

NWT Open File 2010-07

Ts'ude niline Tu'eyeta Candidate Protected Area Phase II Non-renewable Resource Assessment – Minerals

C.A. Ozyer

Recommended Citation: ***Ozyer, C.A., 2010.*** *Ts' ude niline Tu' eyeta (Ramparts River and Wetlands) Candidate Protected Area Phase II Non-renewable Resource Assessment – Minerals, Northwest Territories, Canada; Northwest Territories Geoscience Office, NWT Open File 2010-07, 47 p. and 1 CD.*

>>> NORTHWEST TERRITORIES GEOSCIENCE OFFICE

PO Box 1500, 4601-B 52 Avenue, Yellowknife, NT X1A 2R3

Northwest Territories Geoscience Office
4601-B 52 Avenue
P.O. Box 1500
Yellowknife, NT, X1A 2R3 Canada
867-669-2636
www.nwtgeoscience.ca

This publication may be obtained from the Northwest Territories Geoscience Office (see address, phone number, and website above).

© Copyright 2010
All Rights Reserved

TS'UDE NILINE TU'EYETA CANDIDATE PROTECTED AREA PHASE II NON-RENEWABLE RESOURCE ASSESSMENT – MINERALS

C.A. Ozyer

*Recommended Citation: **Ozyer, C.A., 2010.** Ts' ude niline Tu' eyeta (Ramparts River and Wetlands) Candidate Protected Area Phase II Non-renewable Resource Assessment – Minerals, Northwest Territories, Canada; Northwest Territories Geoscience Office, NWT Open File 2010-07, 47 p. and 1 CD.*

EXECUTIVE SUMMARY

The Northwest Territories Geoscience Office (NTGO) has performed fieldwork as part of a Phase II Non-renewable Resources Assessment (NRA) of the Ts'ude niline Tu'eyeta (Ramparts River and wetlands) Candidate Protected Area required under the Northwest Territories Protected Areas Strategy (PAS). The work consisted of geochemical (stream sediment, water, heavy mineral concentrate, glacial till) sampling in 2007 and 2008.

The NRA was conducted as part of Step 5 of the PAS, to contribute to informed land use decision-making and to comply with the Government of Canada policy. The Phase II NRA followed recommendations made in a Phase I report (Mills, 2008), which evaluated existing data for the study area and identified information gaps.

Most of Ts'ude niline Tu'eyeta lays within the Great Slave Plain, and to a lesser extent the Mackenzie Mountains. The settlement of Fort Good Hope is the closest community to the proposed boundaries of Ts'ude niline Tu'eyeta. The Canadian Wildlife Service is the sponsoring agency of the candidate protected area.

Three-hundred and eighteen heavy mineral concentrate (HMC) samples and 88 glacial till samples were collected and analyzed for kimberlite indicator minerals (KIMs), gold grains, and magmatic/metamorphosed massive sulphide indicator minerals (MMSIMs). To enhance the geochemical knowledge of the area 682 stream silt samples and 666 stream water samples were collected and analyzed. Statistical analyses were applied to the silt and water sample data to produce element anomaly maps for commodity and pathfinder elements.

A review of sample data has determined the highest mineral potential in the Ts'ude niline Tu'eyeta area is located in the southern portion of the study area, within the front ranges of the Mackenzie Mountains. Mississippi Valley Type (MVT) Zinc-Lead potential in the southern portion of the study area is very high just north of the Gayna River MVT Zn-Pb deposits. Moderate sediment-hosted copper potential has been identified in the lower portion of the study area, with stratigraphic exposure appearing to be responsible for copper distribution.

Gold grains recovered from bulk HMC sediment and till samples number from 0 to 9 grains, twenty-three HMC samples contain gold grains, and thirty-four till samples contain gold grains. Samples containing gold grains generally contain only one grain, most of which are characterized as reworked, suggesting abrasion by fluvial or glacial

processes. The relatively low gold values in silt samples and their widespread distribution within the plain area suggest they may have been transported from within or toward the front ranges by glacial processes; the latter is suggested, as gold values in samples from within the front ranges are much lower than samples collected from the plain. Gold potential in the study area is low.

Diamond potential in the study area is low to moderate. Many Kimberlite Indicator Minerals (KIMs) recovered from stream bulk and glacial till samples are derived from kimberlitic sources, but their relative abundance, grain size, and distribution patterns suggest they may have been glacially transported into the area, but this is not conclusive, and much more work would be required to isolate the sources for the KIMs.

The analysis of results of the Phase II fieldwork in the Ts'ude niline Tu'eyeta area increases the potential and confidence for MVT Zinc-Lead, SEDEX Zinc-Lead, sediment-hosted copper, and primary kimberlite diamonds; other deposit types identified in the Phase I report remain unchanged.

TABLE OF CONTENTS

EXECUTIVE SUMMARY i
List of Figures v
List of Tables v
INTRODUCTION 1
Study Area 1
Physiography, Climate and Vegetation 2
REGIONAL GEOLOGY 5
General Tectonic and Geological History of the Study Area 5
Bedrock Lithologies 7
Interior Platform 7
Cordillera 8
Structural Geology 11
Interior Platform 11
Cordillera 11
Quaternary Geology 11
FIELD PROGRAMS 12
2007 Program 12
2008 Program 12
METHODOLOGY 12
Stream Sediment Sampling and Methodology 13
Water Sampling and Methodology 13
HMC Sampling and Methodology 16
Till Sampling and Methodology 18
Heavy Mineral Recovery and Identification 20
RESULTS AND INTERPRETATION: REGIONAL SILT AND WATER SAMPLING 21
Data Processing 21
Mineral Potential Assessment 21
Zn-Pb 22
Copper 25
Gold 26

HEAVY MINERAL CONCENTRATE SAMPLING: RESULTS AND INTERPRETATION .. 27
Gold Grains 27
Results: Bulk HMC Sample Gold Grains 27
Results: Gold Grains from Surficial Materials 28
Results: Kimberlite Indicator Minerals (KIMs) 30
Chromite 32
Diopside 33
Mg-Ilmenite 33
Cr-pyrope 34
Olivine 35
KIM Summary 36
CONCLUSIONS 37
ACKNOWLEDGEMENTS 43
REFERENCES 44
Appendix A 1
Appendix B 1
Appendix C 1
Appendix D 2
Appendix E 3

LIST OF FIGURES

Figure 1. Location of Ts'ude niline Tu'eyeta Candidate Protected Area. 3
Figure 2. Map of ecozones, rivers, and geographic names mentioned in the text.. 4
Figure 3. Geological domains of Ts'ude niline Tu'eyeta..... 6
Figure 4. Bedrock geology map of the study area 9
Figure 5. Stratigraphy of the Mackenzie Mountains..... 10
Figure 6. Locations of 2007-2008 silt and water sample sites..... 15
Figure 7. Locations 2007-2008 bulk sediment and water sample sites. 17
Figure 8. Location of till sample sites collected from Great Slave Plain area..... 19
Figure 9. Geology map showing sample site locations, known deposits, and anomalous sample locations..... 24
Figure 10. Locations of stream bulk and till samples containing visible gold grains..... 29
Figure 11. Distribution of kimberlite indicator minerals from stream bulk sedminet and till samples 31
Figure 12. Cr_2O_3 vs. MgO for chromite and Cr-spinel.. 32
Figure 13. MgO vs. TiO_2 for ilmenites..... 34
Figure 14. CaO vs. Cr_2O_3 for garnets..... 35
Figure 15. NiO vs. Fo content for olivine grains. 36
Figure 16. Location of very high MVT Zn-Pb potential..... 39
Figure 17. Area with moderate copper potential..... 40
Figure 18. Areas with low to moderate diamond potential..... 41

LIST OF TABLES

Table 1. Mineral potential summary 42

INTRODUCTION

The mineral potential of the Ts'ude niline Tu'eyeta candidate protected area has been evaluated by the Northwest Territories Geoscience Office (NTGO) as part of a Non-renewable Resource Assessment under Step 5 of the Northwest Territories Protected Areas Strategy. The Phase I report (Mills, 2008) provided a compilation of existing geological information, detailed potential mineral deposit types, identified information gaps and provided recommendations for Phase II work.

Recommendations for Phase II listed in the Phase I report are: stream sediment sampling to determine anomalous chemistries; heavy mineral concentrate (HMC) sampling to assess diamond potential by detecting KIMs, gold grains, Platinum Group Minerals, and MMSIMs; prospecting, structural analysis, stratigraphic and paleontological studies, lithogeochemical sampling; targeted thematic bedrock mapping.

The purpose of the Phase II work is to address information gaps identified in Phase I (Mills, 2008) and increase the confidence level of the Non-Renewable Resource Assessment (NRA) of mineral potential for the Ts'ude niline Tu'eyeta area. The magnitude of information gaps is large, therefore only certain aspects could be addressed with available resources. Reconnaissance geochemical surveys were selected to enhance mineral potential confidence because important information could be collected promptly and economically over large tracts of land. This report is a compilation of results from work conducted between 2007 and 2008, and provides an interpretation of element and mineral data from silt, HMC, till, and water sample analyses.

Study Area

The Ts'ude niline Tu'eyeta Candidate Protected Area (Fig. 1) covers 15,063 km^2 and lies between 65°03’05”N and 66°40’05”N latitude and 128°41’55”W and 132°00’00”W longitude. Ts'ude niline Tu'yeta lies west of the Mackenzie River, and includes parts of the Ramparts, Hume, and Ontaratue river watersheds. The area is covered by 1:250 000 NTS map sheets 106G, 106H, 106I, and 106J. The settlement of Fort Good Hope is the community closest to the proposed boundaries of Ts'ude niline Tu'eyeta.

Concentrations of traditional trails can be found along the lower Ramparts and Hume rivers (Hunter et al., 2002). Recently established trails tend to follow lines cut for seismic surveys of petroleum exploration. The nearby Mackenzie River is a major transportation corridor for the area.

There is an airport at Fort Good Hope, but there is no year round road access to the community or to Ts'ude niline Tu'eyeta. Access to the field area is restricted to power boats along the larger river systems or by helicopter.

A few unmaintained landing strips exist in the region and in spite of the numerous lakes only a few are deep enough to be suitable for float plane access.

Physiography, Climate and Vegetation

The following description of the Ts'ude niline Tu'eyeta area is summarized from Gal (2007). The study area lies mainly within Great Slave Plain, a physiographic region of generally low relief (average elevation is less than 350 m above sea level). The Mackenzie Mountains in the southern part of the study area comprises rugged upland ranges, with elevations up to 1990 m.

The study area lies within the Taiga Plains and Taiga Cordillera ecozones (Fig. 2) (Environment Canada, 2005; Gal, 2007). The study area within Taiga Plains ecozone includes several ecoregions: Fort McPherson Plain, Mackenzie River Plain, and Peel River Plateau. The climate of these regions is characterized by short cool summers and long cold winters, and is classified as high subarctic, ranging to subhumid boreal along the Mackenzie River. Mean annual summer temperatures range from 9.5 to 11.5°C; Mean winter temperatures range from –22.5 to –25°C (Environment Canada, 2005). Climactic conditions in the Mackenzie Mountains are similar, though somewhat cooler in summer, and with more precipitation (up to 500 mm).

Vegetation in the region is dominated by open, stunted stands of black spruce and tamarack, with secondary white spruce and ground cover of willow, birch, shrubs, cotton grass, lichen, and moss (Environment Canada, 2005). Wetlands constitute a significant portion of the study area (Figure 2), and support sedge, cotton grass and moss. Along the Mackenzie River, taller stands of black spruce and jack pine dominate, with a lower cover of shrubs, moss, and lichen. Higher elevations in the Mackenzie Mountains are covered by alpine tundra vegetation (lichen, dwarf shrubs, sedge), with bare rock and talus. Lower elevations in the mountains support white spruce, willow, and birch.

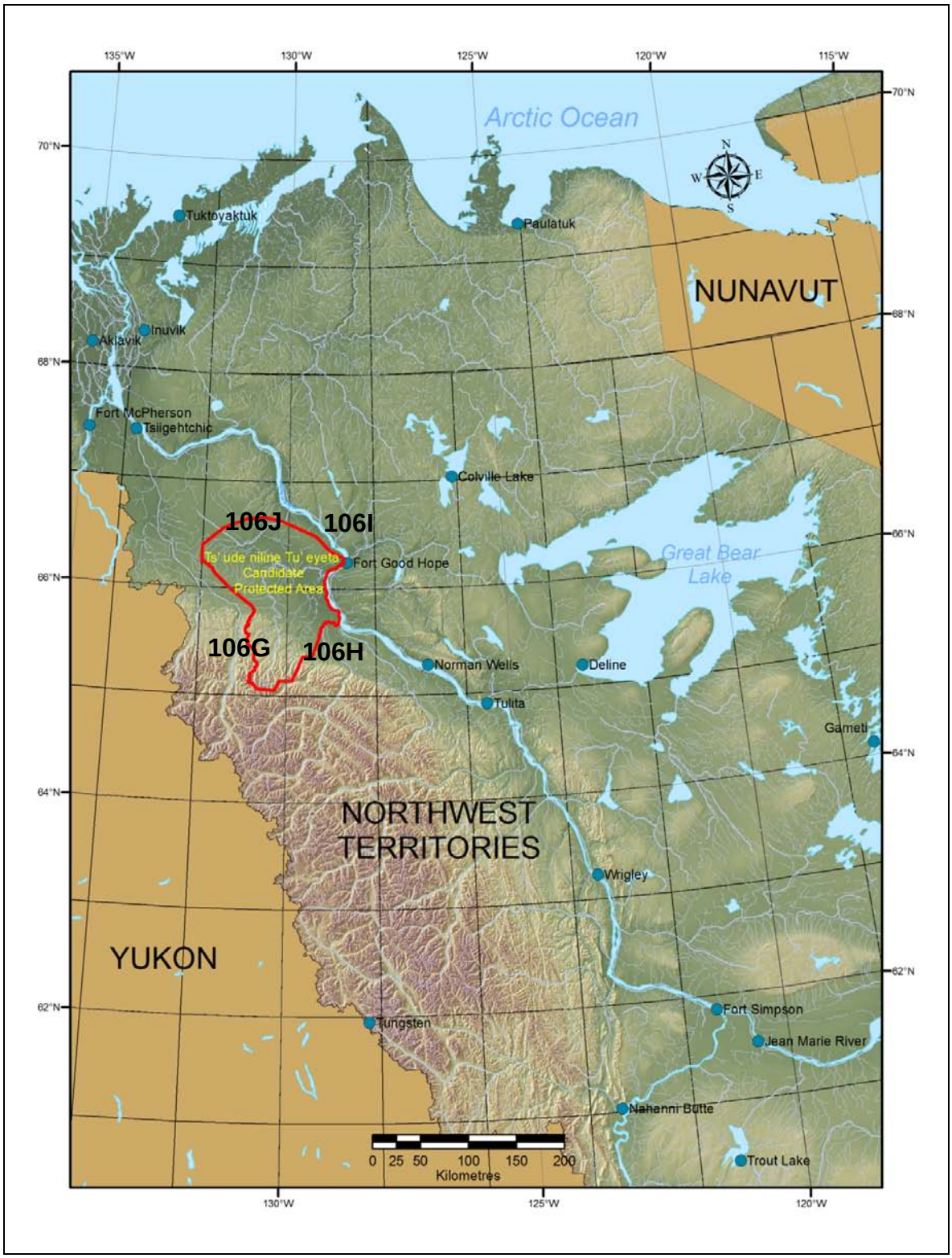


Figure 1. *Map showing location of Ts'ude niline Tu'eyeta Candidate Protected Area (red outline) and communities of the region.*



Figure 2. *Ecozones, rivers, and geographic names mentioned in the text (from Gal, 2007).*

REGIONAL GEOLOGY

General Tectonic and Geological History of the Study Area

The following geologic description is summarized from Gal (2007) and the reader is referred to that report for a more detailed description of regional geology.

Most of Ts'ude niline Tu'eyeta lies within the Interior Platform geological province (Fig. 3), a vast basin of Phanerozoic sedimentary rocks between the Canadian Shield to the east and the Cordillera to the west and south. Sedimentary rocks within the Interior platform are typically shallowly dipping, forming a west-southwest thickening wedge overlying Proterozoic basement rocks (Fig. 4).

The southern portion of Ts'ude niline Tu'eyeta lays within the Mackenzie Mountains, a belt of uplifted, deformed rocks which include the same Phanerozoic rocks as the Interior Platform, and Proterozoic rocks.

The oldest rocks of the study area consist of Proterozoic sediments deposited in an ocean basin along the flank of ancestral North America during rifting, which was followed by quiescent platform conditions. This sedimentation led to the deposition of several kilometers of dominantly siliciclastic and carbonate sedimentary rocks. These rocks were subsequently subjected to episodes of uplift, tilting, deformation and erosion. There is an indication of ancient glaciation within the Proterozoic lithologies (e.g. Aitken, 1993).

Deposition of sediments in the marine environment continued in the Phanerozoic. The continental margin was a tectonically quiet passive margin setting, which underwent voluminous deposition of Mackenzie Platform carbonate rocks (Aitken, 1993).

In the late Devonian, the Ellesmerian Orogeny began in northern Canada, resulting in deposition of siliciclastic sediments into the study area from a landmass to the north and west (Moore, 1993). Sediment deposition continued into the Carboniferous (Richards et al., 1993), followed by an extended period of non-deposition and erosion, through to the Jurassic (Poulton et al., 1993).

During the Cretaceous, the Columbian and Laramide orogenies uplifted the older sediments and formed the Mackenzie Mountains. Eroded sediments were shed into a Cretaceous sea from the newly uplifted lands to the west and south (Stott et al., 1993; Dixon, 1999). In the Late Cretaceous, regression of the sea occurred leading to deposition of continental alluvial and fluvial sediments.

Erosion and glaciation during the Pleistocene transformed the landscape, depositing a veneer of glaciofluvial unconsolidated sediments over most of the study area. Fluvial activity continues to erode the landscape today, especially in the upland areas, with the nearby Mackenzie River and its tributaries transporting large volumes of sediment.

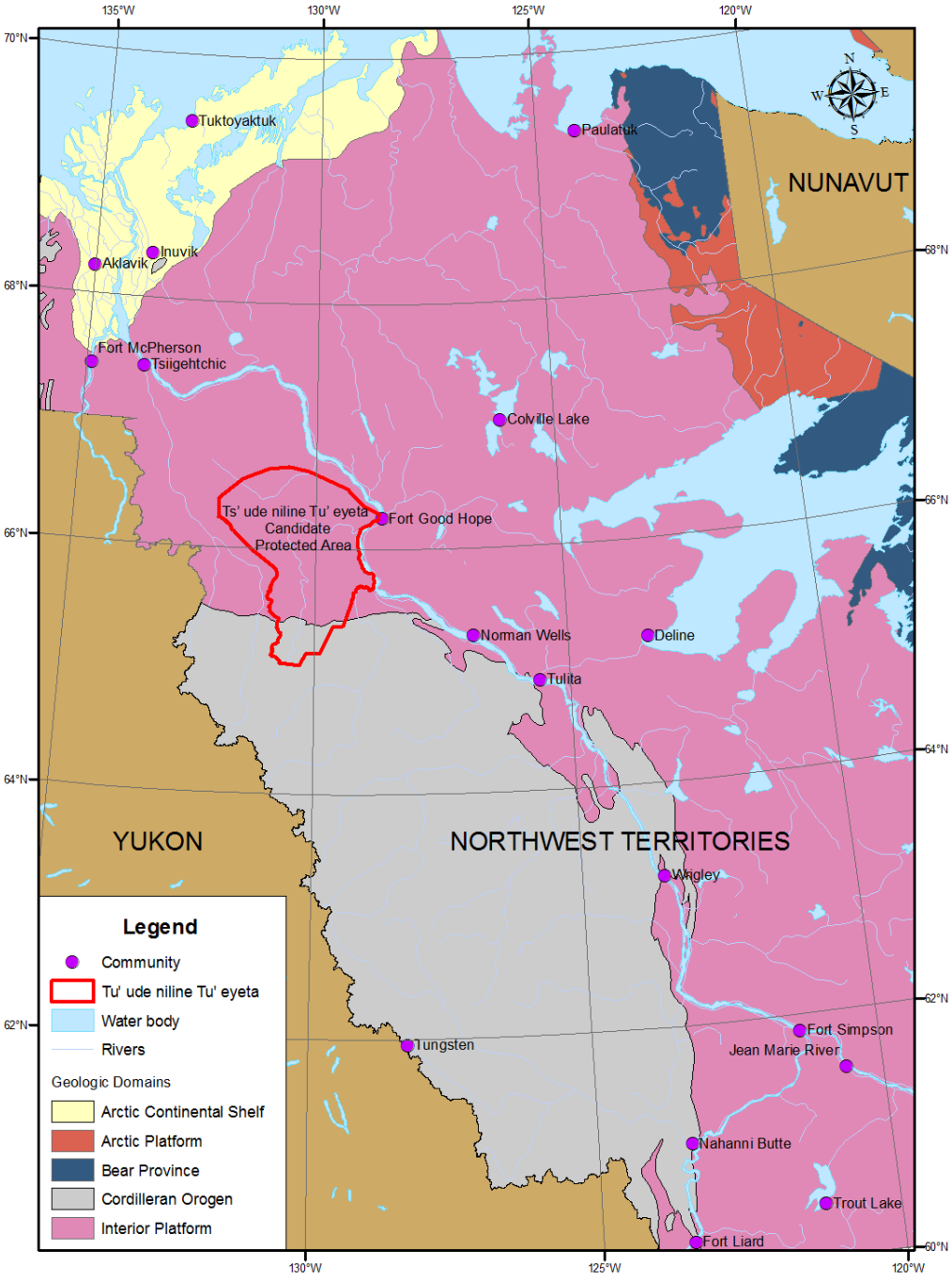


Figure 3. *Geological domains and location of Ts'ude niline Tu'eyeta candidate protected area.*

Bedrock Lithologies

Interior Platform

The erosional event that is responsible for the sub-Cretaceous unconformity has cut downward through Devonian units from southwest to northeast throughout the study area. This partial removal of units, along with the regional southwest dip, has resulted in the oldest rock exposure occurring in the northeast portion of the study area (Fig. 4). In general, although many of the lithological units underlie the entire study area, outcrops are rare on the Interior Platform due to the lack of topography, horizontal nature of the bedrock, abundance of easily erodible shales, and the thick (laterally extensive) veneer of Quaternary surficial deposits. However, many units can be recognized along the cut riverbanks of the major river systems in the study area. The following units have been mapped in the study area, from oldest to youngest they are:

The Hume Formation (Fig. 5) outcrops in several locations south of Hare Indian River, near the eastern boundary of the study area. These exposures consist of dense, brown, thin to medium-bedded fossiliferous limestone (Aitken et al., 1969).

The Hare Indian Formation (Fig. 5), a shale unit is poorly exposed in the study area due to its recessive nature. Exposures of this formation are composed of greenish-grey, grey, and pale brown shales, interbedded with thin horizons of calcareous siltstone and fossiliferous limestone, particularly toward the top of the Hare Indian Formation

The Ramparts Formation (Fig. 5) outcrops considerably in the northeast portion of the study area. Notable outcrops occur at the Ramparts on Mackenzie River, Ramparts Plateau west of Loon Lake, between Rorey and Manuel lakes, Yelta Lake, and Tieda River. This formation is characterized by medium-bedded, brown, partially argillaceous limestone with abundant tabulate coral (Aitken, et al., 1969).

The Canol Formation (Fig. 5) rarely outcrops, and exposures occur mainly on the river banks downstream from Tieda River. The formation consists of dark grey to black bituminous shales with a several silty beds, clay-ironstone concretions, and pyritic nodules (Aitken et al., 1969). Outcrops are stained with yellow and red iron oxides.

The Imperial Formation (Fig. 5) is exposed in the Mackenzie River valley, downstream from Fort Good Hope. It consists of brown and greenish-brown fissile shale, with lesser brown fine-grained sandstone and siltstone beds (Aitken et al., 1969).

Subcrops of Cretaceous strata appear throughout Interior Platform in the western and south-central portions of the study area, and plateaus near Yeltea Lake, south of Loon Lake, south of Fort Good Hope, and near Chick Lake. Cretaceous beds unconformably overlie Paleozoic beds, with more than 120 m of relief on the sub-Cretaceous unconformity apparent near Rorey Lake (Aitken et al., 1969).

Basal Cretaceous sandstone (Sans Sault member of the Arctic Red Formation, or Martin House Formation) is usually white and quartzose, with local oil staining. Abundance of chert, quartz, and grain size varies between beds; calcite cement is common. This basal

sandstone is overlain by shale that rarely outcrops. On the lower Ramparts River the exposures are dark grey to black, slightly silty with abundant ironstone concretions. Shale, siltstone, and minor sandstone are exposed in the lower Ramparts River as a series of gently dipping beds outlining open folds.

Cordillera

In contrast to the Interior Platform, outcrop is abundant in the Cordillera, where more resistant lithological facies are exposed at the surface by tectonic folding and faulting processes. Beds dipping at steep angles often expose thick sedimentary sections. Most stratigraphic units previously described in the Interior Platform are widely exposed in the Cordillera portion of the study area, therefore, not described again here.

Large volumes of Precambrian sedimentary rocks, brought to the surface on fault planes and within cores of large folds, are visible in the Mackenzie Mountains. The Tonian Tsezotene Formation (Fig. 5) is a coarsening up sequence divisible into two subdivisions; the lower member is comprised of dominantly grey argillaceous rock, and the upper member is formed of varicoloured argillite, sandstone, and minor carbonate (Aitken et al., 1978). The (Tonian) Katherine Group (Fig. 5), which overlies the Tsezotene Formation, is predominately arenaceous. The Tsezotene Formation and Katherine Group have both been intruded by sills and northwest oriented dykes composed of greenish-black gabbro. These are the only known igneous intrusions in the study area (Aitken et al., 1978), and could be a source of metals and heat for forming mineral deposits.

The Little Dal Group (Fig. 5) overlies the Katherine Group and is composed of a varied package of limestone, dolostone, anhydrite, gypsum, mudstone, and sandstone. Scattered Zn-Pb showings are present in most stratigraphic units within the Gayna River deposit area, but it is the Grainstone Formation within the Little Dal Group that is most important in terms of size and grade (Eagle Plains Resources Ltd., 2009). Gallium has been identified as the impurity responsible or the distinctive orange coloured sphalerite within the Little Dal Group and is being assessed for economic potential (Wallace, 2009; Eagle Plains Resources Ltd., 2009).

The Cambrian-Ordovician Franklin Mountain Formation (Fig. 5) is dominated by grey, fine-grained dolostone and outcrops widely in the Mackenzie and Franklin mountains (Norman Range) within the study area (Gal, 2009) and may be a suitable host for MVT Zn-Pb mineralization.

The lower Devonian Landry Formation (Fig. 5), comprised of lower pale buff and upper, brown, fine-grained and variably argillaceous and/or pelletal limestone with interbedded shale outcrops in the southwestern part of the study area (Gal, 2007); Zn-Pb showings have been reported in the Landry Formation (Dewing et al., 2006). The Arnica Formation (Fig. 5) overlies the Landry Formation and consists of dark grey-brown and buff crystalline dolostone. The Arnica Formation is widely distributed throughout the study area; several Zn-Pb showing have been reported in the Arnica Formation (Dewing et al., 2006).

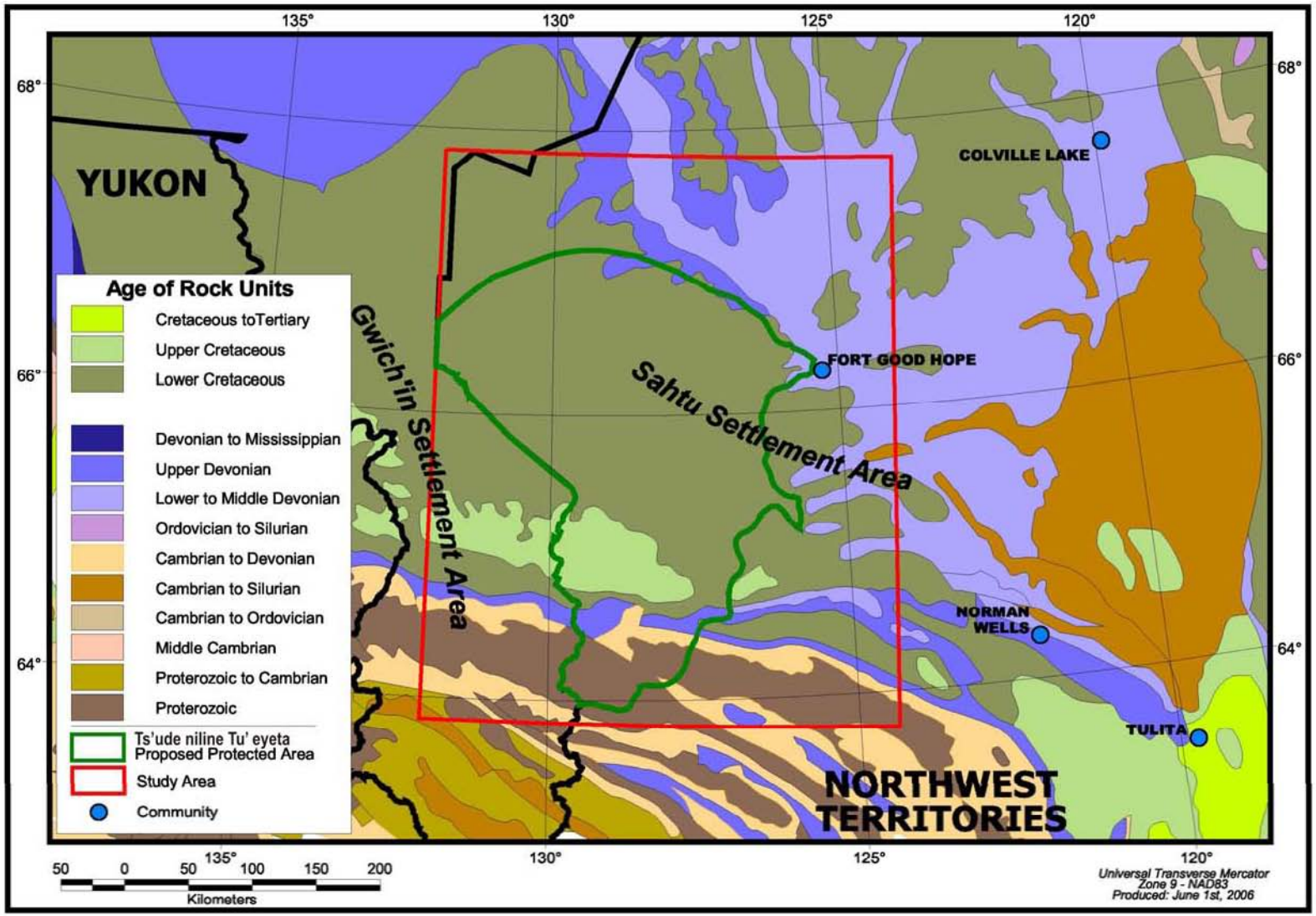


Figure 4. *Bedrock geology map of the study area (from Wheeler et al., 1996)*



Figure 5. *A) Neoproterozoic stratigraphy of the Mackenzie Mountains with mineral occurrences highlighted. Modified from Narbonne and Aitken (1995). B) Simplified Phanerozoic stratigraphy of the Mackenzie Mountains with mineral occurrences denoted. Modified after Dewing et al. (2006) with the addition of Cretaceous-Tertiary units after Dixon (1999) and T. Hadlari (personal comm., 2008). Figure provided by Ootes et al. (in prep.).*

Structural Geology

Interior Platform

For the most part, strata in the Interior Platform have been subjected to little deformation. Regionally, the structural style consists of a southwest dipping monocline (Gal, 2007). Seismic surveys have revealed minor faults and structures such as synclines and anticlines in the subsurface. Evidence of deformation is more pronounced as the Cordilleran front is approached. Mild open folds trending northeast and northwest are generally parallel to the mountain front in Cretaceous beds at Sans Sault Rapids and along the lower Mountain River (Aitken and Cook, 1974).

Cordillera

In general, large structures of the Mackenzie Mountains in the study area are composed of typical fold and thrust morphology, which are interpreted to have resulted from the Laramide Orogeny in the Cretaceous. There is evidence of earlier deformational events but the majority of structural features visible at 1:250 000 map scale are the product of the Cretaceous events. The structural trend of the Franklin Mountains swings markedly to the west in the study area from a northwest trend further south. Large-scale structures in the region consist of north and south-directed thrust faults, and open to slightly overturned folds (Gal, 2007).

Quaternary Geology

Geology in the northern portion of the study area is dominantly Quaternary deposits composed of glacial moraine plain, hummocky and rolling plain, glaciolacustrine deposits, and organics. The northern half of the study area is underlain by till, with minor lenses of glaciolacustrine, glaciofluvial, and organic deposits. Major glaciolacustrine deposits are present along the Hume, lower Ramparts, and lower Hare Indian river areas. Basal till in this area is overlain by these thick glaciolacustrine sediments. Sites for till samples collected in this area were only accessible along rivers that had cut through the glaciolacustrine sediments. Within the southeastern sector of the study area, along the lower Mountain River is a large area composed of glaciolacustrine deposits. Colluvial and sheetwash deposits form thin veneers in mountainous regions. An area trending west–northwest across the middle part of the study area from the Mackenzie River to the western boundary of study area is dominated by significant peat deposits and thermokarst depressions.

FIELD PROGRAMS

2007 Program

The 2007 program was conducted in NTS map sheets 106 J and 106 G. Prior to fieldwork, available geological and topographic maps were studied to determine suitable locations for collection of silt and bulk samples. Sites for bulk samples were selected based on identification of secondary, tertiary, quaternary streams within catchment areas, allowing for isolation of individual catchments should anomalies be identified in a particular sample. Sites selected for silt and water sample collection targeted only primary and secondary streams in catchment areas. Major rivers were also sampled for bulk sediments, but to a lesser extent than the aforementioned streams. In addition to bulk sample collection, silt and water samples were also collected from each bulk site.

2008 Program

The 2008 program was conducted in NTS map sheets 106 H, 106 I, and 106 J. The same sample site selection process was used as in 2007. In addition to collection of stream silt, bulk, and water samples, glacial till samples were also collected in the northern half of the study area, as the area was not conducive to collection of suitable silt and bulk samples due to dense vegetation preventing helicopter access, and vast wetland areas.

METHODOLOGY

Geochemical surveys adhering to National Geochemical Reconnaissance (NGR) protocols were completed for silt, bulk, and water samples within the lower 5,793 km^2 of the Ts'ude niline Tu'eyeta candidate protected area in a collaborative agreement with the NTGO and the Geological Survey of Canada (GSC). Objectives of the survey are to provide geochemical information, which is used to assess mineral potential of the study area.

Stream sediments (silts), heavy mineral concentrates (HMCs), and water samples were collected from the Ts'ude niline Tu'eyeta area employing protocols and methodology used by the NGR program (Day et al., 2005; 2007). In addition, surface material (glacial till) samples were collected in 2008 by personnel from the NTGO. In total, 682 stream silt sediment samples (Fig. 6), 666 stream water samples, 318 bulk sediment samples, and 88 till samples were collected.

Duplicate samples were taken at some locations as part of QA/QC. Sampling and analytical methods used are summarized by Day et al. (2005; 2007). Silt and water geochemistry were reviewed by the NTGO, and geo-statistical interpretation conducted by Aurora Geosciences Ltd. (Robinson, 2010), an independent geological consulting company (Appendix A). See Appendix C for sample field card data.

Stream Sediment Sampling and Methodology

Stream sediments (silt) samples were collected from the Ts'ude niline Tu'eyeta area employing protocols and methodology used by the NGR program (Day et al., 2005; 2007). A total, 682 stream silt sediment samples were collected. Locations and field observations were recorded at each site on a standard NGR stream sediment and water form. Silt samples consisting of silt and/or fine sand were collected from various points in the active stream channel. A sampler typically collects handfuls of silt/fine sand while moving upstream at every site, and prior to bulk sediment collection if the site is designated for collection of such. Sites consisting of only clay or coarse materials not suitable for collection may have had moss mat material collected, as organic fibres tend to trap a variety of grain sizes. Pre-labelled Kraft paper bags (12.5 cm × 28 cm) were two thirds filled with the silt/fine sand and placed into plastic bags and secured with electrical tape. The silt samples were shipped to a commercial laboratory where they were air-dried and sieved through a minus 80-mesh screen. Control reference and blind duplicate samples were inserted into each block of twenty sediment samples at the laboratory for QA/QC purposes.

Silt samples were analyzed by Acme Analytical Laboratories Ltd. for 36 elements using inductively coupled plasma mass spectrometry (ICP-MS); analyses for tin (Sn) was by fusion and ICP-MS (Appendix C). Silt samples were also analyzed for 26 elements using Neutron Activation Analysis (NAA) by Becquerel Laboratories Inc. (Appendix C).

Water Sampling and Methodology

A total of 666 water samples were collected in 125 ml Nalgene high density polyethelene (HDPE) bottles from the active part of the stream channel at each site. Prior to collection of a water sample, each sample bottle was rinsed twice in the stream channel prior to final collection. Within 24 hours of collection 50 ml of water from each water sample was filtered through a single-use Millipore Sterivex-HV 0.45 μm filter attached to a 50 ml sterile plastic syringe into new 60-ml HDPE bottles. The remainder of the water was used to determine pH and conductivity before being discarded. Using an Eppendorf pipette repeater with disposable plastic tips, 0.5 ml of 8M HNO_3 was added to the filtered water samples. Syringes were re-used after rinsing with DDI water, but replaced daily.

Filtered and acidified waters were kept in a cool dark place until shipped to the laboratory. Control references were inserted into the block of 20 water samples; no blind duplicates were inserted for the water samples.

At the end of each water filtering and acidification session, control reference samples (filter, acid, travel blanks) were inserted. Filter blanks consist of a 60-ml HDPE bottle of filtered and acidified double de-ionized (DDI); acid blanks consist of a 60-ml HDPE bottle filled with DDI and acidified (but not filtered); travel blanks consist of a 60-ml HDPE bottle pre-filled with DDI at the lab in advance of sample collection, then acidified with routine samples.

Water samples were analyzed for 51 elements by ICP-MS and 9 elements by inductively coupled plasma emission spectroscopy (ICP-ES) by the Geological Survey of Canada. Results of water sample analyses are located in Appendix C.

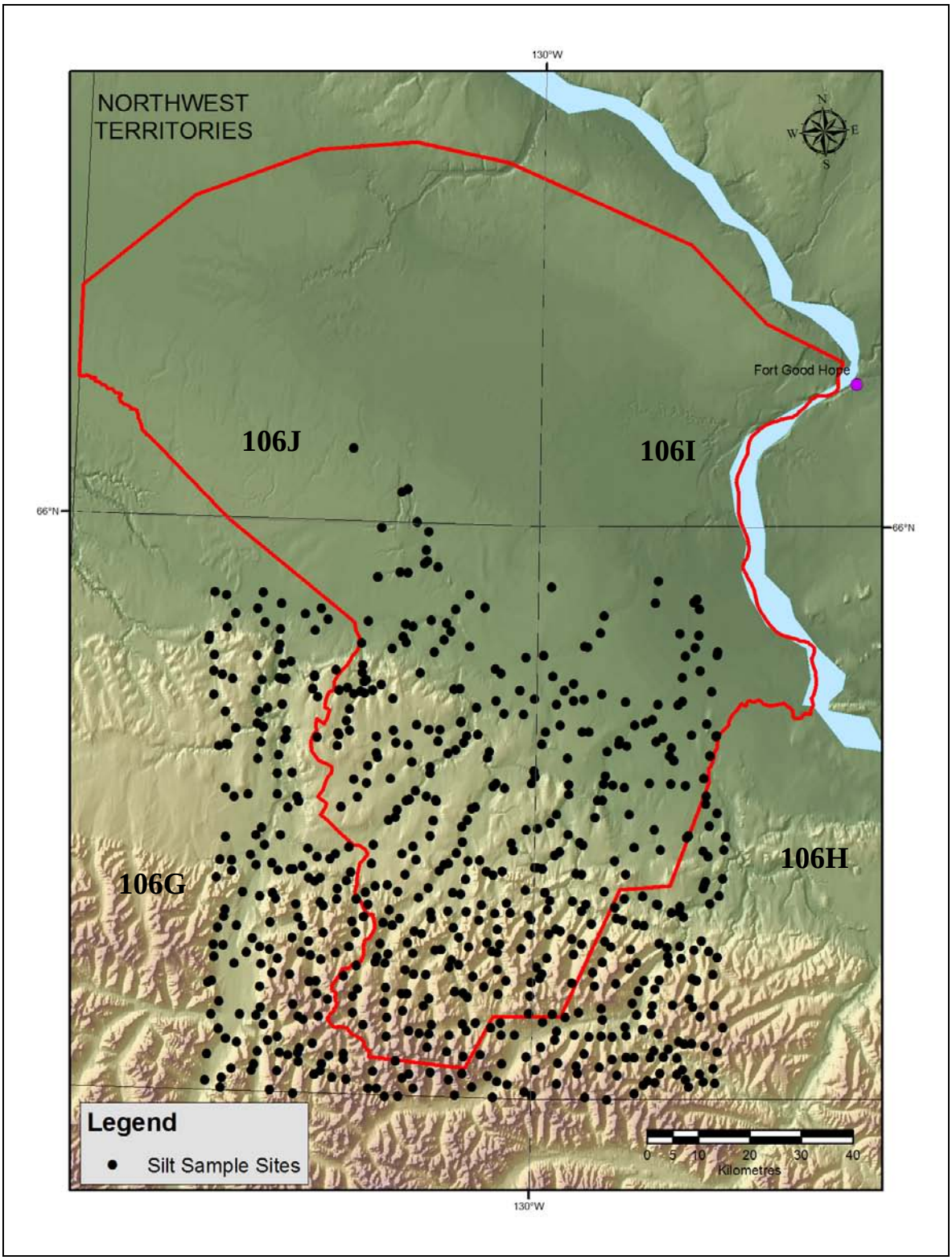


Figure 6. *Locations of 2007–2008 silt and water sample sites.*

HMC Sampling and Methodology

Heavy mineral concentrate (HMC) sampling studies were conducted to test for the presence of kimberlite indicator minerals (KIMs) and to determine the regional distribution of KIMs in the area. Additionally, samples were analyzed for gold grains and MMSIMs to determine presence and possible distribution patterns. Analytical results of stream HMC samples are provided in Appendix D.

A total of 318 bulk HMC samples were collected with an approximate density of one sample per 17 km^2. Locations for sample sites were determined prior to the field season and identified on 1:50 000 topographic map sheets. Sample sites were strategically placed in areas exhibiting topographic gradients where heavy minerals are likely to accumulate. Specific sample sites were dependent upon helicopter access and availability of appropriate material. Variances of actual sample sites from original target sites were recorded using a portable Global Positioning System (GPS). Bulk (HMC) sample locations are shown in Figure 7.

Primary sample medium was alluvium as it provides a relatively fast, low-cost means to obtain heavy mineral signatures for individual drainage basins. Material collected represents products of erosion of bedrock and overburden, reflecting collective bedrock and overburden located upstream of the sample site. HMCs extracted from stream sediment samples were characterized by composition, grain size, maturity and colour, which reflect geology, terrain, and climate of the catchment area upstream of the sample site. The objective of HMC sampling is to identify anomalous material within the catchment area, and to interpret those anomalies in light of the known geology of the area.

The main target areas within streams were dominantly the upstream apices of point and longitudinal bars and to a lesser extent boulder and vegetation traps. These areas were selected because they represent areas where marked reductions in stream energy occur, thus locations where heavy minerals are likely deposited. Samples were collected by wet-sieving material through a 2 mm mesh sieve into a 5-gallon plastic pail lined with a heavy-duty sample bag until 12–15 kg of material was attained. Samples were weighed, double-bagged, and opening sealed with plastic electrical tape, then shipped to a commercial laboratory for preparation and analysis.

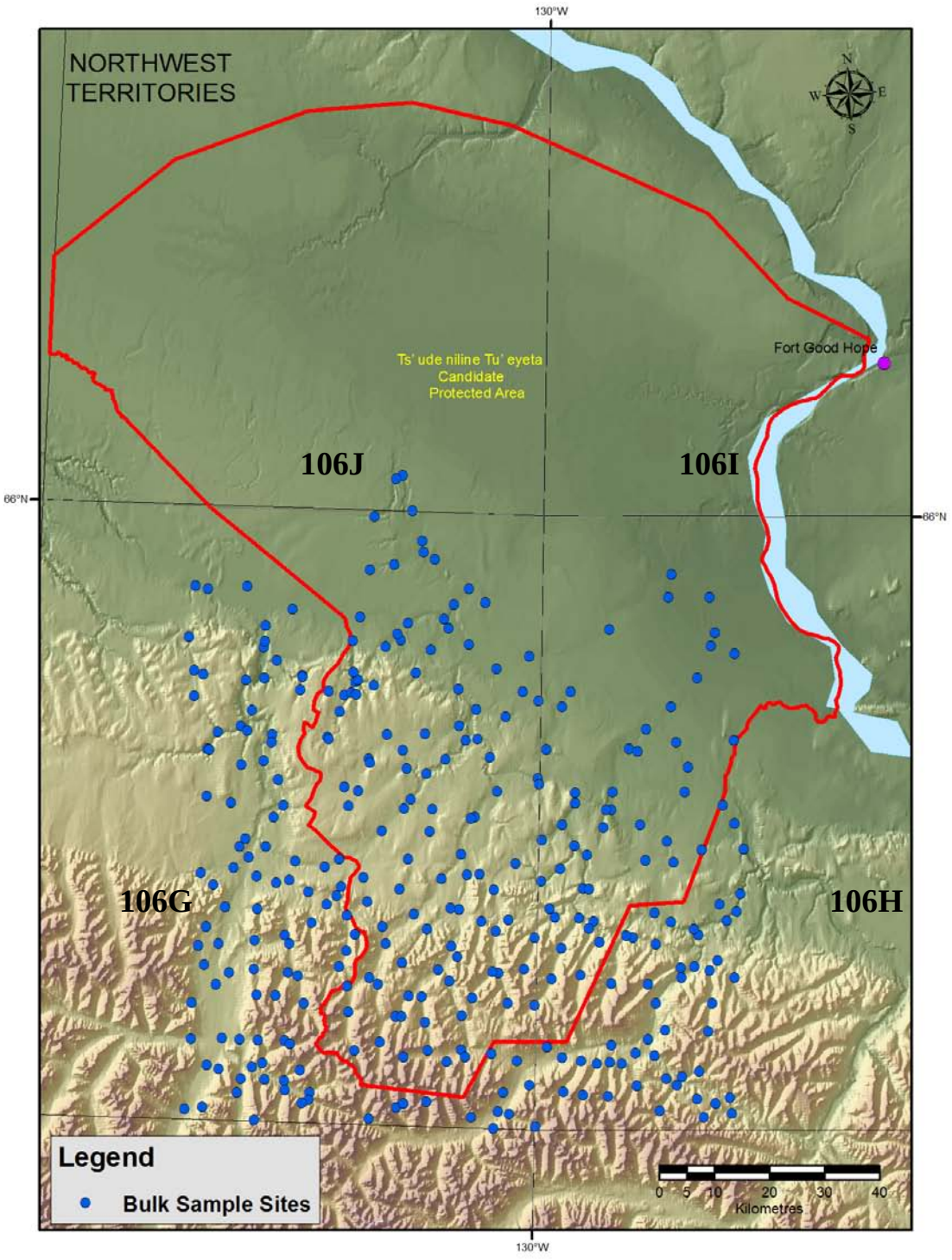


Figure 7. *Locations of 2007–2008 bulk sediment and water sample sites.*

Till Sampling and Methodology

Eighty-eight samples of surficial (till) materials were collected from the northern portion of the study area in the Great Slave Plain (Fig. 8), a physiographic region of generally low relief. This work was included as part of the PAS-NRA work to complement bulk samples collected from sites to the south. Some rivers and streams in the northern portion of the study area contain a mixture of sediments transported from mountainous areas and glacially transported material. But most surficial material in the area is composed of glacial till or glaciofluvial sediments. Glacial till was selected as the prime material for HMC sampling as it often possible to trace anomalous materials in the till to its bedrock source through paleo-ice flow studies. Samples were collected and double bagged in heavy-duty plastic sample bags with average sample weights of 21 kg, which is a typical weight for till samples. Due to significant glaciolacustrine sediments overlying basal till, samples were collected from stream cuts where glacial till was exposed.

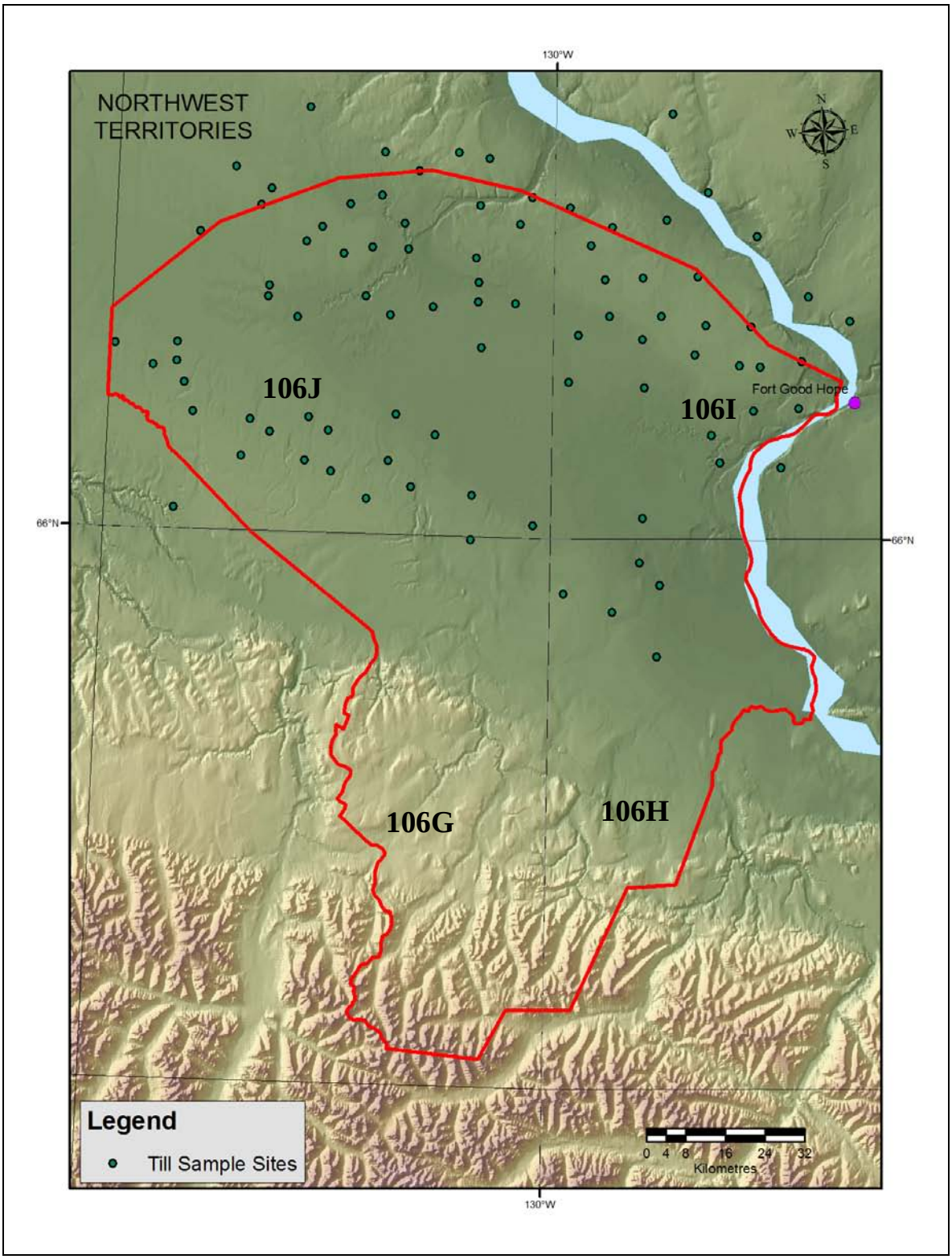


Figure 8. *Location of till sample sites collected from Great Slave Plain area.*

Heavy Mineral Recovery and Identification

Overburden Drilling Management (ODM) was contracted to process the stream HMC samples and till samples. Initially, a 500 g character sample was extracted and stored prior to further laboratory procedures. The remaining material was wet sieved to <2.0 mm with any oversize material stored. The <2.0 mm material was examined for visible gold (V.G.) grains and a calculation of assay value was conducted. The material was dry sieved to extract the –0.25 mm size fraction for geochemical analysis. The remaining 0.25 to 2.0 mm size fraction was subjected to Heavy Liquid Separation using methylene iodide diluted with acetone to achieve a specific gravity of 3.20. Fractions with specific gravities lighter than 3.20 were separated and stored. Remaining material with specific gravities greater than 3.2 then underwent ferromagnetic separation, which was extracted and stored. The remaining 0.25–2.0 mm nonferromagnetic fraction was subjected to an oxalic acid wash with any liberated –0.25 mm material stored. The sample was then dry sieved into three size fractions, 0.25–0.5 mm, 0.5–1.0 mm, and 1.0–2.0 mm. The 0.25–0.5 size fraction underwent paramagnetic separation with a Carpo drum and was logged/picked for indicator minerals as were the other two size fractions. Picked grains were visually identified; ambiguous grains were additionally examined by Scanning Electron Microscope (SEM).

Stream bulk sediment and till samples were analyzed for magmatic/metamorphosed massive sulphide indicator minerals (MMSIMs) as these minerals are also extracted from the samples during KIM picking and SEM checks. Results of these analyses are presented in Appendix E. Heavy minerals extracted from bulk sediment samples collected in 2008 were also subjected to a 100 grain count from the 0.25–0.5 mm size fraction to identify grain species, results of these counts are also presented in Appendix D.

Kimberlite indicator mineral grains recovered from HMC and till samples were identified by electron microprobe analyses by the Geological Survey of Canada and Renaud Geological Consulting Ltd. to determine their composition (Appendix E). KIM data was categorized and interpreted by Dr. Ingrid Kjarsgaard, an independent consulting mineralogist (Appendix B).

RESULTS AND INTERPRETATION: REGIONAL SILT AND WATER SAMPLING

Geo-statistical analysis and interpretation of silt and water sample geochemical data from the Ts'ude niline Tu'eyeta area was completed by Aurora Geosciences Ltd. (Robinson, 2010) on behalf of the NTGO. This section summarizes the report, which is included in Appendix A. Results of silt and water geochemical analyses are provided in Appendix C.

Data Processing

Procedures used for statistical analysis of the Ts'ude niline Tu'eyeta geochemistry are described in Appendix A. Univariate statistics such as sample quantity, mean, median, skewness, kurtosis, and standard deviation were used to determine which elements to include in the multivariate statistical analysis. Multivariate statistics was applied to the data because it can extract geochemical patterns associated with underlying geology, weathering, alteration and mineralization (Grunsky and Smee, 2003). Principle Component Analysis (PCA) was employed to reduce the number of variables (elemental analyses) necessary to describe the response by grouping them into small, linear combinations, which are frequently found to reflect underlying features and processes, such as surficial geology, bedrock lithology, and mineralization systems where present (Robinson, 2010).

Mineral Potential Assessment

Based on the chemical analyses from the stream sediment and water survey, a set of single element plots have been assembled for key commodity and pathfinder elements. The plots were studied to help identify areas with anomalous elemental values. These single element plots display an area of anomalous values in the southern portion of the Ts'ude niline Tu'eyeta proposed area.

Several deposit types should be considered in the Ts'ude niline Tu'eyeta study area based on known geology of the area. Mississippi Valley-Type (MVT) Zn-Pb, Sedimentary Exhalative (SEDEX) Zn-Pb, and sediment hosted copper are favourable deposit types for the area.

To evaluate the MVT potential of the study area the following criteria should be considered: presence of Proterozoic to Carboniferous platformal carbonate rocks, especially if adjacent to sedimentary basins; features that allow fluid migration such as paleokarsts, faults, unconformities, breccias, basement highs, reef complexes, depositional margins and shale cap; hydrothermal dolomitization of precursor carbonate rocks. The Mackenzie Mountains are underlain by Proterozoic to Devonian sedimentary rocks, deposited in a carbonate platformal setting. Many showings of galena and sphalerite occur in dolostone and associated vugs in these carbonate rocks.

SEDEX deposits are most prevalent in Proterozoic to Paleozoic rocks and are usually basinal sedimentary rocks with tabular bodies of Zn, Pb, and Ag mineralization (in sphalerite and galena), which were deposited by hydrothermal fluids on the seafloor and into deep water basins associated with continental rifts under reducing conditions (Goodfellow and Lydon, 2007). SEDEX and MVT deposits are both found within marine platforms of sedimentary basins, and are thought to have formed due to migration of metalliferous saline fluids. SEDEX and Volcanogenic Massive Sulphides (VMS) deposits are both formed by vented fluids onto the seafloor from hydrothermal systems, thus host rocks are of similar age. MVT deposits however, were formed in the subsurface allowing for greater age differences between ores and host rocks (Goodfellow and Lydon, 2007). In Canada, SEDEX deposits were formed during several hydrothermal events, often occurring in clusters within second-order basins adjacent to extensional structures separating basinal facies from platformal carbonate sequences (Goodfellow and Lydon, 2007).

Sediment hosted copper is known to exist southeast of the study area in the Redstone Copper Belt. The Redstone Copper Belt is considered to host Kupferschiefer-type copper mineralization, which extends at least 240 km from Coates Lake to north of the Godlin River. Copper mineralization in the Redstone Copper Belt is within the Copper Cap Formation of the Coates Lake Group. The copper belt appears as a narrow arcuate band on surface maps, but its lateral extent is unknown. The Coates Lake Group has not been identified in the study area, but latest Windermere Supergroup (which hosts the Coates Lake Group) strata outcrop in the in extreme southwest corner of the study area in the interior ranges of the Mackenzie Mountains (Gal, 2007).

The geochemical report prepared by Robinson (2010) suggests favourability for SEDEX, MVT, or Redbed type deposits within the study area. Similar to SEDEX deposits, the Gayna River deposits are considered to be Mississippi Valley-Type. MVT deposits occur in clusters from a few to hundreds of individual bodies which have variation in character and shape, and are often interconnected (Paradis et al., 2007).

Zn-Pb

Analyses of silt samples from the sampling programs have revealed samples with anomalously high values of Zn and Pb (Fig. 9). Nine samples returned Zn values greater than 350 ppm, the highest 634 ppm. Thirteen samples analysed for lead returned values at or exceeding the ninety-eighth percentile, and are considered anomalous; the highest Pb value returned was 47 ppm. Many samples with anomalous lead values also contained elevated levels of copper. Numerous sphalerite and galena grains were picked as MMSIMs in the HMC samples (Appendix E), suggesting a proximal source.

Samples with anomalous values of Zn, Pb and Cu also have elevated Ag and Au values (Fig. 9). The anomalous samples appear concentrated in a 22 km wide, west-northwest–trending belt across the southern portion of the study area just north of the Gayna River Zn-Pb deposits and satellite showings.

The multivariate statistical analysis of silt samples in the geochemical report produced by Aurora Geosciences Ltd. (Appendix A) for this report reveals a strong positive

correlation between Ga and Cu, similar to that reported by Wallace (2009) for Ga and Cu in sphalerite from the Gayna River deposits.

Wallace (2009) determined several trace elements in the Gayna River sphalerite were unusual, with high Ga values, whereas most other carbonate-hosted zinc-lead deposits in the Mackenzie Platform do not contain detectable Ga (Carrière and Sangster, 1999). The Wallace (2009) study suggests a strong positive correlation between Ga and Cu values in sphalerite, and suggests these impurities may be responsible for the orange colour of sphalerite in the Gayna River deposit. Recent microprobe analyses, has also revealed gallium is also concentrated in galena (Eagle Plains Resources Ltd., 2009). This correlation is important because it indicates the potential to discover Gayna River MVT style mineralization in the study area.

The Mackenzie Mountains consists of a series of fault blocks and grabens, therefore, the west-northwest trend of anomalous samples may represent exposure of mineralized stratigraphic horizons similar, if not the same as those found at the Gayna River deposits and showings.

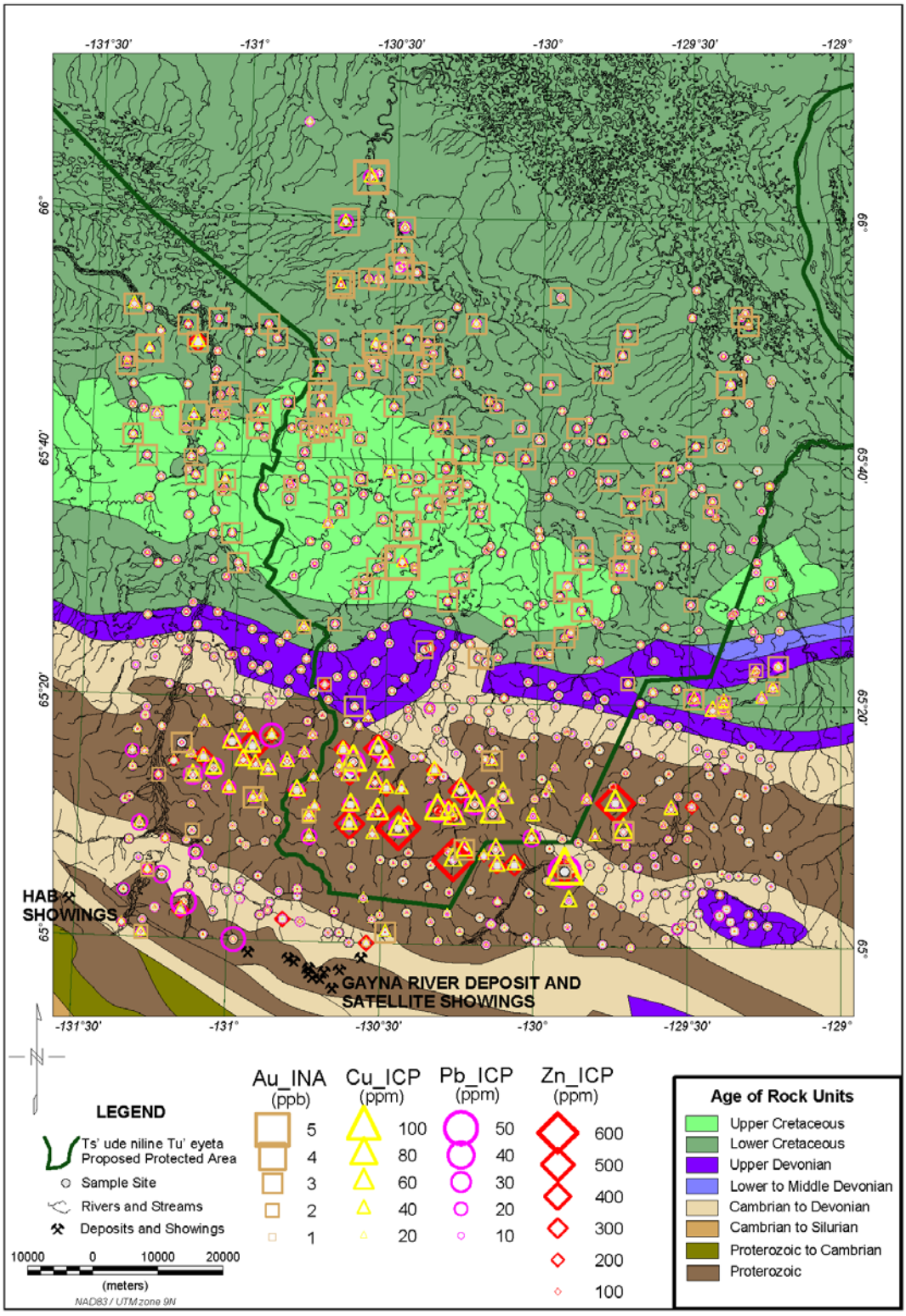


Figure 9. *Geology map of study area showing sample site locations, known deposits, and anomalous sample locations (from Robinson, 2010).*

In the mid-1970s, Cordilleran Engineering Ltd conducted a regional silt sampling survey in the Gayna River area at a density of one sample per 2.6 km^2 which resulted in one single sample containing 980 ppm Zn and 11 ppm Pb (Hewton, 1982). Surveys conducted for this report were collected at a density of one sample per 17 km^2, a lower density than the survey, which led to the discovery of the Gayna River Zn-Pb deposits. Although the surveys are not of sufficient coverage density to discover location of deposits, they do indicate their presence. Targeted, high density follow-up surveys would increase the resolution of areas with anomalously high values, and a prospecting program would aid to identify source rocks.

The Gayna River deposits are one of the world's largest undeveloped Zn-Pb properties (Lydon, 2007). Additional discoveries could increase the value of the Gayna River camp. This study suggests the southern portion of the proposed Ts'ude niline Tu'eyeta protected area has very high potential for discovery of significant MVT Zn-Pb deposits.

Copper

Eleven silt samples returned anomalous values of copper, the highest value is 106 ppm; nine samples exhibiting elevated zinc values were also anomalous for copper. Similarly, many samples with anomalous lead values also contained elevated copper values. Figure 9 in the Aurora Geosciences Ltd. report (Appendix A) illustrates the relationship between gridded PCA F1 values and copper, nickel and silver, suggesting the southern portion of the study area has potential for the presence of SEDEX or red bed type deposits. The Redstone Copper Belt is located approximately 150 km southeast of the study area, and is described as Kupferschiefer-type copper mineralization. The majority of copper showings in the Redstone Copper Belt occur at a stratigraphic position referred to as the "Tranzition Zone" of the upper Coppercap Formation and lower Redstone River Formation of the Coates Lake Group (Fig. 5). Primary copper sulphides in the Redstone Copper Belt include chalcocite, covellite, chalcopyrite, digeonite, and bornite (Ruelle and Bond, 1976). Chalcopyrite is the primary copper-bearing mineral, while chalcocite and bornite make up less than 15% of the copper sulphide content of the showings. Extensive supergene alteration in the Redstone Copper Belt includes malachite, limonite, covellite, minor azurite, and chalcocite mineralization. Malachite, a mineral found in the oxidized zones of copper deposits was recovered from several HMC samples in the study area. Samples containing malachite grains are located predominately in the southeastern portion of the study area.

This study suggests that although some silt samples returned anomalous values of copper, their association is likely not related to the Redstone Copper Belt as rocks of the Coates Lake Group, Rapitan Group (Fig. 5), and Wernecke Supergroup are not known to exist within the study area (Mills, 2008); however, late Windermere Supergroup strata outcrop in the extreme southwest corner of the study area (Gal, 2007). It is possible an improvement upon existing geological maps could result in identification of favourable stratigraphic sequences.

Based on samples with anomalous copper values (Fig. 11; Appendix A) and recovery of malachite grains from HMC samples in a west-northwest trending belt, copper potential is ranked moderate in the southern portion of the study area.

Gold

Gold values in silt samples are higher in the plains area compared to samples in the cordillera. It may seem logical to attribute samples with elevated gold values in the plains to glacial dispersion of auriferous debris from distal sources such as the shield area, but it does not explain the correlation with mercury and silver, barium and phosphorous reported by Robinson (2010).

Ten silt sample locations exhibiting elevated metal values also correlate with highly acidic pH values, suggesting a local concentrated source for the metals. Of the ten anomalous locations, two showed elevated responses for copper, lead and gold, two for copper and gold, and one for copper, zinc and gold.

Intrusions are known to host gold, but the only known intrusions in the study area are related to the Tsezotene Sills, with several exposures located within the southern boundary of the Ts'ude niline Tu'eyeta proposed protected area. A recent study of the Tsezotene Sills by Ootes et al. (2008) revealed either no gold values, or insignificant gold values from rock samples analyses and determined the sills are of little economic interest, thus not a significant source of gold.

Although silt samples from varying locations across the survey exhibited elevated gold values, numerous stream HMC and till samples also contain gold grains. Results of gold grains recovered from stream HMC and till samples are discussed in the Heavy Mineral Concentrate and Surficial Materials sections.

The relatively low values of gold in the silt samples and their fairly even widespread distribution, predominately in the plains region, suggests they were likely transported to the area by continental glaciers during the last glaciation and then redistributed by glaciofluvial or glaciolacustrine processes, and subsequently fluvial processes. Although Robinson (2010) determined a correlation with mercury and silver, barium and phosphorous, the gold values are low, and likely represent background values.

HEAVY MINERAL CONCENTRATE SAMPLING: RESULTS AND INTERPRETATION

Laboratory results of kimberlite indicator mineral HMC and gold picking data are presented in Appendix D.

Gold Grains

Twenty-three of the 318 stream bulk HMC samples and thirty-four of the 88 till samples collected contained visible gold grains (Fig. 10). Gold grain results are discussed separately for stream bulk HMC samples and till samples.

Results: Bulk HMC Sample Gold Grains

One sample located west of the Arctic Red River contained seven gold grains, two samples contained two gold grains, and the remaining twenty samples contained one grain of visible gold. One sample containing two gold grains is located in the plains area along the Ramparts River, and the other sample was collected from a tributary to the Gayna River. The number of visible gold grains recovered in the HMC samples is relatively low, and the morphological characteristics of most gold grains indicate they have been reworked. Gold grains recovered from HMC samples are categorized into three grain morphologies; pristine, modified, and reworked.

Pristine gold grains are described as those that do not appear to have been damaged and retain primary surface textures such as crystal faces or grain moulds which may have held gangue minerals which may have been broken or weathered out (DiLabio, 1990). Modified gold grains are described as those that appear to represent their original shape with some primary textures still visible, but all edges appear curled, blunted, or bent, likely through grain to grain contact and abrasion (DiLabio, 1990). Reshaped gold grains are described as those that retain none of their pristine shapes or textures, with most having a rounded outline. The surface texture and shape of these grains are typically the result of weathering and fluvial abrasion, not glacial abrasion, therefore, cannot be used to determine distance of glacial transport. Reworked gold grains can be problematic where they are found in large numbers recycled in till, or where concentrated by glaciolacustrine or glaciofluvial processes into small placers that have no known sources (DiLabio, 1990).

Sources for gold grains recovered in proximity to the front ranges may be ambiguous as they may have been distributed by Cordilleran ice from deeper in the mountains, or their presence may represent distribution of auriferous debris from the shield area by continental glaciers into the Mackenzie Mountains, and subsequent redistribution by streams. Similar to elevated gold values in the silt samples, gold grains in the stream HMC samples are widely distributed near the front ranges and plain area, and for the most part consist of one grain. The low gold grain count and broad distribution suggests dispersal by glaciers and redistribution by fluvial processes.

Results: Gold Grains from Surficial Materials

Of 88 samples analyzed, a total of 51 gold grains were recovered from 34 samples (Fig. 10). Most samples containing gold grains had one or two grains, but one sample contained nine grains. Most gold grain morphologies were identified as reshaped, suggesting they were subjected to weathering and fluvial abrasion. However, the gold grains were recovered from glacial till exposed in stream cuts, suggesting the gold grains may have been subjected to fluvial abrasion and modification prior to entrainment in the glacial till. Similar to silt samples elevated in gold values, and gold grains in the stream HMC samples, low gold grains in till are widely dispersed throughout the northern part of the study area, suggesting their origin was likely derived from auriferous debris in glacial overburden.

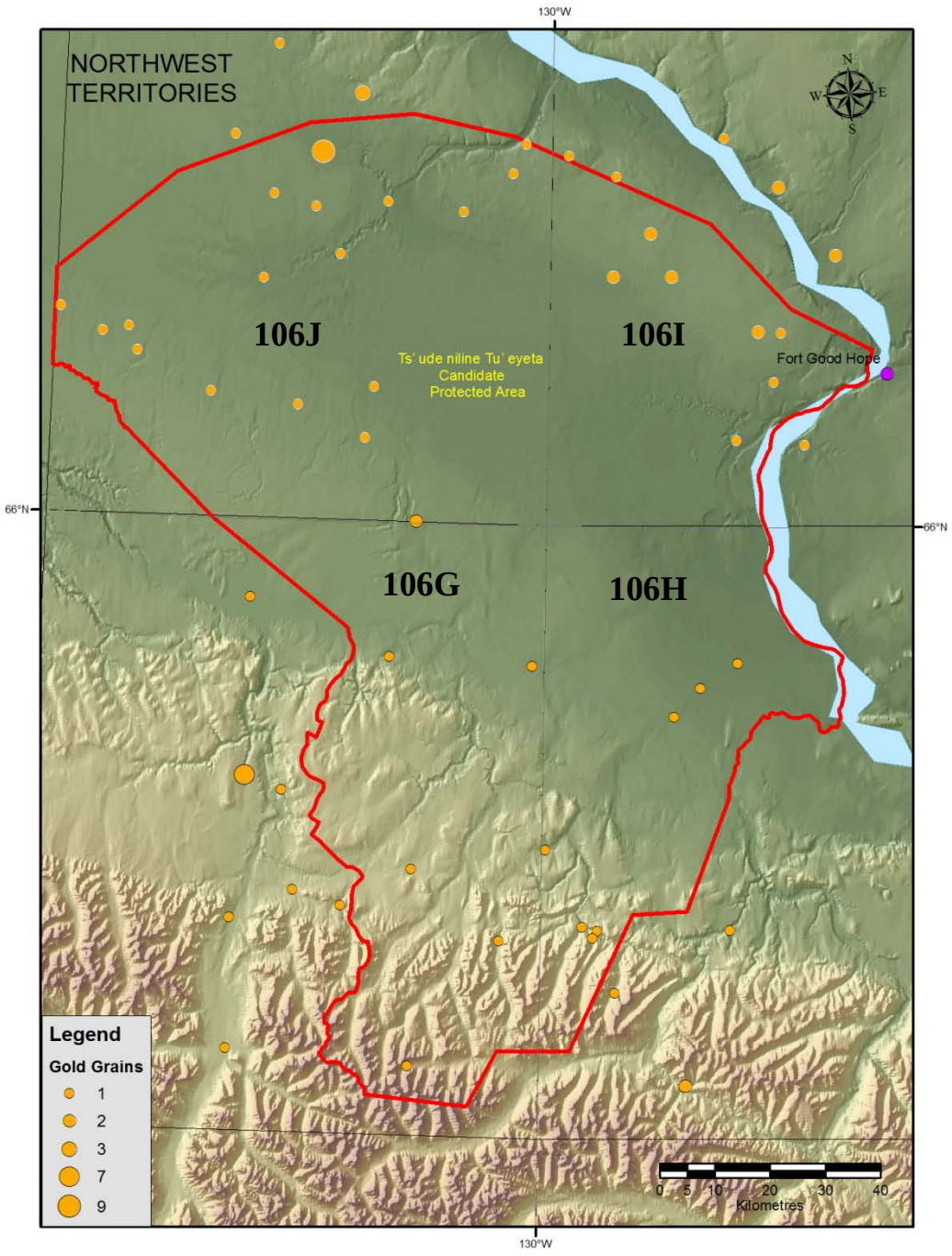


Figure 10. *Locations of stream bulk (black outline) and till (white outline) samples containing visible gold grains.*

Results: Kimberlite Indicator Minerals (KIMs)

Kimberlite indicator mineral grains recovered from bulk HMC and till samples were analyzed by electron microprobe to determine their crystal chemistry. This process enables categorization of the grains into either kimberlitic or non-kimberlitic sources. Data collected from electron microprobe analyses conducted by the Katherine Venance (Geological Survey of Canada) and Renaud Geological Consulting Ltd. (Appendix E) were interpreted by Dr. Ingrid Kjarsgaard, a consulting mineralogist specializing in classification of kimberlite indicator minerals. Two reports on interpretation of kimberlite indicator minerals recovered from bulk samples and one report for till samples were prepared by Dr. Kjarsgaard and can be found in Appendix B.

The following is summarized from Kjarsgaard (Appendix B). A total of 714 mineral grains were recovered and analyzed from 124 bulk stream sediment samples and 43 till samples, the remainder of samples were barren of KIMs. Pie charts in Figure 11 illustrate the quantity, distribution, and KIM types recovered from bulk (black outline) and till samples (white outline), note the central portion of the upper part of the study area is void of samples due to inaccessibility.

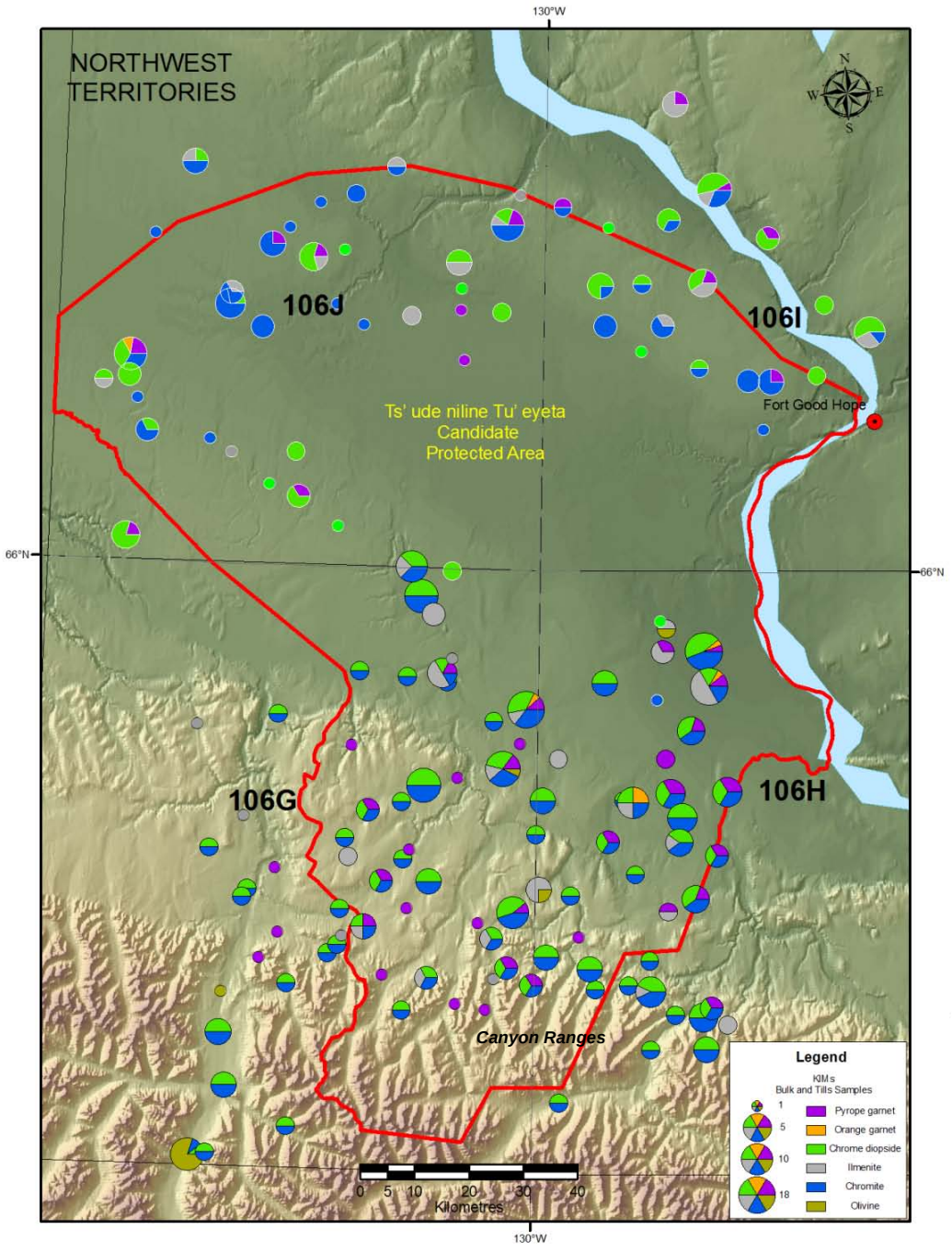


Figure 11. *Size proportional pie chart map illustrating distribution of kimberlite indicator minerals from stream bulk (black outline) and till (white outline) samples collected from NTS map sheets 106G to 106J.*

Chromite

Chromite, represented by 344 grains, is the most abundant mineral in the samples. Most samples containing chromite have less than 6 grains, but 50% of chromite grains are concentrated in only five samples, with one sample containing 60 grains (106G-2007-2188). Compositions vary considerably from 25 to 62 wt.% Cr_2O_3 and from 2.5 to 17.7 wt.% MgO. The geochemical composition of chromite grains can be used to determine if a particular grain is associated with diamond by plotting the MgO wt.% vs. Cr_2O_3 wt.% to see if it plots within areas of geochemical composition known to be associated with diamond inclusions or intergrowth with diamonds.

One Cr-rich grain falls within the compositional field of diamond inclusion chromites, and a few grains plot immediately below the diamond inclusion and intergrowth fields (Fig. 12) and are likely from garnet-peridotite xenoliths.

Many of the chromites could have originated from mantle peridotite, except MgO-poor ferrochromites, but many could also be derived from crustal ultramafic rocks, which have a compositional overlap. Several grains are Fe-rich and Al- and Mg-poor ferrochromites, suggestive of chromite originating from ultramafic layered intrusions.

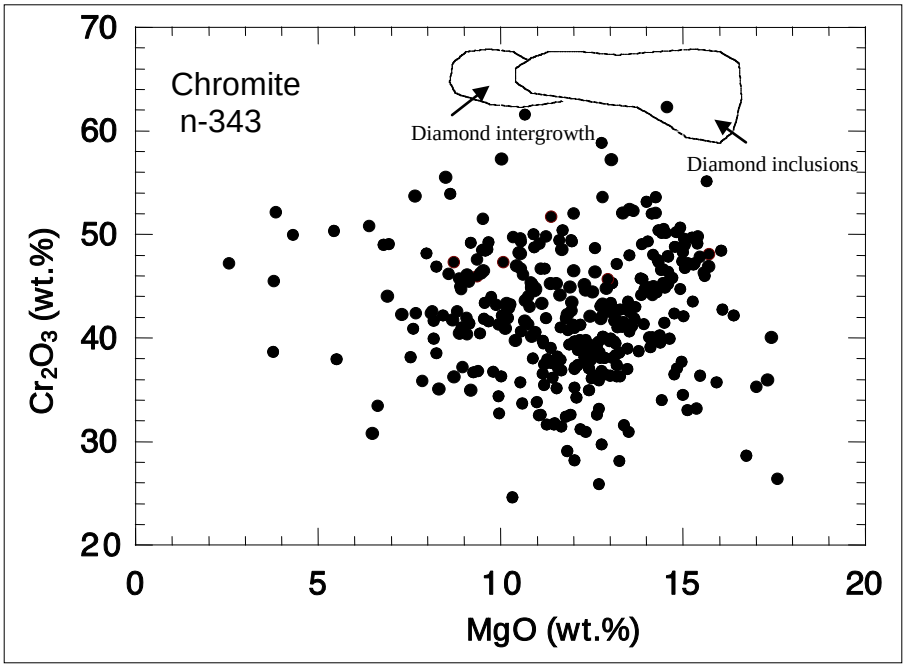


Figure 12. *Cr_2O_3 vs. MgO for chromite and Cr-spinel. The black outlined fields are the compositional ranges of chromite inclusions in diamond (right) and of chromite intergrown with diamond (left) after Fipke et al. (1995).*

Diopside

Cr-diopside with 174 grains is the second most abundant kimberlite indicator mineral in the samples. It is the most widespread mineral in the samples and is relatively evenly distributed throughout the sample set, with the highest concentration (n = 8) occurring in sample 106H-2008-3011BS, which also contained one pyrope and one eclogitic garnet. Diopside compositions vary from mg-#76 to 96 and Cr_2O_3 from 0.20 to 1.6 wt.% and a few grains enriched in Na_2O (1.2 to 2.5 wt.%), most contain less than 0.5 wt.% Na_2O. Many Cr-diopsides are compositionally similar to Cr-diopsides from garnet-lherzolite, but it is suspected many Cr-diopsides recovered from bulk and till samples in this study are from crustal ultramafic rocks (such as peridotite, komatiite, gabbro or pyroxenite from layered intrusions (Deer et al., 1978) because pyrope garnet and mantle olivine, which are usually found in relative abundance with Cr-diopsides from kimberlitic sources are sparse in the bulk stream sediments, thus may not originate from a peridotitic source.

Five Cr-rich diopsides are likely derived from mantle peridotitic xenoliths because Cr-levels >1.4 wt.% are rarely found in diopside from crustal rocks. Most Cr-diopsides with Cr_2O_3 >0.5 wt.% fall into the garnet-peridotite field of Nimis (1998), but diopside from ultramafic crustal rocks are similar in composition, with Cr_2O_3 up 1.4 wt.% and mg-#s in the mid to high 80s.

Mg-Ilmenite

Ninety-one Mg-ilmenite grains were recovered and analyzed. Sixty of the grains were magnesian with MgO varying between 7 to 15 wt.% and Cr_2O_3 ranging from 0.3 to 6.7 wt.% and fall within the compositional range of kimberlitic megacryst ilmenite (MgO vs. TiO_2; Fig. 13) of Wyatt et al. (2004). Eight MgO-rich ilmenite grains could only be derived from crustal ultramafic rocks such as those found in ultramafic layered intrusions (e.g. dunite, peridotite, pyroxenite). The remaining twenty-three have low MgO ($\leq$1.15 wt.%) and are derived from crustal rocks.

The report indicates the kimberlitic ilmenites have approximately the same distribution as pyrope garnets in the lowlands north of the Canyon Ranges. The report also indicates one sample contained half of the kimberlitic ilmenite grains, and suggests this is possibly the result of a larger grain breaking apart, or pocket of heavy mineral accumulation.

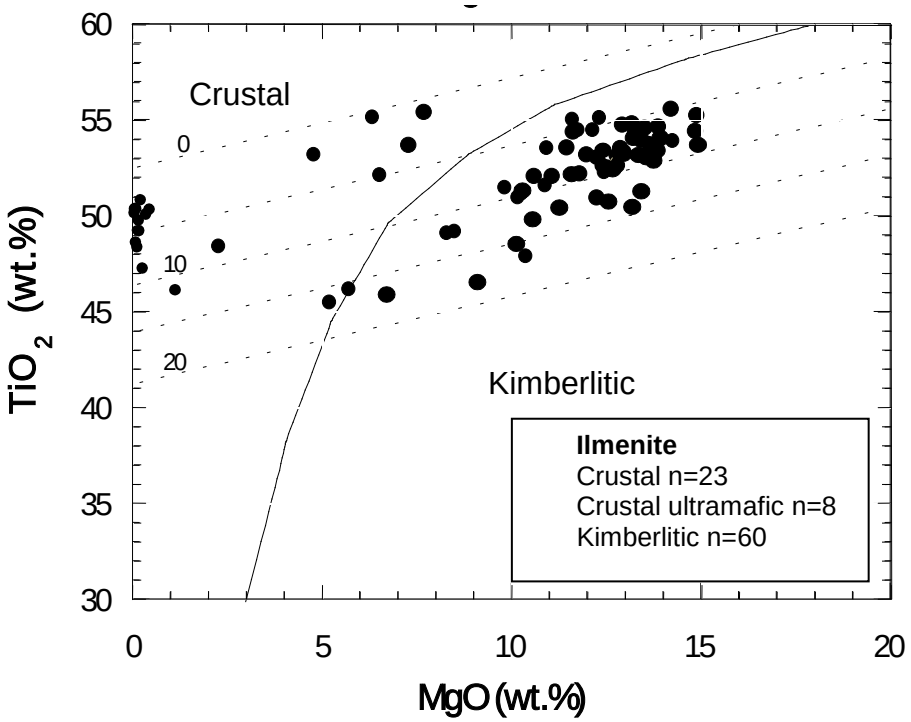


Figure 13. *MgO vs. TiO2 for ilmenites. The curve separates low MgO crustal ilmenites from high MgO kimberlitic megacryst ilmenite. The stippled lines are lines of equal hematite content — an indication of oxidation (curve and lines after Wyatt et al., 2004).*

Cr-pyrope

Fifty-nine Cr-pyrope garnets recovered from stream HMC and till samples were analyzed by electron microprobe. Cr-pyrope garnets that have been microprobed to determine their geochemical composition are usually classified into one of a number of categories based on oxide weight percent (wt.%) such as Cr_2O_3 wt.% vs. CaO wt.%. Lherzolitic G-9 garnet is the most abundant Cr-pyrope garnet recovered in diamond exploration (Grutter et al., 2004), but their statistical association with diamond is weak because they represent only 15% of peridotitic inclusions in diamond (Gurney, 1984). Harzburgitic G-10 garnet is the garnet standard with which diamond potential is judged (Grutter et al., 2004). Harzburgitic G-10 garnets are Ca-poor and Cr-rich, and are correlated with 85% of peridotitic garnet inclusions in diamonds from global sources (Gurney, 1984). The reader should refer to Grutter et al. (2004) for descriptions of other Cr-pyrope garnet classifications.

Most Cr-pyrope garnets (39) recovered from samples are derived from garnet-lherzolite and are classified as G-9 garnets, with the exception of one garnet classified as wehrlitic (G-12), two garnets classified as low Cr_2O_3 (<1 wt.%) and elevated TiO_2 (>0.5 wt.%) titanian pyrope (G-1), and one garnet that is likely from fertile harzburgite classified as a G-10 Cr-pyrope associated with the diamond stability field (Fig. 14). All of the aforementioned garnets are typically found in kimberlites, but are not always indicative of the presence of diamonds. One eclogitic (e-type) garnet was recovered, and another grain originally picked as an orange garnet (OG) was reclassified (by electron microprobe verification) as crustal almandine with >27 wt.% FeO.

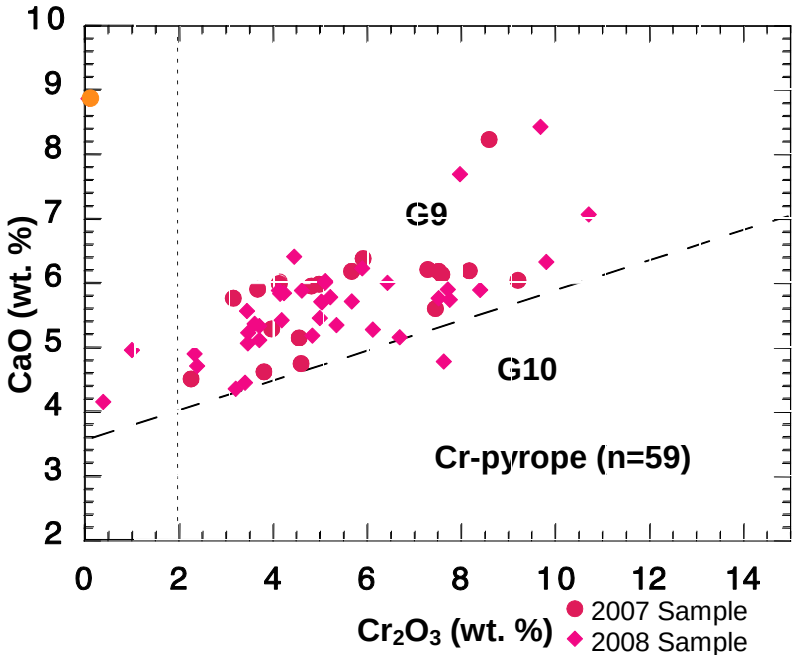


Figure 14. *CaO vs. Cr_2O_3 for garnets. The diagonal dashed line is the 85% line from Gurney (1984) that divides Ca-rich lherzolitic garnets (G9) from Ca-depleted harzburgitic garnets (G10). The vertical dashed line separates peridotitic Cr-pyrope (at right) from Cr-poor megacrystic and eclogitic garnet (at left). A potentially eclogitic garnet is shown in orange.*

Olivine

Twelve olivine grains were recovered from the samples, eleven grains have a forsteritic olivine (Fo) content of 81–87 and variable NiO content from 0.15 to 0.46 wt.% (Fig. 14), the Fo content is too low to be derived from mantle peridotite, which is typically between Fo88 and 93, and NiO> 0.25 wt.% (Deer et al., 1997). These olivines match the characteristics of crustal ultramafic rocks such as peridotite, olivine pyroxenite, komatiite, or olivine-gabbro from ultramafic layered intrusion. One olivine from sample 106H-2007-1002 plots within the compositional field of kimberlitic megacryst olivine, or mantle peridotite (Fig. 15).

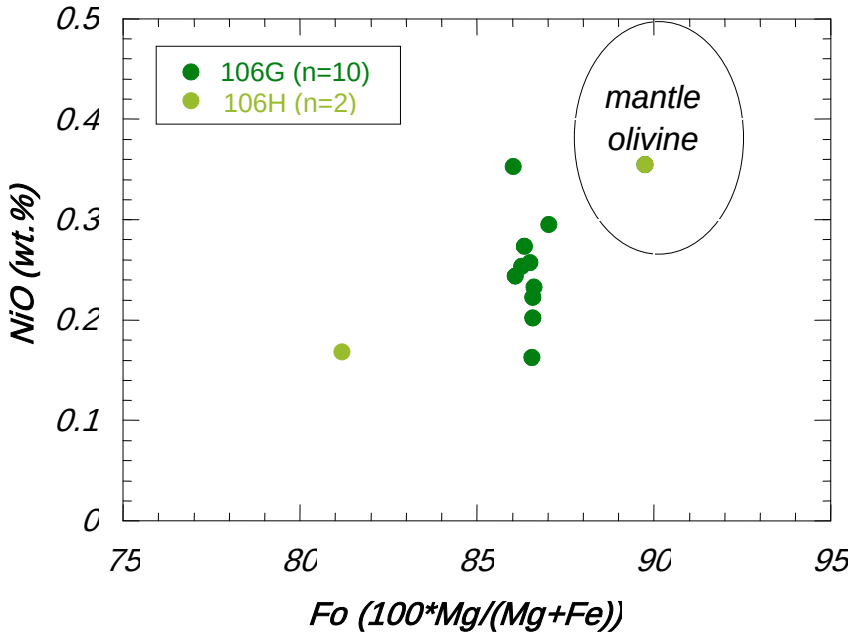


Figure 15. *NiO vs. Fo content for olivine grains. The oval shows the compositional range of olivine from mantle peridotite and kimberlite megacrysts (after Deer et al., 1997).*

KIM Summary

Many grains recovered from bulk and till samples are bona fide kimberlite indicator minerals, Cr-pyrope occurs only in garnet-peridotitic mantle xenoliths which have been transported to the surface by a kimberlite intrusion, and are not found in crustal rocks. Mg-ilmenite also indicates a kimberlitic source, especially when found in conjunction with Cr-pyrope grains indicative of lherzolitic and wehrlitic mantle xenoliths. KIMs such as olivine, chromite and Cr-diopside although used as kimberlite indicator minerals, are not exclusive to kimberlite, since they are also found in mafic to ultramafic crustal rocks and compositionally overlap with those from mantle peridotite.

The distribution of chromite and (Cr)-diopside outnumber Cr-pyrope and Mg-ilmenite, suggesting they have sources other than kimberlite, as peridotitic mantle xenoliths typically have low modal abundances of Cr-diopside and minor to trace amounts of chromite. Sample locations for Cr-pyrope, Mg-ilmenite, olivine and chromite widely overlap, making it difficult to determine which proportion is crustally derived, and which is from mantle peridotite. The relatively low abundance and wide distribution of Cr-pyrope and Mg-ilmenite in comparison to number of chromites and diopsides suggest two sources, kimberlite and mafic to ultramafic crustal rocks.

An additional challenge to assessing the diamond potential of this region is that while many KIMs recovered in this survey are sourced from kimberlite, it is not known if the material is from a kimberlite intrusion in the area, or if it is kimberlite debris transported

into the area by glaciers during the last glacial period from external sources. The definitive location of the source cannot be determined with this level of study. The low KIM numbers and wide distribution favours glacial transportation, but is not conclusive and requires significantly more investigation to confidently determine the source.

CONCLUSIONS

To enhance current knowledge of mineral potential in the proposed Ts'ude niline Tu'eyeta area 682 silt, 324 bulk, 666 water, and 88 till samples were collected between 2007 and 2008. The samples were submitted to laboratories to determine their geochemical compositions. Aurora Geosciences Ltd. provided an interpretation of analytical results for silt and water samples (Appendix A), and mineralogist Dr.Ingrid Kjarsgaard provides an interpretation of KIMs extracted from stream bulk sediment samples (Appendix B). Table 1 illustrates mineral potential of the study area based on criteria for assessing mineral potential by Scoates et al. (1986).

Geostatistical analysis of silt sediment and water data has identified an area within the southern portion of the Ts'ude niline Tu'eyeta proposed boundary with very high Zn-Pb potential. The trend of silt and water samples with anomalous values of Pb, Zn, Cu, and elevated Ag, Au values parallel the Gayna River Zn-Pb deposits suggesting geological control. Silt samples in this area have a strong Ga-Cu correlation, as does sphalerite in the Gayna River Zn-Pb deposits. This relationship is not found elsewhere in the Mackenzie Mountains and suggests there may be a relationship between the Gayna River MVT deposits and anomalous Zn-Pb silt samples in the study area. It is likely undiscovered Zn-Pb deposits exist in the southern portion of the study area, which is located just 12 km north of the world class Gayna River Zn-Pb deposits. Discovery of Zn-Pb deposits in the study area could contribute to the development of the Gayna River MVT district. Zinc-lead potential in the southern portion of the study area is ranked very high. Figure 16 illustrates an area with very high MVT Zn-Pb potential based on sample results from surveys conducted to produce this report and known geologic information. The full extent of the MVT zinc-lead potential has not been determined by this study and results should only be considered valid within the boundaries of the Ts'ude niline Tu'eyeta study area.

Many samples returned elevated copper values (see Fig. 8 in Appendix A) in the southern portion of the proposed boundaries. The anomalous copper values in the samples follow the same west-northwest oriented trend as samples with anomalous zinc values, indicating geological (exposure) control is likely responsible for their distribution. PCA Factor F1 was selected as the best overall copper factor and is the dominant copper-silver factor in the data set as well as the dominant overall PCA factor. It is likely due to the underlying bedrock geology, reflecting large-scale regional lithogeochemical patterns. Figure 11 in Appendix A illustrates the distribution of copper values with gridded Principal Component Analysis Factor 21. This factor may be a vector to sediment-hosted copper. The trend of anomalous copper values appears concentrated within the

Ts'ude niline Tu'eyeta proposed boundary, but also extends to the east and west of the boundary. Copper potential in the southern portion of the study area is moderate. Figure 17 illustrates an area with moderate copper potential based on sample results from

surveys conducted to produce this report and known geologic information. Extent of copper potential outside of the Ts'ude niline Tu'eyeta proposed boundary may not constitute the areal extent of moderate copper potential as there are no further data beyond the samples collected for this study.

Gold grains were found in many stream bulk sediment and till samples, along with elevated gold values in silt samples. Low gold grain counts, broad distribution pattern, and generally reworked grain morphology from stream bulk sediment and till samples suggests most gold gains recovered from these samples were likely subjected to several transportation processes, including fluvial, glaciofluvial, glaciolacustrine, and entrainment within glacial till.

Robinson (2010) determined a correlation exists with mercury and silver, barium and phosphorous in silt samples from the study area, suggesting an epigenetic source, but gold values are low, and likely represent background values. Gold potential within the study area is ranked low, with very little information.

Diamond potential in the study area was determined by evaluation of kimberlite indicator minerals recovered from stream bulk sediment and glacial till samples. Many KIMs were recovered from both bulk and till samples. KIMs recovered from till samples were glacially transported into the study area from either distal or proximal sources, in contrast to KIMs recovered from bulk stream sediment samples, which may represent primary, secondary (or tertiary) dispersal by fluvial and/or glaciofluvial processes. It is unknown if the primary source of KIMs recovered from bulk sediment samples were derived from materials originating in mountainous areas, or from glacial till transported into the mountains by continental glaciers. Kimberlites have been known to intrude sedimentary rocks (i.e. Fort a la Corne, Buffalo Head Hills), therefore the possibility exists a kimberlite may have intruded within or near the study area. But the wide distribution of KIMs and their relatively low abundance suggests dispersal of KIM-rich material into the area by continental glaciers, however, this is not conclusive and further studies would be required to help determine likely sources for the KIMs.

The Kjarsgaard reports (Appendix B) suggests numerous samples contain bona fide KIMs as well as minerals originating from crustal mafic to ultramafic rocks. The mineral composition of some grains suggest a source from within the diamond stability field and compositional ranges of inclusions in diamonds, thus may be associated with the presence of diamonds.

No samples were collected from a large area within the central northern wetland area due to access, thus diamond (or other mineral) potential in this area cannot be assessed. Primary diamond potential within the areas identified in Figure 18 is ranked low to moderate with very little information.

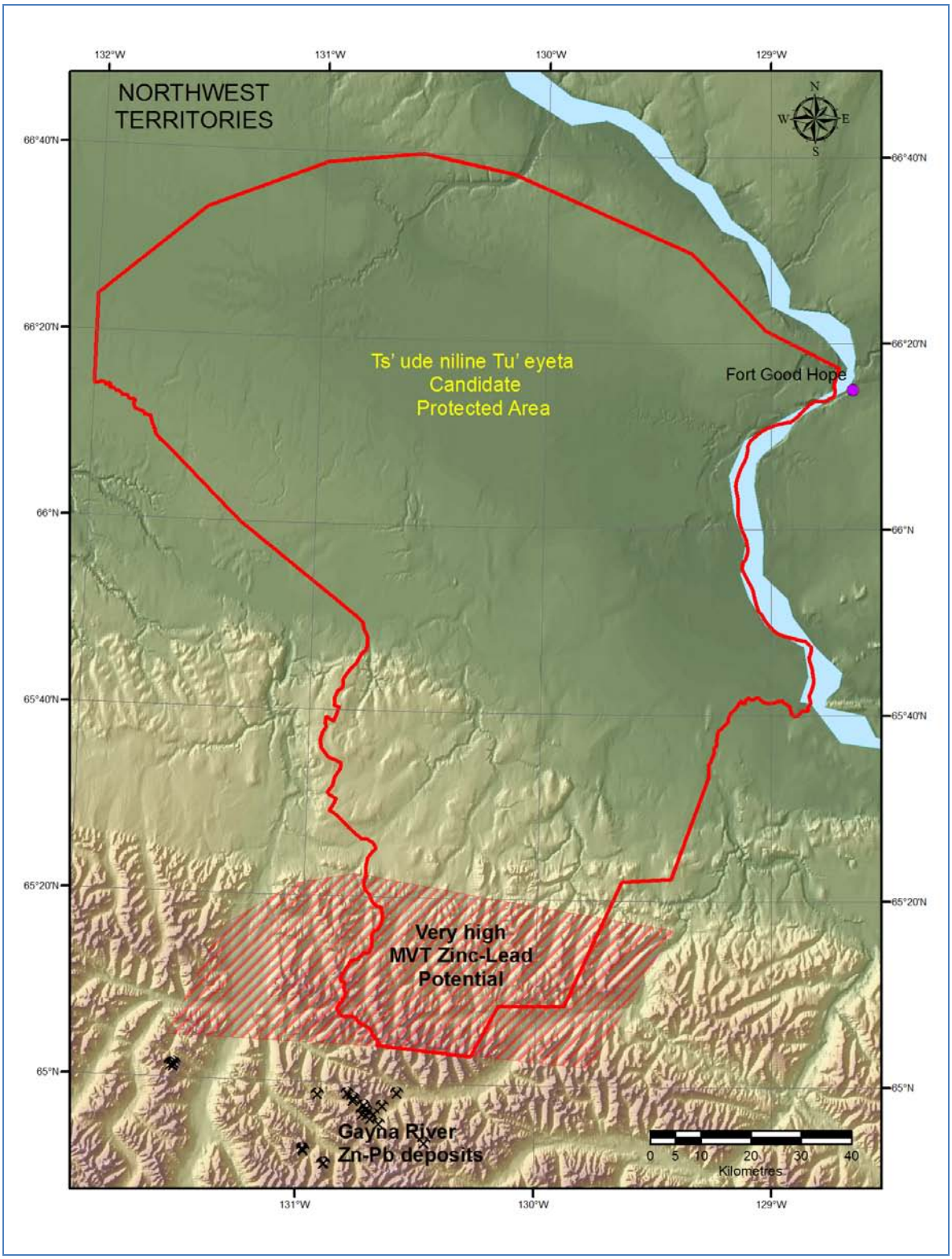


Figure 16. *Location of area within Ts'ude niline Tu'eyeta proposed boundary with very high MVT Zn-Pb potential.*

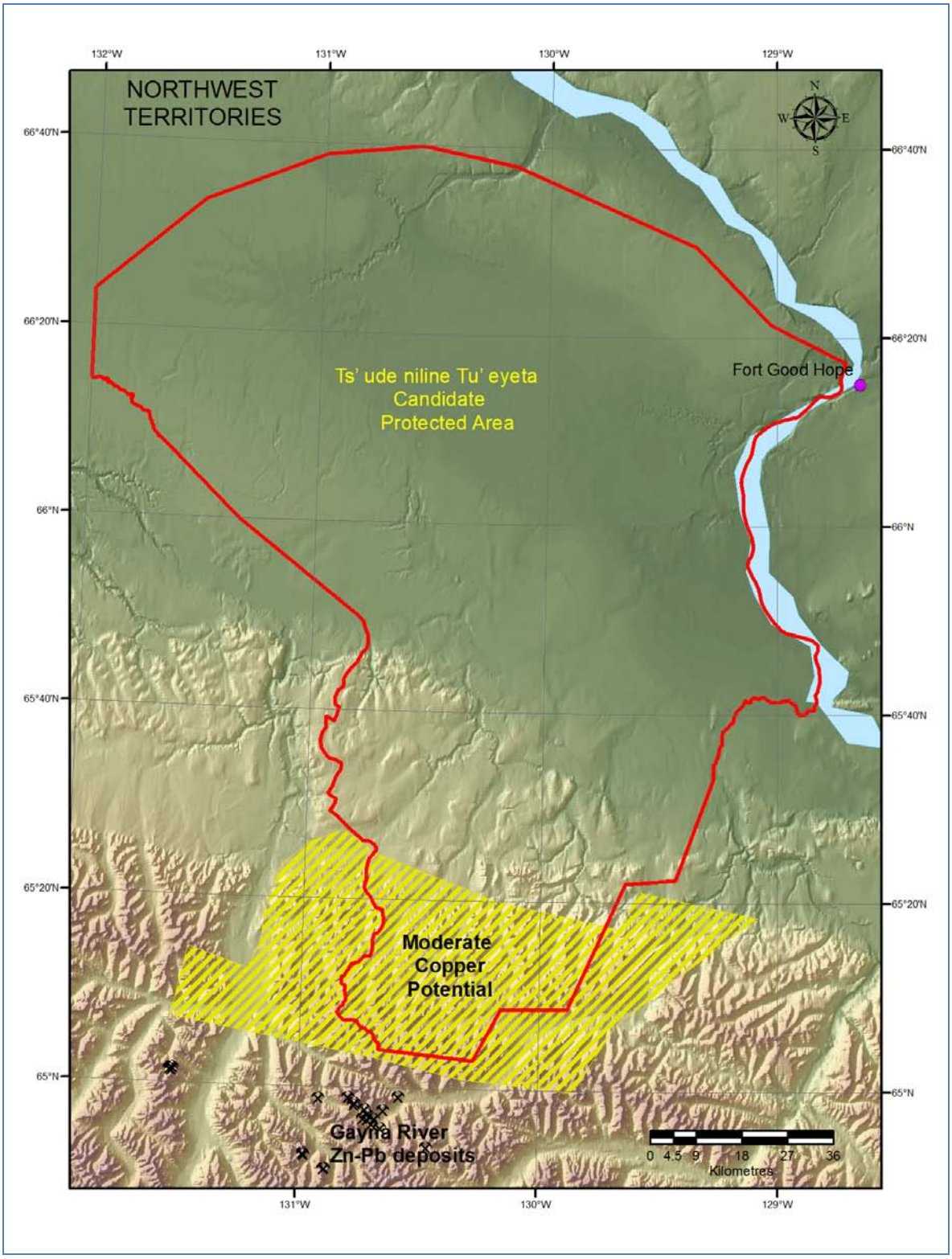


Figure 17. *Area with moderate copper potential.*

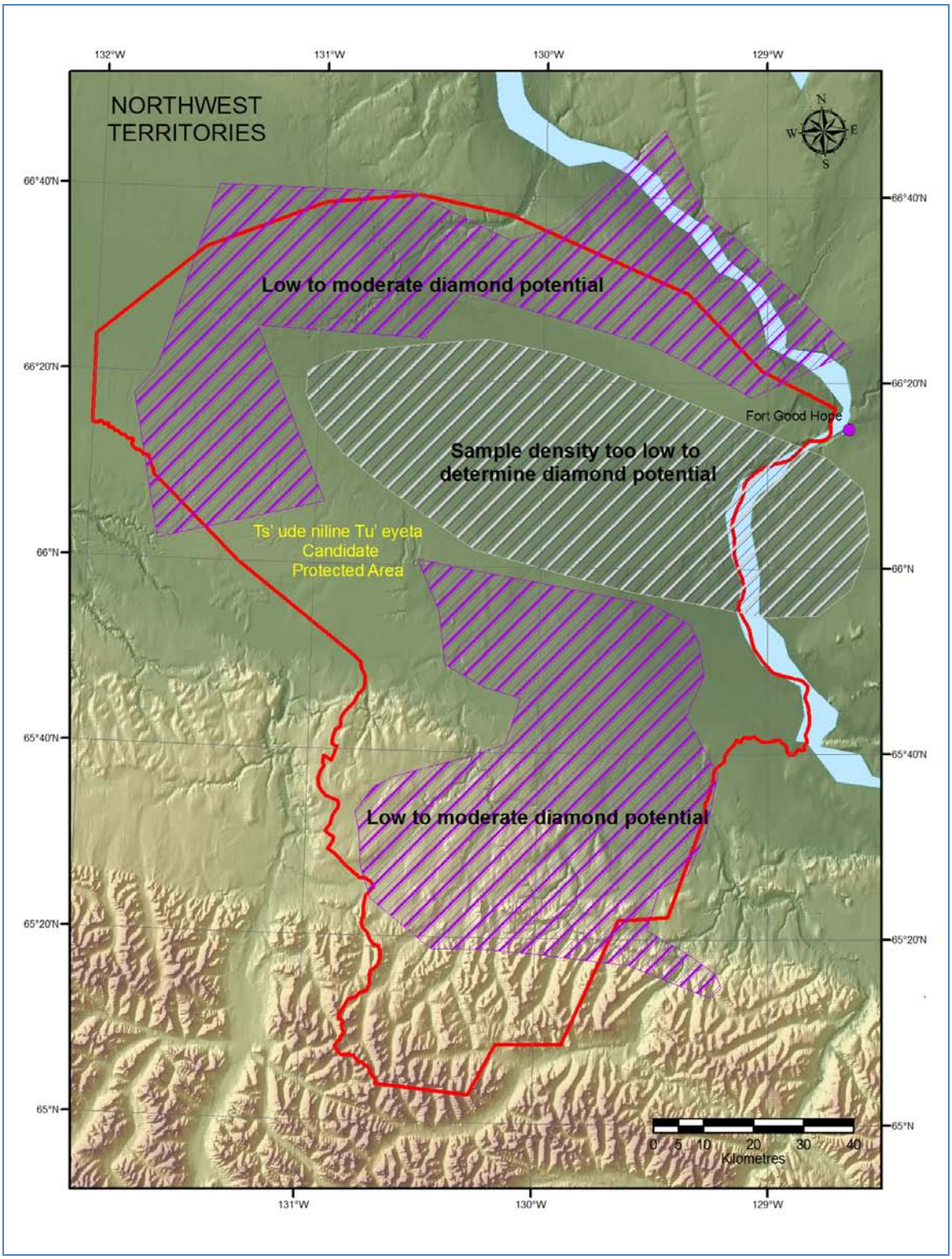


Figure 18. *Areas with low to moderate diamond potential and area with insufficient sample density to determine diamond potential.*

POTENTIAL Ranking	CONFIDENCE Ranking			
	Rank 1: Abundant reliable information	Rank 2: Moderate amount of information	Rank 3: Some information	Rank 4: Very little and/or unreliable information
Rank A: Very High: Geologic environment is favourable. Significant deposits are known. Presence of undiscovered deposits is very likely.		MVT Zinc-Lead		
Rank B: High: Geologic environment is favourable. Occurrences are present but significant deposits are not known. Presence of undiscovered deposits is likely.				
Rank C: Moderate to High: Intermediate between moderate and high potential.				
Rank D: Moderate: Geological environment is favourable. Occurrences may or may not be known. Presence of undiscovered deposits is possible.			Sediment-hosted copper SEDEX Zn-Pb deposits (Mackenzie Mountains)	
Rank E: Low to Moderate: Intermediate between low and moderate.			Primary kimberlite diamonds Coal (wetlands)	Ni-Cu-PGE deposits (Mackenzie Mountains)
Rank F: Low: Some aspects of the geological environment may be favourable but are limited in extent. Few if any occurrences are known. Low probability that undiscovered deposits are present.				Gold Iron-Formation deposits
Rank G: Very Low: Geologic environment is unfavourable. No occurrences are known. Very low probability that undiscovered deposits are present.				Breccia-hosted IOCG deposits SEDEX Zn-Pb deposits (wetlands)
Rank H: Not Assessed: Deposit types unknown, overlooked, beyond the scope of the assessment, or not worth mentioning at the time the assessment was done. A higher rating could be assigned during future assessments.				Uranium
Criteria for assessing mineral potential follows the Geological Survey of Canada's Mineral and Energy Resource assessment rating scale (Scoates et al., 1986).				

Table 1. *Mineral potential summary*

ACKNOWLEDGEMENTS

Constructive reviews by Lee Pigage of the Yukon Geological Survey and Hendrik Falck of the Northwest Territories Geoscience Office were much appreciated and helped to improve the paper.

REFERENCES

Aitken, J.D., 1993. Proterozoic sedimentary rocks, Subchapter 4A; *in* Sedimentary Cover of the Craton in Canada, edited by D.F. Stott and J.D. Aitken, Geological Survey of Canada, no. 5, p. 81–95.

Aitken, J.D., Ayling, M.E., Balkwill, H.R., Cook, D.G., Mackenzie, W.D. and Yorath, C.J., 1969. Fort Good Hope, District of Mackenzie; Geological Survey of Canada, Preliminary Map 4-1969.

Aitken, J.D. and Cook, D.G., 1974. Carcajou Canyon map-area, District of Mackenzie; Geological Survey of Canada, Paper 74-13.

Aitken, D., Long, D.G.F. and Semikhatov, M.A., 1978. Progress in Helikian stratigraphy, Mackenzie Mountains; *in* Current Research, Part A, Geological Survey of Canada, Paper 78-1A, p. 481–484.

Carrière, J.J. and Sangster, D.F., 1999. A multidisciplinary study of carbonate-hosted zinc-lead mineralization in the Mackenzie Platform (a.k.a. Blackwater and Lac de Bois platforms), Yukon and Northwest Territories, Canada; Geological Survey of Canada, Open File 3700, 146 p.

Day, S.J.A., Lariviere, J.M., Friske, P.W.B., NcNeil, R.J., Cairns, S.R., and McCurdy, M.W., 2005. Regional stream sediment and water geochemical data, lower Willowlake River area, Northwest Territories (parts of NTS 95-I and 95 J) including analytical, mineralogical and kimberlite indicator mineral data from silts, heavy mineral concentrates and waters; Geological Survey of Canada, Open File 4674.

Day, S.J.A., Lariviere, J.M., McNeil, R.J., Friske, P.W.B., Cairns, S.R., McCurdy,M.W. and Wilson, R.S., 2007. National Geochemical Reconnaissance (NGR): Regional stream sediment and water geochemical data, Horn Plateau area, Northwest Territories (Parts of NTS 85E, 85F, 85K, 85L, 95H, 95I and 95J) including analytical, mineralogical and kimberlite indicator mineral data; Geological Survey of Canada, Open File 5478.

Deer, W.A., Howie, R.A. and Zussman, J., 1978. Rock-Forming Minerals, Volume 2A Single-Chain Silicates, 2nd edition. Longman Group Ltd., London. 668 p.

Deer, W.A., Howie, R.A. and Zussman, J., 1997. Rock-Forming Minerals, Volume 1A Ortho-Silicates, 2nd edition. The Geological Society, London. 919 p.

Dewing, K., Sharp, R.J., Ootes, L., Turner, E.C. and Gleeson, S., 2006. Geological assessment of known Zn-Pb showings, Mackenzie Mountains, Northwest Territories, Geological Survey of Canada, Current Research 2006-A4, 12 p.

DiLabio, R.N.W., 1990. Classification and interpretation of the shapes and surface textures of gold grains from till on the Canadian Shield; *in* Current Research, Part C, Geological Survey of Canada, Paper 90-1C, p. 329–332.

Dixon, J., 1999. Mesozoic-Cenozoic stratigraphy of the northern Interior Plains and Plateau, Northwest Territories; Geological Survey of Canada, Bulletin 536.

Eagle Plains Resources Ltd., 2009. Gayna River Project Summary 2009-01, extracted 2010/11/27; http://www.eagleplains.bc.ca/projects/nwt/gayna/documents/GaynaRiverProjectSummary2009_001.pdf.

Environment Canada, 2005. State of the Environment Infobase, extracted August 25, 2009; http://www.ec.gc.ca/soer-ree/English/default.cfm.

Fipke, C.E., Gurney, J.J. and Moore, R.O. 1995. Diamond exploration techniques emphasizing indicator mineral geochemistry and Canadian examples; Geological Survey of Canada, Bulletin 423, 86 p.

Gal, L.P., 2007. Ts'ude niline Tu'eyeta (Ramparts River and Wetlands) Candidate Protected Area Phase I Non-Renewable Assessment – Petroleum, Northwest Territories, Canada, NTS 106G, H, I, J; Northwest Territories Geoscience Office, NWT Open File 2007-01, 115 p.

Goodfellow, W.D. and Lydon, J.W. 2007. Sedimentary exhalative (SEDEX) deposits; *in* Mineral Deposits of Canada: A Synthesis of Major Deposit Types, District Metallogeny, the Evolution of Geological Provinces, and Exploration Methods, edited by W.D. Goodfellow; Geological Association of Canada, Mineral Deposits Division, Special Publication No. 5, p. 163–183.

Grunsky, E.C. and Smee, B.W., 2003. Enhancements in the interpretation of geochemical data using multivariate methods and digital topography; CIM Bulletin, v. 96, n. 1068, p. 39–43.

Gurney, J.J. 1984. A correlation between garnets and diamonds in kimberlites; *in* Kimberlite occurrence and origin a basis for conceptual models in exploration, Geology Department and University Extension, University of Western Australia, Publication No. 8, p. 143–166.

Hewton, R.S., 1982. Gayna River: A Proterozoic Mississippi Valley-Type Zinc-Lead Deposit; *in* Precambrian Sulphide Deposits, H.S. Robinson Memorial Volume, edited by R.W. Hucthinson, C.D. Spence and J.M. Franklin, Geological Association of Canada, Special Paper 25.

Hunter, B., Geirholm, S., Krokosh, S. and McNeely, L., 2002. Protected Area Initiative: Ramparts River and Wetlands (Tsodehniline and Tuyat'ah) in the Sahtu Region of the Northwest Territories; unpublished report for Ducks Unlimited Canada.

Lydon, J.W., 2007. An overview of the economic and geological contexts of Canada's major mineral deposit types, *in* Mineral Deposits of Canada: A Synthesis of Major Deposit-Types, District Metallogeny, the Evolution of Geological Provinces, and

Exploration Methods, edited by W.D. Goodfellow; Geological Association of Canada, Mineral Deposits Division, Special Publication No. 5, p. 3–48.

Kjarsgaard, I., 2008. Interpretation of Kimberlite Indicator Minerals in Stream Sediment (Map Areas 106G & 106H), *in* Ts' ude niline Tu' eyeta (Ramparts River and Wetlands) Candidate Protected Area Phase II Non-renewable Resource Assessment – Minerals, Northwest Territories, Canada, NTS 106G, 106H, 106I, and 106J, Appendix B; Northwest Territories Geoscience Office, NWT Open File 2010-07.

Kjarsgaard, I., 2010a. Kimberlite Indicator Mineral Distribution in Map Sheet 106G and 106H of The Ramparts Area, NWT, *in* Ts' ude niline Tu' eyeta (Ramparts River and Wetlands) Candidate Protected Area Phase II Non-renewable Resource Assessment – Minerals, Northwest Territories, Canada, NTS 106G, 106H, 106I, and 106J, Appendix B; Northwest Territories Geoscience Office, NWT Open File 2010-07.

Kjarsgaard, I. 2010b. Kimberlite Indicator Mineral Distribution in Till Samples from Map Sheets 106G, 106H, 106I and 106J of the Ramparts Area, NWT, *in* Ts' ude niline Tu' eyeta (Ramparts River and Wetlands) Candidate Protected Area Phase II Non-renewable Resource Assessment – Minerals, Northwest Territories, Canada; NTS 106G, 106H, 106I, and 106J, Appendix B; Northwest Territories Geoscience Office, NWT Open File 2010-07.

Mills, A.J., 2008. Ts'ude niline Tu'eyeta (Ramparts River and Wetlands) Candidate Protected Area Phase I Non-renewable Resource Assessment – Minerals; Northwest Territories Geoscience Office, NWT Open File 2008-01, 33 p.

Moore, P.F., 1993. Devonian; Subchapter 4D; *in* Sedimentary Cover of the Craton in Canada, edited by D.F. Stott and J.D. Aitken; Geological Survey of Canada, Geology of Canada, no. 5, p. 150–201.

Nimis, P., 1998. Evaluation of diamond potential from the composition of peridotitic chromian diopside; European Journal of Mineralogy, v. 10, p. 505–519.

Ootes, L., Sandeman, H., Lemieux, Y. and Leslie, C., 2008. The 780 Ma Tsezotene Sills, Mackenzie Mountains: a field, petrographical, and geochemical study; Northwest Territories Geoscience Office, NWT Open Report 2008-011, 21 p. and appendices.

Paradis, S., Hannigan, P. and Dewing, K., 2007. Mississippi Valley-type lead-zinc deposits, *in* Mineral Deposits of Canada: A Synthesis of Major-Types, District Metallogeny, the Evolution of Geological Provinces, and Exploration Methods, edited by W.D. Goodfellow; Geological Association of Canada, Mineral Deposits Division, Special Publication No. 5, p. 185–203.

Poulton, T.P., Braun, W.K., Brooke, M.M. and Davies, E.H., 1993. Jurassic; Subchapter 4H; *in* Sedimentary Cover of the Craton in Canada, edited by D.F. Stott and J.D. Aitken, Geological Survey of Canada, no. 5, p. 321–357.

Richards, B.C., Bamber, E.W., Higgins, A.C. and Utting, J., 1993. Carboniferous; Subchapter 4E, *in* Sedimentary Cover of the Craton in Canada, edited by D.F. Stott and J.D. Aitken, Geological Survey of Canada, Geology of Canada, No. 5, p. 202–271.

Robinson, R.J., 2010. Statistical Geochemical Analysis of Stream Sediment and Water Samples from the Southern Portion of the Proposed Ts' ude niline Tu' eyeta Candidate Protected Area, Aurora Geosciences Ltd., Yellowknife, NWT, 96 p.

Ruelle, J.C.L. and Bond, I.J., 1976. Geological Assessment Report on Backbone Project Claims south and west of Permit 361 and extending from Keele River to Coates Lake, N.W.T.; submitted by Shell Canada Resources Ltd.; Dept. of Indian Affairs and Northern Development, NWT Geology Division, Yellowknife; unpublished Assessment Report 080570.

Scoates, R.F.J., Jefferson, C.W. and Findlay, D.C., 1986. Northern Canada mineral resource assessment; in Prospects for Mineral Resource Assessment on Public Lands: Proceedings of the Leesburg Workshop, edited by S.M. Cargill and S.B. Green, U.S. Geological Survey, Circular 980, p. 111-139.

Stott, D.F., Caldwell, W.G.E., Cant, D.J., Christopher, J.E., Dixon, J., Koster, E.H., McNeil, D.H. and Simpson, F., 1993. Cretaceous, Subchapter 4I; *in* Sedimentary Cover of the Craton in Canada, edited by D.F. Stott and J.D. Aitken, Geological Survey of Canada, Geology of Canada, No. 5, p. 358–438.

Wallace, S.R.B., 2009. The Genesis of the Gayna River Carbonate-Hosted Zn-Pb Deposit, unpublished M.Sc. Thesis, University of Alberta.

Wheeler, J.O., Hoffman, P.F., Card, K.D., Davidson, A., Sanford, B.V., Okulitch, A.V. and Roest, W.R., 1996. Geological Map of Canada; Geological Survey of Canada, "A" Series Map, 1860A.

Wyatt, B.A., Baumgartner, M., Anckar, E. and Grütter, H., 2004. Compositional classification of "kimberlitic" and "non-kimberlitic" ilmenite; Lithos, v. 77, p. 819–840.

APPENDIX A

Statistical Geochemical Analysis of Stream Sediment and Water Samples
from the southern portion of the proposed
Ts'ude niline Tu'eyeta Candidate Protected Area
Ramparts River Area,
Northwest Territories

Appendix A

Statistical Geochemical Analysis

of

Stream Sediment and Water Samples

from the Southern Portion of the

Ts’ ude niline Tu’ eyeta

(Ramparts River and Wetlands)

Candidate Protected Area

Phase II Non-renewable Resource Assessment - Minerals

STATISTICAL GEOGHEMICAL ANALYSIS OF STREAM SEDIMENT AND WATER SAMPLES FROM THE SOUTHERN PORTION OF THE PROPOSED TS' UDE NILINE TU' EYETA CANDIDATE PROTECTED AREA

RAMPARTS RIVER AREA

NORTHWEST TERRITORIES

PARTS OF N.T.S. 106G, H, I and J

65° - 66°10'N, 129°10' - 131°40' W

Prepared on behalf of The Northwest Territories Geoscience Office

March 29, 2010

Report prepared by:

R. James Robinson, B.Sc., P. Geol.

Aurora Geosciences Ltd.
3506 McDonald Drive
Yellowknife, NT X1A 2H1

AURORA GEOSCIENCES

Summary

The Northwest Territories Geoscience Office conducted a stream sediment sampling program across portions of NTS map sheets 106G, 106H, 106I and 106J during the summers of 2007 and 2008. This survey was completed to help assess the potential for the presence of economic mineral deposits in the Ts' ude niline Tu' eyeta Candidate Protected Area in west central Northwest Territories.

Aurora Geosciences Ltd., of Yellowknife, NT was contracted to assess the mineral potential of the area based on a statistical multivariate review of the stream sediment geochemical sampling data. This report documents the statistical geochemical analyses performed on those data and the conclusions drawn from those analyses.

The stream sampling program was carried out according to the protocols established for the National Geochemical Reconnaissance Program and described in Day et al. (2007). A total of 644 separate locations were sampled over the course of the survey program. The sampling protocol included analyzing duplicate samples and standards to ensure quality assurance and quality control.

Analysis of the sampling data suggests the potential exists for several deposits of several different mineralisation types. The most obvious deposits to be expected in the southern, mountainous portion of the study area are limestone hosted, lead-zinc deposits similar to the Mississippi Valley type Gayna River deposit and satellite showings just south of the survey area. The sample data show several locales with anomalous zinc and lead values in this area. There is also strong potential for the discovery of other base and precious metal deposits in the region. There are several locations which returned anomalous results for copper, silver, gold and nickel, often with several elements elevated in the same sample. There are also numerous coincident anomalies for silt and water samples in many locations.

Further mapping and exploration work will no doubt result in the discovery of several showings and deposits in the cordillera region of the candidate protected area.

Table of Contents

Summary i

1 Location, Area and Access 1

2 Physiography, Climate and Vegetation 1

3 Regional Geology 3

3.1 General Tectonic and Geological History of the Study Area 3

3.1 Proterozoic Geology 5

3.2 Middle to Late Proterozoic Tectonic and Depositional History 8

3.3 Phanerozoic Geology 9

4 Local Geology 11

4.1 Bedrock Lithologies 11

4.2 Structural Geology 13

5 Previous Work 15

5.1 Regional Government surveys 15

5.2 Mineral Exploration History 15

6 Potential Mineral Resources 17

7 Stream Geochemical Survey 19

7.1 Sample Procedure 19

7.1.1 Silt Samples 19

7.1.2 Stream Waters 20

7.2 Analytical Methodology 20

8 Data Treatment 23

8.1 Silts 23

8.2 Water 24

9 Statistical Analysis of the Stream Sediment Data 24
9.1 Univariate Statistics 24
9.2 Multivariate Statistics 29
9.3 Principal Component Analysis 34
10 Statistical Analysis of the Water Sample Data 40
10.1 Univariate Analysis 40
10.2 Multivariate Statistics 48
10.3 Principal Component Analysis 53
10.3.1 5x detection limit PCA 53
10.3.2 Major element association PCA 56
10.3.3 Carbonate association PCA 59
10.3.4 Black shale elemental association PCA 60
11 Discussion 64
11.1 Stream Sediment Results 64
11.2 Water Sample Results 72
12 Conclusion 86
13 References 87

LIST OF FIGURES

Figure 1 General topography of the sample area 3
Figure 2 Regional Geology of the Sample Area 6
Figure 3 Contributions of the PCA factors to the total geochemical response. Factors F1 through F3 account for about 78% of the observed geochemical response 35
Figure 4 Scree Plot for five times detection limit PCA 54
Figure 5 Scree plot for major element association PCA 56

Figure 6 Scree plot for the carbonate association PCA 59
Figure 7 Scree plot for the black shale elemental association PCA 61
Figure 8 Map of Study Area Showing Sample Sites, Known Deposits and Showings, 65
Figure 9 Gridded Principal Component Analysis Factor 1 with Copper, Nickel and Silver 67
Figure 10 Gridded Principal Component Analysis Factor 9 with Lead, Zinc and Silver Values Plotted 69
Figure 11 Gridded Principal Component Analysis Factor 21 with Copper Values Plotted 70
Figure 12 Gridded Principal Component Analysis Factor 3 with Gold, Silver and Mercury Values Plotted 71
Figure 13 Gridded F1 factor values from the Principal Component Analysis for the five times detection limit model 73
Figure 14 Gridded F2 factor values from the Principal Component Analysis for the five times detection limit model 74
Figure 15 Gridded F3 factor values from the Principal Component Analysis for the five times detection limit model 75
Figure 16 Gridded F6 factor values from the Principal Component Analysis for the five times detection limit model 76
Figure 17 Gridded F1 factor values from the Principal Component Analysis for the Major Element mineral assemblage model 77
Figure 18 Gridded F2 factor values from the Principal Component Analysis for the Major Element mineral assemblage model 78
Figure 19 Gridded F10 factor values from the Principal Component Analysis for the Major Element mineral assemblage model 79
Figure 20 Gridded F11 factor values from the Principal Component Analysis for the Major Element mineral assemblage model 80
Figure 21 Gridded F1 factor values from the Principal Component Analysis for the Carbonate mineral assemblage model 81
Figure 22 Gridded F2 factor values from the Principal Component Analysis for the Carbonate mineral assemblage model 82

Figure 23 Gridded F1 factor values from the Principal Component Analysis for the Black Shale mineral assemblage model..... 83
Figure 24 Gridded F2 factor values from the Principal Component Analysis for the Black Shale mineral assemblage model..... 84
Figure 25 Gridded F6 factor values from the Principal Component Analysis for the Black Shale mineral assemblage model..... 85

LIST OF TABLES

Table 1 Table of Formations (From Gal (2007)) 10
Table 2 Potential Mineral Deposit Types in the Ts' ude niline Tu' eyeta area (From Mills (2008)) 18
Table 3 Elements in Stream Silt Sediments Determined by Instrumental Neutron Activation analysis. 21
Table 4 Elements in Stream Silt Sediments Determined by ICP - MS and other methods 23
Table 5 Regional Geochemical Survey silt data - Univariate statistics 25
Table 6 Regional Geochemical Survey silt data - Univariate statistics (continued) 26
Table 7 Summary of Element Response Distributions 28
Table 8 Multivariate Statistical Summary 31
Table 9 Multivariate Statistical Summary (Part 2) 32
Table 10 Multivariate Statistical Summary (Part 3) 33
Table 11 Principal Component Analysis - Element Contributions 36
Table 12 Principal Component Analysis - Factor Loading for Each Element. 37
Table 13 Factor Associations for Elements of Principal Economic Interest 38
Table 14 Univariate statistics for water sample, by element 41

LIST OF APPENCICES

Appendix 1 Figure A Univariate Statistical Plots For Silt Samples (At Back)
Appendix 2 Figure B Univariate Scatter Plots For Silt Samples (At Back)
Appendix 3 Figure C Univariate Statistical Plots For Water Samples (At Back)
Appendix 4 Figure D Univariate Scatter Plots For Water Samples (At Back)

1 Location, Area and Access

The following four sections are adapted from Gal (2007), and the reader is directed to that document for a far more in-depth discussion of these topics. Proposed boundaries of the Ts' ude niline Tu' eyeta Candidate Protected Area lie between 65°03'05" N and 66°40'05" N latitude and 128°41'55" W and 132°00'00" W longitude and cover an area of 15,063 km^2 (1.5 million hectares). Ts' ude niline Tu' eyeta lies west of Mackenzie River, and includes parts of the watersheds of the Ramparts, Hume, and Ontaratue rivers. The candidate protected area is covered by 1:250,000 scale National Topographic System map sheets 106G, 106H, 106I, and 106J. These four map sheets cover the study area that is the focus of this report, bounded by 65° and 66°10'N latitude, and 129°10' and 131°30'W longitude (Figure 1).

This report is concerned with the southern portion of the candidate Protected Area where the increased topographic relief allows exposure of bedrock. The hilly and mountainous topography also enable ground water runoff in drainages to carry and concentrate silts and other weathering by-products.

There are no roads in the area. Traditional trails are concentrated along the lower Ramparts and Hume rivers (Hunter et al., 2002). Recent trails tend to follow seismic survey cut lines. Access to the survey area is limited to hiking, canoe and helicopter. The survey was conducted with continuous helicopter support.

2 Physiography, Climate and Vegetation

The Mackenzie Mountains in the study area are rugged upland ranges, with elevations up to 1990 m. The study area lies within the Taiga Plains and Taiga Cordillera ecozones (Environment Canada, 2005). The portion of the study area within the Taiga Plains ecozone includes several ecoregions: Fort McPherson Plain, Mackenzie River Plain, and Peel River Plateau. The climate of these regions is marked by short cool summers and long cold winters, and is classified as high subarctic, ranging to subhumid boreal

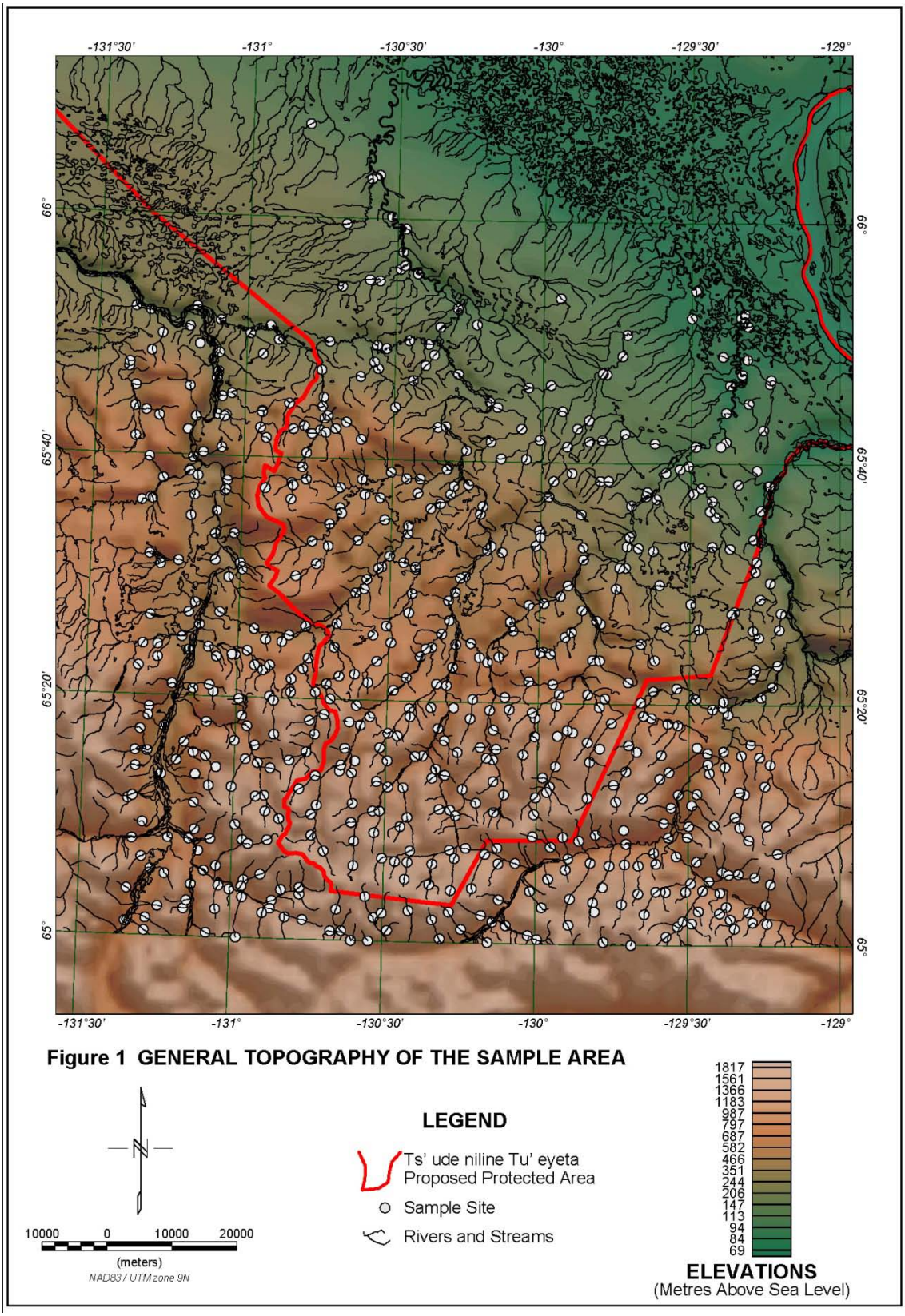


Figure 1 GENERAL TOPOGRAPHY OF THE SAMPLE AREA

Figure 1 General topography of the sample area

along the Mackenzie River. Mean annual summer temperatures range from 9.5 to 11.5°C; winter temperatures range from –22.5 to –25°C (Environment Canada, 2005). Mean annual temperatures in the Mackenzie Mountains are similar, if somewhat cooler in summer, and with more precipitation (up to 500 mm). Vegetation in the region (Environment Canada, 2005) is dominated by open, stunted stands of black spruce and tamarack, with secondary white spruce and ground cover of willow, birch, shrubs, cotton grass, lichen, and moss. Wetlands make up a significant portion of the northern part of the study area, and these areas support sedge, cotton grass, and moss. Along the Mackenzie River, taller stands of black spruce with jack pine dominate, with a lower cover of shrubs, moss, and lichen.

Higher elevations in Mackenzie Mountains are dominantly alpine tundra vegetation (lichen, dwarf shrubs, sedge), with bare rock and talus. Lower elevations in the mountains feature white spruce, willow, and birch.

3 Regional Geology

3.1 General Tectonic and Geological History of the Study Area

Pyle et al. (2006) present a good review of the geology of Peel Plateau and Plain, which includes much of the northern portion of the current study area.

Ts' ude niline Tu' eyeta lies mainly within the Interior Platform geological province, a vast basin of Phanerozoic sedimentary rocks lying between the Canadian Shield to the east and the Cordillera to the west and south. Sedimentary rocks of Interior Platform are generally shallowly dipping, and form a west-south westward thickening wedge. These lie upon a "basement" of Proterozoic rocks, which are also largely sedimentary.

In the southern part of Ts' ude niline Tu' eyeta are the Mackenzie Mountains, a belt of uplifted and deformed rocks. These include the same Phanerozoic rocks as the Interior Platform, with a basement of Proterozoic rocks except that in the

Mackenzie Mountains, these rocks are uplifted, and exposed in folds and faulted slices.

Proterozoic sediments were deposited in an ocean basin at the western edge of the ancestral North American continent. Early rifting events marking the breakup of Rhodinia were followed by quiescent platform conditions. A thickness of several kilometres of dominantly siliciclastic and carbonate sedimentary rocks was deposited. Episodes of uplift, tilting, deformation, and erosion during the Forward Orogeney (Thorkleson, 2003; Cook and MacLean 1999) affected these rocks. Ancient glaciation is also indicated by the Proterozoic lithologies (e.g., Aitken, 1993).

The early Phanerozoic saw continued marine deposition of sedimentary rocks. Through much of the Cambrian to Middle Devonian periods, the continental margin was a relatively tectonically quiet passive margin setting that saw the deposition of voluminous Mackenzie Platform carbonate rocks (Aitken, 1993).

The Ellesmerian orogeny began in Late Devonian time and resulted in siliciclastic sediments being shed into the study area from a landmass to the north and west (Moore, 1993). Siliciclastic deposition continued into the Carboniferous (Richards et al., 1993). A long period of no deposition and erosion followed, through to the Jurassic (Poulton et al., 1993).

The Columbian and Laramide orogenies occurred during the Cretaceous, and formed the modern Mackenzie Mountains. Uplifted lands to the west and south shed sediments into a Cretaceous sea (Stott et al., 1993; Dixon, 1999). Upon withdrawal of the sea in the Late Cretaceous, continental alluvial and fluvial sediments were deposited.

Subsequent erosion and Pleistocene glaciation events modified the landscape and left a veneer of glacio-fluvial unconsolidated sediments covered by glaciolacustrine sediments over much of the study area. Fluvial erosion continues today, particularly in the upland areas, and the Mackenzie River and its tributaries carry a

large volume of sediment. Figure 2 on the following page is a simplified bedrock geology map.

3.1 Proterozoic Geology

A basement of Proterozoic rocks underlies the Phanerozoic succession throughout the study area. Proterozoic rocks are known from outcrops in the Mackenzie Mountains, and from petroleum wells within the study area that penetrated the basement. Morphology of the basement surface can be inferred from seismic surveys. In the north half of the study area, the surface dips gently west-southwest, while in the south, the dip is relatively steep and south trending. Gentle warps and flexures were also identified on basement surface (MacLean, 1999), which could be tectonic and/or erosional features.

The lithology of basement rocks in the Interior Platform has been inferred from geophysical surveys (magnetics, gravity) and from rare borehole intersections. Four assemblages of Middle and Late Proterozoic unmetamorphosed sedimentary rocks have been identified, including two that are exposed in the Mackenzie Mountains. These four assemblages were deposited over a time period of more than 1 billion years, and they overlie still older metamorphic, igneous, and volcanic rocks. Brief lithological descriptions below are taken primarily from Aitken (1993).

Sedimentation associated with the Hornby Bay/Dismal Lakes assemblages began before 1660 Ma and ended before eruption of Coppermine basalts (1270-1210 Ma), northeast of the study area. The Hornby Bay assemblage was deposited in an extensional basin, with minor associated volcanism. Faults were periodically reactivated. The Dismal Lakes assemblage was deposited in a trangressive regime ranging from earlier fluvial clastic environments to later marine carbonate shelf carbonate rocks. The continental margin faced north and west.

Locally significant unconformities between Hornby Bay and Dismal Lakes assemblages indicate an intervening period of uplift and erosion. Both assemblages, as well as overlying Coppermine basalts were subsequently deformed during the Racklan / Forward Orogeny.

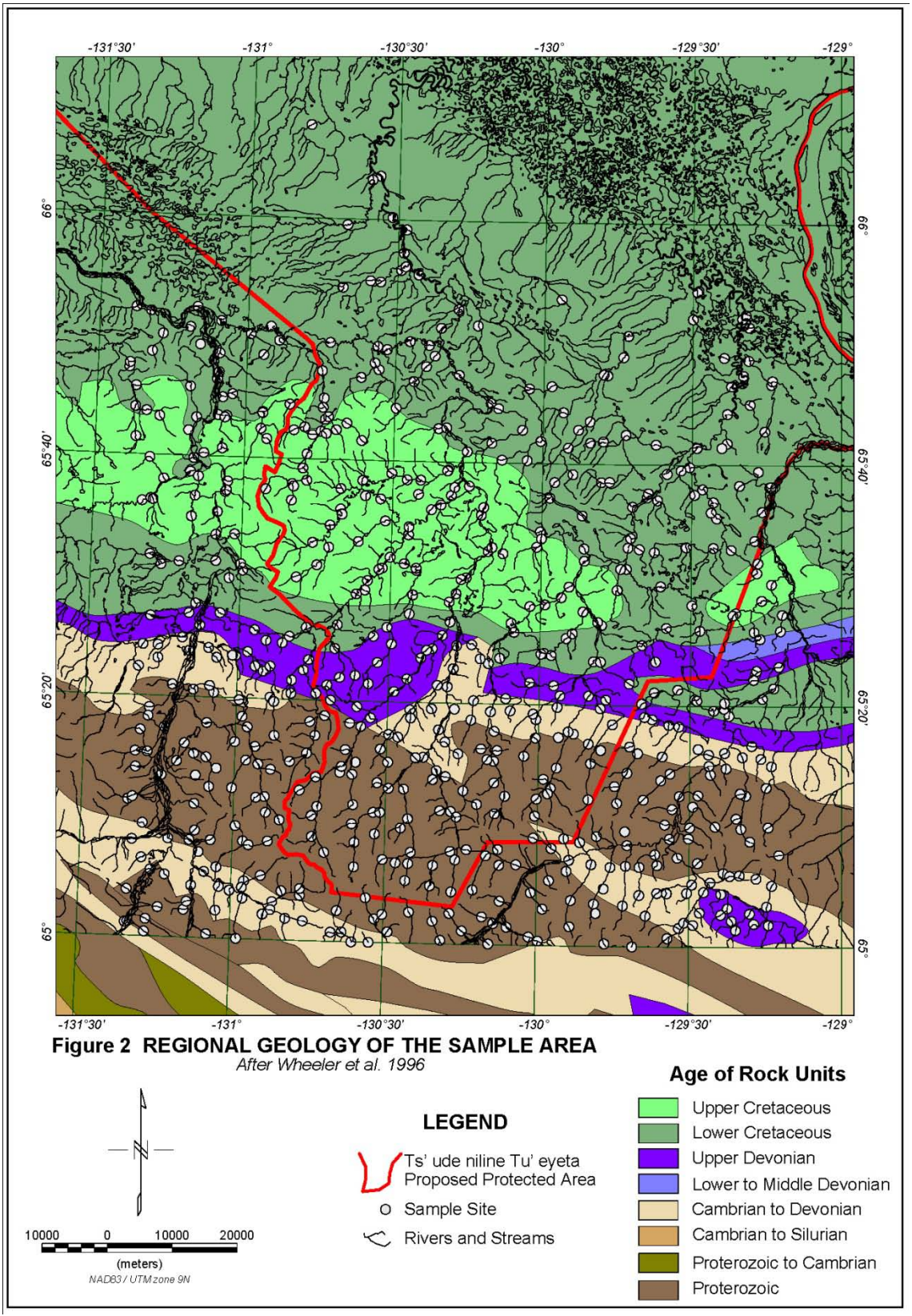


Figure 2 Regional Geology of the Sample Area

Hornby Bay assemblage

Hornby Bay assemblage rocks comprise feldspathic sandstones, conglomerates, and mudrocks, with a significant amount of carbonate beds in the upper part of the section.

Dismal Lakes assemblage

The Dismal Lakes assemblage overlies the Hornby Bay assemblage. Lithologies include mainly siliciclastic rocks in the lower third of the unit, and carbonate rocks in the upper part. The Hornby Bay and Dismal Lakes assemblages together were deposited from about 1660 to 1210 million years ago.

Mackenzie Mountains Supergroup

Mackenzie Mountains supergroup outcrops in Mackenzie Mountains in the southern part of the study area. Uplift and erosion preceded deposition of the Supergroup. A maximum age for these deposits may be 1000 Ma (Rainbird et al., 1996), and they are cut by basic intrusions dated 780 Ma (Harlan et al., 2003). The sedimentary environment was a continental platform margin. Individual units thicken basinward, toward the southwest. Some workers suggest that the Mackenzie Mountains supergroup was deposited in a “two-sided basin”, i.e., with continental margins to northeast and south or west (Aitken, 1993).

The lower part of the Mackenzie Mountains Supergroup is composed of sandstones, shales, and siltstones overlain by grey cherty dolostone belonging to the H1 unit. The H1 unit is overlain by mudstones with subordinate sandstones and carbonates of the Tsezotene Formation. Above these lie quartz sandstone, minor shale, and carbonate rock of the Katherine Group. The supergroup is capped by the Little Dal Formation; a lithologically varied package of limestone, dolostone, anhydrite, gypsum, mudstone, and sandstone. Flows of basaltic lava are locally preserved at the top of Little Dal Formation. The Mackenzie Mountains supergroup is up to four km thick, and was deposited from about 1,000 to 780 Ma (Pyle et al., 2006).

Uplift, tilting, and erosion followed deposition of the Mackenzie Mountains supergroup, as indicated by regional unconformities. Rifting was initiated, accompanied by local volcanism. Diamictite deposits indicate glacio-marine sedimentation. By the latest Proterozoic, rifting had subsided and there was widespread subsidence along a passive continental margin hinge. A series of shale-carbonate cycles were deposited as sea levels rose and fell in a marine platform to basin environment.

These latest Proterozoic marine deposits were followed by another phase of uplift and local erosion, and then finally by marine transgression, and deposition of the basal Cambrian beds.

Windermere Supergroup

Latest Proterozoic Windermere Supergroup strata outcrop in the interior ranges of Mackenzie Mountains, in the extreme southwest corner of the study area.

3.2 Middle to Late Proterozoic Tectonic and Depositional History

The summary below is taken from Aitken (1993). Sedimentation associated with the Hornby Bay/Dismal Lakes assemblages began before 1660 Ma and ended before eruption of Coppermine basalts (1270-1210 Ma), northeast of the study area . The Hornby Bay assemblage was deposited in an extensional basin, with minor associated volcanism. Faults were periodically reactivated. Dismal Lakes assemblage was deposited in a trangressive regime ranging from earlier fluvial clastic environments to later marine carbonate shelf carbonate rocks. The continental margin faced north and west.

Locally significant unconformities between Hornby Bay and Dismal Lakes assemblages indicate an intervening period of uplift and erosion. Both assemblages, as well as overlying Coppermine basalts were subsequently deformed during the Racklan Orogeny.

Uplift and erosion preceded deposition of the Mackenzie Mountains supergroup. A maximum age for these deposits may be 1000 Ma (Rainbird et al., 1996), and

they are cut by basic intrusions dated 780 Ma (Harlan et al., 2003). The sedimentary environment was a continental platform margin. Individual units thicken basinward, toward the southwest. Some workers suggest that the Mackenzie Mountains supergroup was deposited in a “two-sided basin”, i.e., with continental margins to northeast and south or west (Aitken, 1993).

Uplift, tilting, and erosion followed deposition of the Mackenzie Mountains supergroup, as indicated by regional unconformities. Rifting was initiated, accompanied by local volcanism. Diamictite deposits indicate glacio-marine sedimentation. By the latest Proterozoic, rifting had subsided and there was widespread subsidence along a passive continental margin hinge. A series of shale-carbonate cycles were deposited as sea levels rose and fell in a marine platform to basin environment.

These latest Proterozoic marine deposits were followed by another phase of uplift and local erosion, and then finally by marine transgression, and deposition of the basal Cambrian beds.

3.3 Phanerozoic Geology

Throughout the study area, the total thickness of Phanerozoic rocks increases from northeast to southwest, from less than 2,100 m in the northeast to over 4,000 m in the southwest (Morrell, 1995). Cambrian through Cretaceous rocks are present. Unconsolidated Quaternary deposits of varying thickness cover much of the north portion of the study area, effectively obscuring bedrock, except in the mountain regions and the larger stream valleys. Table 3 summarizes the Phanerozoic stratigraphic units of the study area. The lithology, nature of contacts, distribution, and thickness of the formations, ordered from oldest to youngest, are described in great detail in Gal (2007).

PERIOD (EPOCH)		FORMATION (OR GROUP/ASSEMBLAGE)			MAJOR LITHOLOGIES
		West part of study area		East part of study area	
Quaternary	Pleistocene	Laurentide till, glaciofluvial deposits		Laurentide till, glaciofluvial deposits; Columbian till	sand, gravel, till,
Unconformity					
Cretaceous	Late (?)	Slater River		--	Shale
		Trevor		--	Sandstone
	Unconformity				
	Early-Middle	Trevor		--	shale, sandstone (?)
		Arctic Red		Arctic Red	shale, siltstone, sandstone
		Martin House		Martin House	sandstone, siltstone, shale
Unconformity					
Carbon-iferous	Early	Tuttle		--	sandstone, conglomerate, siltstone
Unconformity					
Devonian	Late	Imperial		Imperial	siltstone, shale, sandstone
		Canol		Canol	Shale
	Unconformity				
	Middle	--		Ramparts	limestone, siltstone, shale
		Hare Indian		Hare Indian	shale, siltstone
		Hume		Hume	limestone, shale
	Early	Landry		Landry (Bear Rock at surface)	limestone, dolostone, carbonate breccias
		Arnica		Arnica (Bear Rock at surface)	dolostone, limestone, carbonate breccias
				Fort Norman	anhydrite, dolostone
		Tatsieta		--	limestone, dolostone, shale,
		Peel		--	dolostone, limestone
Unconformity					
Ordovician–Silurian		Mount Kindle		Mount Kindle	Dolostone
Unconformity					
Cambrian–Ordovician		Franklin Mountain		Franklin Mountain	Dolostone
Cambrian (Early-Middle)		Saline River		Saline River	shale, dolostone, evaporites
		unconformity (?)			
		Mount Cap		Mount Cap	dolostone, shale, quartzose sandstone
		Mount Clark (?)		Mount Clark	quartzose sandstone
Unconformity					
Proterozoic	Late	Windermere supergroup	Risky	--	Carbonate
			Blueflower	--	mudstone, sandstone, limestone
			Gametrail	--	Carbonate
			Sheepbed	--	mudstone, sandstone
			Keele	--	dolostone, limestone, shale
			Twitya	--	mudstone, turbidite
			Shezal	--	diamictite, sandstone, mudstone
			Sayunei	--	siltstone, argillite, sandstone, conglomerate, diamictite, iron formation
			Unconformity		
			Coppercap	--	Carbonate
			Redstone River	--	fanglomerate, redbeds, anhydrite
			Thundercloud	--	sandstone, conglomerate, mudstone, dolostone, shale
		Mackenzie Mountains supergroup	Little Dal	Little Dal	limestone, dolostone, evaporates, mudstone, sandstone, gabbro
			Katherine Group	Katherine Group	quartz sandstone, carbonate, shale
			Tsezotene	Tsezotene	mudstone, sandstone, carbonate
			unnamed	unnamed	sandstone, shale, siltstone, dolostone
	Unconformity				
	Early-Middle Proterozoic	--		Dismal Lakes assemblage	siliciclastic and carbonate
		Unconformity			
		Hornby Bay assemblage		Hornby Bay assemblage	sandstone, conglomerate, mudstone, carbonate

Table 1 Table of Formations (From Gal (2007))

4 Local Geology

The description of the local geology of the Ts' ude niline tu' eyeta study area is adapted from Gal (2007) and Mills (2008).

4.1 Bedrock Lithologies

Stratigraphic units discussed above occur in the subsurface of all or parts of the study area. This section focuses on the lithological character and structure of bedrock exposed within the study area.

Interior Platform

Throughout the study area, the sub-Cretaceous unconformity has cut progressively downward through Devonian units from southwest to northeast. This, coupled with the regional southwest dip, has resulted in the oldest rocks being exposed in the northeast corner of the study area. However, outcrops are relatively rare on the Interior Platform due to topography, flat lying nature of the bedrock, predominance of soft shales, and overlying veneer of Quaternary deposits.

The Hume Formation outcrops in a few places south of Hare Indian River on the east boundary of the study area. Exposed rock consists of dense, brown, thin to medium-bedded, fossiliferous limestone (Aitken et al., 1969). An east-northeast trending, down to the northwest normal fault marks the contact with the Hare Indian Formation at this location.

The Hare Indian Formation is very rarely exposed within the study area, due to the recessive nature of the shale. One outcrop was mapped by Aitken et al. (1969) on the Bluefish River, another section was measured on lower Gossage River (Cook and Aitken, 1975), and outcrops occur along the Mackenzie River at the Ramparts and just downstream from the Tieda River. Exposures are of greenish-grey, grey, and pale brown shale, with thin beds of calcareous siltstone and fossiliferous limestone, especially near the top of the Hare Indian Formation.

The Ramparts Formation outcrops extensively in the northeast corner of the study area. Outcrops occur at the Ramparts on the Mackenzie River, Ramparts Plateau west of Loon Lake, between Rorey and Manuel lakes, and along Yeltea Lake and Tieda River. The platform member is characterized by medium-bedded, brown, partly argillaceous limestone, with abundant tabulate corals (Aitken et al., 1969). The Kee Scarp member is thick-bedded to massive, pale brown limestone with abundant globular stromatoporoids.

The projected pattern of Canol Formation outcrop forms a narrow band along the Mackenzie River in the northeast part of the study area. Actual outcrops are rare, occurring mainly on the river banks downstream from Tieda River. The unit in outcrop is composed of dark grey to black bituminous shales with some silty beds, clay-ironstone concretions, and pyrite nodules (Aitken et al., 1969). Yellow and red iron oxide staining coats outcrops. Better exposures display closely spaced joints resulting in a blocky appearance.

Imperial Formation rocks outcrop mainly in the Mackenzie River valley downstream from Fort Good Hope. Exposures consist of brown and greenish-brown fissile shale, with subordinate brown fine-grained sandstone and siltstone beds (Aitken et al., 1969). Several outcrops occur on lower Ontaratue River (Cook and Aitken, 1975).

Cretaceous beds subcrop throughout the Interior Platform in the south-central and western parts of the study area, and in outlying plateaus around Yeltea Lake, southeast of Loon Lake, south of Fort Good Hope and around Chick Lake. Cretaceous beds overlie Palaeozoic beds in obvious unconformity. Near Rorey Lake, over 120 m of relief is apparent on the sub-Cretaceous unconformity (Aitken et al., 1969). About 17 km northwest of Fort Good Hope, Aitken et al. (1969) observed a Cretaceous channel filled with sandstone and conglomerate, cut into underlying Hare Indian Formation.

Basal Cretaceous sandstone (Martin House Formation or Sans Sault member of Arctic Red Formation) is commonly white and quartzose, and locally oil-stained.

Grain size, and relative abundance of chert and quartz varies between beds. Calcite cement is common. The basal sandstone is overlain by shale that rarely crops out. Exposures on lower Ramparts River are dark grey to black, slightly silty, blocky-weathering with abundant ironstone concretions. On lower Mountain River, Arctic Red Formation shale, siltstone, and minor sandstone are exposed in a series of gently dipping beds outlining open folds.

Additional Cretaceous outcrops occur along Ontaratue River, Arctic Red River, southern Grandview Hills, Yellow Hills, and Lichen Ridge.

Cordillera

Most of the units described above in the stratigraphy section are exposed in the Cordillera portion of the study area, and will not be described again here. The Mackenzie Mountains feature ranges of Precambrian sedimentary rocks brought to surface along thrust fault planes and in the cores of large folds. Sills and northwest trending dykes of medium-grained, greenish-black gabbro intrude Tsezotene Formation and Katherine Group rocks. These are the only known intrusive rocks in the study area. Rocks as old as Franklin Mountain Formation are brought to surface by thrust faults in the northern Franklin Mountains.

4.2 Structural Geology

Interior Platform

Generally, bedding in the Interior Platform is little deformed. The regional structural style is a southwest dipping monocline. Minor faults and structures have been outlined in the subsurface by seismic surveys. As the Cordilleran front is approached, deformation becomes more pronounced. Gentle open folds trending northeast and northwest, but generally parallel to the mountain front, were mapped in Cretaceous beds at Sans Sault Rapids and along lower Mountain River (Aitken and Cook, 1974). Lichen Syncline is a broad, gentle warp, cored by Cretaceous strata, that extends along the Mackenzie Mountain Front west of the Imperial Hills. Only rarely have minor faults been mapped or interpreted near surface in Cretaceous strata.

Cordillera

Generally, larger structures of the Mackenzie Mountains in the study area are of typical fold-and thrust morphology. Structures are interpreted to have resulted from Laramide (plus Columbian?) orogenies in the Cretaceous. Earlier deformational features have not been identified at a 1:250,000 map scale.

The Beavertail Anticline is overturned to the south and associated with a south-directed thrust, while the East Mountain anticline and its associated fault are north verging (Aitken et al., 1982). Reversals in vergence along strike have been interpreted to be the result of salt tectonics southeast of the study area (MacLean and Cook, 2000). The East Mountain anticline is doubly plunging, trends almost due east, and may be traced across the Mackenzie River to West Mountain, which trends northeast. Along strike from West Mountain is the Whirlpool Fault, a southeast directed thrust fault that carries a sliver of Imperial Formation, exposed in its hanging-wall where it crosses Mountain River (Aitken et al., 1982).

The Imperial Hills comprise a large anticlinorium outboard of the main Mackenzie ranges in the southeast part of the study area. The north flank of the anticlinorium dips steeper than that on the south. A number of sub-parallel folds make up the anticlinorium, which is cored by Mount Kindle Formation (Aitken et al., 1982). Several west to northwest trending faults cut the flanks of the constituent folds.

The Imperial syncline, a broad gentle down-warp, separates the Imperial Hills from the main Mackenzie Mountains. At its west end, the south-directed Southbound Fault carries Lichen Syncline up against the north limb of Imperial Syncline (Aitken et al., 1982).

The mountain front is marked by the Stony Anticline, which is a broad open fold cored by Precambrian strata, in the southeast part of the study area. The Stony Anticline is bounded to the south by the comparatively tight Houdini Synclinorium, and the Tawu Anticline (Aitken et al., 1982).

The south-western part of the study area is dominated by the Tawu Anticline, and to the southwest, by a number of northeast and southwest-directed thrust faults and associated folds, in a typical fold-and-thrust structural pattern. The steeper northeast flank of the Tawu Anticline is marked by the southwest-directed Tabasco Fault, which repeats the fold limb. A number of northwest, and lesser west- or north-trending faults have been mapped in Proterozoic sedimentary rocks (Aitken et al., 1982). Some faults, such as Grand Forks Fault, offset beds as young as Middle Devonian (Aitken et al., 1982).

5 Previous Work

5.1 Regional Government surveys

The geology of the study area is covered by Geological Survey of Canada (GSC) 1:250,000 scale maps for NTS sheets 106G and H (Aitken et al., 1982), 106J (Cook and Aitken, 1975), and 106I (Aitken et al., 1969). This mapping was carried out during the GSC's Operation Norman in the late 1960s and early 1970s. Smaller scale compilation maps covering the area include works by Yorath and Cook (1981) and more recently Journeay and Williams (1995), and Wheeler et al. (1996).

GSC surficial geology maps are published at 1:250,000 scale (or larger) for the north part of the study area (Rampton and Fulton, 1970; Duk-Rodkin and Hughes, 1992a, b) and the southern half (Hughes, 1970; Hanley et al., 1973; Monroe, 1973; Duk-Rodkin and Hughes, 1993a, b). The GSC has published gravity anomaly maps at 1:1,000,000 scale covering the study area (Seemann et al., 1988). Aeromagnetic total field maps at 1:100,000 scale are available for NTS map sheet 106H (Dumont, 2000a-d), part of 106G (Dumont et al., 2000), 106I (Dumont et al., 2001a, b), and 106J (Dumont et al., 2001c, d). Older vintage aeromagnetic surveys (GSC G-series maps at 1:250,000 scale) cover the balance of the study area.

5.2 Mineral Exploration History

The area at the headwaters of the Gayna River was explored by Rio Tinto Canadian Exploration Limited during the mid to late 1970s and a small portion of this ground is

currently being investigated by Eagle Plains Resources Limited. A number of Zinc showings and deposits have been outlined. An historical resource estimate in excess of fifty million tons grading 4.7% Zinc, has been suggested by Rio Tinto (Hewton, 1982). Thus Gayna River may be one of Canada's largest undeveloped Zinc camps.

Zinc sulphide concentrations are hosted by carbonate rocks of the Mesoproterozoic H5 unit that overlies coarse grained quartz arenite of the Katherine Group, and is overlain by the Little Dal Group (limestone, dolostone, anhydrite, gypsum, mudstone and sandstone) (Hewton, 1976; Aitken, 1981, 1993, Aitken et al., 1982). The mineralized H5 unit (named the Basinal formation of the Little Dal Group by Aitken, 1981) grades upward from deep water shale and carbonate through shallow marine carbonate to lagoonal rocks. Large stromatolitic pinnacle reef structures within the Basinal formation constitute a north-south chain and record deep to shallow water carbonate environments. The reefs are conformably overlain by shallow platformal marine carbonate rocks - oolitic and stromatolitic tabular units of the Grainstone formation. These in turn are overlain by the variably thick Gypsum formation (bedded deep to shallow water gypsum evaporite) and the laterally continuous stromatolitic carbonate rocks of the Upper Carbonate formation (formerly Upper Little Dal Formation). The Basinal, Grainstone and Gypsum formations of the Little Dal Group are only locally exposed over the Gayna River area, as these units have been partially eroded beneath an Upper Cambrian unconformity.

Basinal limestone and dolostone constitute the Upper and Lower Host units of Hewton (1982), and are separated by about 10 m of argillite, all part of the Basinal formation of Aitken (1981). Several forms of carbonate alteration including intense hydrothermal, early calcite, early quartz, and pyrite alteration are common to both the Upper and Lower hosts, Wallace, 2009. Sphalerite, pyrite and galena are the main sulphide minerals. Sphalerite is most commonly intergrown with calcite and dolomite in primary (syn-sedimentary) breccias, and in recrystallized zones of bedded carbonate rocks where it ranges from massive to disseminated in form. Sphalerite ranges from pale yellow to colourless in primary breccias and is bright yellow,

orange, red or green in secondary breccias. Concentrations of massive sphalerite with associated fine disseminations may represent migration of mineralizing fluids along bedding planes away from fluid conduits such as fractures or faults. Pyrobitumen, dodecahedrons of pyrite, euhedral quartz crystals, dolomite crystals, barite and rare fluorite are also located in vugs within the Lower and Upper Host units (Hewton, 1976).

6 Potential Mineral Resources

The mineral potential of the Ts' ude niline Tu' eyeta area has never before been assessed, as it has received little exploration attention. This likely stems from the lack of geologic information available for the area, in part due to poor outcrop exposure. Areas with better bedrock exposure have naturally seen more mineral exploration activity in the past**.**

From known and extrapolated geologic information, a number of mineral deposit-types may possibly occur within the study area. These include primary diamond deposits, Zn-Pb deposits (including MVT, SEDEX and their subtypes), breccia-hosted IOCG deposits, sedimentary-hosted Cu, Ni-Cu-PGE deposits, stratiform iron, coal and Industrial Minerals.

In order to properly evaluate the stream sediment sampling results and perform meaningful statistical analyses on them, it was necessary to determine what deposit types were likely to be found in the study area and determine statistical factors which would assist in discovering potential deposits. The mineral deposit-types considered in this assessment were selected based upon conceptual models of deposit types and comparison of these models to the geology of the area being assessed (Sangster, 1983). This method is based upon the best currently available scientific knowledge. The existence of deposit types not listed here cannot be ruled out. The mineral deposit-types considered are based on descriptions provided in *Geology of Canadian Mineral Deposit Types* (Eckstrand et al., 1996).

The various assessment criteria outlined in the literature (e.g., Rogers et al., 1995; Eckstrand et al., 1996) have been applied to the mineral deposit-types determined to have the best potential (Table 2) within the study area.

Table 2 Potential Mineral Deposit Types in the Ts' ude niline Tu' eyeta area (From Mills (2008))

Mineral Deposit Type	**Examples with emphasis on Canada & Northwest Territories**
Potential Mineral Deposit Types Occurring In Phanerozoic Cover Rocks	
Diamonds	Ekati Diamond Mine, Lac de Gras, NWT Diavik Diamond Mine, Lac de Gras, NWT DeBeer.s Snap Lake Mine, NWT Kennady Lake, Jericho, NWT Buffalo Head Hills, Alberta Fort a la Corne, Saskatchewan
Mississippi Valley Type Zn-Pb	Pine Point, NWT Wrigley, NWT Nanisivik, Nunavut Polaris, Nunavut Gayna River, NWT
Sedimentary Exhalative (SEDEX) Zn-Pb-Cu	Red Dog, Alaska Anvil Range (Faro, Dy, Grum, Swim, Vangorda), Yukon Tom, Jason, NWT-Yukon Border Howards Pass, NWT Sullivan Mine, B.C.
Sedimentary-Hosted Cu	Redstone (Coates Lake), NWT Hottah Lake occurrences, NWT
Coal	Coal Mine Lake, NWT Douglas Bay, Great Bear Lake Perry Creek and Brule Mine, northeast B.C.
Banded Iron Formation (BIF)	Crest BIF, NWT Mary River BIF, NU
Breccia-hosted IOCGs	Wernecke Breccia, YT Ernest Henry, Australia Olympic Dam, South Australia Sue-Dianne, NWT
Ni-Cu-PGEs (Nick-type, sediment-hosted, or mafic to ultramafic magmatic-hosted)	Nick deposit, YT Ferguson Lake, NU Norilsk, Siberia
Industrial Minerals (Potash, Gypsum, Aggregate)	Esterhazy, Saskatchewan

7 Stream Geochemical Survey

The Northwest Territories Geoscience Office conducted a stream sediment sampling program across portions of NTS map sheets 106G, 106H, 106I and 106J during the summers of 2007 and 2008. This survey was completed to help assess the potential for the presence of economic mineral deposits in the southern portion of the Ts' ude niline Tu' eyeta Candidate Protected Area in west central Northwest Territories.

The stream sampling program was carried out according to the protocols established for the National Geochemical Reconnaissance Program and described in Day et al. (2007). A total of 644 separate locations were sampled over the course of the survey program. The sampling protocol included analyzing duplicate samples and standards to ensure quality assurance and quality control.

Aurora Geosciences Ltd., of Yellowknife, NT was contracted to assess the mineral potential of the area based on a statistical multivariate review of the stream sediment geochemical sampling data. This report documents the statistical geochemical analyses performed on those data and the conclusions drawn from those analyses.

7.1 Sample Procedure

7.1.1 Silt Samples

At each site, a pre-labelled Kraft paper bag (12.5 cm x 28 cm) with side gusset) was two thirds filled with silt or fine sand collected from the active stream channel. In practice, the silt sample was collected after water samples were collected, but before a bulk sediment sample. Commonly, the sampler collected handfuls of silt from various points in the active stream channel while moving gradually upstream. If the stream channel consisted of solely of clay or coarse materials from which suitable sample silt was scarce or absent, a moss mat sample might be collected as the organic fibres tend to trap a variety of grain sizes.

The Kraft paper bags containing the silt samples were placed into plastic bags, taped with electrical tape and shipped directly to a commercial lab,

where they were air-dried at temperatures below 40°C and sieved through a minus 80-mesh (177 pm) screen. At the laboratory, control reference and blind duplicate samples were inserted into each block of twenty sediment samples.

At the time of collection, site-specific field observations were recorded on a standard NGR stream sediment and water form. Sample site locations were recorded using a Garmin GPSMAP 76.

7.1.2 Stream Waters

Waters were sampled in mid-channel, from flowing water where possible, at every site. Samples were contained in 125-ml Nalgene high density polyethylene (HDPE) bottles. Samples were collected after first rinsing bottles two or three times in flowing water before a final fill.

Within 24 hours of collection, water samples were filtered through single-use Millipore Sterivex-HV 0.45 gm filter units attached to 50-ml sterile plastic syringes. After 50 ml of water was filtered into new 60-ml bottles, the remainder was used for the determination of pH and conductivity before being discarded. Using an Eppendorf pipette repeater with disposable plastic tips, 0.5 ml 8M HNO_3 was added to filtered water samples. Syringes were re-used after rinsing with distilled, de- ionized water, but replaced daily. At this point, control reference samples (filter, acid and travel blanks) were inserted. Filtered and acidified waters were kept in a cool dark place until shipment to the lab. For the water samples, only control reference samples were inserted into the block of 20 water samples. There were no blind duplicate water samples.

7.2 Analytical Methodology

Instrumental Neutron Activation Analysis (INAA)

Weighed and encapsulated samples, normally 30 g, were packaged for irradiation along with internal standards and international reference materials. Samples and standards were irradiated together with neutron flux monitors in a two-megawatt pool

type reactor. After a seven-day decay period, samples were measured with a high-resolution germanium detector. Typical counting times were 500 seconds. Elements determined by INAA are listed in Table 3.

Data for Ag, Cd, Ir, Se, Sn, Te, Zn, and Zr are not published because of inadequate detection limits and/or precision.

ELEMENT		DETECTION LEVEL	
As	Arsenic	0.5	ppm
Au	Gold	2	ppb
Ba	Barium	50	ppm
Br	Bromine	0.5	ppm
Ce	Cerium	5	ppm
Co	Cobalt	5	ppm
Cr	Chromium	20	ppm
Cs	Cesium	0.5	ppm
Eu	Europium	1	ppm
Fe	Iron	0.2	pct
Hf	Hafnium	1	ppm
La	Lanthanum	2	ppm
Lu	Lutetium	0.2	ppm
Mo	Molybdenum	1	ppm
Na	Sodium	0.02	pct
Ni	Nickel*	10	ppm
Rb	Rubidium	5	ppm
Sb	Antimony	0.1	ppm
Sc	Scandium	0.2	ppm
Sm	Samarium	0.1	ppm
Ta	Tantalum	0.5	ppm
Tb	Terbium	0.5	ppm
Th	Thorium	0.2	ppm
Ti	Titanium*	500	ppm
U	Uranium	0.2	ppm
W	Tungsten	1	ppm
Yb	Ytterbium	2	ppm

Table 3 Elements in Stream Silt Sediments Determined by Instrumental Neutron Activation analysis.

Inductively Coupled Plasma Mass Spectrometry (ICP-MS) and Other Analyses

For the determination of 36 elements listed in Table 4, a one-gram sample was leached with 6 ml of a mixture of HCl, HNO_3, and distilled, deionised water (2:2:2 v/v) at 95° C for one hour. The sample solution was diluted to 20 ml and analysed by inductively coupled plasma emission spectroscopy on a Jarell-Ash instrument and inductively coupled plasma mass spectroscopy on a Perkin-Elmer Elan instrument.

ELEMENT		DETECTION LEVEL	
Ag	Silver	2	ppb
Al	Aluminum	0.01	pct
As	Arsenic	0.1	ppm
Ba	Barium	0.5	ppm
Bi	Bismuth	0.02	ppm
Ca	Calcium	0.01	pct
Cd	Cadmium	0.01	ppm
Co	Cobalt	0.1	ppm
Cr	Chromium	0.5	ppm
Cu	Copper	0.01	ppm
F	Fluorine	10	ppm
Fe	Iron	0.01	pct
Ga	Gallium	0.2	ppm
Hg	Mercury	5	ppb
K	Potassium	0.01	pct
La	Lanthanum	0.5	ppm
LOI	Loss-on-ignition*	1	pct
Mg	Magnesium	0.01	pct
Mn	Manganese	1	ppm
Mo	Molybdenum	0.01	ppm
Na	Sodium	0.001	pct
Ni	Nickel	0.1	ppm
P	Phosphorus	0.001	pct
Pb	Lead	0.01	ppm
S	Sulphur	0.01	pct
Sb	Antimony	0.02	ppm
Sc	Scandium	0.1	ppm
Se	Selenium	0.1	ppm
Sn	Tin	1	ppm
Sr	Strontium	0.5	ppm
Te	Tellurium	0.02	ppm
Th	Thorium	0.1	ppm

Ti	Titanium	0.001	pct
T1	Thallium	0.02	ppm
U	Uranium	0.1	ppm
V	Vanadium	2	ppm
W	Tungsten	0.1	ppm
Zn	Zinc	0.1	ppm

Table 4 Elements in Stream Silt Sediments Determined by ICP - MS and other methods

Loss-on-ignition was determined using a one-gram sample. The sample, weighed into a Leco® crucible, was placed into a 100°C muffle furnace and brought up to 500° C for one hour. The oven was cooled to 100°C and crucibles transferred to a desiccator for cooling to room temperature. The crucibles were re- weighed, and the difference was reported as loss-on-ignition.

Tin in stream sediments was determined by heating a 200 mg sample with NH_4I: the sublimed SnI_4 was dissolved in acid and the tin determined by atomic absorption spectrometry after solvent extraction of the tin into methyl isobutyl ketone containing trioctylphosphine oxide (TOPO). Welsch and Chao (1976) describe the method.

Fluorine was determined using 0.25-gram sample splits weighed into Ni crucibles. One gram of sodium hydroxide was added and the mixture was fused at 600°C in a muffle furnace. The fusion product was dissolved in 7 ml of de-ionized water and 5 ml of 30% sulphuric acid. The solutions were transferred to plastic beakers and 5 ml of 30% ammonium acetate added. The volume was made up to 90 ml with de- ionized water. The pH was tested and adjusted to 7.8 with either of sodium hydroxide or sulphuric acid. Fluorine content was determined using a fluorine selective ion electrode.

8 Data Treatment

8.1 Silts

Separate data sets collected in 2007 and 2008 were examined. The data sets were not levelled but are assumed to be levelled by virtue of the analytical

procedures and quality control measures taken by the Geological Survey of Canada and the assay laboratory. The data were edited as follows:

1. **Faulty analyses indicated by negative numbers not equal to half the analytical detection limit were deleted.**

2. **All analyses less than the detection limit indicated in the records by half the negative detection limit or an equivalent notation were replaced by values equal to half the detection limits.**

3. **Values above the maximum detection limit were cut to the value of the maximum detection limit. This was principally in Mn.**

4. **Where analyses were repeated at a single sample site, the average value of the two samples was used.**

5. **Where elements were analyzed by different methods, those analyses with higher detection limits were deleted from the data set and the results from the method with the lower detection limit were used in subsequent statistical analysis.**

8.2 Water

Statistical analysis of the water datasets was conducted using the same procedures as outlined with the stream sediment sample data. Separate data sets were collected in 2007 and 2008 concurrent with the stream sediment sampling. The datasets were not leveled but are assumed to be leveled by virtue of the analytical procedures and quality control measures taken by the Geological Survey of Canada. The data were edited as listed immediately above.

9 Statistical Analysis of the Stream Sediment Data

9.1 Univariate Statistics

Statistical analysis in this report was performed with the XLSTAT^{TM} package unless otherwise stated. Univariate statistics for all elements are contained in Tables 5

and 6. In this analysis, standard deviations are normalized by n-1, and both kurtosis and skewness are calculated using Pearson's equations. A normal distribution will show skewness and kurtosis of 0 with these measures. Percentile ranks are calculated for the 25th, median, 75th, 95th and 98th percentiles.

Table 5 Regional Geochemical Survey silt data - Univariate statistics

Analysis	Units	Missing values	Minimum	Maximum	Mean	Standard deviation	Detection limit	Skewness (Pearson)	Kurtosis (Pearson)
LOI_Grav	pct	0	0.1	78.2	5.1	6.6	0.1	5.7	44.6
Ag_ICP	ppb	0	6	272	71	45	2	1	1
Al_ICP	pct	0	0.06	6.84	0.69	0.54	0.01	4.47	35.98
As_ICP	ppm	0	1.7	74.8	7.9	5.0	0.1	5.9	59.2
Au_INA	ppb	2	1	5	1	1	2	2	2
B_ICP	ppm	0	10	10	10	0	20	na	na
Ba_ICP	ppm	0	15.2	1475.8	297.0	213.4	0.5	1.2	2.3
Bi_ICP	ppm	0	0.01	0.53	0.15	0.08	0.02	1.20	2.60
Br_INA	ppm	2	0.3	64.9	3.3	4.6	0.5	7.5	74.2
Ca_ICP	pct	0	0.01	22.84	3.89	5.53	0.01	1.74	1.91
Cd_ICP	ppm	0	0.02	2.77	0.22	0.25	0.01	5.00	34.62
Ce_INA	ppm	2	0	110	50	19	5	0	0
Co_ICP	ppm	0	0.9	445.8	14.8	27.9	0.1	8.6	103.8
Cr_ICP	ppm	0	1.3	34.6	11.0	5.6	0.5	0.3	-0.2
Cs_INA	ppm	2	0.3	11.0	3.6	1.8	0.5	0.6	0.8
Cu_ICP	ppm	0	2.57	106.12	20.01	12.10	0.01	1.87	6.45
Eu_INA	ppm	2	1	4	1	1	1	2	5
F_Fusion	ppm	0	68	1760	428	178	10	2	9
Fe_INA	pct	2	0.3	21.5	2.9	2.2	0.2	3.3	16.2
Ga_ICP	ppm	0	0.1	6.3	1.8	0.9	0.2	0.3	0.8
Hf_INA	ppm	2	1	36	9	5	1	1	4
Hg_ICP	ppb	0	0	149	39	29	5	1	-1
K_ICP	pct	0	0.01	0.24	0.08	0.03	0.01	0.90	2.08
La_ICP	ppm	0	0.7	11.8	3.8	1.6	0.5	1.4	4.0
Lu_INA	ppm	2	0.1	1.5	0.3	0.2	0.2	1.1	2.3
Mg_ICP	pct	0	0.04	12.60	2.04	2.82	0.01	1.91	2.67
Mn_ICP	ppm	0	48	10000	475	799	1	7	72
Mo_ICP	ppm	0	0.11	17.11	1.14	1.27	0.01	6.02	52.96
Na_ICP	pct	0	0.001	0.117	0.007	0.008	0.001	6.747	73.224
Ni_ICP	ppm	0	1.8	301.2	22.5	20.6	0.1	5.5	56.3
P_ICP	pct	0	0.006	0.226	0.049	0.029	0.001	0.719	1.168
Pb_ICP	ppm	0	1.83	46.95	10.75	5.02	0.01	2.20	8.78
Rb_INA	ppm	2	3	160	73	31	5	0	0
S_ICP	pct	0	0.01	3.42	0.11	0.22	0.02	9.00	107.87

Analysis	Units	Missing values	Minimum	Maximum	Mean	Standard deviation	Detection limit	Skewness (Pearson)	Kurtosis (Pearson)
Sb_ICP	ppm	0	0.06	1.42	0.24	0.13	0.02	3.39	21.49
Sc_ICP	ppm	0	0.5	25.2	2.5	1.7	0.1	5.8	61.1
Se_ICP	ppm	0	0.1	3.8	0.6	0.5	0.1	2.5	10.4
Sm_INA	ppm	2	0.3	14.1	4.5	2.0	0.1	0.7	2.1
Sn_Fusion	ppm	0	1	6	2	1	1	1	2
Sr_ICP	ppm	0	2.2	393.5	37.8	42.0	0.5	4.4	26.4
Ta_INA	ppm	2	0.3	1.6	0.8	0.3	0.5	-0.6	-0.4
Tb_INA	ppm	2	0.3	3.6	0.7	0.4	0.5	2.3	9.7
Te_ICP	ppm	0	0.01	0.23	0.03	0.03	0.02	2.77	10.96
Th_ICP	ppm	0	0.1	6.4	2.3	1.1	0.1	0.4	-0.3
Ti_ICP	pct	0	0.001	0.149	0.003	0.006	0.001	19.571	445.077
Tl_ICP	ppm	0	0.01	0.98	0.09	0.06	0.02	6.61	71.74
U_ICP	ppm	0	0.3	7.4	0.7	0.5	0.1	6.4	62.4
V_ICP	ppm	0	3	83	20	10	2	1	2
W_ICP	ppm	0	0.1	0.1	0.1	0.0	0.1	25.3	639.0
Yb_INA	ppm	2	1	9	2	1	2	1	2
Zn_ICP	ppm	0	4.7	634.4	80.7	68.9	0.1	3.4	19.6

Table 6 Regional Geochemical Survey silt data - Univariate statistics (continued)

Analysis	Units	Freq of minimum	Freq of maximum	1st Quartile	Median	3rd Quartile	95th Percentile	98th Percentile
LOI_Grav	pct	1	1	1.8	3.6	6.3		
Ag_ICP	ppb	1	1	35	62	99	162	192
Al_ICP	pct	1	1	0.38	0.68	0.83	1.39	2.35
As_ICP	ppm	1	1	5.5	7.2	9.0	13.7	22.3
Au_INA	ppb	475	2	1	1	2	3	4
B_ICP	ppm	644	644	10	10	10	0	0
Ba_ICP	ppm	1	1	118.3	269.2	422.3	681.4	849.3
Bi_ICP	ppm	4	1	0.09	0.14	0.18	0.30	0.37
Br_INA	ppm	15	1	1.5	2.5	3.6	6.8	15.0
Ca_ICP	pct	1	1	0.39	1.22	4.68	17.69	19.85
Cd_ICP	ppm	5	1	0.09	0.17	0.24	0.61	0.96
Ce_INA	ppm	1	2	42	52	61	81	87
Co_ICP	ppm	1	1	6.6	9.4	12.3	42.9	100.2
Cr_ICP	ppm	1	1	6.1	11.3	15.4	19.4	22.0
Cs_INA	ppm	17	1	2.4	3.6	4.6	6.8	7.7
Cu_ICP	ppm	1	1	12.41	18.21	23.84	43.42	55.50
Eu_INA	ppm	392	1	1	1	1	3	3
F_Fusion	ppm	1	1	310	400	510	720	885
Fe_INA	pct	3	1	1.9	2.7	3.2	6.7	10.7

Analysis	Units	Freq of minimum	Freq of maximum	1st Quartile	Median	3rd Quartile	95th Percentile	98th Percentile
Ga_ICP	ppm	6	1	1.1	1.9	2.4	3.2	3.6
Hf_INA	ppm	21	1	6	8	10	19	24
Hg_ICP	ppb	30	1	12	35	63	87	100
K_ICP	pct	2	2	0.06	0.08	0.10	0.15	0.17
La_ICP	ppm	1	1	2.7	3.7	4.5	6.6	8.4
Lu_INA	ppm	242	1	0.1	0.3	0.4	0.7	0.8
Mg_ICP	pct	1	1	0.34	0.70	2.34	9.23	10.88
Mn_ICP	ppm	1	2	233	305	410	13	2679
Mo_ICP	ppm	1	1	0.65	0.86	1.15	3.07	4.80
Na_ICP	pct	16	1	0.003	0.005	0.008	0.015	0.031
Ni_ICP	ppm	1	1	10.0	21.1	27.1	48.9	87.9
P_ICP	pct	4	1	0.024	0.046	0.071	0.098	0.109
Pb_ICP	ppm	1	1	7.80	10.05	12.41	20.13	25.19
Rb_INA	ppm	2	3	55	71	91	132	143
S_ICP	pct	119	1	0.03	0.06	0.11	0.32	0.50
Sb_ICP	ppm	2	1	0.16	0.23	0.29	0.45	0.55
Sc_ICP	ppm	1	1	1.7	2.3	2.8	4.7	6.9
Se_ICP	ppm	38	1	0.3	0.5	0.7	1.3	2.0
Sm_INA	ppm	1	1	3.7	4.4	5.3	8.2	10.0
Sn_Fusion	ppm	76	2	1	1	2	4	4
Sr_ICP	ppm	1	1	15.7	29.2	45.0	84.9	174.0
Ta_INA	ppm	99	1	0.7	0.9	1.1	1.3	1.5
Tb_INA	ppm	123	1	0.6	0.7	0.8	1.6	2.0
Te_ICP	ppm	186	1	0.01	0.03	0.04	0.08	0.14
Th_ICP	ppm	1	1	1.4	2.2	3.1	4.2	4.8
Ti_ICP	pct	25	1	0.002	0.002	0.003	0.008	0.011
Tl_ICP	ppm	1	1	0.06	0.07	0.10	0.170	0.228
U_ICP	ppm	15	1	0.5	0.7	0.8	1.5	2.2
V_ICP	ppm	6	1	12	22	27	35	39
W_ICP	ppm	643	1	0.1	0.1	0.1	0.0	0.0
Yb_INA	ppm	212	1	1	2	3	5	6
Zn_ICP	ppm	1	1	34.2	81.0	100.2	170.5	277.9

Figure A in Appendix 1 (at back) contains, for each element, histograms, Box plots and Q-Q diagrams for the raw data, and histograms and cumulative probability plots for the logarithmic (base 10) data. The natural distributions of most elements which are not left censored show either negative or positive skew. The log or log normal distributions of such elements more closely approximate a normal distribution and thus it is common practice to examine logarithmic or log

normal distributions of geochemical analyses when computing statistics on these measurements. A normal distribution in log space will be symmetric about a mean value with 66% of all analyses within one standard deviation of the mean. A normal distribution will show a symmetric Box plot and symmetric cumulative probability plot. In the latter case, the inflection point will be mean value of the data set (i.e. the mean and median are the same value in a normal distribution). Outliers in the Box plots are shown as individual points above the 95th percentile values indicated by the "whiskers".

The responses of the various elements vary depending upon their general abundance and the detection limit of the analytical methods used to measure them. Some elements showed no significant response above detection limit including B and W. The following elements are heavily left censored with a large percentage of analyses below detection limit (in brackets): Au (74%), Eu (61%), Lu (38%) and Te (29%). Other left censored elements with proportions of analyses below detection limit ranging from 2% to 20% include Hf, Hg, S, Se, Sn, Ta, Tb, Te, Ti, and U. The remaining elements show either log normal distribution, a skewed response or a two population distribution. The table below summarizes observations on the logarithmic population distributions.

Table 7 Summary of Element Response Distributions

Element	Distribution	Elem	Distribution
Ag	Log normal	Mn	Positive skew
Al	Negative skew	Mo	Positive skew
As	Log normal	Na	Left censored, two populations
Au	Left censored, discretized	Ni	Two populations
B	No response	P	Two populations; negative skew
Ba	Negative skew	Pb	Positive skew
Bi	Two populations, positive skew	Rb	Two populations; negative skew
Br	Positive skew	S	Left censored; positive outliers
Ca	Positive skew	Sc	Log normal
Cd	Positive skew	Sb	Log normal
Ce	Negative skew	Se	Left censored
Co	Positive skew	Sm	Negative skew
Cr	Negative skew	Sn	Log normal, discretized
Cs	Negative skew	Sr	Two populations
Cu	Log normal	Ta	Two populations, left censored

Element	Distribution	Elem	Distribution
Eu	Left censored, discretized	Tb	Two populations, left censored
F	Positive skew	Te	Left censored, positive skew
Fe	Positive skew	Th	Negative skew
Ga	Non normal, multiple populations	Ti	Log normal
Hf	Positive skew	Tl	Log normal
Hg	Left censored, two populations	U	Positive skew
K	Negative skew	V	Two populations
La	Log normal	W	No response
Lu	Left censored	Yb	Left censored
Mg	Positive skew	Zn	Two populations

Elements with two populations including Bi, Ni, P, Na, Rb, Sr, Ta, Tb, V and Zn appear to have been derived from two separate geochemical domains. Negatively skewed responses including Th, Sm, K, Ba, Cr, Cs, and Al indicate that one of these domains is especially enriched in these dominantly lithophile elements.

9.2 Multivariate Statistics

Multivariate statistics are summarized in Table 8 below which lists the Pearson correlation constant for each pair of elements in the distribution. Correlation constants range between 1.0 (perfect positive correlation) and -1.0 (perfect negative correlation) while a correlation constant of zero indicates no correlation exists between the data sets.

Figure B in Appendix 2 is a scatter plot matrix showing the correlation between the various element pairs. The ellipse in each scatter plot indicates the 95% confidence region of a bivariate distribution with the same mean and covariance. Element pairs with no significant correlation (<5% probability that the correlation is entirely random) are shown in blue.

The principal commodities likely to be found in the study area based on the available geological research and prospecting include Au, Cu, Pb and Zn. These are highlighted in Tables 8, 9, and 10, below. Gold response correlates with P, Hg, Ag and Se, suggesting a possible epithermal signature. There is much lower and less significant correlation between gold and Bi, Mo and As; elements which are

normally elevated in Tombstone style gold deposits. Copper response correlates strongly with Bi, Ce, Sc, Sm and Tb and less intensely with Pb, Zn and Fe. This strong association with lithophile and REE suggests a basement source for elevated copper values while the absence of a strong Co correlation does not support a strong primary red-bed copper geochemical affiliation. Lead response correlates with Al, Bi, Cu and Fe while zinc response correlates with Al, Co, Cd and Ni. There are less significant correlations between zinc, and both Fe and Cu.

Table 8 Multivariate Statistical Summary

	LOI Grav	Ag ICP	Al ICP	As ICP	Au INA	Ba ICP	Bi ICP	Br INA	Ca ICP	Cd ICP	Ce INA	Co ICP	Cr ICP	Cs INA	Cu ICP	Eu INA	F Fusion
LOI_Grav	1	0.285	0.216	0.330	0.092	0.171	0.142	0.737	-0.272	0.228	0.073	0.083	0.261	0.181	0.115	0.045	-0.012
Ag_ICP	0.285	1	0.431	0.443	0.658	0.541	0.480	-0.064	-0.414	0.317	0.447	0.085	0.709	0.638	0.454	0.088	0.287
Al_ICP	0.216	0.431	1	0.215	0.176	0.079	0.593	-0.009	-0.407	0.424	0.523	0.601	0.549	0.542	0.689	0.557	0.290
As_ICP	0.330	0.443	0.215	1	0.288	0.310	0.366	0.129	-0.166	0.186	0.177	0.054	0.393	0.356	0.218	0.065	0.102
Au_INA	0.092	0.658	0.176	0.288	1	0.397	0.326	-0.139	-0.293	0.007	0.284	-0.036	0.501	0.459	0.270	0.001	0.094
Ba_ICP	0.171	0.541	0.079	0.310	0.397	1	0.066	-0.041	-0.171	0.208	0.023	-0.090	0.476	0.155	0.061	-0.223	0.126
Bi_ICP	0.142	0.480	0.593	0.366	0.326	0.066	1	-0.086	-0.560	0.212	0.826	0.376	0.568	0.866	0.830	0.562	0.393
Br_INA	0.737	-0.064	-0.009	0.129	-0.139	-0.041	-0.086	1	0.028	0.156	-0.151	0.063	-0.147	-0.124	-0.054	0.022	-0.044
Ca_ICP	-0.272	-0.414	-0.407	-0.166	-0.293	-0.171	-0.560	0.028	1	-0.058	-0.765	-0.182	-0.535	-0.631	-0.479	-0.305	0.016
Cd_ICP	0.228	0.317	0.424	0.186	0.007	0.208	0.212	0.156	-0.058	1	0.206	0.579	0.231	0.222	0.375	0.269	0.333
Ce_INA	0.073	0.447	0.523	0.177	0.284	0.023	0.826	-0.151	-0.765	0.206	1	0.359	0.537	0.874	0.720	0.577	0.303
Co_ICP	0.083	0.085	0.601	0.054	-0.036	-0.090	0.376	0.063	-0.182	0.579	0.359	1	0.098	0.280	0.536	0.581	0.263
Cr_ICP	0.261	0.709	0.549	0.393	0.501	0.476	0.568	-0.147	-0.535	0.231	0.537	0.098	1	0.693	0.488	0.163	0.212
Cs_INA	0.181	0.638	0.542	0.356	0.459	0.155	0.866	-0.124	-0.631	0.222	0.874	0.280	0.693	1	0.701	0.453	0.360
Cu_ICP	0.115	0.454	0.689	0.218	0.270	0.061	0.830	-0.054	-0.479	0.375	0.720	0.536	0.488	0.701	1	0.630	0.472
Eu_INA	0.045	0.088	0.557	0.065	0.001	-0.223	0.562	0.022	-0.305	0.269	0.577	0.581	0.163	0.453	0.630	1	0.240
F_Fusion	-0.012	0.287	0.290	0.102	0.094	0.126	0.393	-0.044	0.016	0.333	0.303	0.263	0.212	0.360	0.472	0.240	1
Fe_INA	0.353	0.409	0.660	0.434	0.181	0.083	0.670	0.197	-0.428	0.287	0.554	0.472	0.403	0.585	0.713	0.567	0.260
Ga_ICP	0.243	0.616	0.670	0.365	0.409	0.317	0.755	-0.115	-0.653	0.296	0.729	0.294	0.892	0.793	0.707	0.385	0.323
Hf_INA	-0.229	-0.230	-0.071	-0.252	-0.128	-0.238	0.100	-0.157	-0.494	-0.189	0.380	0.032	-0.204	0.060	0.074	0.167	-0.188
Hg_ICP	0.414	0.741	0.258	0.450	0.587	0.620	0.289	0.027	-0.416	0.135	0.243	-0.054	0.737	0.471	0.174	-0.110	0.104
K_ICP	0.213	0.410	0.288	0.199	0.266	0.089	0.597	0.065	-0.569	0.137	0.677	0.182	0.357	0.667	0.509	0.293	0.369
La_ICP	0.146	0.411	0.352	0.106	0.095	0.307	0.259	-0.050	-0.217	0.549	0.331	0.279	0.505	0.313	0.363	0.135	0.439
Lu_INA	-0.053	0.110	0.330	-0.060	0.032	-0.132	0.422	-0.071	-0.401	0.149	0.498	0.382	0.047	0.343	0.459	0.291	0.178
Mg_ICP	-0.295	-0.448	-0.408	-0.158	-0.283	-0.219	-0.552	0.015	0.967	-0.144	-0.766	-0.175	-0.554	-0.635	-0.474	-0.280	-0.027
Mn_ICP	0.264	0.054	0.404	0.176	-0.077	0.096	0.275	0.355	-0.149	0.520	0.241	0.757	0.039	0.182	0.372	0.401	0.183
Mo_ICP	0.209	0.320	0.049	0.395	0.130	0.230	0.092	0.134	0.086	0.511	0.014	0.017	0.128	0.194	0.104	-0.044	0.151
Na_ICP	0.161	0.389	-0.045	0.316	0.311	0.063	0.063	0.122	0.197	-0.005	-0.093	-0.084	0.099	0.167	-0.003	-0.088	0.142
Ni_ICP	0.139	0.319	0.674	0.192	0.134	0.131	0.499	-0.014	-0.308	0.697	0.455	0.888	0.394	0.460	0.608	0.541	0.313
P_ICP	0.429	0.769	0.234	0.427	0.562	0.674	0.244	0.063	-0.409	0.202	0.245	-0.067	0.733	0.396	0.187	-0.154	0.139
Pb_ICP	0.040	0.412	0.571	0.299	0.199	0.055	0.637	-0.076	-0.026	0.305	0.387	0.348	0.379	0.536	0.692	0.432	0.492
Rb_INA	0.019	0.284	0.337	0.090	0.210	-0.119	0.704	-0.115	-0.731	0.084	0.901	0.249	0.312	0.780	0.586	0.507	0.182
S_ICP	0.421	0.337	0.391	0.213	0.150	-0.014	0.282	0.334	-0.152	0.154	0.126	0.111	0.189	0.241	0.293	0.178	0.089
Sb_ICP	0.083	0.511	0.221	0.273	0.174	0.323	0.349	-0.045	-0.171	0.569	0.341	0.150	0.300	0.352	0.440	0.120	0.484
Sc_ICP	0.144	0.408	0.906	0.184	0.161	0.027	0.630	-0.029	-0.323	0.349	0.512	0.501	0.441	0.545	0.741	0.552	0.346
Se_ICP	0.403	0.690	0.162	0.586	0.479	0.441	0.264	0.168	-0.225	0.320	0.184	-0.045	0.488	0.432	0.172	-0.088	0.138
Sm_INA	0.025	0.278	0.606	0.066	0.130	-0.123	0.766	-0.101	-0.676	0.299	0.900	0.577	0.333	0.727	0.775	0.721	0.301
Sn_Fusion	0.020	0.199	0.340	0.063	0.162	-0.148	0.668	-0.090	-0.522	0.075	0.726	0.263	0.252	0.651	0.564	0.447	0.229
Sr_ICP	-0.089	0.132	-0.130	0.025	-0.044	0.254	-0.231	-0.032	0.539	0.398	-0.294	-0.116	-0.029	-0.192	-0.155	-0.248	0.300
Ta_INA	0.005	0.507	0.297	0.102	0.458	0.150	0.571	-0.257	-0.806	0.023	0.805	0.125	0.526	0.720	0.463	0.314	0.065
Tb_INA	0.017	0.158	0.616	-0.007	0.048	-0.196	0.610	-0.055	-0.509	0.336	0.691	0.677	0.185	0.527	0.710	0.707	0.245
Te_ICP	0.099	0.410	0.118	0.549	0.325	0.245	0.332	-0.084	-0.091	0.047	0.133	-0.041	0.393	0.348	0.109	0.004	0.096
Th_ICP	0.112	0.756	0.376	0.385	0.571	0.543	0.528	-0.253	-0.515	0.181	0.505	0.022	0.834	0.664	0.367	0.023	0.235
Ti_ICP	-0.069	-0.042	0.068	-0.078	-0.060	-0.079	0.073	-0.012	-0.061	0.093	0.102	0.044	0.067	0.030	0.325	0.119	0.173
Tl_ICP	0.197	0.175	0.074	0.260	-0.024	0.200	0.073	0.083	-0.043	0.425	0.067	-0.011	0.196	0.200	0.025	-0.046	0.054
U_ICP	0.329	0.243	0.395	0.141	0.064	0.068	0.242	0.245	-0.086	0.497	0.162	0.381	0.148	0.221	0.367	0.224	0.227
V_ICP	0.282	0.701	0.463	0.449	0.426	0.505	0.480	-0.099	-0.480	0.334	0.468	0.088	0.882	0.603	0.488	0.112	0.273
Yb_INA	-0.026	0.041	0.462	-0.070	0.004	-0.313	0.560	-0.039	-0.496	0.153	0.685	0.526	0.053	0.483	0.609	0.683	0.141
Zn_ICP	0.217	0.413	0.718	0.240	0.173	0.187	0.488	0.056	-0.295	0.696	0.432	0.788	0.450	0.460	0.659	0.560	0.354

Table 9 Multivariate Statistical Summary (Part 2)

	F Fusion	Fe INA	Ga ICP	Hf INA	Hg ICP	K ICP	La ICP	Lu INA	Mg ICP	Mn ICP	Mo ICP	Na ICP	Ni ICP	P ICP	Pb ICP	Rb INA
LOI_Grav	-0.012	0.353	0.243	-0.229	0.414	0.213	0.146	-0.053	-0.295	0.264	0.209	0.161	0.139	0.429	0.040	0.019
Ag_ICP	0.287	0.409	0.616	-0.230	0.741	0.410	0.411	0.110	-0.448	0.054	0.320	0.389	0.319	0.769	0.412	0.284
Al_ICP	0.290	0.660	0.670	-0.071	0.258	0.288	0.352	0.330	-0.408	0.404	0.049	-0.045	0.674	0.234	0.571	0.337
As_ICP	0.102	0.434	0.365	-0.252	0.450	0.199	0.106	-0.060	-0.158	0.176	0.395	0.316	0.192	0.427	0.299	0.090
Au_INA	0.094	0.181	0.409	-0.128	0.587	0.266	0.095	0.032	-0.283	-0.077	0.130	0.311	0.134	0.562	0.199	0.210
Ba_ICP	0.126	0.083	0.317	-0.238	0.620	0.089	0.307	-0.132	-0.219	0.096	0.230	0.063	0.131	0.674	0.055	-0.119
Bi_ICP	0.393	0.670	0.755	0.100	0.289	0.597	0.259	0.422	-0.552	0.275	0.092	0.063	0.499	0.244	0.637	0.704
Br_INA	-0.044	0.197	-0.115	-0.157	0.027	0.065	-0.050	-0.071	0.015	0.355	0.134	0.122	-0.014	0.063	-0.076	-0.115
Ca_ICP	0.016	-0.428	-0.653	-0.494	-0.416	-0.569	-0.217	-0.401	0.967	-0.149	0.086	0.197	-0.308	-0.409	-0.026	-0.731
Cd_ICP	0.333	0.287	0.296	-0.189	0.135	0.137	0.549	0.149	-0.144	0.520	0.511	-0.005	0.697	0.202	0.305	0.084
Ce_INA	0.303	0.554	0.729	0.380	0.243	0.677	0.331	0.498	-0.766	0.241	0.014	-0.093	0.455	0.245	0.387	0.901
Co_ICP	0.263	0.472	0.294	0.032	-0.054	0.182	0.279	0.382	-0.175	0.757	0.017	-0.084	0.888	-0.067	0.348	0.249
Cr_ICP	0.212	0.403	0.892	-0.204	0.737	0.357	0.505	0.047	-0.554	0.039	0.128	0.099	0.394	0.733	0.379	0.312
Cs_INA	0.360	0.585	0.793	0.060	0.471	0.667	0.313	0.343	-0.635	0.182	0.194	0.167	0.460	0.396	0.536	0.780
Cu_ICP	0.472	0.713	0.707	0.074	0.174	0.509	0.363	0.459	-0.474	0.372	0.104	-0.003	0.608	0.187	0.692	0.586
Eu_INA	0.240	0.567	0.385	0.167	-0.110	0.293	0.135	0.291	-0.280	0.401	-0.044	-0.088	0.541	-0.154	0.432	0.507
F_Fusion	1	0.260	0.323	-0.188	0.104	0.369	0.439	0.178	-0.027	0.183	0.151	0.142	0.313	0.139	0.492	0.182
Fe_INA	0.260	1	0.548	-0.035	0.204	0.344	0.198	0.333	-0.427	0.496	0.211	0.074	0.491	0.201	0.552	0.416
Ga_ICP	0.323	0.548	1	-0.021	0.586	0.522	0.522	0.265	-0.650	0.214	0.066	0.009	0.528	0.560	0.492	0.529
Hf_INA	-0.188	-0.035	-0.021	1	-0.295	0.301	-0.135	0.430	-0.451	0.001	-0.290	-0.367	-0.076	-0.267	-0.266	0.530
Hg_ICP	0.104	0.204	0.586	-0.295	1	0.217	0.323	-0.098	-0.433	0.003	0.163	0.210	0.230	0.808	0.131	0.088
K_ICP	0.369	0.344	0.522	0.301	0.217	1	0.290	0.418	-0.565	0.173	0.098	0.212	0.237	0.273	0.243	0.737
La_ICP	0.439	0.198	0.522	-0.135	0.323	0.290	1	0.095	-0.292	0.244	0.119	-0.063	0.423	0.463	0.327	0.113
Lu_INA	0.178	0.333	0.265	0.430	-0.098	0.418	0.095	1	-0.383	0.249	-0.137	-0.144	0.359	-0.045	0.177	0.513
Mg_ICP	-0.027	-0.427	-0.650	-0.451	-0.433	-0.565	-0.292	-0.383	1	-0.156	0.015	0.213	-0.319	-0.459	-0.032	-0.718
Mn_ICP	0.183	0.496	0.214	0.001	0.003	0.173	0.244	0.249	-0.156	1	0.098	-0.087	0.666	-0.027	0.222	0.169
Mo_ICP	0.151	0.211	0.066	-0.290	0.163	0.098	0.119	-0.137	0.015	0.098	1	0.370	0.180	0.178	0.189	-0.006
Na_ICP	0.142	0.074	0.009	-0.367	0.210	0.212	-0.063	-0.144	0.213	-0.087	0.370	1	-0.036	0.193	0.177	-0.094
Ni_ICP	0.313	0.491	0.528	-0.076	0.230	0.237	0.423	0.359	-0.319	0.666	0.180	-0.036	1	0.194	0.406	0.289
P_ICP	0.139	0.201	0.560	-0.267	0.808	0.273	0.463	-0.045	-0.459	-0.027	0.178	0.193	0.194	1	0.099	0.042
Pb_ICP	0.492	0.552	0.492	-0.266	0.131	0.243	0.327	0.177	-0.032	0.222	0.189	0.177	0.406	0.099	1	0.230
Rb_INA	0.182	0.416	0.529	0.530	0.088	0.737	0.113	0.513	-0.718	0.169	-0.006	-0.094	0.289	0.042	0.230	1
S_ICP	0.089	0.424	0.190	-0.170	0.201	0.177	-0.025	0.043	-0.175	0.055	0.316	0.325	0.143	0.180	0.293	0.080
Sb_ICP	0.484	0.339	0.333	-0.078	0.214	0.276	0.479	0.146	-0.278	0.127	0.438	0.076	0.287	0.341	0.405	0.220
Sc_ICP	0.346	0.721	0.561	-0.064	0.139	0.302	0.267	0.328	-0.337	0.325	0.105	-0.025	0.555	0.139	0.667	0.357
Se_ICP	0.138	0.252	0.382	-0.315	0.640	0.306	0.193	-0.032	-0.247	0.066	0.627	0.511	0.189	0.594	0.163	0.113
Sm_INA	0.301	0.603	0.594	0.436	0.034	0.600	0.286	0.629	-0.666	0.394	-0.066	-0.184	0.605	0.030	0.398	0.853
Sn_Fusion	0.229	0.392	0.461	0.348	0.030	0.541	0.112	0.456	-0.507	0.186	-0.036	-0.112	0.282	0.000	0.326	0.751
Sr_ICP	0.300	-0.185	-0.183	-0.435	-0.032	-0.193	0.292	-0.244	0.378	-0.080	0.367	0.174	-0.046	0.131	0.116	-0.378
Ta_INA	0.065	0.299	0.611	0.477	0.394	0.577	0.179	0.419	-0.792	0.010	-0.088	-0.076	0.254	0.381	0.108	0.797
Tb_INA	0.245	0.604	0.438	0.396	-0.063	0.423	0.211	0.684	-0.490	0.453	-0.093	-0.187	0.671	-0.079	0.366	0.650
Te_ICP	0.096	0.137	0.303	-0.252	0.441	0.183	0.081	-0.096	-0.059	-0.027	0.219	0.387	0.107	0.318	0.210	0.074
Th_ICP	0.235	0.263	0.724	-0.115	0.728	0.462	0.497	0.126	-0.548	-0.031	0.177	0.207	0.309	0.743	0.261	0.333
Ti_ICP	0.173	0.058	0.207	0.116	-0.158	0.214	0.294	0.058	-0.042	0.047	-0.055	-0.083	0.007	-0.082	0.267	0.118
Tl_ICP	0.054	0.098	0.170	-0.155	0.242	0.090	0.179	-0.109	-0.087	0.078	0.676	0.088	0.162	0.088	0.102	0.070
U_ICP	0.227	0.416	0.203	-0.158	0.150	0.124	0.171	0.217	-0.145	0.287	0.498	0.051	0.457	0.145	0.243	0.103
V_ICP	0.273	0.387	0.833	-0.213	0.682	0.355	0.622	0.028	-0.506	0.071	0.275	0.133	0.379	0.716	0.385	0.238
Yb_INA	0.141	0.506	0.340	0.567	-0.196	0.466	0.028	0.658	-0.459	0.358	-0.140	-0.171	0.452	-0.215	0.277	0.720
Zn_ICP	0.354	0.618	0.571	-0.151	0.292	0.216	0.502	0.291	-0.318	0.588	0.192	-0.004	0.869	0.260	0.523	0.243

Table 10 Multivariate Statistical Summary (Part 3)

	S ICP	Sb ICP	Sc ICP	Se ICP	Sm INA	Sn Fusion	Sr ICP	Ta INA	Tb INA	Te ICP	Th ICP	Ti ICP	Tl ICP	U ICP	V ICP	Yb INA	Zn ICP
LOI_Grav	0.421	0.083	0.144	0.403	0.025	0.020	-0.089	0.005	0.017	0.099	0.112	-0.069	0.197	0.329	0.282	-0.026	0.217
Ag_ICP	0.337	0.511	0.408	0.690	0.278	0.199	0.132	0.507	0.158	0.410	0.756	-0.042	0.175	0.243	0.701	0.041	0.413
Al_ICP	0.391	0.221	0.906	0.162	0.606	0.340	-0.130	0.297	0.616	0.118	0.376	0.068	0.074	0.395	0.463	0.462	0.718
As_ICP	0.213	0.273	0.184	0.586	0.066	0.063	0.025	0.102	-0.007	0.549	0.385	-0.078	0.260	0.141	0.449	-0.070	0.240
Au_INA	0.150	0.174	0.161	0.479	0.130	0.162	-0.044	0.458	0.048	0.325	0.571	-0.060	-0.024	0.064	0.426	0.004	0.173
Ba_ICP	-0.014	0.323	0.027	0.441	-0.123	-0.148	0.254	0.150	-0.196	0.245	0.543	-0.079	0.200	0.068	0.505	-0.313	0.187
Bi_ICP	0.282	0.349	0.630	0.264	0.766	0.668	-0.231	0.571	0.610	0.332	0.528	0.073	0.073	0.242	0.480	0.560	0.488
Br_INA	0.334	-0.045	-0.029	0.168	-0.101	-0.090	-0.032	-0.257	-0.055	-0.084	-0.253	-0.012	0.083	0.245	-0.099	-0.039	0.056
Ca_ICP	-0.152	-0.171	-0.323	-0.225	-0.676	-0.522	0.539	-0.806	-0.509	-0.091	-0.515	-0.061	-0.043	-0.086	-0.480	-0.496	-0.295
Cd_ICP	0.154	0.569	0.349	0.320	0.299	0.075	0.398	0.023	0.336	0.047	0.181	0.093	0.425	0.497	0.334	0.153	0.696
Ce_INA	0.126	0.341	0.512	0.184	0.900	0.726	-0.294	0.805	0.691	0.133	0.505	0.102	0.067	0.162	0.468	0.685	0.432
Co_ICP	0.111	0.150	0.501	-0.045	0.577	0.263	-0.116	0.125	0.677	-0.041	0.022	0.044	-0.011	0.381	0.088	0.526	0.788
Cr_ICP	0.189	0.300	0.441	0.488	0.333	0.252	-0.029	0.526	0.185	0.393	0.834	0.067	0.196	0.148	0.882	0.053	0.450
Cs_INA	0.241	0.352	0.545	0.432	0.727	0.651	-0.192	0.720	0.527	0.348	0.664	0.030	0.200	0.221	0.603	0.483	0.460
Cu_ICP	0.293	0.440	0.741	0.172	0.775	0.564	-0.155	0.463	0.710	0.109	0.367	0.325	0.025	0.367	0.488	0.609	0.659
Eu_INA	0.178	0.120	0.552	-0.088	0.721	0.447	-0.248	0.314	0.707	0.004	0.023	0.119	-0.046	0.224	0.112	0.683	0.560
F_Fusion	0.089	0.484	0.346	0.138	0.301	0.229	0.300	0.065	0.245	0.096	0.235	0.173	0.054	0.227	0.273	0.141	0.354
Fe_INA	0.424	0.339	0.721	0.252	0.603	0.392	-0.185	0.299	0.604	0.137	0.263	0.058	0.098	0.416	0.387	0.506	0.618
Ga_ICP	0.190	0.333	0.561	0.382	0.594	0.461	-0.183	0.611	0.438	0.303	0.724	0.207	0.170	0.203	0.833	0.340	0.571
Hf_INA	-0.170	-0.078	-0.064	-0.315	0.436	0.348	-0.435	0.477	0.396	-0.252	-0.115	0.116	-0.155	-0.158	-0.213	0.567	-0.151
Hg_ICP	0.201	0.214	0.139	0.640	0.034	0.030	-0.032	0.394	-0.063	0.441	0.728	-0.158	0.242	0.150	0.682	-0.196	0.292
K_ICP	0.177	0.276	0.302	0.306	0.600	0.541	-0.193	0.577	0.423	0.183	0.462	0.214	0.090	0.124	0.355	0.466	0.216
La_ICP	-0.025	0.479	0.267	0.193	0.286	0.112	0.292	0.179	0.211	0.081	0.497	0.294	0.179	0.171	0.622	0.028	0.502
Lu_INA	0.043	0.146	0.328	-0.032	0.629	0.456	-0.244	0.419	0.684	-0.096	0.126	0.058	-0.109	0.217	0.028	0.658	0.291
Mg_ICP	-0.175	-0.278	-0.337	-0.247	-0.666	-0.507	0.378	-0.792	-0.490	-0.059	-0.548	-0.042	-0.087	-0.145	-0.506	-0.459	-0.318
Mn_ICP	0.055	0.127	0.325	0.066	0.394	0.186	-0.080	0.010	0.453	-0.027	-0.031	0.047	0.078	0.287	0.071	0.358	0.588
Mo_ICP	0.316	0.438	0.105	0.627	-0.066	-0.036	0.367	-0.088	-0.093	0.219	0.177	-0.055	0.676	0.498	0.275	-0.140	0.192
Na_ICP	0.325	0.076	-0.025	0.511	-0.184	-0.112	0.174	-0.076	-0.187	0.387	0.207	-0.083	0.088	0.051	0.133	-0.171	-0.004
Ni_ICP	0.143	0.287	0.555	0.189	0.605	0.282	-0.046	0.254	0.671	0.107	0.309	0.007	0.162	0.457	0.379	0.452	0.869
P_ICP	0.180	0.341	0.139	0.594	0.030	0.000	0.131	0.381	-0.079	0.318	0.743	-0.082	0.088	0.145	0.716	-0.215	0.260
Pb_ICP	0.293	0.405	0.667	0.163	0.398	0.326	0.116	0.108	0.366	0.210	0.261	0.267	0.102	0.243	0.385	0.277	0.523
Rb_INA	0.080	0.220	0.357	0.113	0.853	0.751	-0.378	0.797	0.650	0.074	0.333	0.118	0.070	0.103	0.238	0.720	0.243
S_ICP	1	0.176	0.451	0.373	0.114	0.083	0.025	0.017	0.119	0.192	0.165	-0.047	0.138	0.591	0.139	0.081	0.205
Sb_ICP	0.176	1	0.297	0.311	0.286	0.188	0.488	0.218	0.199	0.086	0.321	0.122	0.293	0.330	0.402	0.094	0.368
Sc_ICP	0.451	0.297	1	0.123	0.593	0.379	-0.068	0.250	0.583	0.075	0.313	0.102	0.073	0.399	0.367	0.468	0.603
Se_ICP	0.373	0.311	0.123	1	0.002	0.011	0.150	0.207	-0.092	0.556	0.574	-0.121	0.456	0.337	0.532	-0.156	0.232
Sm_INA	0.114	0.286	0.593	0.002	1	0.728	-0.333	0.681	0.905	-0.007	0.286	0.131	-0.015	0.245	0.276	0.842	0.561
Sn_Fusion	0.083	0.188	0.379	0.011	0.728	1	-0.319	0.579	0.588	0.024	0.229	0.089	0.030	0.115	0.178	0.640	0.233
Sr_ICP	0.025	0.488	-0.068	0.150	-0.333	-0.319	1	-0.351	-0.318	0.076	0.058	-0.028	0.152	0.176	0.033	-0.416	-0.001
Ta_INA	0.017	0.218	0.250	0.207	0.681	0.579	-0.351	1	0.516	0.137	0.568	0.025	-0.031	0.004	0.422	0.533	0.236
Tb_INA	0.119	0.199	0.583	-0.092	0.905	0.588	-0.318	0.516	1	-0.096	0.116	0.089	-0.076	0.329	0.132	0.866	0.635
Te_ICP	0.192	0.086	0.075	0.556	-0.007	0.024	0.076	0.137	-0.096	1	0.504	-0.142	0.151	0.026	0.340	-0.124	0.114
Th_ICP	0.165	0.321	0.313	0.574	0.286	0.229	0.058	0.568	0.116	0.504	1	-0.027	0.193	0.131	0.751	-0.013	0.326
Ti_ICP	-0.047	0.122	0.102	-0.121	0.131	0.089	-0.028	0.025	0.089	-0.142	-0.027	1	-0.041	-0.019	0.253	0.122	0.135
Tl_ICP	0.138	0.293	0.073	0.456	-0.015	0.030	0.152	-0.031	-0.076	0.151	0.193	-0.041	1	0.304	0.278	-0.104	0.156
U_ICP	0.591	0.330	0.399	0.337	0.245	0.115	0.176	0.004	0.329	0.026	0.131	-0.019	0.304	1	0.190	0.202	0.481
V_ICP	0.139	0.402	0.367	0.532	0.276	0.178	0.033	0.422	0.132	0.340	0.751	0.253	0.278	0.190	1	0.006	0.471
Yb_INA	0.081	0.094	0.468	-0.156	0.842	0.640	-0.416	0.533	0.866	-0.124	-0.013	0.122	-0.104	0.202	0.006	1	0.423
Zn_ICP	0.205	0.368	0.603	0.232	0.561	0.233	-0.001	0.236	0.635	0.114	0.326	0.135	0.156	0.481	0.471	0.423	1

9.3 Principal Component Analysis

Principal component analysis (PCA) is a statistical technique used to analyze large multivariable data sets. The objective of PCA in examining geochemical data is to reduce the number of variables (elemental analyses) necessary to describe the response by grouping them into a smaller number of linear combinations. These linear combinations (principal components) are frequently found to reflect underlying physical features and processes such as bedrock lithology, surficial geology, bedrock alteration and, where present, mineralizing systems. Each sample response in a data set can be expressed as a combination of the principal components in varying proportions. The broad pattern of the principal components over the entire survey area together with the factor components can yield insight into the physical significance of the principal component in question. In analyzing geochemical data sets in areas where economic mineralization is present, it is frequently found that one or more of the principal components are spatially associated with the mineralizing system and have areal distributions which reflect the location and extent of the mineralizing system. The application of PCA to mineral exploration is more fully described in Grunsky (2007).

The assumptions underlying PCA require near-normally distributed variables in order to yield meaningful results. If variables are highly skewed or left censored, the components will be noisy and erratic (Grunsky, 2010, pers. comm.). To mitigate this problem, elements selected for PCA were those which were not left censored and which had means at least five times their detection limits. This set included: Ag, Al, As, Ba, Br, Ca, Co, Cr, Cu, F, Fe, Hf, Hg, La, Mg, Mo, Mn, Na, Ni, P, Pb, Rb, Sb, Sc, Se, Sm, Sr, Th, U, V and Zn. The elements were logarithmically (base 10) transformed prior to analysis and samples with missing analyses for a given element were removed from the data set.

The relative contributions of each factor to the overall geochemical response are depicted in Figure 3. Most of the observed geochemical response in all elements can be attributed to PCA Factors F1 through F3 as shown below. PCA factors are

summarized in Table 11 showing the percent contribution of each element to the factor response. Table 12 shows the factor loading for each element.

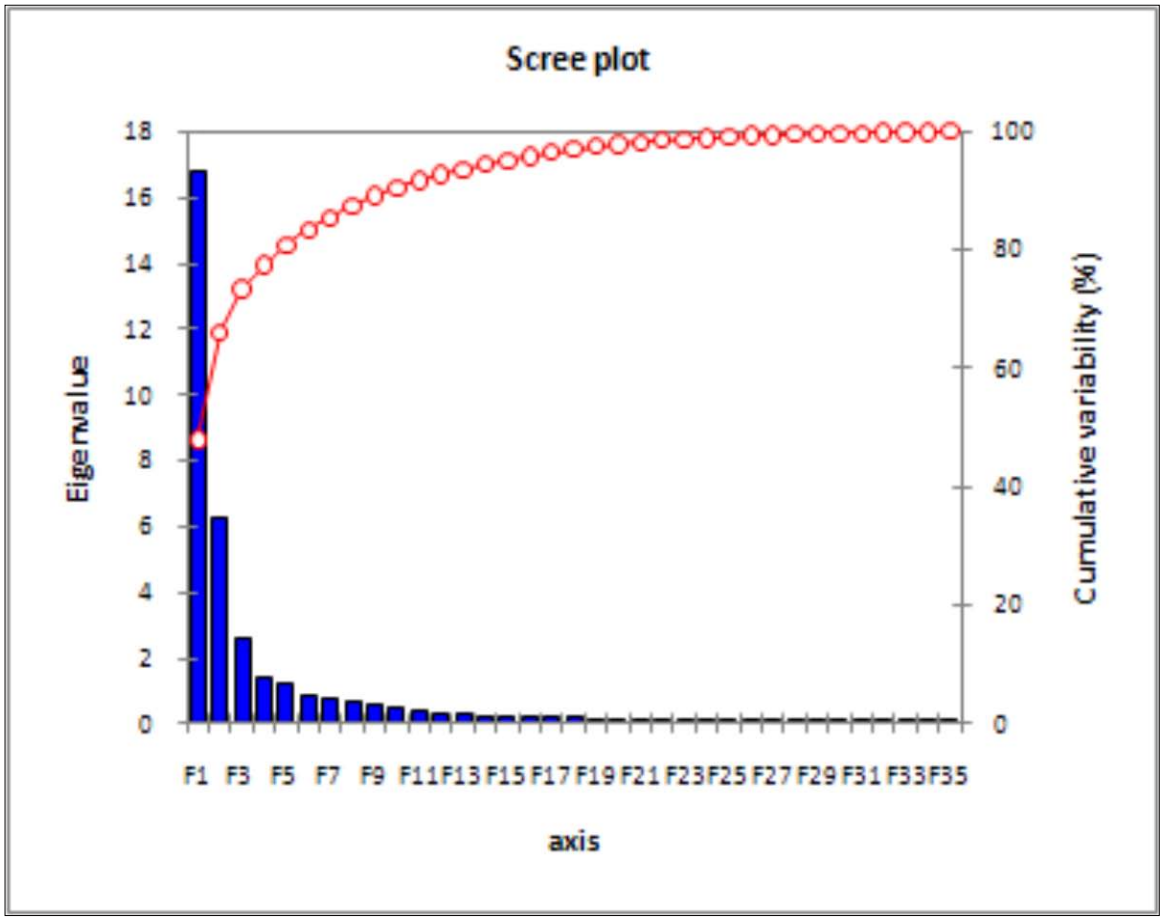


Figure 3 Contributions of the PCA factors to the total geochemical response. Factors F1 through F3 account for about 78% of the observed geochemical response.

Table 13 shows the factor associations for elements of principal economic interest which were analyzed by PCA. These include Ag, Cu, Pb and Zn. Three associations of interest were examined: Pb-Zn-Ag (SEDEX association), Cu-Ag, and Cu (Redbed association). For each, a factor of interest was selected based on the following criteria:

1. **Highest score in cumulative percent rank (sum of percentage contributions of elements of interest).**

	F1	F2	F3	F4	F5	F6	F7	F8	F9	F10	F11	F12	F13	F14	F15	F16	F17	F18	F19	F20	F21	F22	F23	F24	F25	F26	F27	F28	F29	F30	F31	F32	F33	F34	F35
Ag_ICP	4.284	1.007	1.259	1.670	0.318	0.168	0.030	2.922	1.528	1.238	0.882	1.390	4.550	0.152	3.156	0.591	0.383	6.105	18.169	7.895	0.409	0.179	21.720	5.940	0.178	9.229	2.523	0.077	0.055	0.063	0.111	0.431	0.071	1.130	0.184
Al_ICP	5.285	0.160	0.144	0.011	0.789	2.704	0.730	0.031	0.037	2.632	0.003	0.432	2.428	1.281	0.835	0.065	0.136	0.288	0.011	0.086	0.861	2.976	0.132	0.318	14.816	1.283	8.594	0.581	2.924	12.039	3.798	3.843	4.585	1.313	23.850
As_ICP	1.992	2.950	0.012	5.075	3.327	5.973	0.357	14.976	0.133	23.016	5.927	0.510	2.304	2.514	3.655	3.453	11.397	0.123	1.855	1.252	4.188	0.177	0.017	1.583	1.530	0.479	0.001	0.324	0.428	0.170	0.009	0.137	0.086	0.067	0.001
Ba_ICP	1.945	2.554	7.365	3.104	2.081	5.216	0.053	2.581	1.651	3.789	3.553	2.904	3.161	1.520	25.647	9.766	9.280	1.034	0.045	4.173	3.800	2.000	0.308	0.162	0.001	0.000	0.007	2.043	0.141	0.016	0.022	0.004	0.063	0.010	0.000
Br_INA	0.537	0.081	9.569	10.931	11.848	0.260	35.351	1.543	2.404	3.822	4.043	0.223	0.337	5.067	1.739	0.174	0.644	0.004	0.017	1.204	0.000	0.005	3.021	0.319	1.053	0.425	3.662	0.053	0.971	0.011	0.078	0.006	0.180	0.417	0.000
Ca_ICP	1.110	8.038	1.622	11.149	0.511	0.318	0.283	5.068	1.135	1.264	0.098	1.249	0.062	3.496	2.548	0.183	0.248	4.083	0.120	2.660	1.339	0.225	0.732	0.959	2.062	0.771	0.322	0.358	0.438	3.977	0.435	1.210	4.157	31.476	6.292
Ce_INA	3.501	3.940	0.155	0.921	1.447	0.332	3.664	2.269	0.022	0.966	0.551	1.031	0.017	1.724	0.001	0.001	0.308	0.013	1.390	8.360	2.489	9.711	5.182	39.377	2.382	1.098	3.438	0.251	0.502	0.136	2.975	0.908	0.499	0.018	0.421
Co_ICP	3.739	0.815	7.159	0.632	2.745	0.453	4.061	0.273	2.977	1.226	0.015	0.176	0.038	0.598	0.011	1.298	1.404	1.080	0.003	2.213	0.619	0.721	1.479	0.110	0.079	0.260	2.534	14.215	0.111	7.820	0.444	28.705	7.468	3.011	1.506
Cr_ICP	4.754	0.539	2.436	0.027	0.428	3.529	0.112	0.110	0.984	1.899	0.160	0.425	4.655	0.144	1.075	0.093	0.012	3.101	0.125	0.135	0.003	5.816	0.140	0.315	2.345	0.548	0.382	2.183	2.095	42.316	0.012	2.193	15.374	1.006	0.530
Cs_INA	4.732	1.380	0.132	0.002	1.835	0.025	2.228	0.224	0.207	1.696	0.156	3.630	1.152	0.907	2.882	0.092	0.001	0.017	2.725	1.271	0.122	9.883	1.184	3.611	1.505	0.077	4.131	0.890	13.837	1.051	5.605	10.467	10.364	11.956	0.023
Cu_ICP	4.600	0.906	1.882	0.037	1.970	0.277	0.339	0.257	0.280	0.033	1.068	0.005	0.064	0.031	0.218	0.537	7.668	2.213	0.059	4.442	32.294	0.345	0.146	9.680	0.130	0.558	3.919	2.310	14.678	0.125	2.240	5.390	0.004	0.527	0.767
F_Fusion	1.008	1.325	5.657	4.530	10.098	0.134	16.741	22.462	5.355	3.552	0.032	10.221	5.447	1.338	4.276	0.693	3.188	1.415	1.313	0.229	0.005	0.397	0.367	0.000	0.006	0.003	0.044	0.000	0.035	0.005	0.032	0.001	0.000	0.092	0.000
Fe_INA	4.869	0.425	1.437	1.624	0.000	0.486	0.001	2.717	0.028	0.000	0.491	0.470	1.281	0.408	0.628	0.007	1.374	1.475	0.002	1.577	9.146	1.946	0.025	1.455	41.157	10.044	1.420	6.410	2.867	1.111	0.119	0.119	1.858	2.516	0.508
Ga_ICP	5.204	0.427	0.893	0.134	0.080	1.008	0.299	0.288	0.047	1.359	0.001	1.027	3.475	1.724	0.478	0.030	0.041	0.283	0.564	0.271	0.843	4.256	4.487	1.837	3.671	1.632	10.890	0.001	2.932	4.429	6.078	1.719	17.508	0.668	21.417
Hf_INA	0.659	9.331	1.083	4.915	0.467	1.825	0.667	8.207	0.437	0.054	0.071	0.558	0.220	10.567	1.746	2.016	0.144	2.061	36.219	0.508	7.613	0.118	0.985	0.811	0.836	0.007	2.203	0.425	0.178	0.238	3.616	0.201	0.764	0.203	0.045
Hg_ICP	1.986	2.506	3.808	0.605	7.058	0.239	2.460	3.414	11.200	2.532	5.304	38.472	1.990	0.012	2.633	7.783	0.540	2.082	0.006	2.808	0.104	0.318	1.068	0.004	0.001	0.128	0.303	0.550	0.041	0.000	0.000	0.020	0.000	0.024	0.001
La_ICP	2.468	1.030	0.014	12.454	6.651	0.007	5.970	2.860	10.236	1.402	1.832	0.053	28.076	0.254	0.606	0.278	0.046	6.487	0.392	4.274	1.263	1.926	0.610	0.692	0.000	1.886	2.567	2.736	0.845	0.780	1.010	0.003	0.077	0.087	0.128
Mg_ICP	1.491	6.551	2.925	11.774	0.110	0.064	0.084	4.158	1.109	0.969	0.077	1.644	0.656	5.611	1.273	0.486	0.466	1.607	0.104	0.171	0.910	0.005	4.389	3.264	2.102	0.489	6.446	0.009	0.027	4.001	2.385	1.579	3.611	22.995	6.462
Mn_ICP	1.739	0.630	12.620	1.341	11.657	0.137	0.170	2.277	4.463	10.423	0.042	1.291	3.944	8.525	3.451	0.029	0.556	6.692	0.005	3.375	2.581	8.640	1.943	3.423	0.556	0.131	0.465	6.539	0.014	0.331	0.491	1.371	0.042	0.048	0.060
Mo_ICP	0.889	6.776	2.154	2.966	0.356	8.064	0.321	8.747	5.538	0.129	7.525	4.804	4.762	18.946	1.633	3.899	0.591	3.249	8.041	4.785	0.033	0.040	0.267	0.005	1.621	1.398	0.506	0.130	1.094	0.395	0.003	0.040	0.049	0.007	0.235
Na_ICP	0.004	10.591	0.021	0.815	6.267	3.330	0.306	1.835	1.544	6.540	2.450	7.301	0.005	1.946	11.294	29.163	3.552	4.564	0.042	1.842	0.578	1.454	0.126	0.603	0.051	0.547	0.600	0.131	0.506	0.062	0.001	0.016	0.400	1.124	0.391
Ni_ICP	4.891	0.119	0.795	0.246	3.887	0.074	4.636	0.059	0.979	0.033	0.144	0.281	1.596	0.113	0.573	0.087	3.453	5.566	0.191	6.010	0.031	0.258	3.493	0.030	1.942	1.619	2.917	6.325	5.775	4.600	1.715	8.815	23.483	3.135	2.132
P_ICP	3.329	1.684	7.495	0.026	2.015	0.067	0.874	0.205	0.770	0.003	0.935	2.392	0.186	3.996	0.435	1.087	0.228	14.648	4.198	5.817	0.079	1.350	5.064	8.707	1.303	26.462	0.628	0.127	0.178	0.927	0.779	0.031	1.547	2.102	0.325
Pb_ICP	1.830	2.227	6.986	0.350	9.698	11.635	0.352	1.244	3.582	0.428	0.292	11.908	1.765	5.034	9.438	3.856	0.210	0.001	2.748	0.144	0.636	2.497	8.812	0.085	0.043	4.945	1.769	4.503	0.167	0.625	0.148	0.005	1.367	0.531	0.139
Rb_INA	2.838	6.278	0.121	0.112	2.219	0.973	3.156	1.704	0.556	0.921	0.135	1.671	0.055	0.291	2.717	0.080	0.165	1.400	1.320	1.412	1.417	2.655	0.271	5.369	0.001	0.000	2.436	5.669	1.295	0.835	1.248	26.654	2.491	10.068	11.466
S_ICP	2.890	1.267	0.295	5.863	2.130	3.294	1.727	1.258	5.260	7.073	22.264	0.847	16.245	0.045	11.821	5.469	2.610	0.491	0.062	0.547	0.504	4.478	0.149	1.470	0.090	0.095	0.012	0.147	0.859	0.008	0.412	0.038	0.003	0.210	0.066
Sb_ICP	2.959	0.216	0.912	0.032	2.236	23.000	0.022	0.174	14.803	10.793	8.570	0.000	0.731	4.624	0.360	3.564	6.317	0.516	12.176	0.124	4.735	0.127	0.063	0.414	0.663	0.787	0.271	0.129	0.194	0.000	0.000	0.090	0.323	0.006	0.069
Sc_ICP	4.686	0.025	3.249	0.027	0.725	1.691	1.051	0.437	0.193	2.157	0.020	0.448	0.058	0.015	0.024	3.064	1.319	7.274	0.488	4.663	3.919	25.438	2.712	1.237	3.874	0.243	0.403	8.888	11.455	0.972	5.016	1.899	0.330	0.104	1.895
Se_ICP	1.706	3.942	3.693	7.361	0.018	0.006	4.054	0.246	10.241	0.702	10.141	0.879	2.575	7.820	0.009	10.753	30.598	0.002	0.238	0.064	1.483	1.094	0.564	0.089	1.107	0.029	0.065	0.051	0.006	0.059	0.007	0.106	0.218	0.063	0.011
Sm_INA	3.366	5.649	0.182	1.050	0.882	0.288	0.766	0.595	0.567	0.484	0.033	1.258	0.258	0.008	0.164	0.017	0.368	0.234	0.018	0.703	0.003	3.132	0.118	0.956	0.718	0.334	0.002	1.005	0.006	1.198	52.894	3.243	0.186	0.255	19.065
Sr_ICP	0.011	13.253	0.034	3.655	0.142	2.325	0.011	1.152	0.426	1.253	0.003	0.160	0.146	2.240	1.135	0.247	0.014	1.193	0.919	12.068	5.728	0.007	6.465	4.456	4.522	22.207	9.589	0.072	2.205	0.092	0.277	0.182	0.396	3.190	0.225
Th_ICP	4.367	0.032	5.038	1.763	0.456	0.075	0.002	0.015	0.122	1.401	3.963	0.050	3.379	0.002	0.240	0.693	3.324	0.126	5.483	1.089	9.943	3.262	20.659	0.007	0.111	7.641	4.593	1.004	17.286	3.130	0.002	0.017	0.711	0.009	0.003
U_ICP	1.850	0.665	6.419	4.563	1.538	18.938	3.850	5.329	1.265	5.127	17.146	0.002	0.002	8.240	2.025	7.626	8.700	0.259	0.550	0.086	0.466	0.430	3.233	0.058	0.700	0.018	0.047	0.093	0.310	0.212	0.116	0.016	0.063	0.005	0.053
V_ICP	4.460	1.146	1.555	0.211	0.846	1.529	0.019	0.009	6.721	0.977	0.309	1.821	3.957	0.206	1.271	0.191	0.649	0.508	0.137	4.296	1.433	4.000	0.005	2.395	3.530	4.361	20.284	3.112	13.157	7.854	7.812	0.437	0.093	0.122	0.585
Zn_ICP	4.020	1.537	0.880	0.024	3.162	1.555	5.253	0.353	3.201	0.108	1.763	0.469	0.420	0.600	0.007	2.629	0.068	19.806	0.266	9.447	0.425	0.136	0.063	0.256	5.313	0.266	2.028	28.657	2.388	0.411	0.110	0.103	1.628	1.505	1.144

Table 11 Principal Component Analysis - Element Contributions

	F1	F2	F3	F4	F5	F6	F7	F8	F9	F10	F11	F12	F13	F14	F15	F16	F17	F18	F19	F20	F21	F22	F23	F24	F25	F26	F27	F28	F29	F30	F31	F32	F33	F34	F35
Ag_ICP	0.849	0.252	-0.180	-0.154	-0.062	0.038	0.015	0.143	0.095	0.078	0.059	0.068	0.121	0.020	0.090	0.037	0.029	-0.110	0.172	0.108	0.021	-0.013	0.138	0.065	-0.011	-0.077	-0.035	0.006	-0.005	0.004	-0.005	0.009	0.003	0.014	-0.005
Al_ICP	0.943	-0.100	0.061	0.013	0.098	-0.152	-0.074	0.015	-0.015	-0.114	0.004	-0.038	-0.088	-0.058	-0.046	-0.012	-0.017	-0.024	0.004	0.011	-0.031	0.055	-0.011	0.015	-0.098	-0.029	-0.065	-0.015	0.034	-0.055	0.030	-0.026	-0.028	0.015	0.055
As_ICP	0.579	0.431	-0.018	-0.268	-0.201	-0.226	0.052	-0.323	0.028	0.336	-0.154	-0.041	0.086	-0.082	-0.097	0.089	-0.157	0.016	-0.055	0.043	0.068	0.013	0.004	-0.034	-0.032	-0.018	-0.001	0.011	-0.013	0.007	0.001	-0.005	-0.004	-0.003	0.000
Ba_ICP	0.572	0.401	-0.435	0.210	0.159	0.211	-0.020	-0.134	-0.099	0.136	0.119	-0.099	-0.101	-0.063	0.256	-0.149	-0.142	0.045	0.009	-0.079	0.064	0.045	0.016	0.011	-0.001	0.000	-0.002	-0.029	-0.007	0.002	0.002	-0.001	-0.003	0.001	0.000
Br_INA	-0.301	-0.072	0.496	-0.394	0.379	-0.047	0.519	-0.104	0.119	-0.137	0.127	-0.027	-0.033	-0.116	0.067	-0.020	-0.037	0.003	-0.005	0.042	-0.001	0.002	0.052	-0.015	-0.026	0.017	0.043	-0.005	0.019	0.002	-0.004	0.001	0.005	-0.008	0.000
Ca_ICP	-0.432	0.712	0.204	0.398	0.079	0.052	0.046	-0.188	-0.082	-0.079	0.020	0.065	-0.014	-0.096	-0.081	-0.020	0.023	-0.090	-0.014	0.063	0.038	-0.015	0.025	-0.026	0.037	0.022	-0.013	0.012	-0.013	-0.032	-0.010	-0.015	-0.026	0.072	-0.028
Ce_INA	0.768	-0.499	-0.063	0.114	-0.132	0.053	0.167	-0.126	-0.011	-0.069	-0.047	0.059	0.007	0.068	-0.002	-0.001	-0.026	-0.005	-0.047	0.111	0.052	0.099	-0.068	0.168	0.039	0.027	0.041	0.010	0.014	0.006	-0.026	-0.013	-0.009	0.002	0.007
Co_ICP	0.793	-0.227	0.429	0.095	0.182	-0.062	-0.176	-0.044	-0.132	0.078	0.008	-0.024	0.011	0.040	-0.005	0.054	0.055	0.046	0.002	0.057	0.026	0.027	0.036	-0.009	0.007	0.013	0.035	-0.075	0.007	-0.044	-0.010	0.072	-0.035	-0.022	-0.014
Cr_ICP	0.895	0.184	-0.250	0.019	0.072	-0.174	-0.029	0.028	0.076	-0.097	-0.025	-0.038	-0.122	-0.020	-0.052	-0.015	0.005	-0.078	-0.014	-0.014	0.002	-0.076	-0.011	0.015	-0.039	0.019	0.014	-0.030	0.028	0.103	0.002	0.020	-0.051	0.013	-0.008
Cs_INA	0.893	-0.295	-0.058	0.005	-0.149	-0.015	0.130	-0.039	-0.035	-0.091	-0.025	0.110	-0.061	0.049	0.086	-0.014	-0.001	0.006	-0.066	0.043	-0.012	-0.100	0.032	-0.051	0.031	-0.007	-0.045	-0.019	-0.073	-0.016	-0.036	-0.043	-0.042	-0.045	-0.002
Cu_ICP	0.880	-0.239	0.220	0.023	-0.154	0.049	-0.051	0.042	-0.041	-0.013	0.065	0.004	0.014	-0.009	0.024	0.035	0.129	-0.066	0.010	-0.081	0.188	0.019	0.011	-0.083	0.009	-0.019	0.044	0.030	0.075	0.006	-0.023	-0.031	-0.001	-0.009	0.010
F_Fusion	0.412	0.289	0.381	0.253	-0.350	0.034	0.357	0.395	-0.178	0.132	-0.011	-0.185	-0.133	0.060	-0.105	-0.040	-0.083	0.053	0.046	0.018	-0.002	-0.020	0.018	0.000	0.002	0.001	0.005	0.000	0.004	-0.001	0.003	0.000	0.000	0.004	0.000
Fe_INA	0.905	-0.164	0.192	-0.152	0.002	-0.064	-0.003	-0.138	0.013	0.000	0.044	-0.040	-0.064	0.033	-0.040	0.004	-0.055	-0.054	0.002	-0.048	-0.100	0.044	-0.005	-0.032	0.164	-0.081	-0.027	-0.051	0.033	0.017	-0.005	-0.005	0.018	0.020	0.008
Ga_ICP	0.936	-0.164	-0.151	0.044	0.031	-0.093	0.048	-0.045	0.017	-0.082	-0.002	-0.059	-0.106	-0.068	-0.035	0.008	0.009	-0.024	-0.030	-0.020	0.030	-0.065	-0.063	0.036	-0.049	-0.032	-0.073	-0.001	0.034	-0.033	-0.038	0.018	0.054	-0.011	-0.052
Hf_INA	0.333	-0.767	-0.167	0.264	-0.075	0.125	0.071	-0.239	-0.051	0.016	0.017	-0.043	0.027	-0.167	-0.067	0.068	0.018	0.064	0.242	-0.027	-0.091	-0.011	-0.029	-0.024	-0.023	0.002	0.033	0.013	-0.008	0.008	-0.029	-0.006	-0.011	-0.006	0.002
Hg_ICP	0.578	0.398	-0.313	-0.093	0.292	-0.045	0.137	0.154	-0.257	0.111	0.146	0.360	-0.080	0.006	-0.082	0.133	-0.034	0.064	0.003	-0.064	-0.011	0.018	-0.031	0.002	-0.001	-0.009	0.012	0.015	0.004	0.000	0.000	0.002	0.000	0.002	0.000
La_ICP	0.645	0.255	-0.019	0.420	0.284	-0.008	0.213	0.141	0.246	-0.083	-0.086	-0.013	0.301	0.026	-0.039	0.025	-0.010	0.113	-0.025	-0.079	0.037	0.044	-0.023	-0.022	0.000	-0.035	-0.036	-0.033	-0.018	0.014	-0.015	0.001	-0.004	0.004	0.004
Mg_ICP	-0.501	0.643	0.274	0.409	-0.037	-0.023	0.025	-0.170	-0.081	-0.069	-0.018	0.074	-0.046	-0.122	-0.057	0.033	0.032	-0.056	0.013	-0.016	0.031	0.002	0.062	0.048	0.037	0.018	-0.057	0.002	0.003	0.032	0.024	0.017	0.025	-0.062	0.028
Mn_ICP	0.541	-0.199	0.569	0.138	0.376	-0.034	0.036	-0.126	-0.162	0.226	-0.013	-0.066	0.113	0.150	0.094	0.008	0.035	-0.115	-0.003	-0.071	-0.053	-0.093	-0.041	0.050	-0.019	0.009	-0.015	0.051	-0.002	0.009	0.011	-0.016	-0.003	0.003	0.003
Mo_ICP	0.387	0.654	0.235	-0.205	-0.066	0.262	0.049	-0.247	0.181	-0.025	-0.173	0.127	-0.124	0.224	-0.065	-0.094	0.036	0.080	0.114	-0.084	0.006	0.006	0.015	0.002	-0.032	0.030	-0.016	-0.007	0.021	-0.010	-0.001	0.003	-0.003	0.001	-0.005
Na_ICP	0.025	0.817	0.023	-0.107	-0.276	-0.169	0.048	-0.113	-0.095	-0.179	0.099	-0.157	-0.004	0.072	0.170	0.258	0.088	0.095	0.008	-0.052	-0.025	0.038	-0.011	0.021	-0.006	0.019	-0.017	0.007	-0.014	0.004	0.000	-0.002	-0.008	0.014	-0.007
Ni_ICP	0.907	0.087	0.143	0.059	0.217	-0.025	-0.188	-0.020	-0.076	0.013	-0.024	-0.031	-0.072	0.017	-0.038	0.014	0.087	0.105	-0.018	0.094	0.006	-0.016	0.055	-0.005	-0.036	0.032	0.038	-0.050	-0.047	0.034	-0.020	-0.040	0.063	0.023	0.016
P_ICP	0.749	0.326	-0.439	-0.019	0.156	0.024	0.082	0.038	0.067	-0.004	0.061	-0.090	0.025	0.103	-0.033	0.050	-0.022	-0.170	0.082	0.093	0.009	0.037	-0.067	-0.079	0.029	0.131	-0.018	-0.007	-0.008	-0.015	0.014	0.002	0.016	-0.019	0.006
Pb_ICP	0.555	0.375	0.423	0.070	-0.343	-0.315	-0.052	0.093	0.145	0.046	0.034	0.200	0.075	-0.115	0.155	-0.094	-0.021	-0.001	0.067	-0.015	-0.026	-0.050	-0.088	0.008	0.005	0.057	0.030	-0.042	0.008	-0.013	0.006	-0.001	0.015	0.009	0.004
Rb_INA	0.691	-0.629	-0.056	0.040	-0.164	0.091	0.155	-0.109	-0.057	-0.067	-0.023	0.075	-0.013	0.028	0.083	-0.014	0.019	0.053	-0.046	0.046	0.039	-0.052	-0.015	-0.062	0.001	0.000	-0.035	0.048	-0.022	0.014	0.017	0.069	0.020	0.041	0.038
S_ICP	0.697	0.283	0.087	-0.288	-0.161	0.168	-0.115	-0.094	-0.176	-0.186	0.298	-0.053	0.229	0.011	-0.174	-0.112	-0.075	0.031	-0.010	-0.028	0.023	-0.067	-0.011	0.032	-0.008	0.008	0.002	-0.008	-0.018	0.001	0.010	0.003	-0.001	-0.006	0.003
Sb_ICP	0.706	0.117	0.153	0.021	-0.165	0.443	0.013	0.035	0.295	0.230	0.185	0.001	-0.049	-0.111	-0.030	0.090	0.117	-0.032	-0.140	-0.014	-0.072	0.011	-0.007	0.017	-0.021	0.023	-0.012	-0.007	-0.009	0.000	0.000	0.004	-0.007	0.001	0.003
Sc_ICP	0.888	-0.040	0.289	0.020	-0.094	-0.120	-0.089	0.055	-0.034	-0.103	-0.009	0.039	-0.014	-0.006	-0.008	-0.084	-0.054	-0.120	-0.028	-0.083	-0.065	0.160	0.049	-0.030	-0.050	0.013	0.014	0.060	-0.066	0.016	-0.034	0.018	0.007	-0.004	-0.015
Se_ICP	0.536	0.499	-0.308	-0.323	0.015	0.007	0.176	0.041	-0.246	0.059	-0.201	-0.054	0.091	-0.144	0.005	-0.157	0.258	0.002	-0.020	-0.010	-0.040	0.033	-0.022	0.008	0.027	0.004	-0.006	-0.005	-0.002	-0.004	0.001	0.004	-0.006	-0.003	0.001
Sm_INA	0.753	-0.597	0.068	0.122	-0.103	0.050	0.076	-0.064	-0.058	-0.049	-0.011	0.065	0.029	0.004	0.020	0.006	0.028	0.022	-0.005	0.032	-0.002	0.056	0.010	-0.026	-0.022	-0.015	-0.001	-0.020	-0.001	0.017	0.111	-0.024	0.006	-0.006	-0.049
Sr_ICP	-0.044	0.914	-0.029	0.228	-0.042	0.141	0.009	-0.090	-0.050	-0.078	0.003	0.023	0.022	0.077	0.054	-0.024	-0.005	-0.049	-0.039	0.134	-0.079	-0.003	-0.075	-0.057	-0.054	-0.120	0.069	0.005	0.029	0.005	-0.008	0.006	0.008	-0.023	0.005
Th_ICP	0.857	0.045	-0.360	0.158	-0.074	0.025	0.004	-0.010	-0.027	-0.083	-0.126	0.013	0.104	-0.002	0.025	0.040	-0.085	0.016	-0.094	-0.040	-0.104	-0.057	0.135	0.002	0.008	0.070	0.048	0.020	0.082	-0.028	0.001	-0.002	0.011	0.001	0.001
U_ICP	0.558	0.205	0.406	-0.254	0.136	0.402	-0.171	0.193	-0.086	-0.159	-0.262	-0.002	-0.003	-0.148	0.072	0.132	-0.138	-0.023	0.030	0.011	0.023	-0.021	-0.053	0.006	0.021	0.003	-0.005	0.006	-0.011	0.007	0.005	-0.002	-0.003	0.001	-0.003
V_ICP	0.866	0.269	-0.200	0.055	0.101	-0.114	0.012	-0.008	0.199	-0.069	-0.035	-0.078	-0.113	-0.023	-0.057	0.021	0.038	-0.032	0.015	-0.080	0.040	-0.063	-0.002	0.041	0.048	-0.053	0.100	0.035	-0.071	-0.044	0.043	0.009	0.004	-0.004	0.009
Zn_ICP	0.823	0.311	0.150	0.018	0.196	-0.115	-0.200	0.050	0.137	0.023	0.084	-0.040	-0.037	-0.040	0.004	-0.077	0.012	0.198	0.021	0.118	-0.022	0.012	-0.007	-0.014	0.059	0.013	-0.032	0.107	0.030	0.010	0.005	-0.004	-0.016	-0.016	-0.012

Table 12 Principal Component Analysis - Factor Loading for Each Element.

2. **Positive correlation constants for elements of interest and**

3. **Roughly equal contribution to the cumulative percent rank by each of the elements in a multi-element set.**

	Percent contribution				Correlations				Associations		
Factor	Ag_ICP	Cu_ICP	Pb_ICP	Zn_ICP	Ag_ICP	Cu_ICP	Pb_ICP	Zn_ICP	Pb-Zn-Ag	Cu-Ag	Cu
F01	4.28	4.60	1.83	4.02	0.849	0.880	0.555	0.823	10.1	8.9	4.6
F02	1.01	0.91	2.23	1.54	0.252	-0.239	0.375	0.311	4.8	1.9	0.9
F03	1.26	1.88	6.99	0.88	-0.180	0.220	0.423	0.150	9.1	3.1	1.9
F04	1.67	0.04	0.35	0.02	-0.154	0.023	0.070	0.018	2.0	1.7	0.0
F05	0.32	1.97	9.70	3.16	-0.062	-0.154	-0.343	0.196	13.2	2.3	2.0
F06	0.17	0.28	11.64	1.56	0.038	0.049	-0.315	-0.115	13.4	0.4	0.3
F07	0.03	0.34	0.35	5.25	0.015	-0.051	-0.052	-0.200	5.6	0.4	0.3
F08	2.92	0.26	1.24	0.35	0.143	0.042	0.093	0.050	4.5	3.2	0.3
F09	1.53	0.28	3.58	3.20	0.095	-0.041	0.145	0.137	8.3	1.8	0.3
F10	1.24	0.03	0.43	0.11	0.078	-0.013	0.046	0.023	1.8	1.3	0.0
F11	0.88	1.07	0.29	1.76	0.059	0.065	0.034	0.084	2.9	2.0	1.1
F12	1.39	0.00	11.91	0.47	0.068	0.004	0.200	-0.040	13.8	1.4	0.0
F13	4.55	0.06	1.77	0.42	0.121	0.014	0.075	-0.037	6.7	4.6	0.1
F14	0.15	0.03	5.03	0.60	0.020	-0.009	-0.115	-0.040	5.8	0.2	0.0
F15	3.16	0.22	9.44	0.01	0.090	0.024	0.155	0.004	12.6	3.4	0.2
F16	0.59	0.54	3.86	2.63	0.037	0.035	-0.094	-0.077	7.1	1.1	0.5
F17	0.38	7.67	0.21	0.07	0.029	0.129	-0.021	0.012	0.7	8.1	7.7
F18	6.11	2.21	0.00	19.81	-0.110	-0.066	-0.001	0.198	25.9	8.3	2.2
F19	18.17	0.06	2.75	0.27	0.172	0.010	0.067	0.021	21.2	18.2	0.1
F20	7.89	4.44	0.14	9.45	0.108	-0.081	-0.015	0.118	17.5	12.3	4.4
F21	0.41	32.29	0.64	0.42	0.021	0.188	-0.026	-0.022	1.5	32.7	32.3
F22	0.18	0.35	2.50	0.14	-0.013	0.019	-0.050	0.012	2.8	0.5	0.3
F23	21.72	0.15	8.81	0.06	0.138	0.011	-0.088	-0.007	30.6	21.9	0.1
F24	5.94	9.68	0.08	0.26	0.065	-0.083	0.008	-0.014	6.3	15.6	9.7
F25	0.18	0.13	0.04	5.31	-0.011	0.009	0.005	0.059	5.5	0.3	0.1
F26	9.23	0.56	4.95	0.27	-0.077	-0.019	0.057	0.013	14.4	9.8	0.6
F27	2.52	3.92	1.77	2.03	-0.035	0.044	0.030	-0.032	6.3	6.4	3.9
F28	0.08	2.31	4.50	28.66	0.006	0.030	-0.042	0.107	33.2	2.4	2.3
F29	0.06	14.68	0.17	2.39	-0.005	0.075	0.008	0.030	2.6	14.7	14.7
F30	0.06	0.12	0.62	0.41	0.004	0.006	-0.013	0.010	1.1	0.2	0.1
F31	0.11	2.24	0.15	0.11	-0.005	-0.023	0.006	0.005	0.4	2.4	2.2
F32	0.43	5.39	0.00	0.10	0.009	-0.031	-0.001	-0.004	0.5	5.8	5.4
F33	0.07	0.00	1.37	1.63	0.003	-0.001	0.015	-0.016	3.1	0.1	0.0
F34	1.13	0.53	0.53	1.51	0.014	-0.009	0.009	-0.016	3.2	1.7	0.5
F35	0.18	0.77	0.14	1.14	-0.005	0.010	0.004	-0.012	1.5	1.0	0.8

Table 13 Factor Associations for Elements of Principal Economic Interest

Based on these criteria, Factor F1 was selected as the best overall copper factor, Factor F9 is the factor most sensitive to SEDEX deposit style element associations and Factor F21 would be associated with elevated copper alone.

F1 is the dominant copper-silver factor in the data set and is also the dominant overall PCA factor. It is likely determined by the underlying bedrock geology and reflects large scale regional lithogeochemical patterns. There are strong positive contributions to this factor by Ag, Cu, Co, Ni and Cr as well as from the REEs. The association of Cu, Co and Fe in this factor suggest it would be a suitable vector to both precious metal mineralization carrying copper and to sediment-hosted copper (redbed) mineralization. Factor F1 is also heavily loaded by the other base metals and a high response in this factor would also likely be associated with SEDEX style mineralization.

Factor F9 is characterized by modest positive Pb, Zn and Ag correlation in roughly equivalent proportions and thus is a vector to SEDEX style mineralization. It is interesting that Ba and Mn, commonly found with this style of mineralization, are not positively correlated with this factor. Either of factors F1 or F9 would be suitable vectors to SEDEX mineralization.

Factor F21 is a copper-only factor with associated subordinate As and Co responses. This factor might be a vector to sediment-hosted copper mineralization.

Finally, although gold was not included in the PCA because of the left censored nature of its distribution, there is an association between highly anomalous gold values and low factor F3 response. Factor F3 is dominated by strong positive contributions from Br, Pb, Mn and F, and negative contributions from Ag, Ba, P and Hg. Thus elevated gold values seem to correlate with the latter suite of elements.

10 Statistical Analysis of the Water Sample Data

10.1 Univariate Analysis

Statistical analysis in this report was performed with the XLSTAT^{TM} package unless otherwise stated. Univariate statistics for all elements are contained in Table 14. In this analysis, standard deviations are normalized by n-1, and both kurtosis and skewness are calculated using Pearson's equations. A normal distribution will show skewness and kurtosis of 0 with these measures. Percentile ranks are calculated for the 25th, median, 75th, 95th and 98th percentiles. Figure C (in appendix 3) contains, for each element, histograms, Box plots and Q-Q diagrams for the raw data, and histograms and cumulative probability plots for the logarithmic (base 10) data. The natural distributions of most elements which are not left censored show either negative or positive skew.

Table 14 below describes the Univariate statistics for each element analysed for in the water sampling survey.

Table 14 Univariate statistics for water sample, by element

Statistic	Li_w_ICP-MS	Be_w_ICP-MS	B_w_ICP-MS	Al_w_ICP-MS	Ti_w_ICP-MS	V_w_ICP-MS	Cr_w_ICP-MS
No. of observations	592	592	592	592	592	592	592
Analysis Method	ICP-MS	ICP-MS	ICP-MS	ICP-MS	ICP-MS	ICP-MS	ICP-MS
Detection Limit	0.02	0.005	0.5	2	0.5	0.1	0.1
Units	ppb	ppb	ppb	ppb	ppb	ppb	ppb
No. of missing values	0	0	0	0	0	0	0
Minimum	0.023	0.0025	0.25	1	0.25	0.05	0.05
Maximum	471.41	13.848	245	140753	5	10	29
Freq. of minimum	1	267	3	26	460	263	315
Freq. of maximum	1	1	1	1	6	1	1
Range	471.387	13.8455	244.75	140752	4.75	9.95	28.95
1st Quartile	0.6775	0.0025	3.425	7	0.25	0.05	0.05
Median	1.735	0.0061	6.405	20.85	0.25	0.115	0.05
3rd Quartile	5.64475	0.0151	10.53	67.275	0.25	0.22	0.24
95th Percentile	24.93	0.0368	39.42	229.4	1.34	0.42	0.46
98th Percentile	63.086	1.1778	87.73	5885.6	2.58	0.56	0.56
Mean	7.84	0.13	11.30	906.54	0.46	0.18	0.21
Standard deviation (n)	28.51	0.98	19.19	8404.29	0.62	0.46	1.22
Skew ness (Pearson)	10.62	10.89	5.65	13.38	4.95	17.81	22.46
Kurtosis (Pearson)	142.25	132.88	46.21	197.75	29.19	363.92	524.20

Statistic	Mn_w_ICP-MS	Co_w_ICP-MS	Ni_w_ICP-MS	Cu_w_ICP-MS	Zn_w_ICP-MS	Ga_w_ICP-MS	Ge_w_ICP-MS
No. of observations	592	592	592	592	592	592	592
Analysis Method	ICP-MS	ICP-MS	ICP-MS	ICP-MS	ICP-MS	ICP-MS	ICP-MS
Detection Limit	0.1	0.05	0.2	0.1	0.5	0.01	0.02
Units	ppb	ppb	ppb	ppb	ppb	ppb	ppb
No. of missing values	0	0	0	0	0	0	0
Minimum	0.05	0.025	0.1	0.05	0.25	0.005	0.01
Maximum	29273	944.09	1925	302	6211	0.16	0.145
Freq. of minimum	26	289	158	17	225	532	573
Freq. of maximum	1	1	1	1	1	1	1
Range	29272.95	944.065	1924.9	301.95	6210.75	0.155	0.135
1st Quartile	0.4	0.025	0.1	0.3	0.25	0.005	0.01
Median	3.365	0.053	1.03	0.69	0.67	0.005	0.01
3rd Quartile	13.6025	0.177	2.2525	1.9225	1.3675	0.005	0.01
95th Percentile	717.97	17.344	25.94	4.12	24.09	0.016	0.01
98th Percentile	2500.99	97.661	135.6	8.8	268.76	0.038	0.028
Mean	247.35	8.66	13.55	2.26	31.73	0.01	0.01
Standard deviation (n)	1754.50	60.05	101.14	13.53	309.59	0.01	0.01
Skew ness (Pearson)	11.86	11.09	13.98	19.20	15.96	9.38	8.13
Kurtosis (Pearson)	160.83	142.29	231.91	408.59	288.30	122.53	68.90

Statistic	As_w_ICP-MS	Se_w_ICP-MS	Rb_w_ICP-MS	Sr_w_ICP-MS	Y_w_ICP-MS	Zr_w_ICP-MS	Nb_w_ICP-MS
No. of observations	592	592	592	592	592	592	592
Analysis Method	ICP-MS	ICP-MS	ICP-MS	ICP-MS	ICP-MS	ICP-MS	ICP-MS
Detection Limit	0.1	1	0.05	0.5	0.01	0.05	0.01
Units	ppb	ppb	ppb	ppb	ppb	ppb	ppb
No. of missing values	0	0	0	0	0	0	0
Minimum	0.05	0.5	0.025	1.5	0.005	0.025	0.005
Maximum	3.6	11	14.47	2518.91	746.68	1.23	0.05
Freq. of minimum	262	560	19	1	93	331	581
Freq. of maximum	1	1	1	1	1	1	6
Range	3.55	10.5	14.445	2517.41	746.675	1.205	0.045
1st Quartile	0.05	0.5	0.135	22.25	0.017	0.025	0.005
Median	0.13	0.5	0.256	42.24	0.0685	0.025	0.005
3rd Quartile	0.31	0.5	0.38025	97.2125	0.26	0.16525	0.005
95th Percentile	0.58	1.2	0.838	272.15	0.851	0.357	0.01
98th Percentile	0.93	1.8	2.082	471.57	29.99	0.513	0.01
Mean	0.22	0.64	0.37	84.44	3.13	0.11	0.01
Standard deviation (n)	0.26	1.00	0.77	154.24	34.18	0.13	0.00
Skew ness (Pearson)	5.21	8.92	12.44	8.91	18.54	2.65	9.50
Kurtosis (Pearson)	50.78	81.21	201.44	117.00	382.99	12.06	89.64

Statistic	Mo_w_ICP-MS	Ag_w_ICP-MS	Cd_w_ICP-MS	In_w_ICP-MS	Sn_w_ICP-MS	Sb_w_ICP-MS	Te_w_ICP-MS
No. of observations	592	592	592	592	592	592	592
Analysis Method	ICP-MS	ICP-MS	ICP-MS	ICP-MS	ICP-MS	ICP-MS	ICP-MS
Detection Limit	0.05	0.005	0.02	0.01	0.01	0.01	0.02
Units	ppb	ppb	ppb	ppb	ppb	ppb	ppb
No. of missing values	0	0	0	0	0	0	0
Minimum	0.025	0.0025	0.01	0.005	0.005	0.005	0.01
Maximum	2.749	0.025	14.16	0.11	0.053	1.519	0.1
Freq. of minimum	119	580	455	586	576	195	584
Freq. of maximum	1	6	1	1	1	1	6
Range	2.724	0.0225	14.15	0.105	0.048	1.514	0.09
1st Quartile	0.065	0.0025	0.01	0.005	0.005	0.005	0.01
Median	0.1755	0.0025	0.01	0.005	0.005	0.026	0.01
3rd Quartile	0.3665	0.0025	0.01	0.005	0.005	0.06425	0.01
95th Percentile	0.961	0.005	0.171	0.01	0.01	0.154	0.02
98th Percentile	1.441	0.0053	0.687	0.01	0.014	0.204	0.02
Mean	0.29	0.00	0.09	0.01	0.01	0.05	0.01
Standard deviation (n)	0.36	0.00	0.70	0.01	0.01	0.08	0.01
Skew ness (Pearson)	3.13	9.09	15.52	12.65	7.42	11.16	8.80
Kurtosis (Pearson)	13.29	83.11	281.59	183.52	54.82	195.19	76.63

Statistic	Cs_w_ICP-MS	Ba_w_ICP-MS	La_w_ICP-MS	Ce_w_ICP-MS	Pr_w_ICP-MS	Nd_w_ICP-MS	Sm_w_ICP-MS
No. of observations	592	592	592	592	592	592	592
Analysis Method	ICP-MS	ICP-MS	ICP-MS	ICP-MS	ICP-MS	ICP-MS	ICP-MS
Detection Limit	0.01	0.2	0.01	0.01	0.005	0.005	0.005
Units	ppb	ppb	ppb	ppb	ppb	ppb	ppb
No. of missing values	0	0	0	0	0	0	0
Minimum	0.005	2.39	0.005	0.005	0.0025	0.0025	0.0025
Maximum	0.15	937.19	24.63	115.73	28.384	202.201	80.303
Freq. of minimum	556	1	284	236	311	146	244
Freq. of maximum	2	1	1	1	1	1	1
Range	0.145	934.8	24.625	115.725	28.3815	202.1985	80.3005
1st Quartile	0.005	39.23	0.005	0.005	0.0025	0.005075	0.0025
Median	0.005	59.615	0.011	0.019	0.0025	0.0232	0.00805
3rd Quartile	0.005	88.67	0.05025	0.104	0.0222	0.113575	0.039125
95th Percentile	0.014	150.87	0.178	0.396	0.0752	0.4085	0.1447
98th Percentile	0.03	204.65	0.71	2.759	0.5269	3.9512	2.6406
Mean	0.01	72.06	0.14	0.51	0.11	0.77	0.35
Standard deviation (n)	0.01	61.89	1.17	5.27	1.26	8.95	3.69
Skew ness (Pearson)	9.57	6.22	17.53	18.88	19.85	20.04	18.38
Kurtosis (Pearson)	105.99	70.05	342.45	392.58	428.07	435.95	378.46

Statistic	Eu_w_ICP-MS	Tb_w_ICP-MS	Gd_w_ICP-MS	Dy_w_ICP-MS	Ho_w_ICP-MS	Er_w_ICP-MS	Tm_w_ICP-MS
No. of observations	592	592	592	592	592	592	592
Analysis Method	ICP-MS	ICP-MS	ICP-MS	ICP-MS	ICP-MS	ICP-MS	ICP-MS
Detection Limit	0.005	0.005	0.005	0.005	0.005	0.005	0.005
Units	ppb	ppb	ppb	ppb	ppb	ppb	ppb
No. of missing values	0	0	0	0	0	0	0
Minimum	0.0025	0.0025	0.0025	0.0025	0.0025	0.0025	0.0025
Maximum	24.925	22.375	143.501	127.454	23.907	57.133	5.931
Freq. of minimum	331	393	208	218	379	286	525
Freq. of maximum	1	1	1	1	1	1	1
Range	24.9225	22.3725	143.4985	127.4515	23.9045	57.1305	5.9285
1st Quartile	0.0025	0.0025	0.0025	0.0025	0.0025	0.0025	0.0025
Median	0.0025	0.0025	0.01175	0.01	0.0025	0.0055	0.0025
3rd Quartile	0.011825	0.0076	0.050475	0.044725	0.008525	0.0227	0.0025
95th Percentile	0.0382	0.0276	0.1858	0.1547	0.0298	0.0738	0.0092
98th Percentile	0.8142	0.8824	6.1264	4.8929	0.9152	2.4631	0.3233
Mean	0.11	0.10	0.66	0.55	0.10	0.26	0.03
Standard deviation (n)	1.14	1.04	6.77	5.91	1.10	2.67	0.29
Skew ness (Pearson)	18.40	17.75	17.35	18.03	18.14	17.74	16.39
Kurtosis (Pearson)	378.92	355.78	342.54	365.55	369.45	355.38	307.23

Statistic	Yb_w_ICP-MS	Lu_w_ICP-MS	Hf_w_ICP-MS	Ta_w_ICP-MS	W_w_ICP-MS	Re_w_ICP-MS	Tl_w_ICP-MS
No. of observations	592	592	592	592	592	592	592
Analysis Method	ICP-MS	ICP-MS	ICP-MS	ICP-MS	ICP-MS	ICP-MS	ICP-MS
Detection Limit	0.005	0.005	0.01	0.01	0.02	0.005	0.005
Units	ppb	ppb	ppb	ppb	ppb	ppb	ppb
No. of missing values	0	0	0	0	0	0	0
Minimum	0.0025	0.0025	0.005	0.005	0.01	0.0025	0.0025
Maximum	28.871	3.813	0.05	0.05	14.46	0.025	0.084
Freq. of minimum	306	546	518	586	555	576	491
Freq. of maximum	1	1	6	6	1	6	1
Range	28.8685	3.8105	0.045	0.045	14.45	0.0225	0.0815
1st Quartile	0.0025	0.0025	0.005	0.005	0.01	0.0025	0.0025
Median	0.0025	0.0025	0.005	0.005	0.01	0.0025	0.0025
3rd Quartile	0.016825	0.0025	0.005	0.005	0.01	0.0025	0.0025
95th Percentile	0.0487	0.0073	0.015	0.01	0.035	0.0051	0.0083
98th Percentile	1.7103	0.2307	0.02	0.05	0.17	0.0058	0.0215
Mean	0.16	0.02	0.01	0.01	0.05	0.00	0.00
Standard deviation (n)	1.50	0.21	0.01	0.00	0.60	0.00	0.01
Skew ness (Pearson)	14.94	14.34	6.06	9.78	23.76	8.95	8.17
Kurtosis (Pearson)	254.70	232.76	43.46	93.68	569.98	81.15	86.04

Statistic	Pb_w_ICP-MS	U_w_ICP-MS	Ca_w_ICP-ES	Fe_w_ICP-ES	K_w_ICP-ES	Mg_w_ICP-ES	Na_w_ICP-ES
No. of observations	592	592	592	592	592	592	592
Analysis Method	ICP-MS	ICP-MS	ICP-ES	ICP-ES	ICP-ES	ICP-ES	ICP-ES
Detection Limit	0.01	0.005	0.02	0.005	0.05	0.005	0.05
Units	ppb	ppb	ppm	ppm	ppm	ppm	ppm
No. of missing values	0	0	0	0	0	0	0
Minimum	0.005	0.0025	1.343	0.0025	0.025	0.903	0.025
Maximum	4.48	19.074	262.72	594.111	25.61	404.621	383.56
Freq. of minimum	187	13	1	172	3	1	8
Freq. of maximum	1	1	1	1	1	1	1
Range	4.475	19.0715	261.377	594.1085	25.585	403.718	383.535
1st Quartile	0.005	0.053525	13.1805	0.0025	0.27275	5.29445	0.2045
Median	0.0335	0.13785	23.9355	0.02505	0.5075	9.38395	0.6585
3rd Quartile	0.104	0.331875	37.71725	0.214625	0.7355	16.421675	2.57
95th Percentile	0.221	1.2	75.256	0.9428	1.39	37.9121	18.58
98th Percentile	0.519	1.6209	114.69	3.4838	1.912	71.5255	55.18
Mean	0.09	0.34	30.01	1.54	0.63	15.46	5.35
Standard deviation (n)	0.27	0.93	26.93	24.99	1.14	29.53	23.56
Skew ness (Pearson)	10.65	14.61	3.21	22.75	17.99	8.30	10.31
Kurtosis (Pearson)	141.98	274.82	16.54	532.46	386.04	84.28	133.52

Statistic	P_w_ICP-ES	S_w_ICP-ES	Sc_w_ICP-ES	Si_w_ICP-ES
No. of observations	592	592	592	592
Analysis Method	ICP-ES	ICP-ES	ICP-ES	ICP-ES
Detection Limit	0.05	0.05	0.001	0.02
Units	ppm	ppm	ppm	ppm
No. of missing values	0	0	0	0
Minimum	0.025	0.151	0.0005	0.299
Maximum	0.255	1423.94	0.035	18.25
Freq. of minimum	585	1	579	1
Freq. of maximum	1	1	1	1
Range	0.23	1423.789	0.0345	17.951
1st Quartile	0.025	1.66275	0.0005	0.912
Median	0.025	6.31	0.0005	1.221
3rd Quartile	0.025	22.42075	0.0005	1.57425
95th Percentile	0.05	104.172	0.001	2.448
98th Percentile	0.25	182.712	0.0018	4.307
Mean	0.03	27.95	0.00	1.40
Standard deviation (n)	0.02	92.06	0.00	1.15
Skew ness (Pearson)	9.03	9.72	14.02	7.82
Kurtosis (Pearson)	79.60	116.91	216.42	90.73

The log or log normal distributions of such elements more closely approximate a normal distribution and thus it is common practice to examine logarithmic or log normal distributions of geochemical analyses when computing statistics on these measurements. A normal distribution in log space will be symmetric about a mean value with 66% of all analyses within one standard deviation of the mean. A normal distribution will show a symmetric Box plot and symmetric cumulative probability plot. In the latter case, the inflection point will be mean value of the data set (ie. the mean and median are the same value in a normal distribution). Outliers in the Box plots are shown as individual points above the 95th percentile values indicated by the "whiskers".

The responses of the various elements vary depending upon their general abundance and the detection limit of the analytical methods used to measure them. Some elements showed no significant response above detection limit including: Ge, Se, Nb, Ag, In, Sn, Te, Cs, Ta, W, Re, P, and Sc. The following elements show either a log normal distribution, a skewed response or a two population distribution: Li, B, Sr, Ba, Ca, K, Mg, Na, S, and Si. Other left censored elements with proportions of analyses below detection limit ranging from 2% to 20% include Al, Mn, Cu, Rb, Y, and U. The remaining elements are heavily left censored with a large percentage of analyses below detection limit (>20%). The table below summarizes observations on the logarithmic population distributions:

Table 15 Summary of element response distributions

Variable	Description
pH	negative skew
Conductivity	log normal
Li_w_ICP-MS	weak positive skew, two populations
Be_w_ICP-MS	left censored, two populations
B_w_ICP-MS	log normal
Al_w_ICP-MS	positive skew
Ti_w_ICP-MS	left censored, two populations
V_w_ICP-MS	left censored, positive skew, two populations
Cr_w_ICP-MS	left censored, two populations
Mn_w_ICP-MS	positive skew, two populations
Co_w_ICP-MS	left censored, positive skew
Ni_w_ICP-MS	left censored, two populations

Variable	Description
Cu_w_ICP-MS	two populations
Zn_w_ICP-MS	left censored, positive skew
Ga_w_ICP-MS	left censored
Ge_w_ICP-MS	no response
As_w_ICP-MS	left censored, near log normal
Se_w_ICP-MS	no response
Rb_w_ICP-MS	weak positive skew, two populations
Sr_w_ICP-MS	log normal
Y_w_ICP-MS	left censored, positive skew
Zr_w_ICP-MS	left censored, negative skew, two populations
Nb_w_ICP-MS	no response
Mo_w_ICP-MS	left censored, weak positive skew
Ag_w_ICP-MS	no response
Cd_w_ICP-MS	left censored, positive skew
In_w_ICP-MS	no response
Sn_w_ICP-MS	no response
Sb_w_ICP-MS	left censored, two populations
Te_w_ICP-MS	no response
Cs_w_ICP-MS	no response
Ba_w_ICP-MS	log normal
La_w_ICP-MS	left censored, positive skew
Ce_w_ICP-MS	left censored, two populations
Pr_w_ICP-MS	left censored, positive skew
Nd_w_ICP-MS	left censored, positive skew, two populations
Sm_w_ICP-MS	left censored, positive skew, two populations
Eu_w_ICP-MS	left censored, positive skew
Tb_w_ICP-MS	left censored, positive skew, two populations
Gd_w_ICP-MS	left censored, positive skew, two populations
Dy_w_ICP-MS	left censored, positive skew, two populations
Ho_w_ICP-MS	left censored, positive skew
Er_w_ICP-MS	left censored, positive skew, two populations
Tm_w_ICP-MS	left censored
Yb_w_ICP-MS	left censored, positive skew, two populations
Lu_w_ICP-MS	left censored
Hf_w_ICP-MS	left censored
Ta_w_ICP-MS	no response
W_w_ICP-MS	no response
Re_w_ICP-MS	no response
Tl_w_ICP-MS	left censored
Pb_w_ICP-MS	left censored, negative skew, two populations
U_w_ICP-MS	log normal, three populations
Ca_w_ICP-ES	weak positive skew
Fe_w_ICP-ES	left censored, two populations
K_w_ICP-ES	weak negative skew, two populations

Variable	Description
Mg_w_ICP-ES	weak positive skew, two populations
Na_w_ICP-ES	positive skew, two populations
P_w_ICP-ES	no response
S_w_ICP-ES	three populations, near log normal
Sc_w_ICP-ES	no response
Si_w_ICP-ES	near log normal, two populations

Elements with two populations including Li, Ti, Cr, Cu, Mn, Ni, Sb, Nd, Sm, Gd, Dy, Er, Yb, Zr, Pb, Fe, Mg, Na, K and Si appear to have been derived from two separate geochemical domains. Elements Ni, Na, Rb, Tb, and V show two populations in silt and water sample data. Uranium and Sulphur show three populations. Negatively skewed responses including pH, Zr, Pb, and K indicate that one of these domains is especially enriched in these dominantly lithophile elements.

10.2 Multivariate Statistics

Multivariate statistics are summarized in Table 16 below which shows the Pearson correlation constant for each pair of elements in the distribution. Correlation constants range between 1.0 (perfect positive correlation) and -1.0 (perfect negative correlation) while a correlation constant of zero indicates no correlation exists between the data sets.

Interpretation of covariate data are as follows:

- Acid association: REE, Be, An, Cd, Ni, Sc, Fe, Mn, Cs, and Al
- Alkaline association: Ba, Mo, Sb, U
- Organic shale association: Fe, Be, Al, Ti, V, Cr, Mn, Ni, Cu, TREE, As, Zr
- Redox association: Mn, Fe, Ni, Co ±V, As.
- Carbonate association: Sr, Ca, Mg, Li, Be ±Na
- Major element association: U, Ca, K, Mg, Na, P, Ba, Li, conductivity, S, Si, Sr

The acid and alkaline associations reflect elements that are strongly governed by pH. These elements show greater concentrations with decreasing pH as a function of solubility. The REE group shows the strongest correlation with pH. Redox

Table 16 Multivariate statistics: Pearson correlation coefficient for all water sample data pairs

Variables	pH	Conductivity	Li_w	Be_w	B_w	Al_w	Ti_w	V_w	Cr_w	Mn_w	Co_w	Ni_w	Cu_w	Zn_w	GA_w	Ge_w	As_w	Se_w	Rb_w	Sr_w	Y_w	Zr_w	Nb_w	Mo_w	Ag_w
pH	**1**	**-0.151**	**-0.330**	**-0.655**	**-0.150**	**-0.546**	**-0.282**	**-0.149**	**-0.289**	**-0.479**	**-0.540**	**-0.500**	**-0.408**	**-0.625**	**-0.411**	**-0.375**	**-0.146**	**-0.321**	**-0.336**	-0.069	**-0.532**	**-0.125**	**-0.407**	**0.177**	**-0.441**
Conductivity	**-0.151**	**1**	**0.693**	0.078	**0.512**	0.038	**-0.194**	**-0.244**	**-0.238**	**0.310**	**0.367**	**0.322**	-0.055	**0.333**	**0.128**	**0.323**	**-0.146**	**0.348**	**0.491**	**0.797**	-0.004	**-0.351**	**0.291**	**0.327**	**0.336**
Li_w_ICP-MS	**-0.330**	**0.693**	**1**	**0.456**	**0.784**	**0.454**	**0.112**	0.074	**0.129**	**0.667**	**0.635**	**0.704**	**0.364**	**0.586**	**0.270**	**0.385**	**0.222**	**0.349**	**0.723**	**0.762**	**0.459**	0.070	**0.312**	**0.234**	**0.349**
Be_w_ICP-MS	**-0.655**	0.078	**0.456**	**1**	**0.241**	**0.867**	**0.513**	**0.417**	**0.604**	**0.705**	**0.731**	**0.797**	**0.713**	**0.774**	**0.513**	**0.385**	**0.393**	**0.303**	**0.332**	**0.104**	**0.876**	**0.510**	**0.425**	**-0.143**	**0.473**
B_w_ICP-MS	**-0.150**	**0.512**	**0.784**	**0.241**	**1**	**0.243**	**0.124**	**0.095**	**0.108**	**0.371**	**0.327**	**0.392**	**0.311**	**0.329**	**0.261**	**0.350**	**0.217**	**0.358**	**0.782**	**0.655**	**0.312**	**0.096**	**0.271**	**0.212**	**0.302**
Al_w_ICP-MS	**-0.546**	0.038	**0.454**	**0.867**	**0.243**	**1**	**0.479**	**0.406**	**0.511**	**0.743**	**0.730**	**0.772**	**0.689**	**0.691**	**0.484**	**0.337**	**0.340**	**0.276**	**0.338**	**0.119**	**0.840**	**0.440**	**0.363**	**-0.094**	**0.400**
Ti_w_ICP-MS	**-0.282**	**-0.194**	**0.112**	**0.513**	**0.124**	**0.479**	**1**	**0.665**	**0.679**	**0.280**	**0.253**	**0.360**	**0.524**	**0.323**	**0.674**	**0.364**	**0.507**	**0.327**	**0.149**	-0.043	**0.540**	**0.687**	**0.511**	0.027	**0.471**
V_w_ICP-MS	**-0.149**	**-0.244**	0.074	**0.417**	**0.095**	**0.406**	**0.665**	**1**	**0.792**	**0.273**	0.073	**0.360**	**0.676**	**0.118**	**0.412**	**0.258**	**0.823**	**0.225**	-0.011	0.019	**0.607**	**0.820**	**0.297**	**0.322**	**0.282**
Cr_w_ICP-MS	**-0.289**	**-0.238**	**0.129**	**0.604**	**0.108**	**0.511**	**0.679**	**0.792**	**1**	**0.322**	**0.189**	**0.469**	**0.714**	**0.303**	**0.400**	**0.292**	**0.775**	**0.235**	-0.006	-0.028	**0.698**	**0.889**	**0.344**	**0.142**	**0.357**
Mn_w_ICP-MS	**-0.479**	**0.310**	**0.667**	**0.705**	**0.371**	**0.743**	**0.280**	**0.273**	**0.322**	**1**	**0.890**	**0.879**	**0.508**	**0.721**	**0.347**	**0.302**	**0.328**	**0.242**	**0.484**	**0.358**	**0.671**	**0.249**	**0.293**	0.000	**0.336**
Co_w_ICP-MS	**-0.540**	**0.367**	**0.635**	**0.731**	**0.327**	**0.730**	**0.253**	0.073	**0.189**	**0.890**	**1**	**0.846**	**0.365**	**0.831**	**0.397**	**0.329**	0.059	**0.253**	**0.478**	**0.298**	**0.577**	**0.089**	**0.341**	**-0.180**	**0.388**
Ni_w_ICP-MS	**-0.500**	**0.322**	**0.704**	**0.797**	**0.392**	**0.772**	**0.360**	**0.360**	**0.469**	**0.879**	**0.846**	**1**	**0.652**	**0.794**	**0.383**	**0.332**	**0.403**	**0.307**	**0.438**	**0.411**	**0.797**	**0.420**	**0.351**	0.049	**0.387**
Cu_w_ICP-MS	**-0.408**	-0.055	**0.364**	**0.713**	**0.311**	**0.689**	**0.524**	**0.676**	**0.714**	**0.508**	**0.365**	**0.652**	**1**	**0.443**	**0.447**	**0.305**	**0.675**	**0.279**	**0.298**	**0.127**	**0.897**	**0.718**	**0.323**	**0.170**	**0.347**
Zn_w_ICP-MS	**-0.625**	**0.333**	**0.586**	**0.774**	**0.329**	**0.691**	**0.323**	**0.118**	**0.303**	**0.721**	**0.831**	**0.794**	**0.443**	**1**	**0.440**	**0.386**	**0.124**	**0.330**	**0.439**	**0.274**	**0.644**	**0.156**	**0.414**	**-0.142**	**0.473**
Ga_w_ICP-MS	**-0.411**	**0.128**	**0.270**	**0.513**	**0.261**	**0.484**	**0.674**	**0.412**	**0.400**	**0.347**	**0.397**	**0.383**	**0.447**	**0.440**	**1**	**0.522**	**0.259**	**0.442**	**0.376**	**0.133**	**0.479**	**0.338**	**0.599**	0.002	**0.585**
Ge_w_ICP-MS	**-0.375**	**0.323**	**0.385**	**0.385**	**0.350**	**0.337**	**0.364**	**0.258**	**0.292**	**0.302**	**0.329**	**0.332**	**0.305**	**0.386**	**0.522**	**1**	**0.216**	**0.599**	**0.343**	**0.253**	**0.341**	**0.144**	**0.753**	**0.087**	**0.801**
As_w_ICP-MS	**-0.146**	**-0.146**	**0.222**	**0.393**	**0.217**	**0.340**	**0.507**	**0.823**	**0.775**	**0.328**	0.059	**0.403**	**0.675**	**0.124**	**0.259**	**0.216**	**1**	**0.196**	0.080	**0.159**	**0.597**	**0.791**	**0.200**	**0.441**	**0.206**
Se_w_ICP-MS	**-0.321**	**0.348**	**0.349**	**0.303**	**0.358**	**0.276**	**0.327**	**0.225**	**0.235**	**0.242**	**0.253**	**0.307**	**0.279**	**0.330**	**0.442**	**0.599**	**0.196**	**1**	**0.373**	**0.326**	**0.270**	**0.124**	**0.755**	**0.147**	**0.737**
Rb_w_ICP-MS	**-0.336**	**0.491**	**0.723**	**0.332**	**0.782**	**0.338**	**0.149**	-0.011	-0.006	**0.484**	**0.478**	**0.438**	**0.298**	**0.439**	**0.376**	**0.343**	0.080	**0.373**	**1**	**0.559**	**0.316**	-0.059	**0.349**	0.018	**0.383**
Sr_w_ICP-MS	-0.069	**0.797**	**0.762**	**0.104**	**0.655**	**0.119**	-0.043	0.019	-0.028	**0.358**	**0.298**	**0.411**	**0.127**	**0.274**	**0.133**	**0.253**	**0.159**	**0.326**	**0.559**	**1**	**0.153**	-0.056	**0.230**	**0.550**	**0.237**
Y_w_ICP-MS	**-0.532**	-0.004	**0.459**	**0.876**	**0.312**	**0.840**	**0.540**	**0.607**	**0.698**	**0.671**	**0.577**	**0.797**	**0.897**	**0.644**	**0.479**	**0.341**	**0.597**	**0.270**	**0.316**	**0.153**	**1**	**0.668**	**0.359**	0.049	**0.393**
Zr_w_ICP-MS	**-0.125**	**-0.351**	0.070	**0.510**	**0.096**	**0.440**	**0.687**	**0.820**	**0.889**	**0.249**	**0.089**	**0.420**	**0.718**	**0.156**	**0.338**	**0.144**	**0.791**	**0.124**	-0.059	-0.056	**0.668**	**1**	**0.221**	**0.174**	**0.195**
Nb_w_ICP-MS	**-0.407**	**0.291**	**0.312**	**0.425**	**0.271**	**0.363**	**0.511**	**0.297**	**0.344**	**0.293**	**0.341**	**0.351**	**0.323**	**0.414**	**0.599**	**0.753**	**0.200**	**0.755**	**0.349**	**0.230**	**0.359**	**0.221**	**1**	0.052	**0.906**
Mo_w_ICP-MS	**0.177**	**0.327**	**0.234**	**-0.143**	**0.212**	**-0.094**	0.027	**0.322**	**0.142**	0.000	**-0.180**	0.049	**0.170**	**-0.142**	0.002	**0.087**	**0.441**	**0.147**	0.018	**0.550**	0.049	**0.174**	0.052	**1**	0.048
Ag_w_ICP-MS	**-0.441**	**0.336**	**0.349**	**0.473**	**0.302**	**0.400**	**0.471**	**0.282**	**0.357**	**0.336**	**0.388**	**0.387**	**0.347**	**0.473**	**0.585**	**0.801**	**0.206**	**0.737**	**0.383**	**0.237**	**0.393**	**0.195**	**0.906**	0.048	**1**
Cd_w_ICP-MS	**-0.617**	**0.366**	**0.504**	**0.635**	**0.263**	**0.563**	**0.193**	0.011	**0.168**	**0.616**	**0.723**	**0.651**	**0.336**	**0.817**	**0.387**	**0.421**	0.032	**0.384**	**0.439**	**0.236**	**0.500**	-0.015	**0.437**	**-0.152**	**0.516**
In_w_ICP-MS	**-0.434**	**0.324**	**0.305**	**0.420**	**0.245**	**0.353**	**0.428**	**0.256**	**0.316**	**0.296**	**0.345**	**0.348**	**0.302**	**0.423**	**0.520**	**0.736**	**0.166**	**0.787**	**0.343**	**0.238**	**0.339**	**0.172**	**0.935**	0.042	**0.895**
Sn_w_ICP-MS	**-0.305**	**0.224**	**0.238**	**0.309**	**0.187**	**0.255**	**0.355**	**0.232**	**0.255**	**0.237**	**0.248**	**0.270**	**0.243**	**0.299**	**0.413**	**0.583**	**0.179**	**0.602**	**0.268**	**0.184**	**0.257**	**0.159**	**0.721**	0.072	**0.698**
Sb_w_ICP-MS	0.024	0.038	**0.318**	**0.209**	**0.336**	**0.250**	**0.325**	**0.678**	**0.529**	**0.249**	-0.011	**0.354**	**0.637**	0.021	**0.176**	**0.092**	**0.781**	**0.177**	**0.152**	**0.372**	**0.487**	**0.627**	**0.100**	**0.644**	**0.083**
Te_w_ICP-MS	**-0.385**	**0.274**	**0.290**	**0.400**	**0.232**	**0.329**	**0.397**	**0.247**	**0.309**	**0.282**	**0.317**	**0.330**	**0.291**	**0.392**	**0.469**	**0.668**	**0.185**	**0.713**	**0.337**	**0.215**	**0.323**	**0.182**	**0.851**	0.041	**0.814**
Cs_w_ICP-MS	**-0.533**	**0.344**	**0.393**	**0.568**	**0.366**	**0.483**	**0.437**	**0.205**	**0.312**	**0.402**	**0.473**	**0.456**	**0.410**	**0.552**	**0.654**	**0.598**	**0.124**	**0.574**	**0.510**	**0.248**	**0.465**	**0.146**	**0.687**	**-0.088**	**0.711**
Ba_w_ICP-MS	**0.306**	0.004	-0.076	**-0.270**	**-0.100**	**-0.268**	**-0.095**	**0.202**	**0.097**	**-0.156**	**-0.333**	**-0.138**	**0.082**	**-0.374**	**-0.198**	**-0.105**	**0.353**	**-0.147**	**-0.208**	**0.141**	**-0.084**	**0.156**	**-0.207**	**0.499**	**-0.211**
La_w_ICP-MS	**-0.531**	**-0.107**	**0.311**	**0.862**	**0.219**	**0.739**	**0.664**	**0.670**	**0.791**	**0.532**	**0.471**	**0.681**	**0.835**	**0.590**	**0.538**	**0.338**	**0.619**	**0.269**	**0.214**	0.038	**0.917**	**0.760**	**0.382**	-0.014	**0.406**
Ce_w_ICP-MS	**-0.522**	**-0.118**	**0.330**	**0.860**	**0.234**	**0.766**	**0.644**	**0.688**	**0.779**	**0.567**	**0.482**	**0.695**	**0.861**	**0.578**	**0.524**	**0.332**	**0.656**	**0.259**	**0.229**	0.051	**0.937**	**0.755**	**0.355**	0.029	**0.381**
Pr_w_ICP-MS	**-0.558**	-0.056	**0.351**	**0.879**	**0.261**	**0.755**	**0.644**	**0.641**	**0.786**	**0.540**	**0.487**	**0.691**	**0.835**	**0.612**	**0.537**	**0.357**	**0.611**	**0.299**	**0.247**	0.078	**0.917**	**0.734**	**0.405**	0.008	**0.437**
Nd_w_ICP-MS	**-0.494**	**-0.125**	**0.339**	**0.835**	**0.238**	**0.780**	**0.590**	**0.687**	**0.763**	**0.568**	**0.461**	**0.706**	**0.907**	**0.557**	**0.476**	**0.313**	**0.661**	**0.241**	**0.223**	0.062	**0.971**	**0.744**	**0.331**	0.058	**0.359**
Sm_w_ICP-MS	**-0.544**	-0.055	**0.378**	**0.882**	**0.276**	**0.787**	**0.597**	**0.634**	**0.753**	**0.571**	**0.502**	**0.718**	**0.874**	**0.607**	**0.512**	**0.356**	**0.617**	**0.284**	**0.263**	**0.095**	**0.953**	**0.717**	**0.380**	0.036	**0.415**
Eu_w_ICP-MS	**-0.633**	0.066	**0.394**	**0.875**	**0.268**	**0.749**	**0.583**	**0.517**	**0.685**	**0.563**	**0.547**	**0.674**	**0.742**	**0.669**	**0.554**	**0.448**	**0.513**	**0.334**	**0.311**	**0.128**	**0.854**	**0.559**	**0.461**	0.003	**0.504**
Tb_w_ICP-MS	**-0.669**	**0.122**	**0.429**	**0.901**	**0.300**	**0.768**	**0.567**	**0.449**	**0.630**	**0.562**	**0.594**	**0.694**	**0.725**	**0.723**	**0.569**	**0.456**	**0.412**	**0.385**	**0.349**	**0.137**	**0.849**	**0.508**	**0.500**	-0.065	**0.546**
Gd_w_ICP-MS	**-0.548**	-0.029	**0.414**	**0.896**	**0.292**	**0.823**	**0.569**	**0.605**	**0.715**	**0.619**	**0.556**	**0.757**	**0.875**	**0.641**	**0.507**	**0.352**	**0.585**	**0.282**	**0.290**	**0.118**	**0.972**	**0.679**	**0.377**	0.029	**0.413**
Dy_w_ICP-MS	**-0.550**	-0.011	**0.423**	**0.896**	**0.304**	**0.817**	**0.570**	**0.611**	**0.725**	**0.612**	**0.546**	**0.756**	**0.879**	**0.636**	**0.510**	**0.365**	**0.597**	**0.300**	**0.291**	**0.132**	**0.970**	**0.688**	**0.389**	0.043	**0.425**
Ho_w_ICP-MS	**-0.660**	**0.117**	**0.436**	**0.905**	**0.311**	**0.768**	**0.568**	**0.468**	**0.649**	**0.567**	**0.589**	**0.705**	**0.747**	**0.720**	**0.565**	**0.452**	**0.440**	**0.386**	**0.346**	**0.144**	**0.864**	**0.536**	**0.498**	-0.053	**0.543**
Er_w_ICP-MS	**-0.587**	0.029	**0.433**	**0.912**	**0.317**	**0.796**	**0.574**	**0.565**	**0.723**	**0.591**	**0.553**	**0.742**	**0.847**	**0.662**	**0.529**	**0.388**	**0.560**	**0.329**	**0.308**	**0.138**	**0.940**	**0.666**	**0.427**	0.015	**0.465**
Tm_w_ICP-MS	**-0.714**	**0.317**	**0.452**	**0.799**	**0.311**	**0.678**	**0.420**	**0.215**	**0.375**	**0.509**	**0.604**	**0.599**	**0.554**	**0.731**	**0.603**	**0.546**	**0.170**	**0.491**	**0.437**	**0.207**	**0.676**	**0.205**	**0.591**	**-0.105**	**0.642**
Yb_w_ICP-MS	**-0.609**	0.025	**0.409**	**0.918**	**0.293**	**0.792**	**0.579**	**0.546**	**0.712**	**0.571**	**0.546**	**0.719**	**0.826**	**0.664**	**0.543**	**0.401**	**0.529**	**0.340**	**0.302**	**0.118**	**0.922**	**0.645**	**0.442**	-0.010	**0.480**
Lu_w_ICP-MS	**-0.714**	**0.348**	**0.455**	**0.777**	**0.306**	**0.656**	**0.363**	**0.167**	**0.321**	**0.497**	**0.599**	**0.580**	**0.521**	**0.722**	**0.581**	**0.555**	**0.128**	**0.501**	**0.448**	**0.221**	**0.642**	**0.146**	**0.597**	**-0.106**	**0.649**
Hf_w_ICP-MS	**-0.307**	-0.074	**0.154**	**0.505**	**0.138**	**0.441**	**0.769**	**0.555**	**0.636**	**0.271**	**0.276**	**0.385**	**0.471**	**0.358**	**0.590**	**0.463**	**0.442**	**0.445**	**0.113**	0.017	**0.498**	**0.612**	**0.632**	0.047	**0.563**
Ta_w_ICP-MS	**-0.420**	**0.324**	**0.304**	**0.416**	**0.244**	**0.347**	**0.431**	**0.241**	**0.301**	**0.295**	**0.344**	**0.345**	**0.293**	**0.418**	**0.526**	**0.741**	**0.161**	**0.792**	**0.344**	**0.242**	**0.333**	**0.166**	**0.942**	0.043	**0.902**
W_w_ICP-MS	**-0.249**	**0.268**	**0.247**	**0.255**	**0.212**	**0.211**	**0.197**	0.080	**0.155**	**0.220**	**0.262**	**0.256**	**0.154**	**0.320**	**0.260**	**0.355**	0.065	**0.347**	**0.217**	**0.190**	**0.209**	0.031	**0.443**	0.002	**0.445**
Re_w_ICP-MS	**-0.357**	**0.339**	**0.293**	**0.318**	**0.224**	**0.252**	**0.356**	**0.209**	**0.242**	**0.287**	**0.281**	**0.292**	**0.223**	**0.352**	**0.457**	**0.642**	**0.181**	**0.743**	**0.326**	**0.283**	**0.254**	**0.105**	**0.821**	**0.145**	**0.785**
Tl_w_ICP-MS	**-0.414**	**0.392**	**0.421**	**0.372**	**0.394**	**0.332**	**0.202**	**0.185**	**0.206**	**0.321**	**0.324**	**0.411**	**0.405**	**0.463**	**0.401**	**0.420**	**0.224**	**0.453**	**0.467**	**0.425**	**0.393**	**0.087**	**0.461**	**0.301**	**0.506**
Pb_w_ICP-MS	**-0.289**	**-0.299**	-0.019	**0.449**	-0.012	**0.411**	**0.465**	**0.429**	**0.491**	**0.176**	**0.116**	**0.188**	**0.530**	**0.227**	**0.375**	**0.198**	**0.435**	0.049	**0.096**	**-0.164**	**0.496**	**0.451**	**0.170**	0.006	**0.179**
U_w_ICP-MS	-0.015	**0.660**	**0.364**	-0.043	**0.265**	-0.004	-0.059	0.002	**-0.084**	-0.003	-0.022	0.041	0.045	0.010	**0.121**	**0.195**	0.030	**0.277**	**0.213**	**0.650**	-0.025	**-0.140**	**0.187**	**0.648**	**0.202**
Ca_w_ICP-ES	-0.043	**0.916**	**0.594**	-0.018	**0.369**	-0.043	**-0.223**	**-0.186**	**-0.222**	**0.220**	**0.222**	**0.249**	-0.069	**0.202**	0.028	**0.209**	-0.069	**0.245**	**0.333**	**0.831**	-0.042	**-0.291**	**0.190**	**0.495**	**0.209**
Fe_w_ICP-ES	**-0.439**	**-0.177**	**0.281**	**0.738**	**0.204**	**0.634**	**0.574**	**0.703**	**0.810**	**0.526**	**0.351**	**0.604**	**0.805**	**0.461**	**0.384**	**0.286**	**0.767**	**0.182**	**0.164**	0.031	**0.848**	**0.759**	**0.273**	**0.098**	**0.308**
K_w_ICP-ES	-0.073	**0.586**	**0.615**	0.017	**0.753**	0.035	-0.057	**-0.248**	**-0.289**	**0.213**	**0.258**	**0.172**	0.025	**0.201**	**0.201**	**0.222**	**-0.185**	**0.305**	**0.835**	**0.550**	-0.012	**-0.285**	**0.220**	0.038	**0.246**
Mg_w_ICP-ES	**-0.201**	**0.934**	**0.648**	0.080	**0.445**	0.056	**-0.234**	**-0.376**	**-0.358**	**0.318**	**0.423**	**0.296**	**-0.138**	**0.373**	**0.127**	**0.311**	**-0.312**	**0.359**	**0.518**	**0.704**	-0.057	**-0.474**	**0.322**	**0.155**	**0.358**
Na_w_ICP-ES	**-0.261**	**0.568**	**0.871**	**0.401**	**0.802**	**0.407**	**0.165**	**0.280**	**0.274**	**0.589**	**0.476**	**0.638**	**0.463**	**0.446**	**0.263**	**0.379**	**0.440**	**0.363**	**0.624**	**0.709**	**0.510**	**0.227**	**0.292**	**0.361**	**0.325**
P_w_ICP-ES	**-0.390**	**0.314**	**0.317**	**0.412**	**0.270**	**0.348**	**0.457**	**0.291**	**0.329**	**0.295**	**0.339**	**0.337**	**0.296**	**0.401**	**0.567**	**0.820**	**0.202**	**0.729**	**0.333**	**0.221**	**0.337**	**0.195**	**0.932**	0.066	**0.930**
S_w_ICP-ES	**-0.194**	**0.828**	**0.706**	**0.110**	**0.604**	**0.118**	**-0.166**	**-0.379**	**-0.360**	**0.332**	**0.453**	**0.318**	**-0.113**	**0.407**	**0.139**	**0.231**	**-0.316**	**0.315**	**0.645**	**0.686**	-0.014	**-0.432**	**0.253**	**0.109**	**0.280**
Sc_w_ICP-ES	**-0.615**	**0.372**	**0.392**	**0.628**	**0.234**	**0.528**	**0.348**	**0.149**	**0.267**	**0.398**	**0.493**	**0.467**	**0.407**	**0.587**	**0.607**	**0.668**	**0.083**	**0.633**	**0.405**	**0.249**	**0.483**	**0.098**	**0.744**	-0.056	**0.760**
Si_w_ICP-ES	**-0.402**	**0.539**	**0.765**	**0.554**	**0.588**	**0.494**	**0.223**	**0.197**	**0.272**	**0.571**	**0.533**	**0.659**	**0.460**	**0.554**	**0.325**	**0.374**	**0.243**	**0.344**	**0.538**	**0.562**	**0.575**	**0.203**	**0.348**	**0.123**	**0.383**

Table 16 Continued

Variables	Cd_w	In_w	Sn_w	Sb_w	Te_w	Cs_w	Ba_w	La_w	Ce_w	Pr_w	Nd_w	Sm_w	Eu_w	Tb_w	Gd_w	Dy_w	Ho_w	Er_w	Tm_w	Yb_w	Lu_w	Hf_w	Ta_w	W-w
pH	**-0.617**	**-0.434**	**-0.305**	0.024	**-0.385**	**-0.533**	**0.306**	**-0.531**	**-0.522**	**-0.558**	**-0.494**	**-0.544**	**-0.633**	**-0.669**	**-0.548**	**-0.550**	**-0.660**	**-0.587**	**-0.714**	**-0.609**	**-0.714**	**-0.307**	**-0.420**	**-0.249**
Conductivity	**0.366**	**0.324**	**0.224**	0.038	**0.274**	**0.344**	0.004	**-0.107**	**-0.118**	-0.056	**-0.125**	-0.055	0.066	**0.122**	-0.029	-0.011	**0.117**	0.029	**0.317**	0.025	**0.348**	-0.074	**0.324**	**0.268**
Li_w_ICP-MS	**0.504**	**0.305**	**0.238**	**0.318**	**0.290**	**0.393**	-0.076	**0.311**	**0.330**	**0.351**	**0.339**	**0.378**	**0.394**	**0.429**	**0.414**	**0.423**	**0.436**	**0.433**	**0.452**	**0.409**	**0.455**	**0.154**	**0.304**	**0.247**
Be_w_ICP-MS	**0.635**	**0.420**	**0.309**	**0.209**	**0.400**	**0.568**	**-0.270**	**0.862**	**0.860**	**0.879**	**0.835**	**0.882**	**0.875**	**0.901**	**0.896**	**0.896**	**0.905**	**0.912**	**0.799**	**0.918**	**0.777**	**0.505**	**0.416**	**0.255**
B_w_ICP-MS	**0.263**	**0.245**	**0.187**	**0.336**	**0.232**	**0.366**	**-0.100**	**0.219**	**0.234**	**0.261**	**0.238**	**0.276**	**0.268**	**0.300**	**0.292**	**0.304**	**0.311**	**0.317**	**0.311**	**0.293**	**0.306**	**0.138**	**0.244**	**0.212**
Al_w_ICP-MS	**0.563**	**0.353**	**0.255**	**0.250**	**0.329**	**0.483**	**-0.268**	**0.739**	**0.766**	**0.755**	**0.780**	**0.787**	**0.749**	**0.768**	**0.823**	**0.817**	**0.768**	**0.796**	**0.678**	**0.792**	**0.656**	**0.441**	**0.347**	**0.211**
Ti_w_ICP-MS	**0.193**	**0.428**	**0.355**	**0.325**	**0.397**	**0.437**	**-0.095**	**0.664**	**0.644**	**0.644**	**0.590**	**0.597**	**0.583**	**0.567**	**0.569**	**0.570**	**0.568**	**0.574**	**0.420**	**0.579**	**0.363**	**0.769**	**0.431**	**0.197**
V_w_ICP-MS	0.011	**0.256**	**0.232**	**0.678**	**0.247**	**0.205**	**0.202**	**0.670**	**0.688**	**0.641**	**0.687**	**0.634**	**0.517**	**0.449**	**0.605**	**0.611**	**0.468**	**0.565**	**0.215**	**0.546**	**0.167**	**0.555**	**0.241**	0.080
Cr_w_ICP-MS	**0.168**	**0.316**	**0.255**	**0.529**	**0.309**	**0.312**	**0.097**	**0.791**	**0.779**	**0.786**	**0.763**	**0.753**	**0.685**	**0.630**	**0.715**	**0.725**	**0.649**	**0.723**	**0.375**	**0.712**	**0.321**	**0.636**	**0.301**	**0.155**
Mn_w_ICP-MS	**0.616**	**0.296**	**0.237**	**0.249**	**0.282**	**0.402**	**-0.156**	**0.532**	**0.567**	**0.540**	**0.568**	**0.571**	**0.563**	**0.562**	**0.619**	**0.612**	**0.567**	**0.591**	**0.509**	**0.571**	**0.497**	**0.271**	**0.295**	**0.220**
Co_w_ICP-MS	**0.723**	**0.345**	**0.248**	-0.011	**0.317**	**0.473**	**-0.333**	**0.471**	**0.482**	**0.487**	**0.461**	**0.502**	**0.547**	**0.594**	**0.556**	**0.546**	**0.589**	**0.553**	**0.604**	**0.546**	**0.599**	**0.276**	**0.344**	**0.262**
Ni_w_ICP-MS	**0.651**	**0.348**	**0.270**	**0.354**	**0.330**	**0.456**	**-0.138**	**0.681**	**0.695**	**0.691**	**0.706**	**0.718**	**0.674**	**0.694**	**0.757**	**0.756**	**0.705**	**0.742**	**0.599**	**0.719**	**0.580**	**0.385**	**0.345**	**0.256**
Cu_w_ICP-MS	**0.336**	**0.302**	**0.243**	**0.637**	**0.291**	**0.410**	**0.082**	**0.835**	**0.861**	**0.835**	**0.907**	**0.874**	**0.742**	**0.725**	**0.875**	**0.879**	**0.747**	**0.847**	**0.554**	**0.826**	**0.521**	**0.471**	**0.293**	**0.154**
Zn_w_ICP-MS	**0.817**	**0.423**	**0.299**	0.021	**0.392**	**0.552**	**-0.374**	**0.590**	**0.578**	**0.612**	**0.557**	**0.607**	**0.669**	**0.723**	**0.641**	**0.636**	**0.720**	**0.662**	**0.731**	**0.664**	**0.722**	**0.358**	**0.418**	**0.320**
Ga_w_ICP-MS	**0.387**	**0.520**	**0.413**	**0.176**	**0.469**	**0.654**	**-0.198**	**0.538**	**0.524**	**0.537**	**0.476**	**0.512**	**0.554**	**0.569**	**0.507**	**0.510**	**0.565**	**0.529**	**0.603**	**0.543**	**0.581**	**0.590**	**0.526**	**0.260**
Ge_w_ICP-MS	**0.421**	**0.736**	**0.583**	**0.092**	**0.668**	**0.598**	**-0.105**	**0.338**	**0.332**	**0.357**	**0.313**	**0.356**	**0.448**	**0.456**	**0.352**	**0.365**	**0.452**	**0.388**	**0.546**	**0.401**	**0.555**	**0.463**	**0.741**	**0.355**
As_w_ICP-MS	0.032	**0.166**	**0.179**	**0.781**	**0.185**	**0.124**	**0.353**	**0.619**	**0.656**	**0.611**	**0.661**	**0.617**	**0.513**	**0.412**	**0.585**	**0.597**	**0.440**	**0.560**	**0.170**	**0.529**	**0.128**	**0.442**	**0.161**	0.065
Se_w_ICP-MS	**0.384**	**0.787**	**0.602**	**0.177**	**0.713**	**0.574**	**-0.147**	**0.269**	**0.259**	**0.299**	**0.241**	**0.284**	**0.334**	**0.385**	**0.282**	**0.300**	**0.386**	**0.329**	**0.491**	**0.340**	**0.501**	**0.445**	**0.792**	**0.347**
Rb_w_ICP-MS	**0.439**	**0.343**	**0.268**	**0.152**	**0.337**	**0.510**	**-0.208**	**0.214**	**0.229**	**0.247**	**0.223**	**0.263**	**0.311**	**0.349**	**0.290**	**0.291**	**0.346**	**0.308**	**0.437**	**0.302**	**0.448**	**0.113**	**0.344**	**0.217**
Sr_w_ICP-MS	**0.236**	**0.238**	**0.184**	**0.372**	**0.215**	**0.248**	**0.141**	0.038	0.051	0.078	0.062	**0.095**	**0.128**	**0.137**	**0.118**	**0.132**	**0.144**	**0.138**	**0.207**	**0.118**	**0.221**	0.017	**0.242**	**0.190**
Y_w_ICP-MS	**0.500**	**0.339**	**0.257**	**0.487**	**0.323**	**0.465**	**-0.084**	**0.917**	**0.937**	**0.917**	**0.971**	**0.953**	**0.854**	**0.849**	**0.972**	**0.970**	**0.864**	**0.940**	**0.676**	**0.922**	**0.642**	**0.498**	**0.333**	**0.209**
Zr_w_ICP-MS	-0.015	**0.172**	**0.159**	**0.627**	**0.182**	**0.146**	**0.156**	**0.760**	**0.755**	**0.734**	**0.744**	**0.717**	**0.559**	**0.508**	**0.679**	**0.688**	**0.536**	**0.666**	**0.205**	**0.645**	**0.146**	**0.612**	**0.166**	0.031
Nb_w_ICP-MS	**0.437**	**0.935**	**0.721**	**0.100**	**0.851**	**0.687**	**-0.207**	**0.382**	**0.355**	**0.405**	**0.331**	**0.380**	**0.461**	**0.500**	**0.377**	**0.389**	**0.498**	**0.427**	**0.591**	**0.442**	**0.597**	**0.632**	**0.942**	**0.443**
Mo_w_ICP-MS	**-0.152**	0.042	0.072	**0.644**	0.041	**-0.088**	**0.499**	-0.014	0.029	0.008	0.058	0.036	0.003	-0.065	0.029	0.043	-0.053	0.015	**-0.105**	-0.010	**-0.106**	0.047	0.043	0.002
Ag_w_ICP-MS	**0.516**	**0.895**	**0.698**	**0.083**	**0.814**	**0.711**	**-0.211**	**0.406**	**0.381**	**0.437**	**0.359**	**0.415**	**0.504**	**0.546**	**0.413**	**0.425**	**0.543**	**0.465**	**0.642**	**0.480**	**0.649**	**0.563**	**0.902**	**0.445**
Cd_w_ICP-MS	**1**	**0.469**	**0.392**	-0.066	**0.431**	**0.563**	**-0.307**	**0.444**	**0.429**	**0.467**	**0.410**	**0.460**	**0.572**	**0.617**	**0.489**	**0.487**	**0.610**	**0.521**	**0.703**	**0.534**	**0.713**	**0.237**	**0.463**	**0.298**
In_w_ICP-MS	**0.469**	**1**	**0.746**	0.063	**0.897**	**0.646**	**-0.248**	**0.352**	**0.326**	**0.378**	**0.306**	**0.356**	**0.443**	**0.483**	**0.355**	**0.367**	**0.482**	**0.406**	**0.588**	**0.423**	**0.598**	**0.563**	**0.993**	**0.450**
Sn_w_ICP-MS	**0.392**	**0.746**	**1**	**0.085**	**0.678**	**0.485**	**-0.132**	**0.277**	**0.256**	**0.295**	**0.235**	**0.277**	**0.344**	**0.359**	**0.273**	**0.283**	**0.358**	**0.313**	**0.429**	**0.319**	**0.439**	**0.442**	**0.752**	**0.332**
Sb_w_ICP-MS	-0.066	0.063	**0.085**	**1**	**0.081**	0.011	**0.439**	**0.429**	**0.480**	**0.429**	**0.522**	**0.467**	**0.301**	**0.246**	**0.460**	**0.470**	**0.277**	**0.419**	0.048	**0.378**	0.014	**0.290**	0.063	0.014
Te_w_ICP-MS	**0.431**	**0.897**	**0.678**	**0.081**	**1**	**0.577**	**-0.194**	**0.336**	**0.312**	**0.358**	**0.294**	**0.339**	**0.415**	**0.448**	**0.338**	**0.349**	**0.448**	**0.384**	**0.519**	**0.397**	**0.529**	**0.533**	**0.904**	**0.412**
Cs_w_ICP-MS	**0.563**	**0.646**	**0.485**	0.011	**0.577**	**1**	**-0.323**	**0.486**	**0.462**	**0.517**	**0.429**	**0.494**	**0.587**	**0.640**	**0.491**	**0.501**	**0.633**	**0.543**	**0.749**	**0.564**	**0.755**	**0.451**	**0.643**	**0.402**
Ba_w_ICP-MS	**-0.307**	**-0.248**	**-0.132**	**0.439**	**-0.194**	**-0.323**	**1**	**-0.119**	**-0.101**	**-0.134**	-0.055	**-0.109**	**-0.123**	**-0.233**	**-0.130**	**-0.116**	**-0.215**	**-0.148**	**-0.302**	**-0.171**	**-0.307**	**-0.093**	**-0.237**	**-0.181**
La_w_ICP-MS	**0.444**	**0.352**	**0.277**	**0.429**	**0.336**	**0.486**	**-0.119**	**1**	**0.980**	**0.983**	**0.951**	**0.969**	**0.898**	**0.884**	**0.951**	**0.953**	**0.898**	**0.951**	**0.686**	**0.946**	**0.644**	**0.584**	**0.345**	**0.210**
Ce_w_ICP-MS	**0.429**	**0.326**	**0.256**	**0.480**	**0.312**	**0.462**	**-0.101**	**0.980**	**1**	**0.969**	**0.972**	**0.978**	**0.888**	**0.867**	**0.968**	**0.967**	**0.880**	**0.951**	**0.663**	**0.939**	**0.621**	**0.555**	**0.320**	**0.198**
Pr_w_ICP-MS	**0.467**	**0.378**	**0.295**	**0.429**	**0.358**	**0.517**	**-0.134**	**0.983**	**0.969**	**1**	**0.943**	**0.978**	**0.932**	**0.926**	**0.957**	**0.963**	**0.938**	**0.976**	**0.737**	**0.973**	**0.695**	**0.587**	**0.371**	**0.233**
Nd_w_ICP-MS	**0.410**	**0.306**	**0.235**	**0.522**	**0.294**	**0.429**	-0.055	**0.951**	**0.972**	**0.943**	**1**	**0.971**	**0.857**	**0.838**	**0.975**	**0.971**	**0.853**	**0.939**	**0.635**	**0.922**	**0.595**	**0.520**	**0.299**	**0.189**
Sm_w_ICP-MS	**0.460**	**0.356**	**0.277**	**0.467**	**0.339**	**0.494**	**-0.109**	**0.969**	**0.978**	**0.978**	**0.971**	**1**	**0.915**	**0.906**	**0.988**	**0.991**	**0.919**	**0.982**	**0.720**	**0.972**	**0.681**	**0.547**	**0.350**	**0.222**
Eu_w_ICP-MS	**0.572**	**0.443**	**0.344**	**0.301**	**0.415**	**0.587**	**-0.123**	**0.898**	**0.888**	**0.932**	**0.857**	**0.915**	**1**	**0.960**	**0.896**	**0.902**	**0.956**	**0.929**	**0.834**	**0.938**	**0.800**	**0.565**	**0.435**	**0.273**
Tb_w_ICP-MS	**0.617**	**0.483**	**0.359**	**0.246**	**0.448**	**0.640**	**-0.233**	**0.884**	**0.867**	**0.926**	**0.838**	**0.906**	**0.960**	**1**	**0.895**	**0.902**	**0.995**	**0.939**	**0.894**	**0.953**	**0.863**	**0.574**	**0.476**	**0.310**
Gd_w_ICP-MS	**0.489**	**0.355**	**0.273**	**0.460**	**0.338**	**0.491**	**-0.130**	**0.951**	**0.968**	**0.957**	**0.975**	**0.988**	**0.896**	**0.895**	**1**	**0.996**	**0.908**	**0.975**	**0.717**	**0.961**	**0.681**	**0.525**	**0.350**	**0.224**
Dy_w_ICP-MS	**0.487**	**0.367**	**0.283**	**0.470**	**0.349**	**0.501**	**-0.116**	**0.953**	**0.967**	**0.963**	**0.971**	**0.991**	**0.902**	**0.902**	**0.996**	**1**	**0.916**	**0.982**	**0.728**	**0.969**	**0.692**	**0.532**	**0.361**	**0.230**
Ho_w_ICP-MS	**0.610**	**0.482**	**0.358**	**0.277**	**0.448**	**0.633**	**-0.215**	**0.898**	**0.880**	**0.938**	**0.853**	**0.919**	**0.956**	**0.995**	**0.908**	**0.916**	**1**	**0.952**	**0.884**	**0.963**	**0.853**	**0.576**	**0.475**	**0.305**
Er_w_ICP-MS	**0.521**	**0.406**	**0.313**	**0.419**	**0.384**	**0.543**	**-0.148**	**0.951**	**0.951**	**0.976**	**0.939**	**0.982**	**0.929**	**0.939**	**0.975**	**0.982**	**0.952**	**1**	**0.781**	**0.992**	**0.747**	**0.553**	**0.401**	**0.255**
Tm_w_ICP-MS	**0.703**	**0.588**	**0.429**	0.048	**0.519**	**0.749**	**-0.302**	**0.686**	**0.663**	**0.737**	**0.635**	**0.720**	**0.834**	**0.894**	**0.717**	**0.728**	**0.884**	**0.781**	**1**	**0.809**	**0.987**	**0.479**	**0.579**	**0.376**
Yb_w_ICP-MS	**0.534**	**0.423**	**0.319**	**0.378**	**0.397**	**0.564**	**-0.171**	**0.946**	**0.939**	**0.973**	**0.922**	**0.972**	**0.938**	**0.953**	**0.961**	**0.969**	**0.963**	**0.992**	**0.809**	**1**	**0.779**	**0.560**	**0.417**	**0.261**
Lu_w_ICP-MS	**0.713**	**0.598**	**0.439**	0.014	**0.529**	**0.755**	**-0.307**	**0.644**	**0.621**	**0.695**	**0.595**	**0.681**	**0.800**	**0.863**	**0.681**	**0.692**	**0.853**	**0.747**	**0.987**	**0.779**	**1**	**0.425**	**0.590**	**0.368**
Hf_w_ICP-MS	**0.237**	**0.563**	**0.442**	**0.290**	**0.533**	**0.451**	**-0.093**	**0.584**	**0.555**	**0.587**	**0.520**	**0.547**	**0.565**	**0.574**	**0.525**	**0.532**	**0.576**	**0.553**	**0.479**	**0.560**	**0.425**	**1**	**0.567**	**0.241**
Ta_w_ICP-MS	**0.463**	**0.993**	**0.752**	0.063	**0.904**	**0.643**	**-0.237**	**0.345**	**0.320**	**0.371**	**0.299**	**0.350**	**0.435**	**0.476**	**0.350**	**0.361**	**0.475**	**0.401**	**0.579**	**0.417**	**0.590**	**0.567**	**1**	**0.461**
W_w_ICP-MS	**0.298**	**0.450**	**0.332**	0.014	**0.412**	**0.402**	**-0.181**	**0.210**	**0.198**	**0.233**	**0.189**	**0.222**	**0.273**	**0.310**	**0.224**	**0.230**	**0.305**	**0.255**	**0.376**	**0.261**	**0.368**	**0.241**	**0.461**	**1**
Re_w_ICP-MS	**0.439**	**0.867**	**0.652**	**0.098**	**0.788**	**0.552**	**-0.096**	**0.253**	**0.233**	**0.280**	**0.214**	**0.263**	**0.385**	**0.387**	**0.261**	**0.272**	**0.384**	**0.305**	**0.494**	**0.323**	**0.505**	**0.477**	**0.874**	**0.392**
Tl_w_ICP-MS	**0.496**	**0.468**	**0.361**	**0.270**	**0.413**	**0.518**	**-0.092**	**0.340**	**0.349**	**0.385**	**0.349**	**0.391**	**0.448**	**0.469**	**0.400**	**0.411**	**0.470**	**0.421**	**0.544**	**0.431**	**0.549**	**0.251**	**0.467**	**0.296**
Pb_w_ICP-MS	**0.158**	**0.122**	**0.103**	**0.215**	**0.136**	**0.222**	0.055	**0.552**	**0.572**	**0.543**	**0.555**	**0.539**	**0.564**	**0.479**	**0.517**	**0.508**	**0.478**	**0.505**	**0.351**	**0.518**	**0.330**	**0.337**	**0.128**	0.019
U_w_ICP-MS	0.037	**0.209**	**0.149**	**0.268**	**0.167**	**0.201**	**0.213**	-0.073	-0.065	-0.017	-0.066	-0.013	0.068	0.073	-0.020	0.003	0.066	0.021	**0.213**	0.029	**0.231**	0.001	**0.203**	**0.089**
Ca_w_ICP-ES	**0.230**	**0.242**	**0.162**	**0.129**	**0.208**	**0.200**	**0.146**	**-0.146**	**-0.150**	**-0.111**	**-0.143**	**-0.100**	-0.006	0.010	-0.078	-0.062	0.008	-0.042	**0.173**	-0.051	**0.203**	**-0.116**	**0.243**	**0.193**
Fe_w_ICP-ES	**0.324**	**0.252**	**0.217**	**0.519**	**0.255**	**0.352**	0.040	**0.871**	**0.893**	**0.858**	**0.889**	**0.868**	**0.792**	**0.727**	**0.852**	**0.853**	**0.745**	**0.830**	**0.507**	**0.815**	**0.469**	**0.486**	**0.243**	**0.174**
K_w_ICP-ES	**0.220**	**0.207**	**0.167**	0.028	**0.215**	**0.330**	**-0.193**	**-0.097**	**-0.094**	-0.063	**-0.107**	-0.054	-0.015	0.071	-0.028	-0.022	0.066	0.005	**0.217**	0.003	**0.237**	-0.051	**0.218**	**0.174**
Mg_w_ICP-ES	**0.428**	**0.376**	**0.259**	**-0.140**	**0.324**	**0.373**	**-0.151**	**-0.162**	**-0.176**	**-0.112**	**-0.191**	**-0.111**	0.031	**0.101**	-0.078	-0.065	**0.091**	-0.019	**0.343**	-0.015	**0.385**	**-0.110**	**0.377**	**0.264**
Na_w_ICP-ES	**0.379**	**0.270**	**0.206**	**0.504**	**0.261**	**0.356**	0.052	**0.381**	**0.408**	**0.415**	**0.434**	**0.447**	**0.424**	**0.425**	**0.472**	**0.484**	**0.438**	**0.471**	**0.381**	**0.436**	**0.373**	**0.173**	**0.269**	**0.238**
P_w_ICP-ES	**0.439**	**0.917**	**0.729**	0.080	**0.835**	**0.653**	**-0.194**	**0.354**	**0.330**	**0.379**	**0.308**	**0.357**	**0.438**	**0.477**	**0.355**	**0.366**	**0.475**	**0.403**	**0.571**	**0.418**	**0.578**	**0.594**	**0.924**	**0.423**
S_w_ICP-ES	**0.400**	**0.281**	**0.168**	**-0.106**	**0.235**	**0.333**	**-0.304**	**-0.127**	**-0.125**	-0.065	**-0.145**	-0.059	0.052	**0.143**	-0.018	-0.012	**0.130**	0.028	**0.335**	0.028	**0.359**	**-0.083**	**0.280**	**0.240**
Sc_w_ICP-ES	**0.620**	**0.799**	**0.591**	-0.017	**0.714**	**0.727**	**-0.295**	**0.486**	**0.461**	**0.525**	**0.437**	**0.513**	**0.624**	**0.680**	**0.514**	**0.525**	**0.672**	**0.577**	**0.820**	**0.611**	**0.845**	**0.432**	**0.792**	**0.388**
Si_w_ICP-ES	**0.484**	**0.348**	**0.226**	**0.291**	**0.291**	**0.446**	-0.054	**0.475**	**0.466**	**0.499**	**0.489**	**0.522**	**0.526**	**0.565**	**0.544**	**0.555**	**0.572**	**0.563**	**0.579**	**0.552**	**0.578**	**0.255**	**0.339**	**0.296**

Table 16 Continued

Variables	Re_w	Tl_w	Pb_w	U_w	Ca_w	Fe_w	K_w	Mg_w	Na_w	P_w	S_w	Sc_w	Si_w
pH	**-0.357**	**-0.414**	**-0.289**	-0.015	-0.043	**-0.439**	-0.073	**-0.201**	**-0.261**	**-0.390**	**-0.194**	**-0.615**	**-0.402**
Conductivity	**0.339**	**0.392**	**-0.299**	**0.660**	**0.916**	**-0.177**	**0.586**	**0.934**	**0.568**	**0.314**	**0.828**	**0.372**	**0.539**
Li_w_ICP-MS	**0.293**	**0.421**	-0.019	**0.364**	**0.594**	**0.281**	**0.615**	**0.648**	**0.871**	**0.317**	**0.706**	**0.392**	**0.765**
Be_w_ICP-MS	**0.318**	**0.372**	**0.449**	-0.043	-0.018	**0.738**	0.017	0.080	**0.401**	**0.412**	**0.110**	**0.628**	**0.554**
B_w_ICP-MS	**0.224**	**0.394**	-0.012	**0.265**	**0.369**	**0.204**	**0.753**	**0.445**	**0.802**	**0.270**	**0.604**	**0.234**	**0.588**
Al_w_ICP-MS	**0.252**	**0.332**	**0.411**	-0.004	-0.043	**0.634**	0.035	0.056	**0.407**	**0.348**	**0.118**	**0.528**	**0.494**
Ti_w_ICP-MS	**0.356**	**0.202**	**0.465**	-0.059	**-0.223**	**0.574**	-0.057	**-0.234**	**0.165**	**0.457**	**-0.166**	**0.348**	**0.223**
V_w_ICP-MS	**0.209**	**0.185**	**0.429**	0.002	**-0.186**	**0.703**	**-0.248**	**-0.376**	**0.280**	**0.291**	**-0.379**	**0.149**	**0.197**
Cr_w_ICP-MS	**0.242**	**0.206**	**0.491**	**-0.084**	**-0.222**	**0.810**	**-0.289**	**-0.358**	**0.274**	**0.329**	**-0.360**	**0.267**	**0.272**
Mn_w_ICP-MS	**0.287**	**0.321**	**0.176**	-0.003	**0.220**	**0.526**	**0.213**	**0.318**	**0.589**	**0.295**	**0.332**	**0.398**	**0.571**
Co_w_ICP-MS	**0.281**	**0.324**	**0.116**	-0.022	**0.222**	**0.351**	**0.258**	**0.423**	**0.476**	**0.339**	**0.453**	**0.493**	**0.533**
Ni_w_ICP-MS	**0.292**	**0.411**	**0.188**	0.041	**0.249**	**0.604**	**0.172**	**0.296**	**0.638**	**0.337**	**0.318**	**0.467**	**0.659**
Cu_w_ICP-MS	**0.223**	**0.405**	**0.530**	0.045	-0.069	**0.805**	0.025	**-0.138**	**0.463**	**0.296**	**-0.113**	**0.407**	**0.460**
Zn_w_ICP-MS	**0.352**	**0.463**	**0.227**	0.010	**0.202**	**0.461**	**0.201**	**0.373**	**0.446**	**0.401**	**0.407**	**0.587**	**0.554**
Ga_w_ICP-MS	**0.457**	**0.401**	**0.375**	**0.121**	0.028	**0.384**	**0.201**	**0.127**	**0.263**	**0.567**	**0.139**	**0.607**	**0.325**
Ge_w_ICP-MS	**0.642**	**0.420**	**0.198**	**0.195**	**0.209**	**0.286**	**0.222**	**0.311**	**0.379**	**0.820**	**0.231**	**0.668**	**0.374**
As_w_ICP-MS	**0.181**	**0.224**	**0.435**	0.030	-0.069	**0.767**	**-0.185**	**-0.312**	**0.440**	**0.202**	**-0.316**	**0.083**	**0.243**
Se_w_ICP-MS	**0.743**	**0.453**	0.049	**0.277**	**0.245**	**0.182**	**0.305**	**0.359**	**0.363**	**0.729**	**0.315**	**0.633**	**0.344**
Rb_w_ICP-MS	**0.326**	**0.467**	**0.096**	**0.213**	**0.333**	**0.164**	**0.835**	**0.518**	**0.624**	**0.333**	**0.645**	**0.405**	**0.538**
Sr_w_ICP-MS	**0.283**	**0.425**	**-0.164**	**0.650**	**0.831**	0.031	**0.550**	**0.704**	**0.709**	**0.221**	**0.686**	**0.249**	**0.562**
Y_w_ICP-MS	**0.254**	**0.393**	**0.496**	-0.025	-0.042	**0.848**	-0.012	-0.057	**0.510**	**0.337**	-0.014	**0.483**	**0.575**
Zr_w_ICP-MS	**0.105**	**0.087**	**0.451**	**-0.140**	**-0.291**	**0.759**	**-0.285**	**-0.474**	**0.227**	**0.195**	**-0.432**	**0.098**	**0.203**
Nb_w_ICP-MS	**0.821**	**0.461**	**0.170**	**0.187**	**0.190**	**0.273**	**0.220**	**0.322**	**0.292**	**0.932**	**0.253**	**0.744**	**0.348**
Mo_w_ICP-MS	**0.145**	**0.301**	0.006	**0.648**	**0.495**	**0.098**	0.038	**0.155**	**0.361**	0.066	**0.109**	-0.056	**0.123**
Ag_w_ICP-MS	**0.785**	**0.506**	**0.179**	**0.202**	**0.209**	**0.308**	**0.246**	**0.358**	**0.325**	**0.930**	**0.280**	**0.760**	**0.383**
Cd_w_ICP-MS	**0.439**	**0.496**	**0.158**	0.037	**0.230**	**0.324**	**0.220**	**0.428**	**0.379**	**0.439**	**0.400**	**0.620**	**0.484**
In_w_ICP-MS	**0.867**	**0.468**	**0.122**	**0.209**	**0.242**	**0.252**	**0.207**	**0.376**	**0.270**	**0.917**	**0.281**	**0.799**	**0.348**
Sn_w_ICP-MS	**0.652**	**0.361**	**0.103**	**0.149**	**0.162**	**0.217**	**0.167**	**0.259**	**0.206**	**0.729**	**0.168**	**0.591**	**0.226**
Sb_w_ICP-MS	**0.098**	**0.270**	**0.215**	**0.268**	**0.129**	**0.519**	0.028	**-0.140**	**0.504**	0.080	**-0.106**	-0.017	**0.291**
Te_w_ICP-MS	**0.788**	**0.413**	**0.136**	**0.167**	**0.208**	**0.255**	**0.215**	**0.324**	**0.261**	**0.835**	**0.235**	**0.714**	**0.291**
Cs_w_ICP-MS	**0.552**	**0.518**	**0.222**	**0.201**	**0.200**	**0.352**	**0.330**	**0.373**	**0.356**	**0.653**	**0.333**	**0.727**	**0.446**
Ba_w_ICP-MS	**-0.096**	**-0.092**	0.055	**0.213**	**0.146**	0.040	**-0.193**	**-0.151**	0.052	**-0.194**	**-0.304**	**-0.295**	-0.054
La_w_ICP-MS	**0.253**	**0.340**	**0.552**	-0.073	**-0.146**	**0.871**	**-0.097**	**-0.162**	**0.381**	**0.354**	**-0.127**	**0.486**	**0.475**
Ce_w_ICP-MS	**0.233**	**0.349**	**0.572**	-0.065	**-0.150**	**0.893**	**-0.094**	**-0.176**	**0.408**	**0.330**	**-0.125**	**0.461**	**0.466**
Pr_w_ICP-MS	**0.280**	**0.385**	**0.543**	-0.017	**-0.111**	**0.858**	-0.063	**-0.112**	**0.415**	**0.379**	-0.065	**0.525**	**0.499**
Nd_w_ICP-MS	**0.214**	**0.349**	**0.555**	-0.066	**-0.143**	**0.889**	**-0.107**	**-0.191**	**0.434**	**0.308**	**-0.145**	**0.437**	**0.489**
Sm_w_ICP-MS	**0.263**	**0.391**	**0.539**	-0.013	**-0.100**	**0.868**	-0.054	**-0.111**	**0.447**	**0.357**	-0.059	**0.513**	**0.522**
Eu_w_ICP-MS	**0.385**	**0.448**	**0.564**	0.068	-0.006	**0.792**	-0.015	0.031	**0.424**	**0.438**	0.052	**0.624**	**0.526**
Tb_w_ICP-MS	**0.387**	**0.469**	**0.479**	0.073	0.010	**0.727**	0.071	**0.101**	**0.425**	**0.477**	**0.143**	**0.680**	**0.565**
Gd_w_ICP-MS	**0.261**	**0.400**	**0.517**	-0.020	-0.078	**0.852**	-0.028	-0.078	**0.472**	**0.355**	-0.018	**0.514**	**0.544**
Dy_w_ICP-MS	**0.272**	**0.411**	**0.508**	0.003	-0.062	**0.853**	-0.022	-0.065	**0.484**	**0.366**	-0.012	**0.525**	**0.555**
Ho_w_ICP-MS	**0.384**	**0.470**	**0.478**	0.066	0.008	**0.745**	0.066	**0.091**	**0.438**	**0.475**	**0.130**	**0.672**	**0.572**
Er_w_ICP-MS	**0.305**	**0.421**	**0.505**	0.021	-0.042	**0.830**	0.005	-0.019	**0.471**	**0.403**	0.028	**0.577**	**0.563**
Tm_w_ICP-MS	**0.494**	**0.544**	**0.351**	**0.213**	**0.173**	**0.507**	**0.217**	**0.343**	**0.381**	**0.571**	**0.335**	**0.820**	**0.579**
Yb_w_ICP-MS	**0.323**	**0.431**	**0.518**	0.029	-0.051	**0.815**	0.003	-0.015	**0.436**	**0.418**	0.028	**0.611**	**0.552**
Lu_w_ICP-MS	**0.505**	**0.549**	**0.330**	**0.231**	**0.203**	**0.469**	**0.237**	**0.385**	**0.373**	**0.578**	**0.359**	**0.845**	**0.578**
Hf_w_ICP-MS	**0.477**	**0.251**	**0.337**	0.001	**-0.116**	**0.486**	-0.051	**-0.110**	**0.173**	**0.594**	**-0.083**	**0.432**	**0.255**
Ta_w_ICP-MS	**0.874**	**0.467**	**0.128**	**0.203**	**0.243**	**0.243**	**0.218**	**0.377**	**0.269**	**0.924**	**0.280**	**0.792**	**0.339**
W_w_ICP-MS	**0.392**	**0.296**	0.019	**0.089**	**0.193**	**0.174**	**0.174**	**0.264**	**0.238**	**0.423**	**0.240**	**0.388**	**0.296**
Re_w_ICP-MS	**1**	**0.485**	**0.108**	**0.267**	**0.296**	**0.222**	**0.194**	**0.372**	**0.264**	**0.806**	**0.283**	**0.688**	**0.343**
Tl_w_ICP-MS	**0.485**	**1**	**0.171**	**0.404**	**0.333**	**0.268**	**0.329**	**0.362**	**0.413**	**0.460**	**0.379**	**0.515**	**0.392**
Pb_w_ICP-MS	**0.108**	**0.171**	**1**	-0.073	**-0.282**	**0.570**	**-0.158**	**-0.323**	0.036	**0.155**	**-0.314**	**0.265**	0.032
U_w_ICP-MS	**0.267**	**0.404**	-0.073	**1**	**0.763**	**-0.129**	**0.306**	**0.582**	**0.302**	**0.194**	**0.482**	**0.261**	**0.268**
Ca_w_ICP-ES	**0.296**	**0.333**	**-0.282**	**0.763**	**1**	**-0.168**	**0.416**	**0.854**	**0.481**	**0.201**	**0.693**	**0.274**	**0.467**
Fe_w_ICP-ES	**0.222**	**0.268**	**0.570**	**-0.129**	**-0.168**	**1**	**-0.185**	**-0.269**	**0.399**	**0.263**	**-0.239**	**0.346**	**0.416**
K_w_ICP-ES	**0.194**	**0.329**	**-0.158**	**0.306**	**0.416**	**-0.185**	**1**	**0.620**	**0.493**	**0.215**	**0.749**	**0.227**	**0.404**
Mg_w_ICP-ES	**0.372**	**0.362**	**-0.323**	**0.582**	**0.854**	**-0.269**	**0.620**	**1**	**0.456**	**0.331**	**0.862**	**0.443**	**0.495**
Na_w_ICP-ES	**0.264**	**0.413**	0.036	**0.302**	**0.481**	**0.399**	**0.493**	**0.456**	**1**	**0.293**	**0.531**	**0.278**	**0.714**
P_w_ICP-ES	**0.806**	**0.460**	**0.155**	**0.194**	**0.201**	**0.263**	**0.215**	**0.331**	**0.293**	**1**	**0.245**	**0.731**	**0.347**
S_w_ICP-ES	**0.283**	**0.379**	**-0.314**	**0.482**	**0.693**	**-0.239**	**0.749**	**0.862**	**0.531**	**0.245**	**1**	**0.347**	**0.516**
Sc_w_ICP-ES	**0.688**	**0.515**	**0.265**	**0.261**	**0.274**	**0.346**	**0.227**	**0.443**	**0.278**	**0.731**	**0.347**	**1**	**0.478**
Si_w_ICP-ES	**0.343**	**0.392**	0.032	**0.268**	**0.467**	**0.416**	**0.404**	**0.495**	**0.714**	**0.347**	**0.516**	**0.478**	**1**

elements such as Ni, Fe, Mn are included in this association as redox state may correlate with pH.

Elements included in the organic shale group are elements that may be sourced from black shale horizons. Organic-rich shale can host base metal group elements in anomalous, but sub economic concentrations. These elements in association with As, V, TREE, and Zr in the absence of elevated sulphur concentrations are interpreted to be shale-derived rather than base metal sulphide-related. This interpretation does not preclude the potential of a SedEx or related deposit in the study area, but rather that anomalous base metal values may need to be levelled to this baseline. Sulphur shows a strong positive correlation with Ca, Mg, K, and conductivity.

Redox associated elements Fe and Mn are correlative with Ni, Co, and to a lesser degree V and As. These elements partition to solid and liquid phases based on redox state. In this dataset, redox state is inferred from the association of oxidization and low pH.

Elements Sr, Ca, Mg, Li, Be and Na are inferred to be associated with carbonate lithologies. The Sr, Ca, Mg association is most indicative of limestone and dolomite.

The major element association constitutes the majority of the total dissolved solids in the water sample. This is inferred from conductivity. The elements listed in this ground are therefore correlated with conductivity first, and each other second. These elements may geochemically represent major geologic units in the study area.

The stream sediment data indicates principal economic commodities likely to be found in the study area based on the available geology include Au, Cu, Pb and Zn. Copper response in water samples correlates strongly with lithophile and REE similar to the stream sediment data interpretation. Zinc response correlates with Co, Cd, Ni, Be, Tm, Tb and Lu. Lead response correlated with Ce, Fe, Eu, Nd, La, Pr, Sm, and Cu.

10.3 Principal Component Analysis

Principal component analysis (PCA) is a statistical technique used to analyze large multivariable data sets. The theory and practice of principal component analysis has been discussed previously in section 9.3.

Four PCA analyses were completed:

1. 5x detection limit: a factor model considering all qualifying elements
2. Major element associations
3. Carbonate association model
4. Black shale association model

This approach was taken in facilitate the interpretation of anomalous economically interesting metals against the baseline of each metal's assumed deposit type and therefore host lithology.

Factors of interest for each PCA model were selected based on the following criteria:

- Highest score in cumulative percent rank (sum of percentage contributions of elements of interest).
- Positive correlation constants for elements of interest, and
- Roughly equal contribution to the cumulative percent rank by each of the elements in a multi-element set.

10.3.1 5x detection limit PCA

This model considered all elements which showed a mean value greater than or equal to 5x the mean value for that element. This set included: Li, Be, B, Al, Mn, Co, Ni, Cu, Zr, Rb, Sr, Y, Mo, Ba, La, Ce, Pr, Nd, Sm, Eu, Tb, Gd, Dy, Ho, Er, Tm, Yb, Pb, U, Ca, Fe, K, Mg, ,Na, S, Si.

Most of the observed geochemical response in all elements can be attributed to PCA Factors F1 through F3 as shown below and constitute 80% of statistical variability in this dataset.

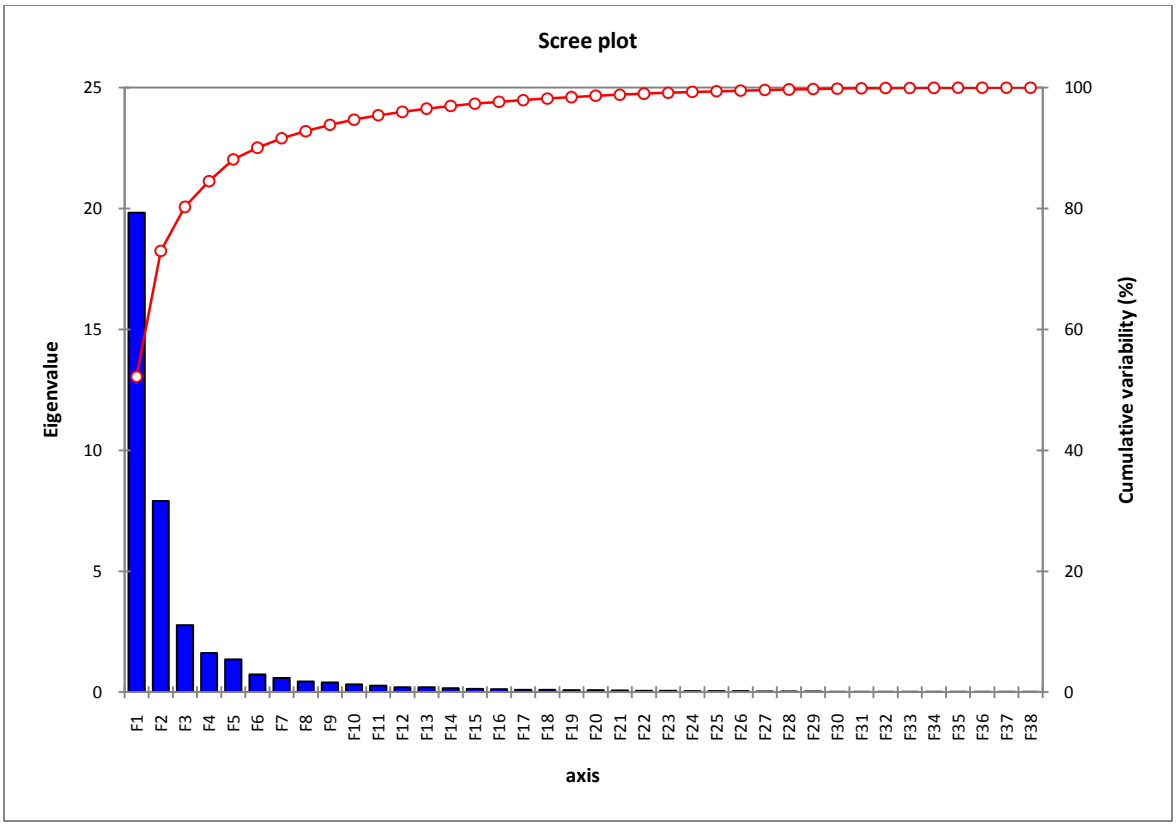


Figure 4 Scree Plot for five times detection limit PCA

Factor F1 explains 52% of the variability in the dataset. This factor contains the most significant element contributions of 23 variables including: all REE elements (TREE), Be, Ce, La, Nd, Al, Ni, Cu, Fe, Zn, Mn, Co, Si, and pH. This factor contains elements from the major, black shale, redox, and acid element associations. This factor is has a strong negative pH factor loading. In the absence of a significant conductivity loading, it is therefore interpreted to be most relevant to the redox, acid, and black shale associations (Figure D, appendix 4).

Factor F2 explains 21% of the variability and shows prominent factor loadings from conductivity, Mg, S, Ca, Sr, K, Li, B, U, and Rb. This factor may be mapping the major and/or carbonate element associations.

Factor F3 explains 7% of the variability. An element association of Mo and Ba, and subordinate U, Co, An, Sr, pH (positive) and Cu may represent the alkaline element association.

Contribution of the variables (%):

	F1	F2	F3	F4	F5	F6	F7	F8	F9	F10	F11	F12	F13	F14	F15	F16	F17	F18	F19	F20	F21	F22	F23	F24	F25	F26	F27	F28	F29	F30	F31	F32	F33	F34	F35	F36	F37	F38
pH	2.091	0.003	3.794	4.424	1.430	3.916	14.025	45.301	12.673	2.949	0.468	0.316	1.215	1.680	2.741	0.740	0.059	0.740	0.032	0.551	0.393	0.216	0.002	0.006	0.096	0.061	0.009	0.013	0.032	0.006	0.000	0.008	0.009	0.001	0.000	0.000	0.000	0.000
Conductiv	0.152	10.513	0.121	4.128	0.000	0.127	0.869	1.002	1.097	0.008	2.781	2.507	2.525	3.679	0.179	0.341	0.690	5.381	0.002	0.085	0.543	0.744	3.461	0.168	0.309	1.176	35.324	3.171	3.441	15.239	0.108	0.055	0.001	0.003	0.068	0.003	0.002	0.000
Li_w_ICP	1.757	6.446	0.021	2.688	1.268	0.000	0.313	0.501	1.432	0.262	2.139	0.284	2.170	1.315	0.054	9.607	0.034	3.270	11.470	8.958	0.669	0.077	27.361	8.284	0.640	7.029	0.446	0.449	0.409	0.282	0.006	0.276	0.008	0.016	0.008	0.045	0.000	0.005
Be_w_ICF	4.390	0.159	1.179	0.773	0.274	0.059	0.038	0.636	0.003	0.004	0.462	0.273	0.618	1.808	0.033	1.290	2.458	12.152	15.121	6.880	3.680	2.682	13.942	2.946	0.010	0.117	3.083	15.866	1.422	5.566	0.717	0.133	0.932	0.101	0.049	0.113	0.024	0.002
B_w_ICP-	0.911	4.898	0.268	17.151	3.699	0.843	0.003	1.782	1.055	2.875	3.600	0.896	2.148	0.628	5.874	2.905	1.904	17.055	1.013	13.634	4.029	2.970	0.036	1.476	0.669	4.281	0.184	1.298	0.362	0.573	0.838	0.001	0.033	0.049	0.006	0.000	0.039	0.017
Al_w_ICP	3.650	0.078	1.063	0.022	2.310	1.841	7.614	1.548	6.376	3.753	21.124	1.268	0.273	3.904	4.918	3.187	8.256	1.628	0.011	0.271	15.891	4.093	0.000	1.854	0.717	0.284	0.245	0.990	0.695	1.939	0.106	0.017	0.022	0.025	0.004	0.003	0.008	0.012
Mn_w_ICI	2.702	0.795	1.471	0.527	17.419	5.467	0.231	0.037	0.830	0.002	0.002	4.112	9.256	9.928	0.002	0.123	2.480	0.002	2.022	4.245	0.089	0.029	5.345	12.027	9.560	0.000	1.967	8.344	0.039	0.026	0.532	0.163	0.037	0.116	0.008	0.046	0.009	0.006
Co_w_ICI	2.427	1.094	7.147	0.165	10.814	3.980	0.419	0.716	0.034	2.889	0.473	0.210	0.360	0.382	2.664	0.845	3.218	2.144	1.555	1.002	3.546	0.376	3.899	6.594	6.297	12.007	5.417	15.743	0.022	0.235	3.010	0.096	0.000	0.053	0.055	0.027	0.014	0.073
Ni_w_ICP	3.595	0.570	0.326	0.063	12.620	0.007	0.164	0.141	0.107	0.360	2.218	0.879	0.562	0.761	1.951	0.008	6.532	6.255	8.945	0.050	1.186	0.009	2.182	1.980	8.254	34.670	3.722	0.016	0.000	0.091	1.566	0.073	0.031	0.039	0.013	0.007	0.000	0.046
Cu_w_ICI	3.476	0.523	3.303	1.705	0.014	0.177	0.253	1.345	9.761	3.227	6.301	1.627	15.081	3.964	2.894	0.297	3.849	1.554	7.149	5.938	0.101	3.148	3.548	0.280	6.770	6.206	5.682	0.047	0.760	0.261	0.332	0.115	0.229	0.003	0.012	0.037	0.031	0.005
Zn_w_ICF	2.965	0.557	5.167	1.480	1.799	0.971	0.011	0.606	5.206	7.087	1.217	35.119	4.893	2.738	11.896	2.992	0.739	0.238	5.695	0.507	1.028	0.056	0.001	4.487	1.813	0.043	0.058	0.002	0.492	0.028	0.013	0.057	0.000	0.005	0.021	0.004	0.007	0.002
Rb_w_ICI	1.046	4.603	1.031	11.251	5.301	7.413	0.110	0.047	4.317	0.038	3.092	0.190	10.207	1.416	2.424	5.171	0.204	5.087	1.096	13.560	11.672	2.565	2.903	0.458	0.813	0.047	2.061	0.968	0.313	0.328	0.231	0.001	0.018	0.006	0.006	0.001	0.002	0.003
Sr_w_ICP	0.374	8.654	4.144	0.006	0.316	0.001	0.741	1.186	1.825	0.038	1.670	0.743	2.753	35.116	0.025	13.468	1.206	0.114	0.697	8.940	1.885	4.492	0.162	1.200	1.397	1.895	1.913	0.590	0.026	4.175	0.126	0.013	0.077	0.004	0.001	0.022	0.000	0.003
Y_w_ICP-	4.523	0.370	0.410	0.354	0.714	0.126	0.313	0.262	1.253	2.313	0.343	0.467	2.093	0.056	0.200	1.372	1.238	0.000	1.277	0.094	1.424	0.033	2.893	0.859	8.617	0.031	2.651	3.581	13.107	0.970	25.903	0.011	15.228	6.110	0.700	0.051	0.001	0.050
Mo_w_ICI	0.004	1.292	24.193	0.831	0.548	0.932	8.084	12.938	0.940	5.709	1.347	15.011	2.361	7.868	2.393	3.649	0.040	5.746	1.162	2.434	0.006	0.623	0.289	1.419	0.001	0.003	0.005	0.005	0.099	0.000	0.007	0.050	0.005	0.000	0.003	0.000	0.001	0.002
Ba_w_ICF	0.164	0.012	19.917	0.011	3.980	6.378	35.497	10.775	4.055	8.014	0.747	0.002	0.314	2.153	0.159	0.861	4.406	0.041	0.788	0.292	0.019	0.202	0.002	0.129	0.211	0.229	0.013	0.019	0.239	0.282	0.022	0.002	0.032	0.000	0.007	0.002	0.022	0.006
La_w_ICF	4.222	1.209	0.358	0.001	0.202	1.017	0.015	0.032	0.628	0.094	3.369	0.181	1.267	0.601	1.450	2.286	1.376	0.419	4.841	1.433	6.768	0.066	2.355	9.290	3.929	0.050	0.015	2.927	1.510	0.606	3.261	15.699	2.473	19.856	0.129	5.899	0.024	0.139
Ce_w_ICI	4.283	1.181	0.612	0.116	0.018	0.249	0.462	0.024	0.107	0.006	2.224	0.369	0.845	0.013	1.324	1.521	0.179	0.187	5.867	0.302	1.574	1.134	0.083	7.635	0.671	0.298	0.039	1.466	0.048	1.222	15.104	30.447	14.549	4.101	0.467	1.241	0.002	0.030
Pr_w_ICP	4.424	0.858	0.334	0.045	0.690	1.099	0.030	0.005	0.466	1.060	0.526	0.628	0.757	0.300	1.152	1.111	1.137	0.031	0.159	0.117	1.962	1.545	0.754	0.761	6.677	0.142	0.328	0.016	0.650	1.424	6.486	1.222	16.811	30.873	0.149	15.000	0.132	0.141
Nd_w_ICF	4.214	1.163	1.107	0.389	0.079	0.394	0.381	0.008	0.369	1.524	1.199	0.152	0.704	0.000	0.000	0.680	0.434	0.224	5.435	0.039	0.121	0.497	1.351	0.463	3.638	1.211	0.581	0.834	2.955	2.211	0.000	10.381	45.506	9.658	0.045	0.997	0.105	0.949
Sm_w_IC	4.535	0.779	0.552	0.008	0.167	0.920	0.230	0.074	0.020	0.005	0.310	0.122	0.003	0.071	1.214	0.029	0.275	0.000	1.061	0.045	1.129	0.107	0.894	0.107	0.018	0.369	0.209	1.579	5.153	0.019	3.543	3.024	0.321	6.071	51.418	13.666	0.834	1.121
Eu_w_ICF	4.312	0.284	0.041	1.425	1.635	0.230	1.175	0.015	1.940	3.612	1.502	1.635	2.549	0.406	0.061	0.896	0.000	4.480	0.131	0.107	0.004	20.021	0.322	0.042	4.739	0.483	8.059	4.524	17.775	11.607	4.059	0.344	0.108	0.557	0.204	0.076	0.605	0.035
Tb_w_ICF	4.424	0.106	0.198	1.781	2.766	0.263	0.512	0.267	0.201	4.129	1.401	0.081	0.217	0.218	0.100	0.686	0.556	1.276	1.402	0.183	1.217	3.389	0.262	1.832	2.170	4.681	0.749	0.268	8.275	0.312	7.153	0.055	0.056	0.060	0.004	2.152	46.582	0.017
Gd_w_ICI	4.622	0.566	0.294	0.049	0.003	0.663	0.694	0.168	0.292	0.145	0.199	0.014	0.477	0.098	1.285	0.208	2.212	0.131	2.562	0.003	2.970	1.191	1.400	0.780	2.084	0.011	0.045	1.006	1.851	0.438	4.469	9.471	0.048	0.657	7.852	10.883	0.424	39.735
Dy_w_ICF	4.653	0.501	0.419	0.019	0.003	0.940	0.412	0.195	0.350	0.044	0.097	0.009	0.481	0.081	0.795	0.051	1.327	0.213	1.075	0.009	2.360	1.080	1.096	1.287	0.639	0.587	0.002	1.571	2.369	0.001	3.183	10.529	0.890	0.172	2.893	2.689	0.012	56.968
Ho_w_ICF	4.501	0.119	0.095	1.392	2.371	0.458	0.597	0.281	0.177	3.956	0.755	0.055	0.040	0.123	0.078	0.342	0.597	0.469	2.108	0.281	0.668	2.371	0.242	2.529	0.195	3.105	1.480	1.176	12.443	1.419	5.256	0.036	0.458	0.637	0.026	0.471	48.622	0.071
Er_w_ICP	4.696	0.375	0.156	0.068	0.428	1.096	0.023	0.193	0.003	0.482	0.031	0.123	0.175	0.123	1.097	0.057	0.061	0.924	1.095	0.098	2.430	0.040	0.502	2.522	3.087	1.170	0.096	4.646	2.909	2.915	3.702	5.152	0.046	1.761	25.106	31.970	0.190	0.451
Tm_w_ICI	3.377	0.172	1.544	5.899	6.421	0.049	1.922	0.688	0.694	1.412	2.725	0.324	0.000	3.574	8.095	9.359	3.340	0.135	0.001	0.423	0.069	31.835	0.768	9.460	0.012	0.292	0.235	3.667	1.463	1.060	0.253	0.259	0.019	0.390	0.020	0.000	0.030	0.013
Yb_w_ICF	4.631	0.418	0.051	0.324	1.019	0.782	0.002	0.240	0.000	0.526	0.010	0.102	0.000	0.167	0.849	0.028	0.034	1.006	3.150	0.114	1.656	0.352	0.213	3.380	4.300	1.498	0.245	2.888	1.009	4.370	7.739	11.667	1.688	18.362	10.658	14.380	2.112	0.031
Pb_w_ICF	1.130	2.265	1.091	0.086	5.076	48.269	0.298	0.541	23.772	8.157	0.459	0.204	2.094	0.074	3.868	0.065	0.352	0.191	0.080	0.383	0.003	0.246	0.009	0.027	0.000	0.525	0.361	0.028	0.108	0.090	0.044	0.073	0.006	0.010	0.002	0.007	0.000	0.005
U_w_ICP-	0.027	4.606	8.691	11.904	3.765	0.880	8.326	0.262	5.303	1.079	3.507	0.766	0.452	0.616	2.530	25.862	3.801	6.634	2.329	0.005	0.626	0.969	1.289	1.889	0.347	0.756	0.012	0.693	0.575	1.309	0.049	0.007	0.016	0.036	0.019	0.041	0.002	0.018
Ca_w_ICI	0.036	9.095	2.642	7.803	0.538	0.035	0.002	0.287	1.750	3.714	7.825	1.079	0.000	0.261	0.891	0.198	0.181	0.773	0.114	0.415	0.234	2.401	0.089	0.117	7.217	2.692	0.201	7.421	3.260	37.967	0.374	0.181	0.062	0.051	0.004	0.076	0.014	0.001
Fe_w_ICF	3.302	1.494	2.131	1.011	0.429	0.012	0.940	3.913	3.579	0.959	3.732	0.721	12.113	5.101	20.179	3.768	12.276	0.434	5.607	2.348	1.612	2.124	0.104	0.381	1.828	0.211	0.409	8.276	0.387	0.076	0.290	0.213	0.000	0.003	0.003	0.000	0.018	0.014
K_w_ICP-	0.094	6.986	1.003	10.199	9.575	1.114	0.169	4.377	5.582	0.616	3.076	1.555	0.629	1.356	3.263	2.645	0.002	2.677	0.532	0.147	24.684	2.507	1.395	4.724	6.721	0.213	0.910	0.044	2.067	0.000	0.837	0.038	0.127	0.071	0.001	0.003	0.061	0.001
Mg_w_ICI	0.093	10.244	0.837	4.999	0.063	0.012	0.303	2.180	0.165	0.818	3.641	1.396	1.144	3.053	0.100	0.967	0.223	2.752	0.483	1.968	0.002	1.318	7.587	0.709	2.984	13.586	20.441	2.728	13.122	1.644	0.301	0.001	0.061	0.001	0.002	0.001	0.068	0.001
Na_w_ICF	1.776	4.149	2.019	6.577	0.962	1.164	0.989	5.966	2.796	0.088	5.797	6.453	10.345	5.036	0.100	2.035	0.013	5.766	3.435	8.579	2.527	3.921	9.988	5.771	0.001	0.001	2.748	0.060	0.091	0.482	0.184	0.084	0.073	0.001	0.007	0.001	0.002	0.012
S_w_ICP-	0.171	10.009	2.189	0.128	1.082	0.337	1.501	0.073	0.099	0.216	0.593	1.237	0.033	1.107	12.184	0.344	31.362	9.476	0.144	15.415	1.224	0.085	2.462	1.986	2.465	0.040	0.000	2.580	0.454	0.632	0.137	0.006	0.016	0.101	0.021	0.078	0.000	0.014
Si_w_ICP	2.251	2.854	0.083	0.199	0.202	7.781	12.332	1.388	0.741	27.827	9.036	18.890	8.844	0.225	0.978	0.004	2.951	0.396	0.356	0.147	0.000	0.485	0.809	0.142	0.102	0.000	0.056	0.498	0.067	0.194	0.062	0.039	0.004	0.040	0.012	0.006	0.001	0.000

Squared cosines of the variables:

	F1	F2	F3	F4	F5	F6	F7	F8	F9	F10	F11	F12	F13	F14	F15	F16	F17	F18	F19	F20	F21	F22	F23	F24	F25	F26	F27	F28	F29	F30	F31	F32	F33	F34	F35	F36	F37	F38
pH	**0.415**	0.000	0.105	0.072	0.019	0.029	0.083	0.203	0.051	0.010	0.001	0.001	0.002	0.003	0.004	0.001	0.000	0.001	0.000	0.000	0.000	0.000	0.000	0.000	0.000	0.000	0.000	0.000	0.000	0.000	0.000	0.000	0.000	0.000	0.000	0.000	0.000	0.000
Conductiv	0.030	**0.831**	0.003	0.067	0.000	0.001	0.005	0.004	0.004	0.000	0.008	0.005	0.005	0.006	0.000	0.000	0.001	0.005	0.000	0.000	0.000	0.000	0.002	0.000	0.000	0.000	0.013	0.001	0.001	0.004	0.000	0.000	0.000	0.000	0.000	0.000	0.000	0.000
Li_w_ICP	0.348	**0.509**	0.001	0.044	0.017	0.000	0.002	0.002	0.006	0.001	0.006	0.001	0.004	0.002	0.000	0.012	0.000	0.003	0.010	0.008	0.000	0.000	0.016	0.004	0.000	0.003	0.000	0.000	0.000	0.000	0.000	0.000	0.000	0.000	0.000	0.000	0.000	0.000
Be_w_ICF	**0.871**	0.013	0.033	0.013	0.004	0.000	0.000	0.003	0.000	0.000	0.001	0.001	0.001	0.003	0.000	0.002	0.003	0.012	0.014	0.006	0.003	0.002	0.008	0.001	0.000	0.000	0.001	0.006	0.000	0.001	0.000	0.000	0.000	0.000	0.000	0.000	0.000	0.000
B_w_ICP-	0.181	**0.387**	0.007	0.278	0.050	0.006	0.000	0.008	0.004	0.009	0.010	0.002	0.004	0.001	0.008	0.003	0.002	0.017	0.001	0.011	0.003	0.002	0.000	0.001	0.000	0.002	0.000	0.000	0.000	0.000	0.000	0.000	0.000	0.000	0.000	0.000	0.000	0.000
Al_w_ICP	**0.724**	0.006	0.029	0.000	0.031	0.014	0.045	0.007	0.025	0.012	0.058	0.003	0.001	0.007	0.007	0.004	0.009	0.002	0.000	0.000	0.011	0.003	0.000	0.001	0.000	0.000	0.000	0.000	0.000	0.000	0.000	0.000	0.000	0.000	0.000	0.000	0.000	0.000
Mn_w_ICI	**0.536**	0.063	0.041	0.009	0.237	0.040	0.001	0.000	0.003	0.000	0.000	0.009	0.019	0.017	0.000	0.000	0.003	0.000	0.002	0.004	0.000	0.000	0.003	0.006	0.004	0.000	0.001	0.003	0.000	0.000	0.000	0.000	0.000	0.000	0.000	0.000	0.000	0.000
Co_w_ICI	**0.481**	0.086	0.198	0.003	0.147	0.029	0.002	0.003	0.000	0.009	0.001	0.000	0.001	0.001	0.004	0.001	0.003	0.002	0.001	0.001	0.002	0.000	0.002	0.003	0.003	0.005	0.002	0.005	0.000	0.000	0.001	0.000	0.000	0.000	0.000	0.000	0.000	0.000
Ni_w_ICP	**0.713**	0.045	0.009	0.001	0.172	0.000	0.001	0.001	0.000	0.001	0.006	0.002	0.001	0.001	0.003	0.000	0.007	0.006	0.008	0.000	0.001	0.000	0.001	0.001	0.001	0.004	0.014	0.001	0.000	0.000	0.000	0.000	0.000	0.000	0.000	0.000	0.000	0.000
Cu_w_ICI	**0.689**	0.041	0.091	0.028	0.000	0.001	0.001	0.006	0.039	0.011	0.017	0.003	0.030	0.007	0.004	0.000	0.004	0.002	0.006	0.005	0.000	0.002	0.002	0.000	0.003	0.003	0.002	0.000	0.000	0.000	0.000	0.000	0.000	0.000	0.000	0.000	0.000	0.000
Zn_w_ICF	**0.588**	0.044	0.143	0.024	0.025	0.007	0.000	0.003	0.021	0.023	0.003	0.074	0.010	0.005	0.017	0.004	0.001	0.000	0.005	0.000	0.001	0.000	0.000	0.002	0.001	0.000	0.000	0.000	0.000	0.000	0.000	0.000	0.000	0.000	0.000	0.000	0.000	0.000
Rb_w_ICI	0.207	**0.364**	0.029	0.182	0.072	0.055	0.001	0.000	0.017	0.000	0.009	0.000	0.021	0.002	0.003	0.006	0.000	0.005	0.001	0.011	0.008	0.002	0.002	0.000	0.000	0.000	0.001	0.000	0.000	0.000	0.000	0.000	0.000	0.000	0.000	0.000	0.000	0.000
Sr_w_ICP	0.074	**0.684**	0.115	0.000	0.004	0.000	0.004	0.005	0.007	0.000	0.005	0.002	0.006	0.060	0.000	0.016	0.001	0.000	0.001	0.008	0.001	0.003	0.000	0.001	0.001	0.001	0.001	0.000	0.000	0.001	0.000	0.000	0.000	0.000	0.000	0.000	0.000	0.000
Y_w_ICP-	**0.897**	0.029	0.011	0.006	0.010	0.001	0.002	0.001	0.005	0.008	0.001	0.001	0.004	0.000	0.000	0.002	0.001	0.000	0.001	0.000	0.001	0.000	0.002	0.000	0.004	0.000	0.001	0.001	0.004	0.000	0.005	0.000	0.001	0.000	0.000	0.000	0.000	0.000
Mo_w_ICI	0.001	0.102	**0.670**	0.013	0.007	0.007	0.048	0.058	0.004	0.019	0.004	0.031	0.005	0.013	0.003	0.004	0.000	0.006	0.001	0.002	0.000	0.000	0.000	0.001	0.000	0.000	0.000	0.000	0.000	0.000	0.000	0.000	0.000	0.000	0.000	0.000	0.000	0.000
Ba_w_ICF	0.032	0.001	**0.551**	0.000	0.054	0.047	0.209	0.048	0.016	0.026	0.002	0.000	0.001	0.004	0.000	0.001	0.005	0.000	0.001	0.000	0.000	0.000	0.000	0.000	0.000	0.000	0.000	0.000	0.000	0.000	0.000	0.000	0.000	0.000	0.000	0.000	0.000	0.000
La_w_ICF	**0.837**	0.096	0.010	0.000	0.003	0.008	0.000	0.000	0.003	0.000	0.009	0.000	0.003	0.001	0.002	0.003	0.001	0.000	0.004	0.001	0.005	0.000	0.001	0.005	0.002	0.000	0.000	0.001	0.000	0.000	0.001	0.002	0.000	0.001	0.000	0.000	0.000	0.000
Ce_w_ICI	**0.849**	0.093	0.017	0.002	0.000	0.002	0.003	0.000	0.000	0.000	0.006	0.001	0.002	0.000	0.002	0.002	0.000	0.000	0.005	0.000	0.001	0.001	0.000	0.004	0.000	0.000	0.000	0.001	0.000	0.000	0.003	0.004	0.001	0.000	0.000	0.000	0.000	0.000
Pr_w_ICP	**0.877**	0.068	0.009	0.001	0.009	0.008	0.000	0.000	0.002	0.003	0.001	0.001	0.002	0.001	0.002	0.001	0.001	0.000	0.000	0.000	0.001	0.001	0.000	0.000	0.003	0.000	0.000	0.000	0.000	0.000	0.001	0.000	0.001	0.002	0.000	0.001	0.000	0.000
Nd_w_ICF	**0.836**	0.092	0.031	0.006	0.001	0.003	0.002	0.000	0.001	0.005	0.003	0.000	0.001	0.000	0.000	0.001	0.000	0.000	0.005	0.000	0.000	0.000	0.001	0.000	0.002	0.000	0.000	0.000	0.001	0.001	0.000	0.001	0.004	0.001	0.000	0.000	0.000	0.000
Sm_w_IC	**0.899**	0.062	0.015	0.000	0.002	0.007	0.001	0.000	0.000	0.000	0.001	0.000	0.000	0.000	0.002	0.000	0.000	0.000	0.001	0.000	0.001	0.000	0.001	0.000	0.000	0.000	0.000	0.001	0.001	0.000	0.001	0.000	0.000	0.000	0.003	0.001	0.000	0.000
Eu_w_ICF	**0.855**	0.022	0.001	0.023	0.022	0.002	0.007	0.000	0.008	0.012	0.004	0.003	0.005	0.001	0.000	0.001	0.000	0.004	0.000	0.000	0.000	0.013	0.000	0.000	0.002	0.000	0.003	0.002	0.005	0.003	0.001	0.000	0.000	0.000	0.000	0.000	0.000	0.000
Tb_w_ICF	**0.877**	0.008	0.005	0.029	0.038	0.002	0.003	0.001	0.001	0.014	0.004	0.000	0.000	0.000	0.000	0.001	0.001	0.001	0.001	0.000	0.001	0.002	0.000	0.001	0.001	0.002	0.000	0.000	0.002	0.000	0.001	0.000	0.000	0.000	0.000	0.000	0.002	0.000
Gd_w_ICI	**0.917**	0.045	0.008	0.001	0.000	0.005	0.004	0.001	0.001	0.000	0.001	0.000	0.001	0.000	0.002	0.000	0.002	0.000	0.002	0.000	0.002	0.001	0.001	0.001	0.000	0.001	0.000	0.000	0.001	0.000	0.001	0.001	0.000	0.000	0.000	0.000	0.000	0.001
Dy_w_ICF	**0.923**	0.040	0.012	0.000	0.000	0.007	0.002	0.001	0.001	0.000	0.000	0.000	0.001	0.000	0.001	0.000	0.001	0.000	0.001	0.000	0.002	0.001	0.001	0.001	0.000	0.000	0.000	0.001	0.001	0.000	0.001	0.001	0.000	0.000	0.000	0.000	0.000	0.001
Ho_w_ICF	**0.893**	0.009	0.003	0.023	0.032	0.003	0.004	0.001	0.001	0.013	0.002	0.000	0.000	0.000	0.000	0.000	0.001	0.000	0.002	0.000	0.000	0.002	0.000	0.001	0.000	0.001	0.001	0.000	0.003	0.000	0.001	0.000	0.000	0.000	0.000	0.000	0.002	0.000
Er_w_ICP	**0.931**	0.030	0.004	0.001	0.006	0.008	0.000	0.001	0.000	0.002	0.000	0.000	0.000	0.000	0.002	0.000	0.000	0.001	0.001	0.000	0.002	0.000	0.000	0.001	0.001	0.000	0.000	0.002	0.001	0.001

Factor F6 explains 2% of the variability but contains Pb as the only significant element. Lead is associated with subordinate Si, Rb, Ba, Mn, Co and pH (negative).

10.3.2 Major element association PCA

This PCA model considers elements with a positive correlation with conductivity and is interpreted to be the major element association for the study area. These elements also meet the criteria of having a statistical mean greater than five times the detection limit for each element. Under this criterion, phosphorous was not considered in the PCA analysis.

Factors F1 and F2 explain most of the observed geochemical response attributed to PCA as shown below and constitute 74% of statistical variability in this dataset.

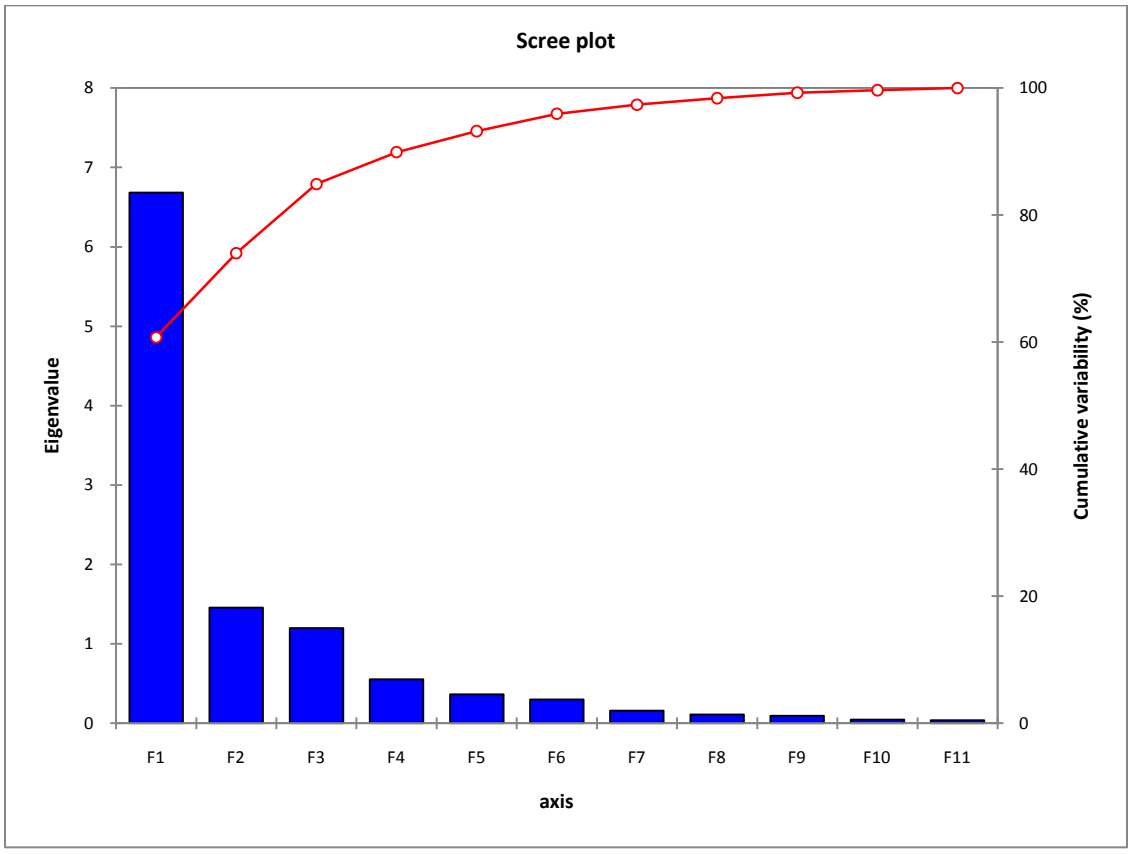


Figure 5 Scree plot for major element association PCA

Factor F1 (61% of variability) has significant contributions from all elements considered except Ba and is therefore considered to be the best approximation of this model (Table 18). Principal elements in this factor include Li, Sr, Ca, Mg, and S together with Conductivity and may be mapping carbonate rocks. Anomalous point analysis of S±Pb±Zn may be a vector to sulphide-bearing carbonate-hosted lead zinc mineralization. Alternatively the S, Ca, Mg±K association may be mapping sulphide-bearing calcareous shales.

Factor F2 (13% of variability) has significant contribution from Ba, and lesser U. These elements share an alkaline affinity and may map the buffering effect of carbonate rocks in the absence of sulphur.

Factor F11 shows the greatest contribution from conductivity and Ca. Factor F10 shows the highest concentrations of Ca and Mg.

Contribution of the variables (%):

	F1	F2	F3	F4	F5	F6	F7	F8	F9	F10	F11
Conductivity	13.010	1.373	3.067	0.621	8.264	1.135	3.485	4.331	2.858	3.409	58.447
Li_w_ICP-MS	11.082	4.211	10.017	0.006	0.442	2.769	3.317	1.945	62.893	2.728	0.590
Sr_w_ICP-MS	11.933	2.589	1.366	0.390	5.795	11.257	53.640	1.202	0.194	9.045	2.589
Ba_w_ICP-MS	0.018	42.972	17.944	17.036	14.509	1.423	1.158	4.470	0.042	0.329	0.099
U_w_ICP-MS	6.430	20.550	3.883	1.113	43.966	15.645	6.870	0.054	0.453	0.881	0.154
Ca_w_ICP-ES	11.299	9.768	2.484	4.252	1.980	2.178	3.206	4.898	0.018	34.958	24.959
K_w_ICP-ES	7.380	8.096	1.543	58.174	0.392	10.681	1.639	10.323	0.000	1.505	0.266
Mg_w_ICP-ES	11.840	0.006	9.733	0.818	14.492	0.099	2.876	3.813	2.877	45.245	8.202
Na_w_ICP-ES	8.329	2.194	25.372	0.107	5.564	11.057	16.787	3.915	22.315	0.769	3.592
S_w_ICP-ES	11.431	4.091	7.170	1.054	0.718	0.000	1.513	65.048	6.793	1.093	1.088
Si_w_ICP-ES	7.248	4.150	17.420	16.429	3.878	43.755	5.509	0.001	1.558	0.039	0.014

Squared cosines of the variables:

	F1	F2	F3	F4	F5	F6	F7	F8	F9	F10	F11
Conductivity	**0.870**	0.020	0.037	0.003	0.030	0.003	0.006	0.005	0.003	0.002	0.022
Li_w_ICP-MS	**0.741**	0.061	0.120	0.000	0.002	0.008	0.005	0.002	0.059	0.001	0.000
Sr_w_ICP-MS	**0.798**	0.038	0.016	0.002	0.021	0.034	0.085	0.001	0.000	0.004	0.001
Ba_w_ICP-MS	0.001	**0.626**	0.215	0.094	0.053	0.004	0.002	0.005	0.000	0.000	0.000
U_w_ICP-MS	**0.430**	0.299	0.046	0.006	0.160	0.047	0.011	0.000	0.000	0.000	0.000
Ca_w_ICP-ES	**0.755**	0.142	0.030	0.024	0.007	0.007	0.005	0.005	0.000	0.015	0.010
K_w_ICP-ES	**0.493**	0.118	0.018	0.322	0.001	0.032	0.003	0.012	0.000	0.001	0.000
Mg_w_ICP-ES	**0.791**	0.000	0.117	0.005	0.053	0.000	0.005	0.004	0.003	0.020	0.003
Na_w_ICP-ES	**0.557**	0.032	0.304	0.001	0.020	0.033	0.027	0.004	0.021	0.000	0.001
S_w_ICP-ES	**0.764**	0.060	0.086	0.006	0.003	0.000	0.002	0.072	0.006	0.000	0.000
Si_w_ICP-ES	**0.484**	0.060	0.209	0.091	0.014	0.131	0.009	0.000	0.001	0.000	0.000

Values in bold correspond for each variable to the factor for which the squared cosine is the largest

Table 18 Contribution of variables for the major element association PCA

10.3.3 Carbonate association PCA

This PCA model considers elements associated with carbonate rocks and follow the same statistical criteria outlined above. Figure 6 summarizes variable contributions and the squared cosines for each factor.

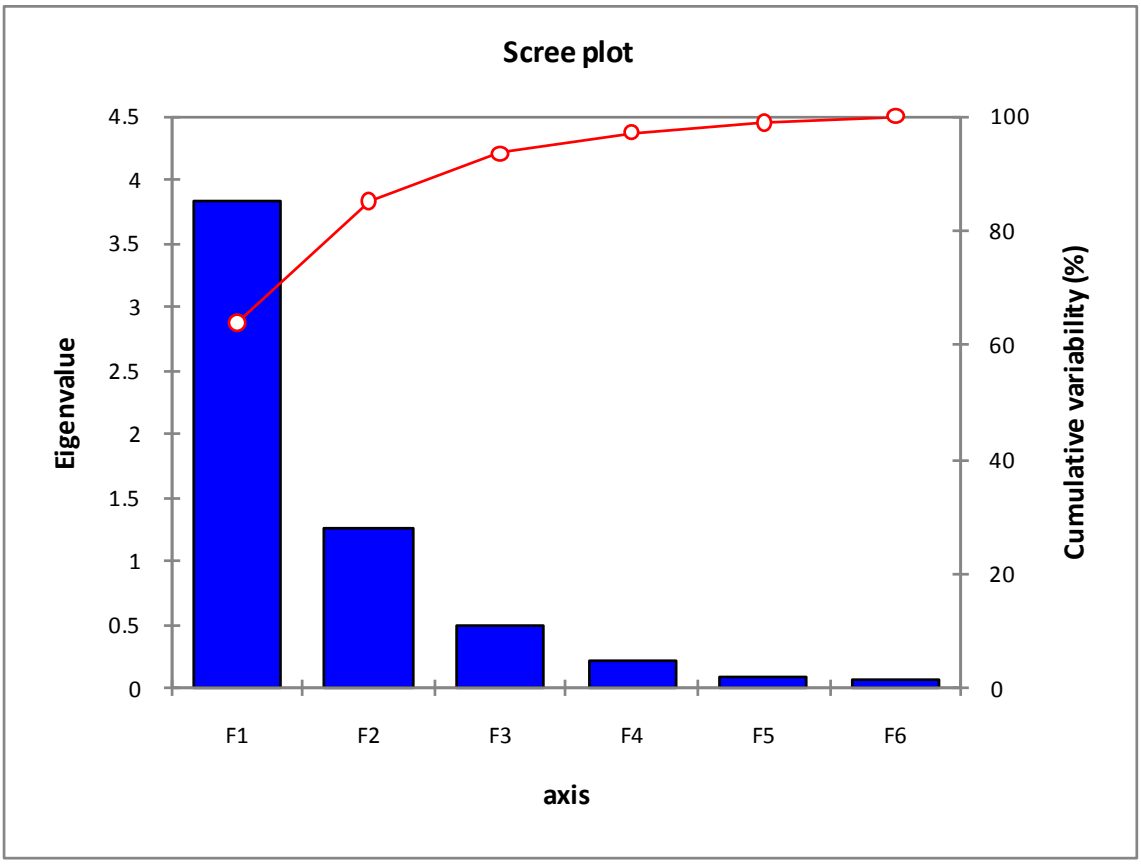


Figure 6 Scree plot for the carbonate association PCA

Factors F1 and F2 consider 85% of the variability in the PCA analysis and explain most of the elemental contributions.

Factor F1 shows significant contribution from Li, Sr, Ca, Mg, Ca, and Na. Factor F2 is dominated by Be. Table 19 below shows the contributions for each element for all the factors in this PCA.

Contribution of the variables (%):

	F1	F2	F3	F4	F5	F6
Li_w_ICP-MS	21.663	6.304	2.555	13.104	24.809	31.565
Be_w_ICP-MS	2.557	57.256	31.138	8.118	0.322	0.608
Sr_w_ICP-MS	21.709	2.575	5.201	35.116	19.938	15.462
Ca_w_ICP-ES	18.464	15.177	6.505	11.884	21.014	26.956
Mg_w_ICP-ES	17.840	9.014	24.996	28.562	0.073	19.515
Na_w_ICP-ES	17.767	9.674	29.606	3.216	33.845	5.893

Squared cosines of the variables:

	F1	F2	F3	F4	F5	F6
Li_w_ICP-MS	**0.832**	0.080	0.013	0.029	0.026	0.020
Be_w_ICP-MS	0.098	**0.727**	0.156	0.018	0.000	0.000
Sr_w_ICP-MS	**0.834**	0.033	0.026	0.076	0.021	0.010
Ca_w_ICP-ES	**0.709**	0.193	0.033	0.026	0.022	0.017
Mg_w_ICP-ES	**0.685**	0.114	0.125	0.062	0.000	0.013
Na_w_ICP-ES	**0.683**	0.123	0.148	0.007	0.035	0.004

Values in bold correspond for each variable
to the factor for which the squared cosine is the largest

Table 19 Contribution of each variable for the carbonate association PCA

10.3.4 Black shale elemental association PCA

This model considered Be, Al, Mn, Ni, Cu, Y, La, Ce, Pr, Nd, Sm, Eu, Tb, Gd, Dy, Ho, Er, Tm, Yb, and Fe associations.

Most of the observed geochemical response in all elements can be attributed to PCA Factors F1 and F2 as shown below which constitute 90% of statistical variability in this dataset (Figure 7).

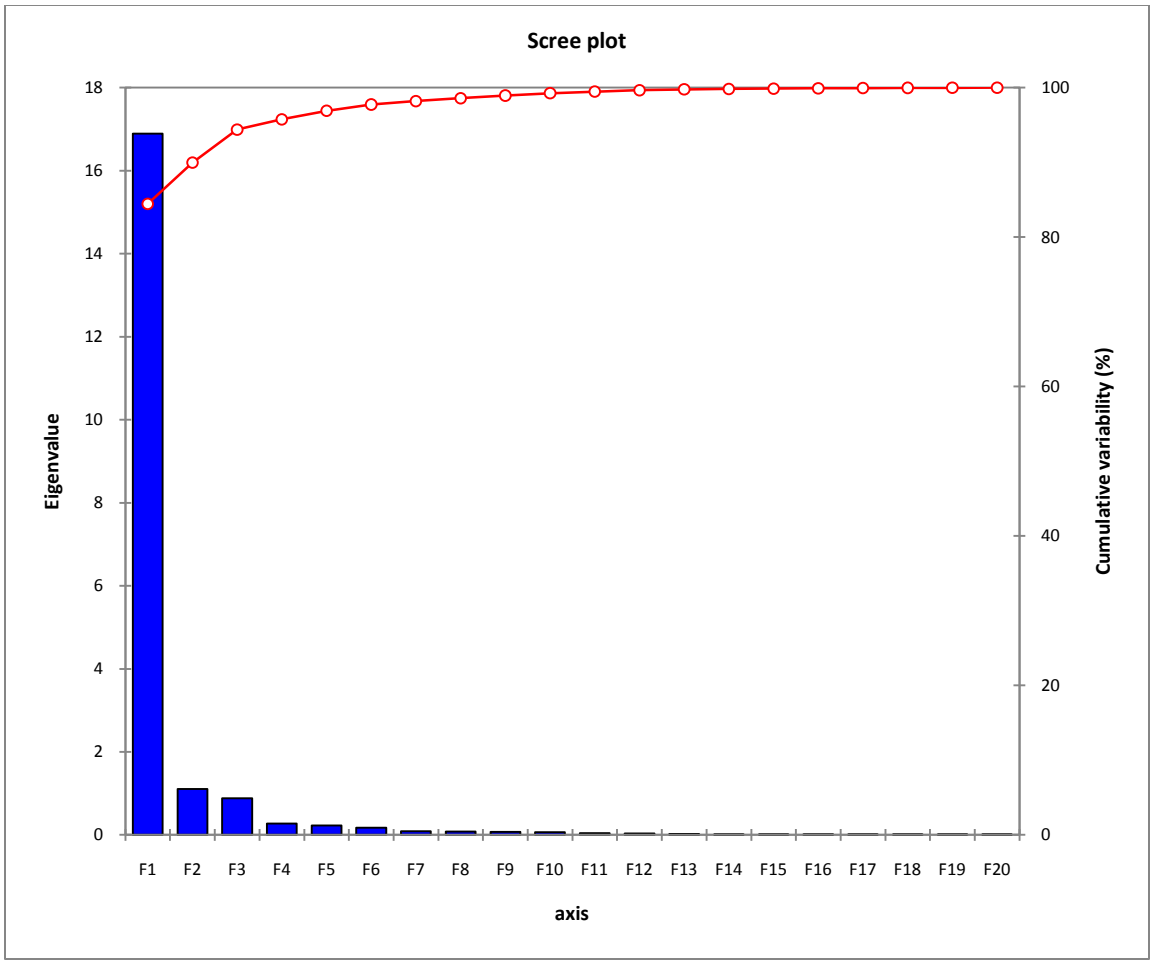


Figure 7 Scree plot for the black shale elemental association PCA

Factor F1 shows balanced contribution from all elements except Mn and covers 84% of statistical variability (Figure 7). Factor F2 accounts for 6% of statistical variability and shows a predominant contribution from Mn (41%). Ni and Mn are both elevated in this factor and may be mapping the redox state of the water rather than a lithological unit up stream. Factor F6 shows elevated concentrations of Fe, Cu and Ni and may map organic-rich shale units.

Table 20 Contribution of the variables for the black shale elemental association PCA

Contribution of the variables (%):

	F1	F2	F3	F4	F5	F6	F7	F8	F9	F10
Be_w_ICP-MS	5.143	3.318	1.545	0.027	9.599	1.112	41.298	0.169	13.934	2.308
Al_w_ICP-MS	4.224	10.016	0.174	30.806	29.808	5.809	1.751	6.050	0.936	3.949
Mn_w_ICP-MS	2.609	41.128	5.021	9.275	0.143	3.677	11.777	9.501	10.853	4.916
Ni_w_ICP-MS	3.697	23.499	3.273	2.295	12.044	15.293	4.863	10.666	11.074	10.271
Cu_w_ICP-MS	4.412	2.427	8.983	14.017	31.998	11.221	0.294	6.671	18.150	0.096
Y_w_ICP-MS	5.514	0.019	3.607	3.306	0.586	0.022	0.090	1.580	10.078	1.269
La_w_ICP-MS	5.444	3.047	0.258	1.930	1.459	4.700	0.748	1.003	7.269	25.266
Ce_w_ICP-MS	5.507	2.337	1.590	0.676	1.900	0.880	1.600	4.761	1.992	9.038
Pr_w_ICP-MS	5.606	2.378	0.097	1.420	0.358	3.006	1.848	0.803	4.326	3.394
Nd_w_ICP-MS	5.431	2.076	4.313	1.188	0.000	0.011	0.686	4.029	4.868	0.545
Sm_w_ICP-MS	5.721	1.654	0.261	0.066	0.024	1.520	0.806	1.134	0.332	1.648
Eu_w_ICP-MS	5.213	0.279	5.679	5.378	0.134	3.449	14.387	15.387	1.223	0.490
Tb_w_ICP-MS	5.223	0.001	11.207	0.497	0.259	0.000	1.884	4.885	0.067	0.774
Gd_w_ICP-MS	5.732	0.349	0.762	1.366	0.032	1.684	0.149	4.628	3.713	4.309
Dy_w_ICP-MS	5.760	0.442	0.483	1.064	0.029	1.604	0.023	2.746	2.769	4.951
Ho_w_ICP-MS	5.333	0.021	9.018	0.520	0.668	0.083	0.628	4.129	0.010	1.510
Er_w_ICP-MS	5.751	0.486	0.295	0.043	0.188	2.663	0.339	0.010	0.202	8.288
Tm_w_ICP-MS	3.639	1.940	33.413	0.736	7.694	12.355	3.237	20.887	1.599	10.745
Yb_w_ICP-MS	5.686	0.572	1.446	0.032	0.012	1.604	1.216	0.004	1.312	6.211
Fe_w_ICP-ES	4.353	4.008	8.575	25.358	3.066	29.307	12.377	0.956	5.295	0.025

	F11	F12	F13	F14	F15	F16	F17	F18	F19	F20
Be_w_ICP-MS	18.89	0.151	0.655	0.059	0.953	0.651	0.019	0.048	0.046	0.066
Al_w_ICP-MS	5.875	0.417	0.000	0.005	0.010	0.079	0.014	0.051	0.020	0.007
Mn_w_ICP-MS	0.120	0.461	0.164	0.039	0.231	0.061	0.008	0.003	0.003	0.010
Ni_w_ICP-MS	0.274	1.642	0.611	0.353	0.041	0.043	0.035	0.012	0.002	0.012
Cu_w_ICP-MS	0.180	0.185	0.954	0.288	0.021	0.007	0.014	0.031	0.028	0.023
Y_w_ICP-MS	8.456	13.813	27.018	0.005	17.599	5.218	1.684	0.019	0.022	0.096
La_w_ICP-MS	0.086	1.023	4.979	17.522	1.445	19.872	0.519	3.218	0.173	0.040
Ce_w_ICP-MS	0.616	0.422	16.591	28.152	19.781	3.281	0.084	0.592	0.096	0.107
Pr_w_ICP-MS	3.942	0.001	8.693	0.491	12.805	38.971	0.004	11.839	0.002	0.015
Nd_w_ICP-MS	5.668	5.147	0.001	13.549	43.962	5.665	0.760	1.003	0.133	0.967
Sm_w_ICP-MS	0.471	4.975	3.488	2.819	1.149	2.388	47.740	21.561	0.428	1.813
Eu_w_ICP-MS	26.63	17.053	1.389	0.023	0.095	0.441	0.319	0.045	0.374	0.005
Tb_w_ICP-MS	0.415	19.819	6.898	0.011	0.019	0.005	0.267	0.379	46.622	0.768
Gd_w_ICP-MS	0.348	0.855	7.827	9.082	0.053	0.345	6.080	13.785	0.814	38.088
Dy_w_ICP-MS	0.284	2.380	3.529	11.387	0.499	0.028	1.492	3.226	0.568	56.736
Ho_w_ICP-MS	3.014	21.012	2.835	0.006	0.370	0.580	0.163	0.007	49.436	0.658

Er_w_ICP-MS	8.040	4.826	4.296	3.314	0.349	0.936	29.822	29.122	0.498	0.532
Tm_w_ICP-MS	0.162	2.674	0.283	0.045	0.133	0.426	0.000	0.001	0.019	0.011
Yb_w_ICP-MS	8.547	3.122	9.703	12.395	0.452	20.997	10.963	15.052	0.668	0.008
Fe_w_ICP-ES	5.969	0.024	0.086	0.455	0.033	0.004	0.014	0.005	0.051	0.038

Squared cosines of the variables:

	F1	F2	F3	F4	F5	F6	F7	F8	F9	F10
Be_w_ICP-MS	**0.869**	0.037	0.014	0.000	0.022	0.002	0.038	0.000	0.010	0.001
Al_w_ICP-MS	**0.713**	0.111	0.002	0.085	0.068	0.010	0.002	0.005	0.001	0.002
Mn_w_ICP-MS	0.441	**0.454**	0.044	0.026	0.000	0.006	0.011	0.008	0.008	0.003
Ni_w_ICP-MS	**0.624**	0.259	0.029	0.006	0.027	0.026	0.004	0.008	0.008	0.006
Cu_w_ICP-MS	**0.745**	0.027	0.079	0.039	0.073	0.019	0.000	0.005	0.013	0.000
Y_w_ICP-MS	**0.931**	0.000	0.032	0.009	0.001	0.000	0.000	0.001	0.007	0.001
La_w_ICP-MS	**0.919**	0.034	0.002	0.005	0.003	0.008	0.001	0.001	0.005	0.016
Ce_w_ICP-MS	**0.930**	0.026	0.014	0.002	0.004	0.001	0.001	0.004	0.001	0.006
Pr_w_ICP-MS	**0.947**	0.026	0.001	0.004	0.001	0.005	0.002	0.001	0.003	0.002
Nd_w_ICP-MS	**0.917**	0.023	0.038	0.003	0.000	0.000	0.001	0.003	0.003	0.000
Sm_w_ICP-MS	**0.966**	0.018	0.002	0.000	0.000	0.003	0.001	0.001	0.000	0.001
Eu_w_ICP-MS	**0.880**	0.003	0.050	0.015	0.000	0.006	0.013	0.012	0.001	0.000
Tb_w_ICP-MS	**0.882**	0.000	0.099	0.001	0.001	0.000	0.002	0.004	0.000	0.000
Gd_w_ICP-MS	**0.968**	0.004	0.007	0.004	0.000	0.003	0.000	0.004	0.003	0.003
Dy_w_ICP-MS	**0.973**	0.005	0.004	0.003	0.000	0.003	0.000	0.002	0.002	0.003
Ho_w_ICP-MS	**0.901**	0.000	0.080	0.001	0.002	0.000	0.001	0.003	0.000	0.001
Er_w_ICP-MS	**0.971**	0.005	0.003	0.000	0.000	0.005	0.000	0.000	0.000	0.005
Tm_w_ICP-MS	**0.615**	0.021	0.295	0.002	0.017	0.021	0.003	0.016	0.001	0.007
Yb_w_ICP-MS	**0.960**	0.006	0.013	0.000	0.000	0.003	0.001	0.000	0.001	0.004
Fe_w_ICP-ES	**0.735**	0.044	0.076	0.070	0.007	0.050	0.011	0.001	0.004	0.000

Values in bold correspond for each variable to the factor for which the squared cosine is the largest

	F11	F12	F13	F14	F15	F16	F17	F18	F19	F20
Be_w_ICP-MS	0.008	0.000	0.000	0.000	0.000	0.000	0.000	0.000	0.000	0.000
Al_w_ICP-MS	0.003	0.000	0.000	0.000	0.000	0.000	0.000	0.000	0.000	0.000
Mn_w_ICP-MS	0.000	0.000	0.000	0.000	0.000	0.000	0.000	0.000	0.000	0.000
Ni_w_ICP-MS	0.000	0.001	0.000	0.000	0.000	0.000	0.000	0.000	0.000	0.000
Cu_w_ICP-MS	0.000	0.000	0.000	0.000	0.000	0.000	0.000	0.000	0.000	0.000
Y_w_ICP-MS	0.004	0.005	0.006	0.000	0.002	0.000	0.000	0.000	0.000	0.000
La_w_ICP-MS	0.000	0.000	0.001	0.002	0.000	0.002	0.000	0.000	0.000	0.000
Ce_w_ICP-MS	0.000	0.000	0.004	0.004	0.002	0.000	0.000	0.000	0.000	0.000
Pr_w_ICP-MS	0.002	0.000	0.002	0.000	0.001	0.003	0.000	0.001	0.000	0.000
Nd_w_ICP-MS	0.002	0.002	0.000	0.002	0.004	0.000	0.000	0.000	0.000	0.000
Sm_w_ICP-MS	0.000	0.002	0.001	0.000	0.000	0.000	0.003	0.001	0.000	0.000
Eu_w_ICP-MS	0.012	0.006	0.000	0.000	0.000	0.000	0.000	0.000	0.000	0.000
Tb_w_ICP-MS	0.000	0.007	0.002	0.000	0.000	0.000	0.000	0.000	0.002	0.000
Gd_w_ICP-MS	0.000	0.000	0.002	0.001	0.000	0.000	0.000	0.001	0.000	0.001
Dy_w_ICP-MS	0.000	0.001	0.001	0.001	0.000	0.000	0.000	0.000	0.000	0.002

Ho_w_ICP-MS	0.001	0.008	0.001	0.000	0.000	0.000	0.000	0.000	0.002	0.000
Er_w_ICP-MS	0.004	0.002	0.001	0.000	0.000	0.000	0.002	0.001	0.000	0.000
Tm_w_ICP-MS	0.000	0.001	0.000	0.000	0.000	0.000	0.000	0.000	0.000	0.000
Yb_w_ICP-MS	0.004	0.001	0.002	0.002	0.000	0.002	0.001	0.001	0.000	0.000
Fe_w_ICP-ES	0.003	0.000	0.000	0.000	0.000	0.000	0.000	0.000	0.000	0.000

11 Discussion

11.1 Stream Sediment Results

Figure 8 below shows all sample locations overlain on a map of the drainages in the study area. Proportional sized symbols are used to indicate the analytical values for the principal minerals determined to be of most interest, namely zinc, lead, copper and gold. It is interesting to note that the Gayna River deposit and satellite showings are located within kilometres of the candidate protected area, hosted in rocks also found within the candidate area. A region of elevated analytical response for the metals is apparent in the southern portion of the proposed protected area. There were nine silt samples collected which returned results greater than 350 ppb Zn. All nine elevated zinc samples were also anomalous for copper. In addition, there were eleven other silt samples which contained anomalously high amounts of copper.

Of the six hundred forty-three samples analysed for lead, 13 of the samples returned values at or exceeding the ninety-eighth percentile and should be considered anomalous. The thirteen samples were collected either from within or just outside the far southern region of the study area. Many of the samples which were anomalous for lead also contained elevated levels of copper, and while none of the samples with anomalous lead also returned anomalous zinc values, the zinc results for several samples were elevated, and definitely bear further study. The samples exhibiting an elevated response for gold are less explicable than the base metals. The samples with elevated gold were collected from settings scattered widely across the survey area. While it seems logical to attribute these elevated gold values to random dispersion of gold grains by glaciation, the gold results

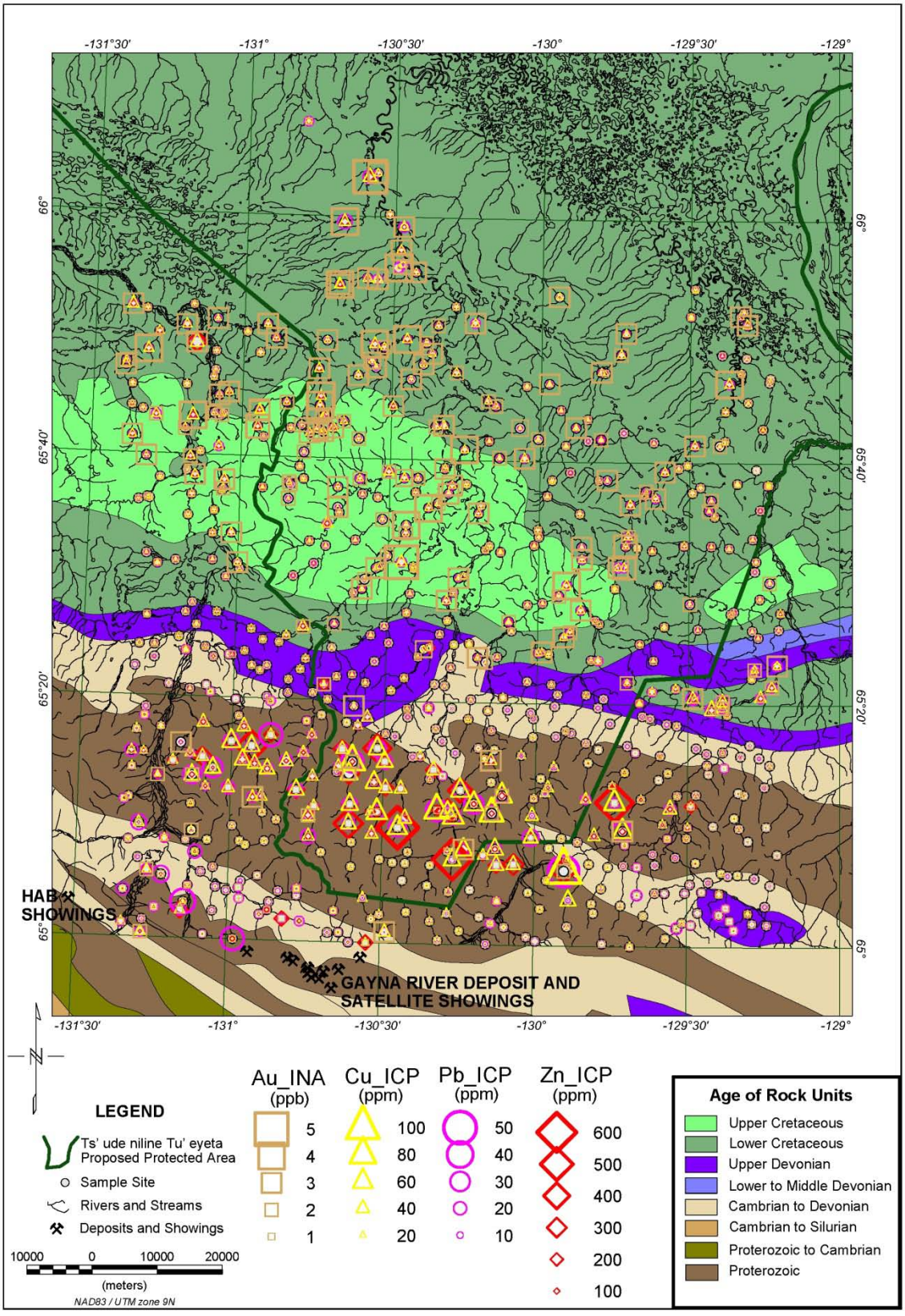


Figure 8 Map of Study Area Showing Sample Sites, Known Deposits and Showings, and Anomalous Sample Locations

correlate well with mercury and silver, barium and phosphorus suggesting that there may be epigenetic sources for some of these elevated gold results.

There were ten sample locations where silt sample analytical results correlated between elevated metal values and highly acidic water pH values. The coincident metal values and acidic stream water would suggest the presence of a local, concentrated source for the metals. Of these ten anomalous locations, five showed elevated responses for copper and lead, two for copper, lead and gold, two for copper and gold, and one for copper, zinc and gold.

Figure 9 illustrates the relationship between gridded PCA F1 values and copper, nickel and silver. It is interesting to note the zone of elevated F1 values in the southern portion of the study area corresponding with anomalously high nickel, silver and copper values. As discussed above, this association has the potential to indicate the presence of SEDEX or RED BED type deposits. With the corresponding elevated metal analysis values in this area, there is good potential for metallic mineral deposits in the southern portion of the survey area. The region of greatest potential for these types of deposits is bounded by 65° - 65° 20'N, and 129° 30' - 131° West.

Figure 10 below shows gridded PCA F9 values with corresponding lead, zinc and silver. F9 is the factor most likely to provide a vector to discovering SEDEX type deposits. Figure 10 shows that there are several locations where elevated PCA Factor 9 and high lead and silver values coincide. These locations would be prospective for silver and base metals. The area with the highest prospectivity demonstrated in Figure 10 is roughly coincident with but somewhat larger than the area indicated in Figure 9. It extends across the entire southern end of the survey area and includes several extensions as far north as 66°N.

Factor 21 is optimized to identify areas prospective for copper. Figure 13 on following pages compares gridded PCA F21 values with elemental values for copper. Areas most prospective for copper are indicated

within the southern extension of the proposed protected area south of 65° 20'N latitude, but there are

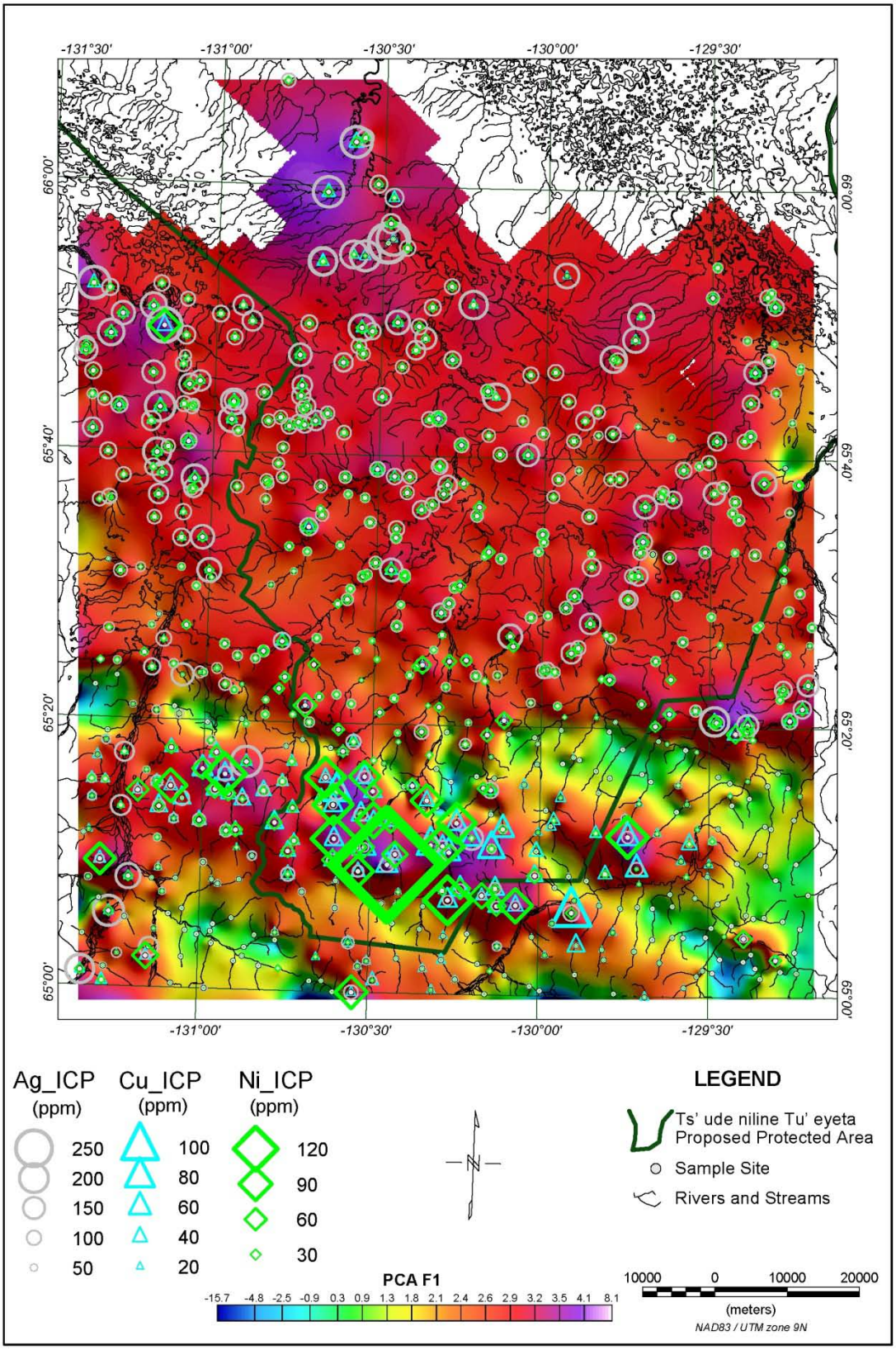


Figure 9 Gridded Principal Component Analysis Factor 1 with Copper, Nickel and Silver Proportional Size Symbols Plotted

several other locales showing good potential for copper mineralization as far north as 65° 50’N latitude

Figure 12 also following compares gridded PCA F3 values with plotted gold, silver and mercury values. As indicated by the statistical analysis, sample sites with coincident higher values for gold, silver and mercury coincide with gridded lows in the F3 plot. Several areas with elevated potential to host gold and/or silver deposits are displayed in this figure. They are well dispersed across the central and northern reaches of the sample survey are, and extend as far north as 66° 5’N latitude.

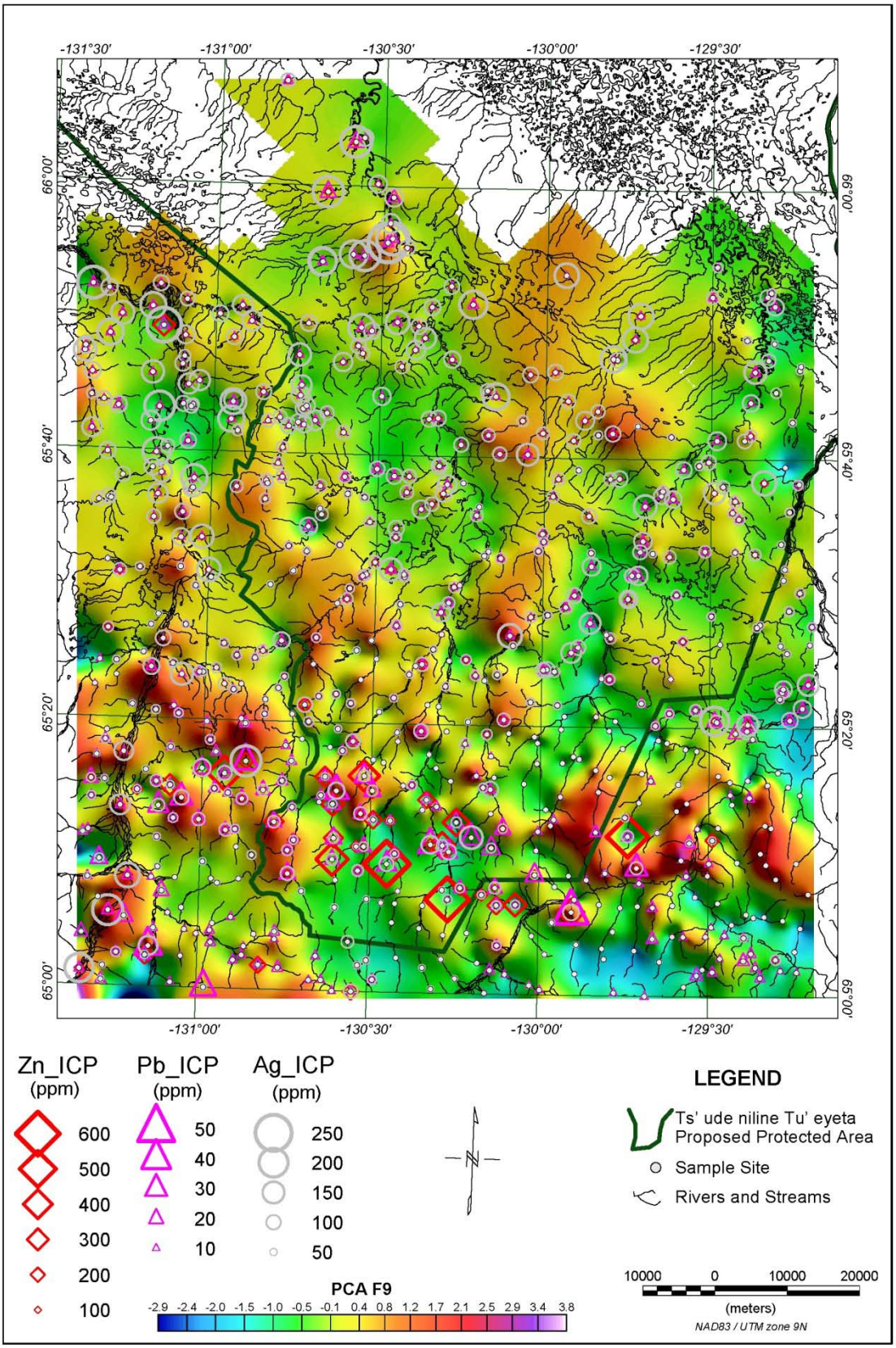


Figure 10 Gridded Principal Component Analysis Factor 9 with Lead, Zinc and Silver Values Plotted

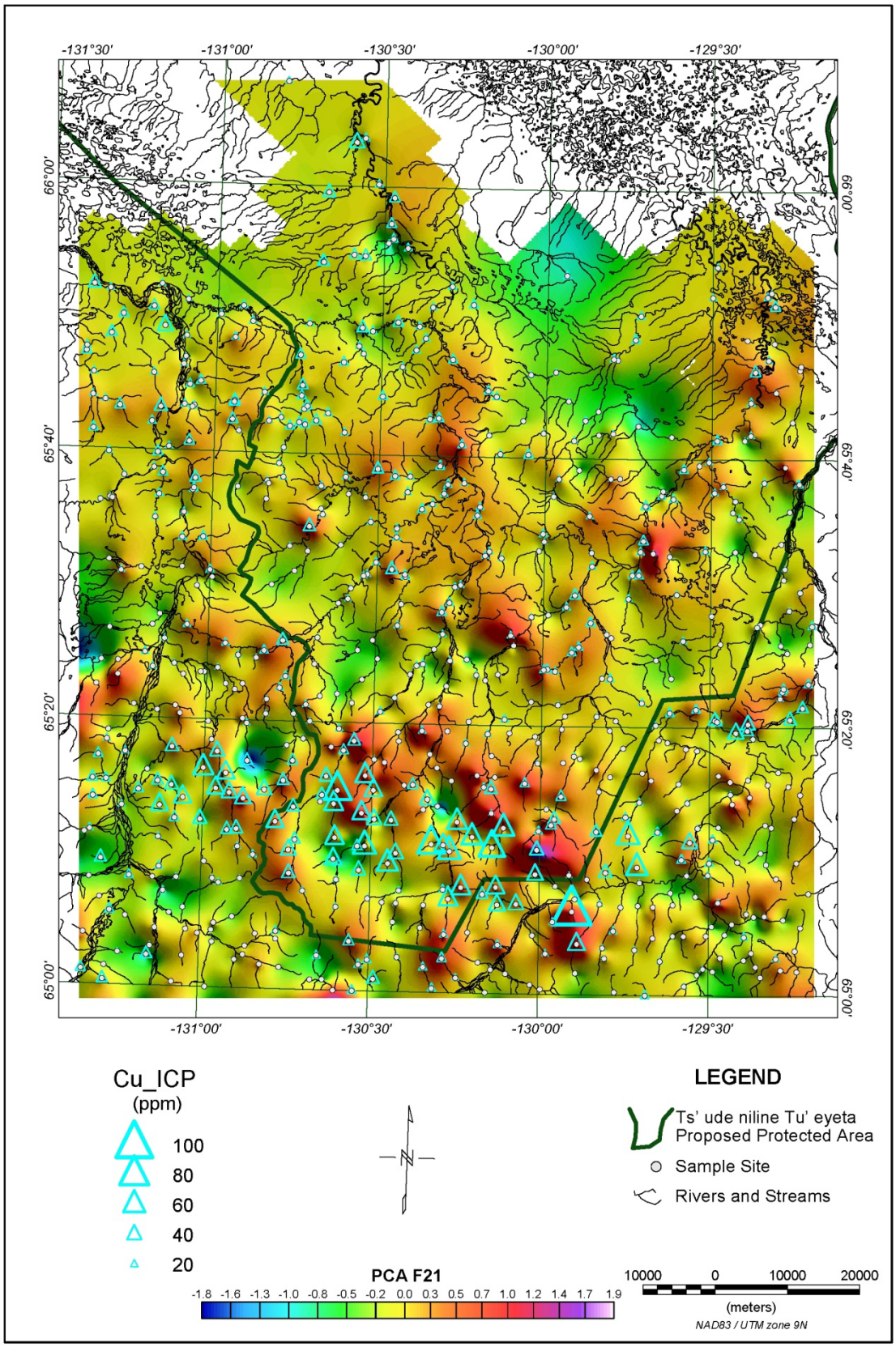


Figure 11 Gridded Principal Component Analysis Factor 21 with Copper Values Plotted

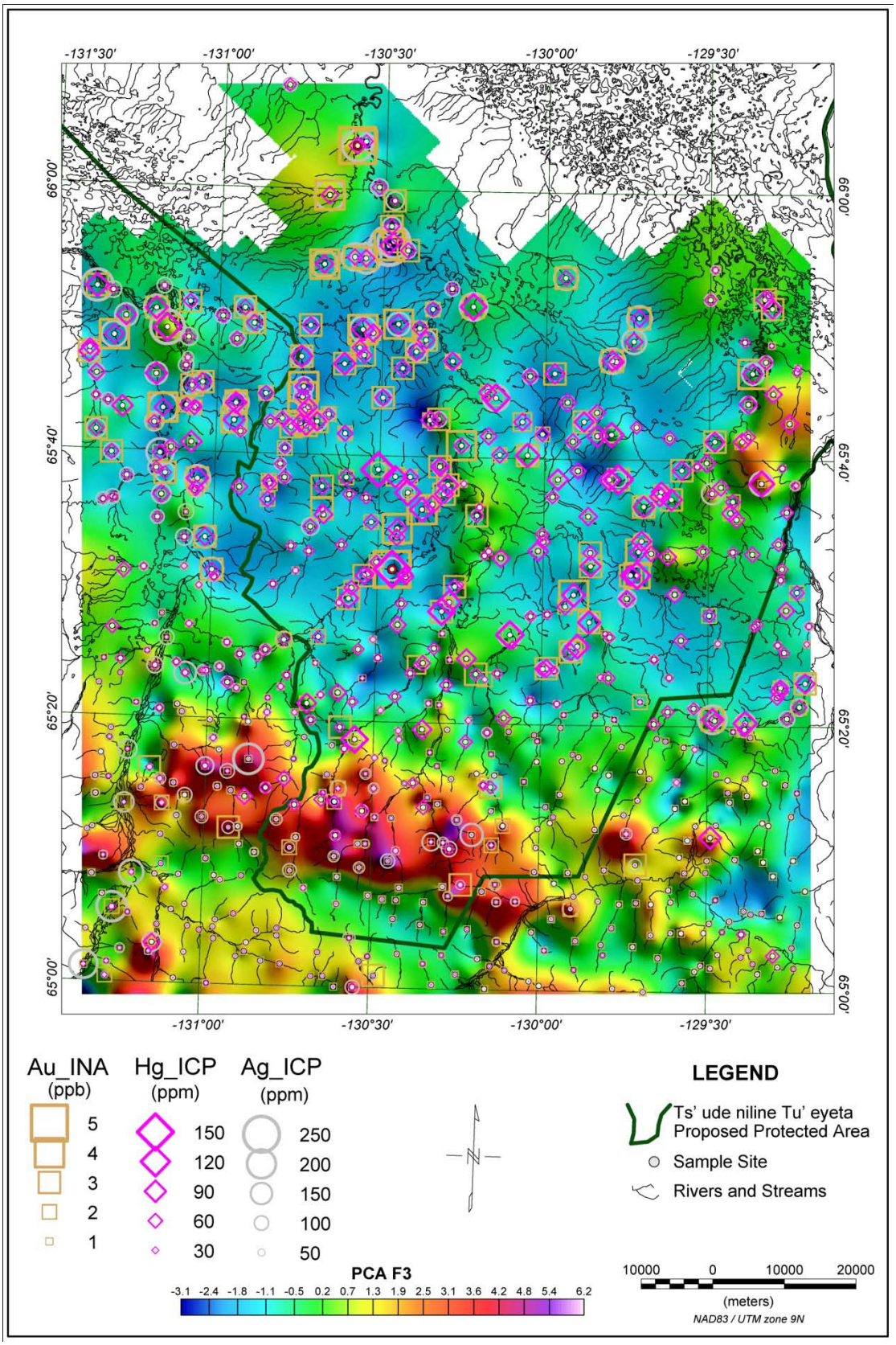


Figure 12 Gridded Principal Component Analysis Factor 3 with Gold, Silver and Mercury Values Plotted

11.2 Water Sample Results

The results of the analysis of the stream water sampling program are very similar to those of the sediment sampling. Plots of gridded PCA Factors show significantly elevated factor values and coincident anomalies in water samples in the southern portion of the sample area for most of the different factors in the different principal component analyses which were carried out. Almost every factor in each PCA is elevated in the area between 65° 5’ and 65° 15’N and between 130° and 130° 30’ W.

The following thirteen plots are gridded PCA Factors for the most important factors calculated for each of the four analyses; the five times background association, the principal Element association, the carbonate association, and the black shale association.

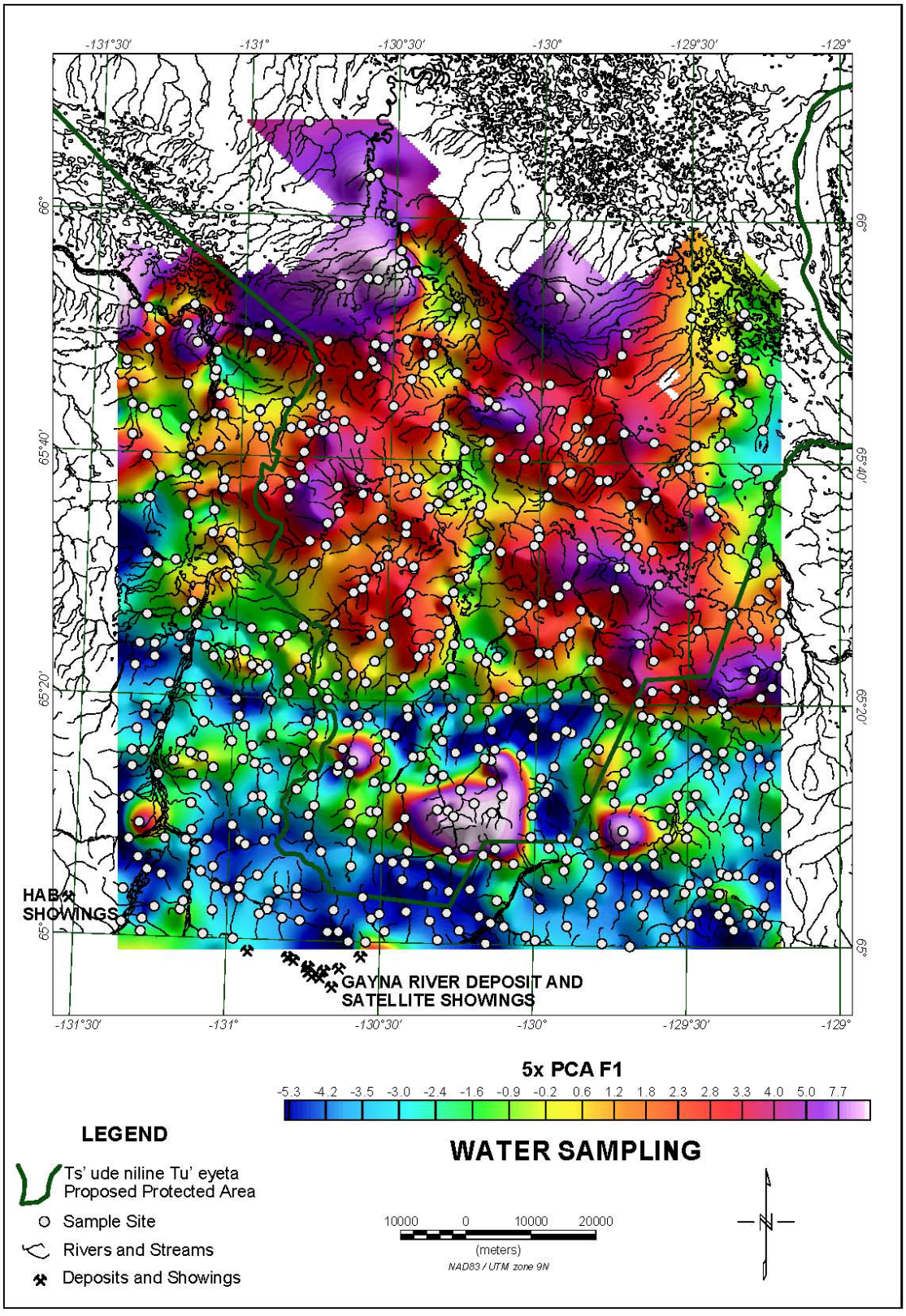


Figure 13 Gridded F1 factor values from the Principal Component Analysis for the five times detection limit model. It shows contributions from all REE elements, Be, Ce, La, Nd, Al, Ni, Cu, Fe, Zn, Mn, Co, Si, and pH. Perhaps most relevant to the redox, acid, and black shale associations

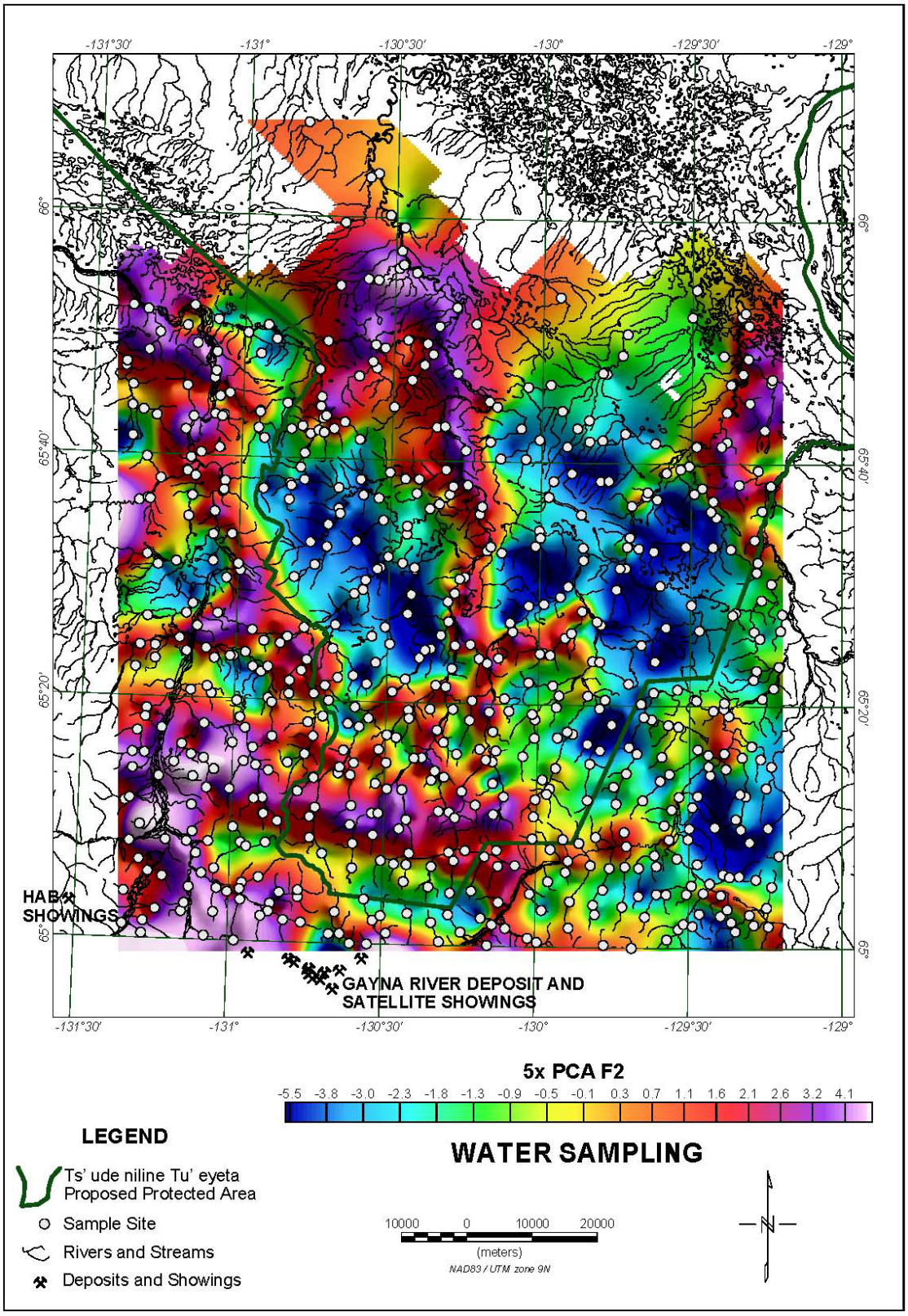


Figure 14 Gridded F2 factor values from the Principal Component Analysis for the five times detection limit model. It shows prominent factor loadings from conductivity, Mg, S, Ca, Sr, K, Li, B, U, and Rb. This factor may be mapping the major and/or carbonate element associations.

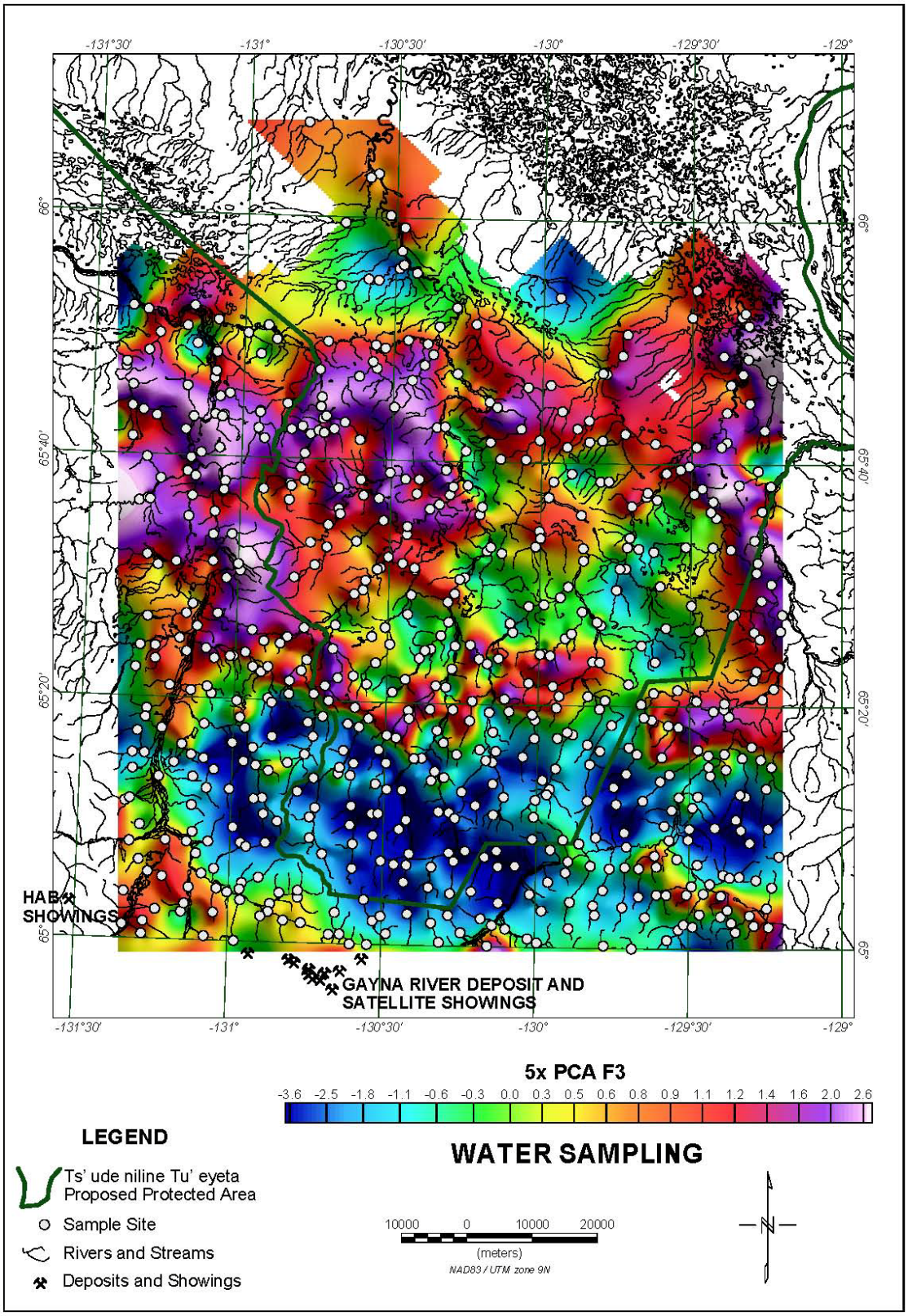


Figure 15 Gridded F3 factor values from the Principal Component Analysis for the five times detection limit model. An element association of Mo and Ba, and subordinate U, Co, An, Sr, pH (positive) and Cu may represent the alkaline element association.

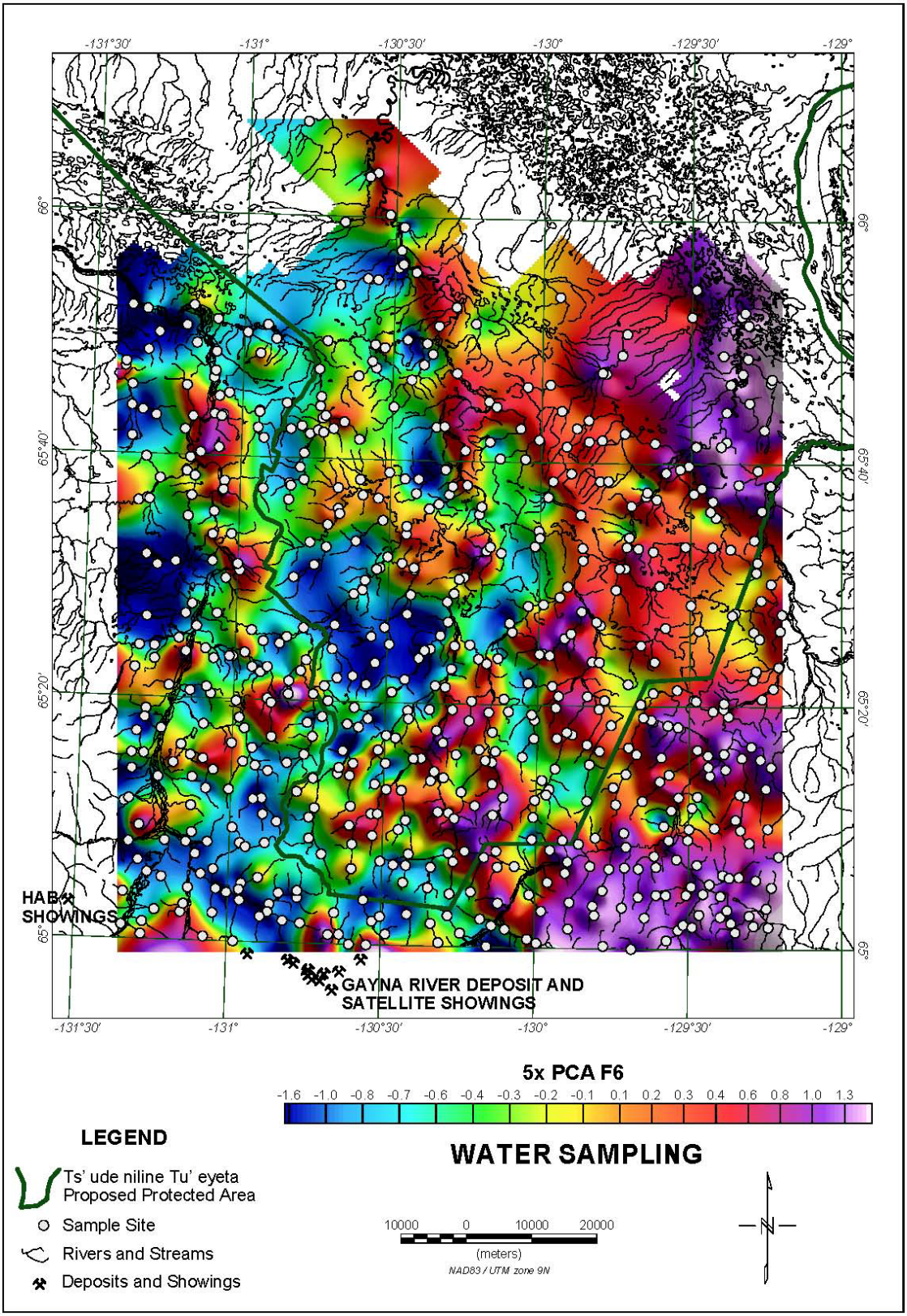


Figure 16 Gridded F6 factor values from the Principal Component Analysis for the five times detection limit model. It contains Pb as the only significant contributing element. Lead is associated with subordinate Si, Rb, Ba, Mn, Co and pH (negative).

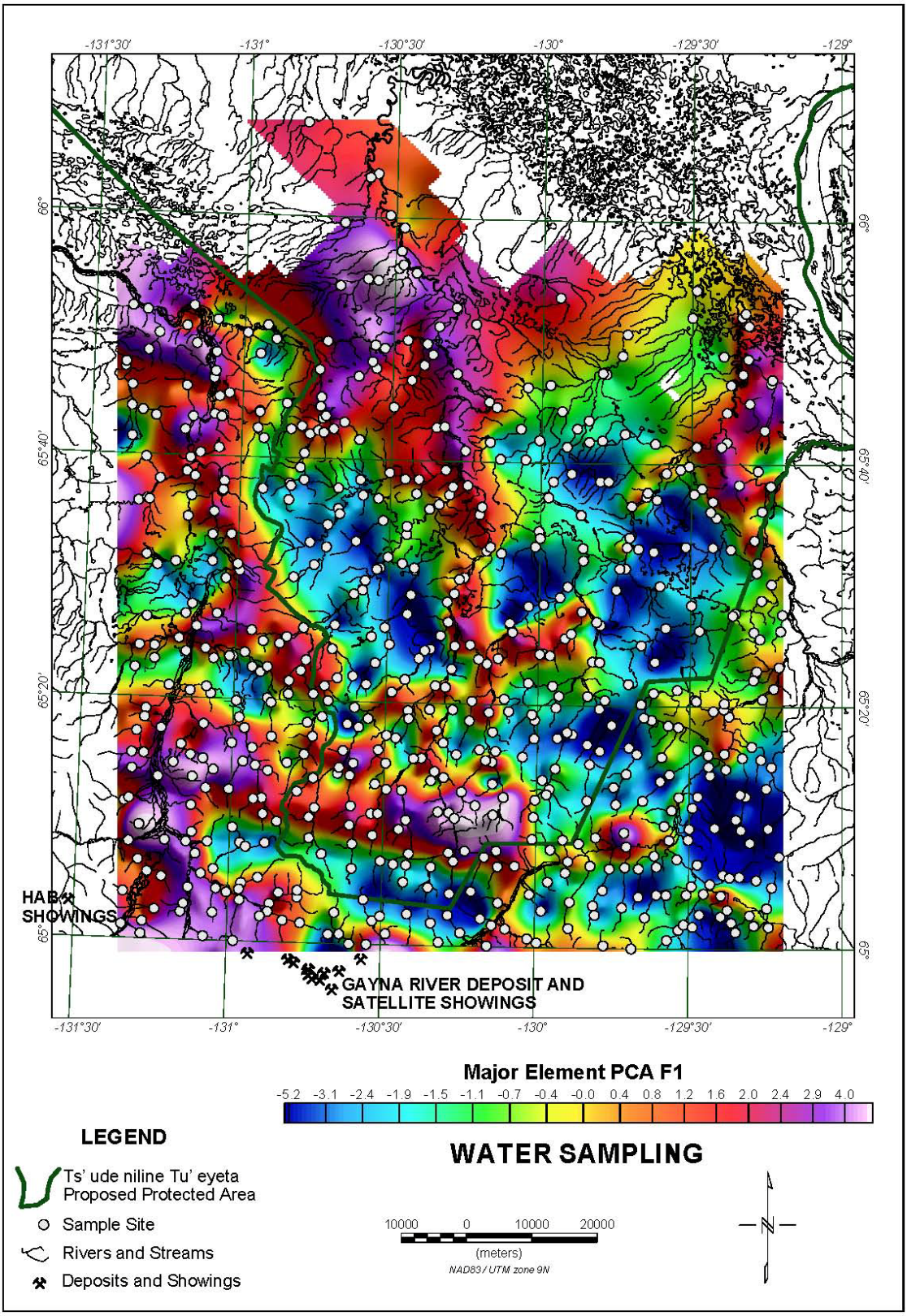


Figure 17 Gridded F1 factor values from the Principal Component Analysis for the Major Element mineral assemblage model. Principal elements in this factor include Li, Sr, Ca, Mg, and S together with Conductivity and may be mapping carbonate rocks.

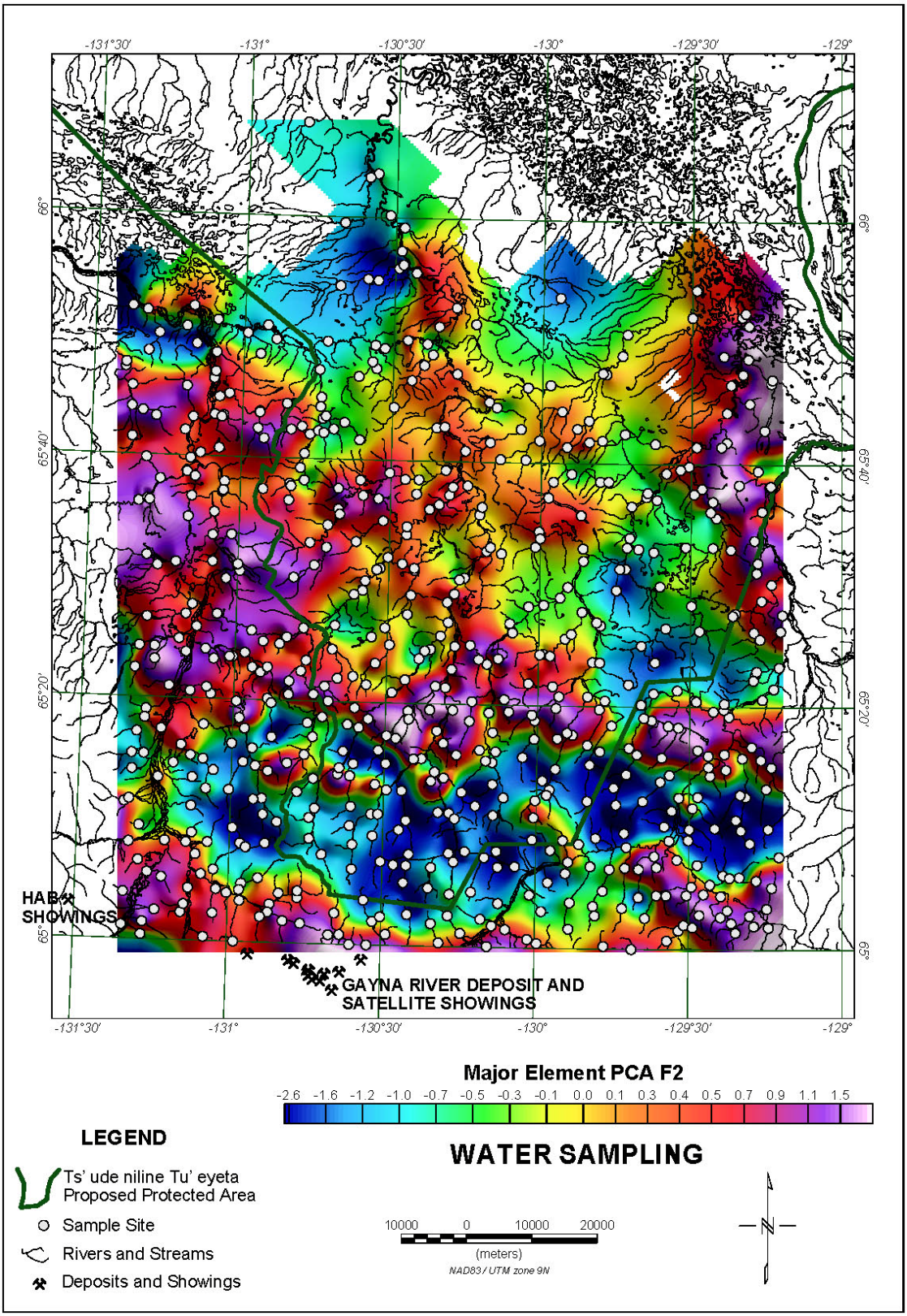


Figure 18 Gridded F2 factor values from the Principal Component Analysis for the Major Element mineral assemblage model. It has significant contribution from Ba, and lesser U. These elements share an alkaline affinity and may map the buffering effect of carbonate rocks in the absence of sulphur.

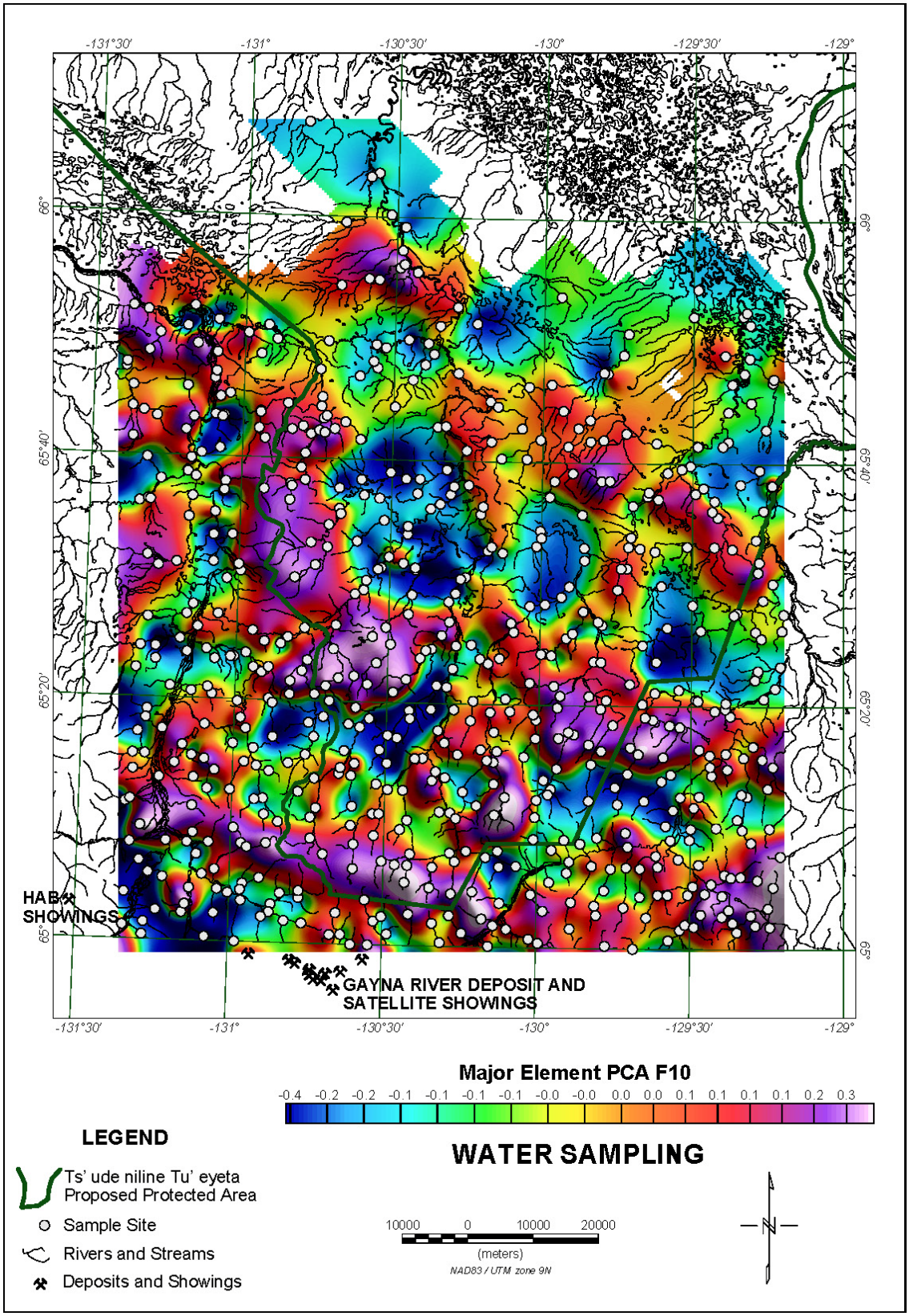


Figure 19 Gridded F10 factor values from the Principal Component Analysis for the Major Element mineral assemblage model. It shows the highest concentrations of Ca and Mg.

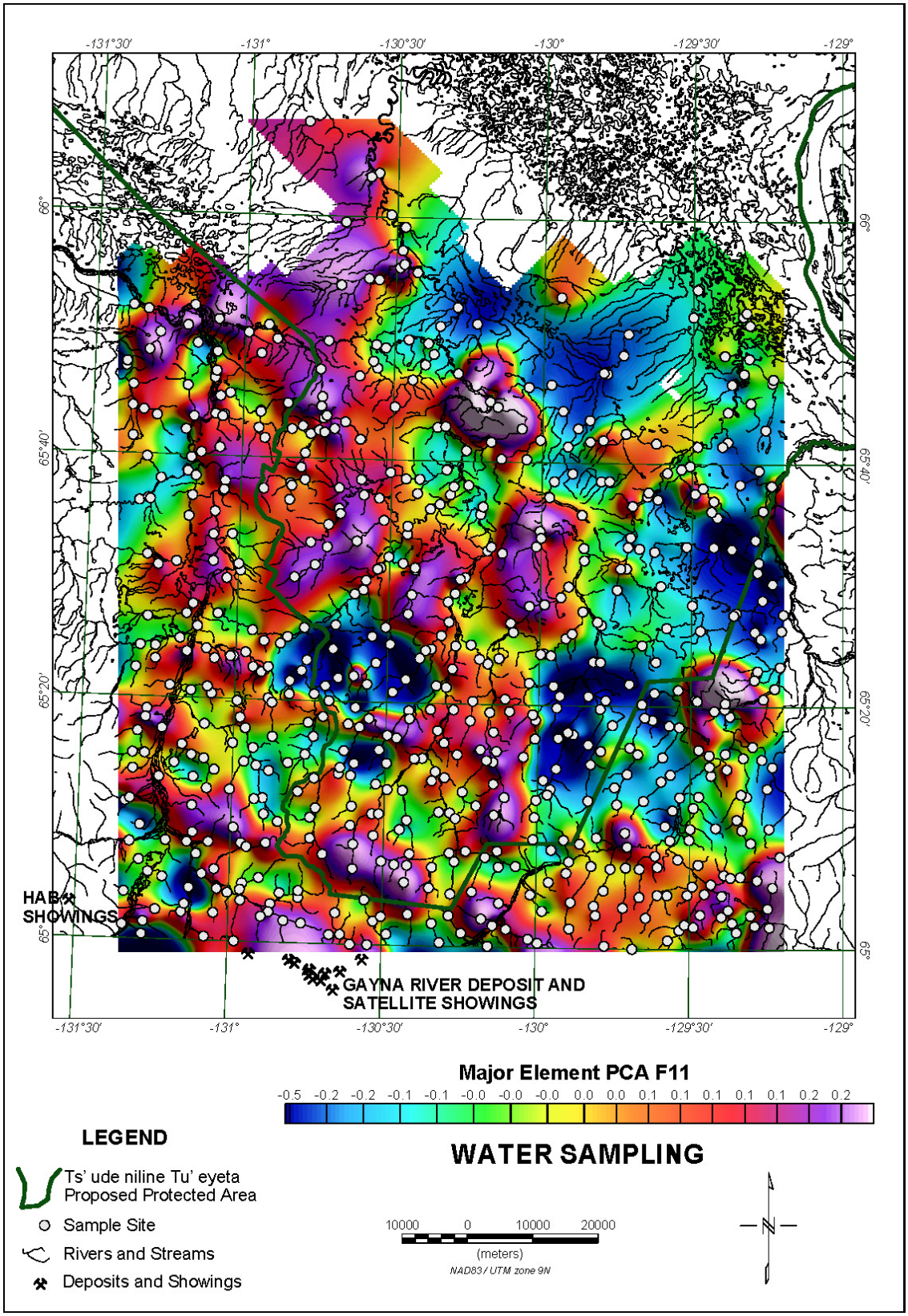


Figure 20 Gridded F11 factor values from the Principal Component Analysis for the Major Element mineral assemblage model. It shows the greatest contribution from conductivity and Ca.

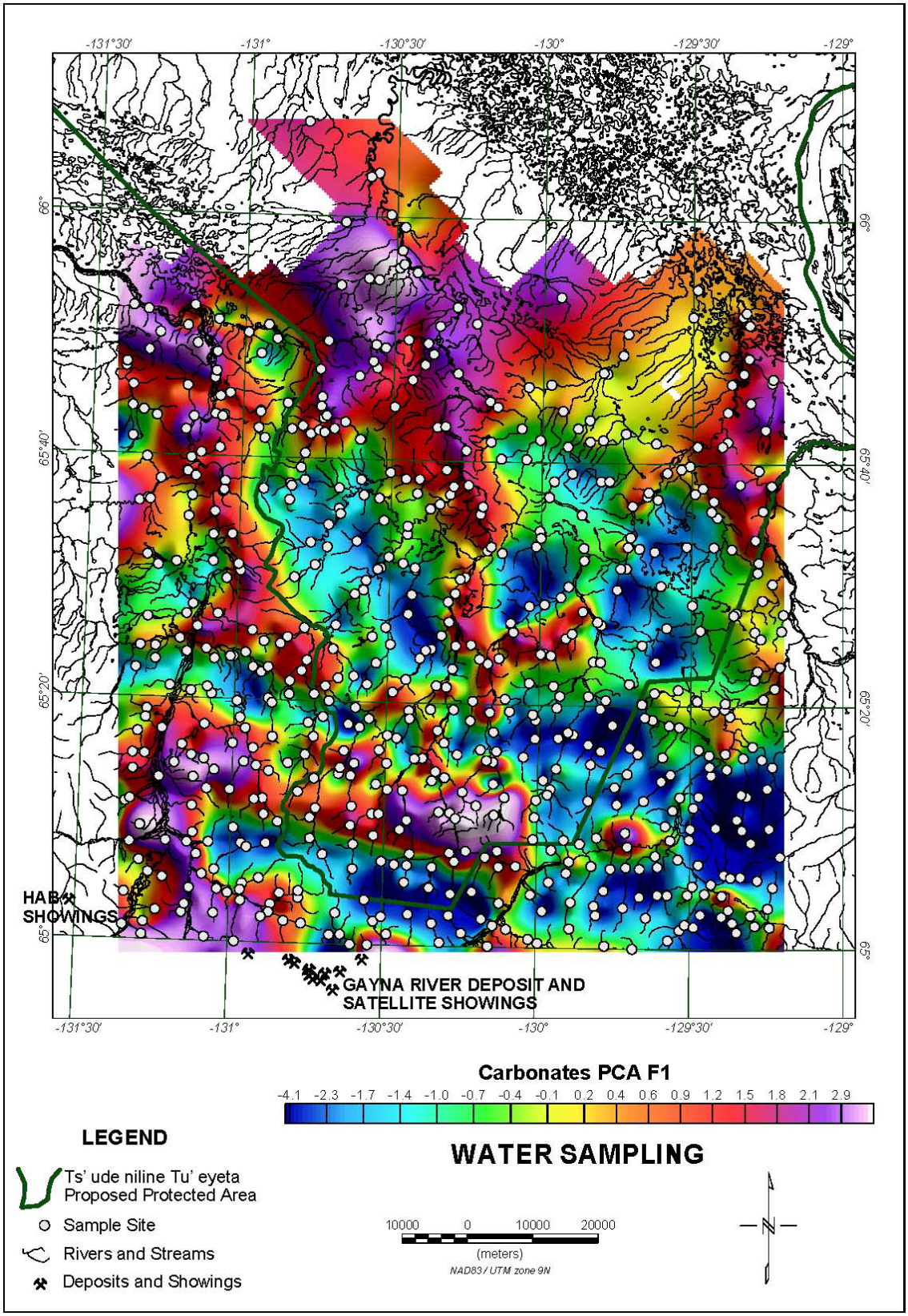


Figure 21 Gridded F1 factor values from the Principal Component Analysis for the Carbonate mineral assemblage model. It shows significant contribution from Li, Sr, Ca, Mg, Ca, and Na.

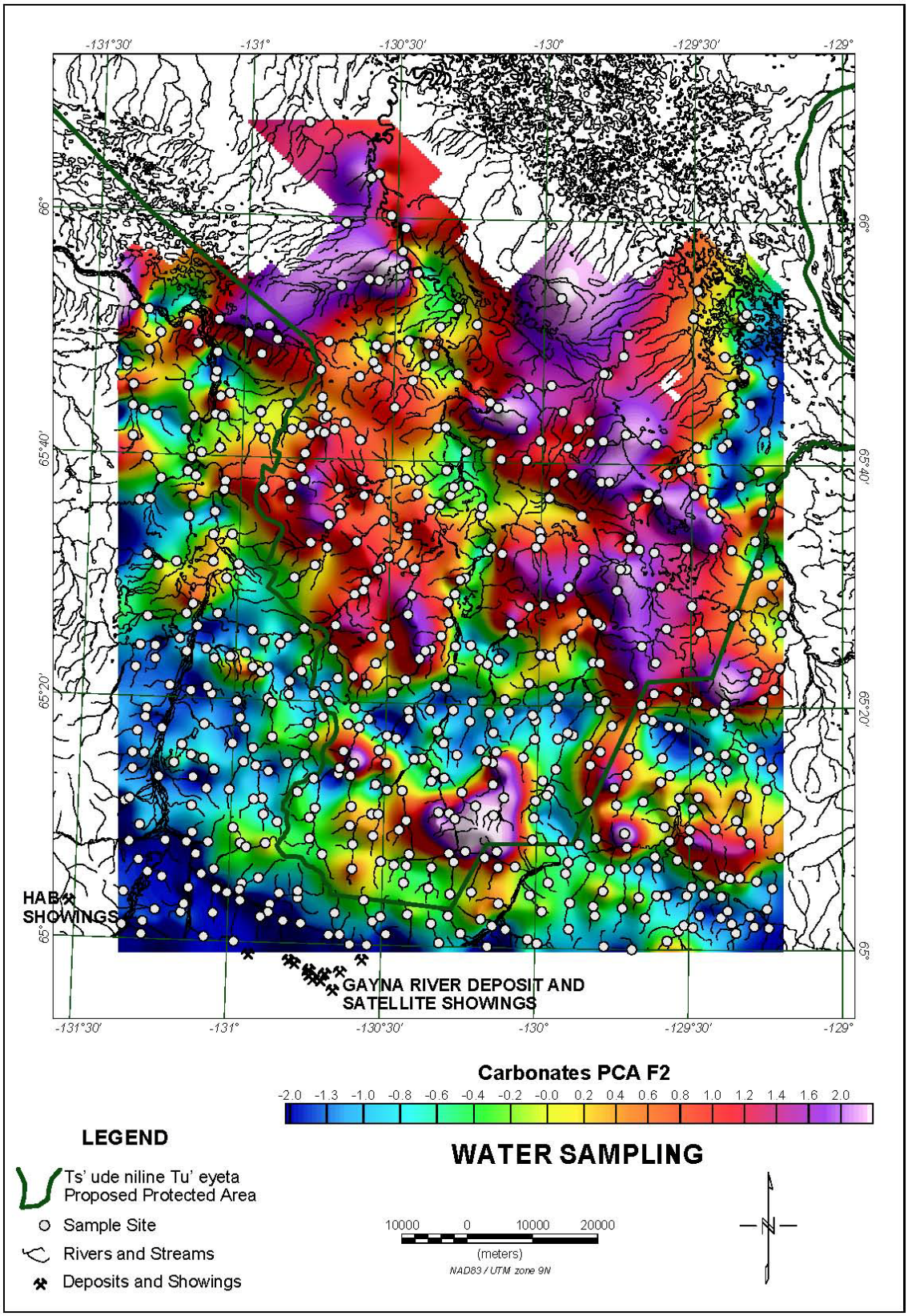


Figure 22 Gridded F2 factor values from the Principal Component Analysis for the Carbonate mineral assemblage model. It is dominated by Be.

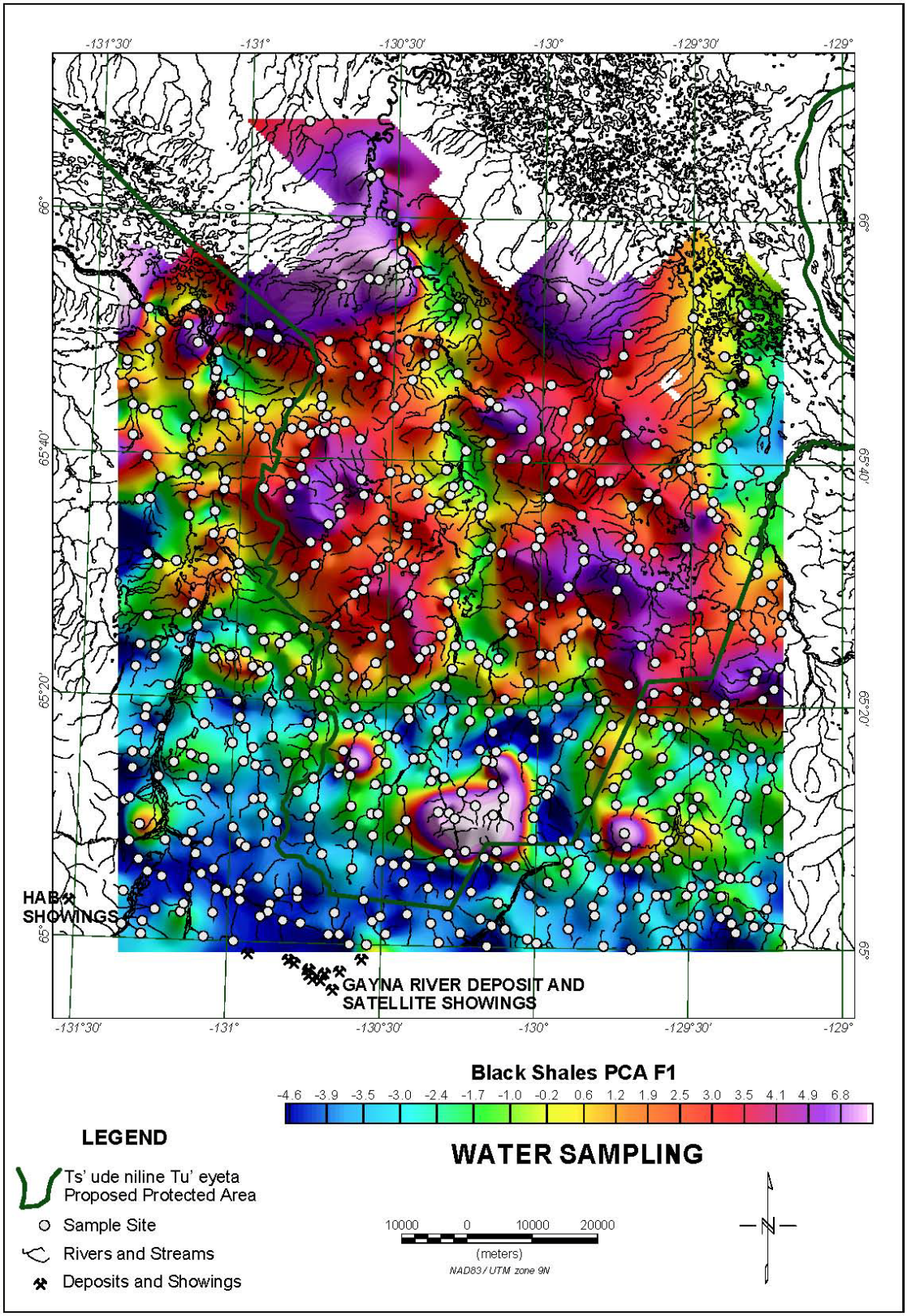


Figure 23 Gridded F1 factor values from the Principal Component Analysis for the Black Shale mineral assemblage model. It shows balanced contribution from all elements except Mn and covers 84% of statistical variability

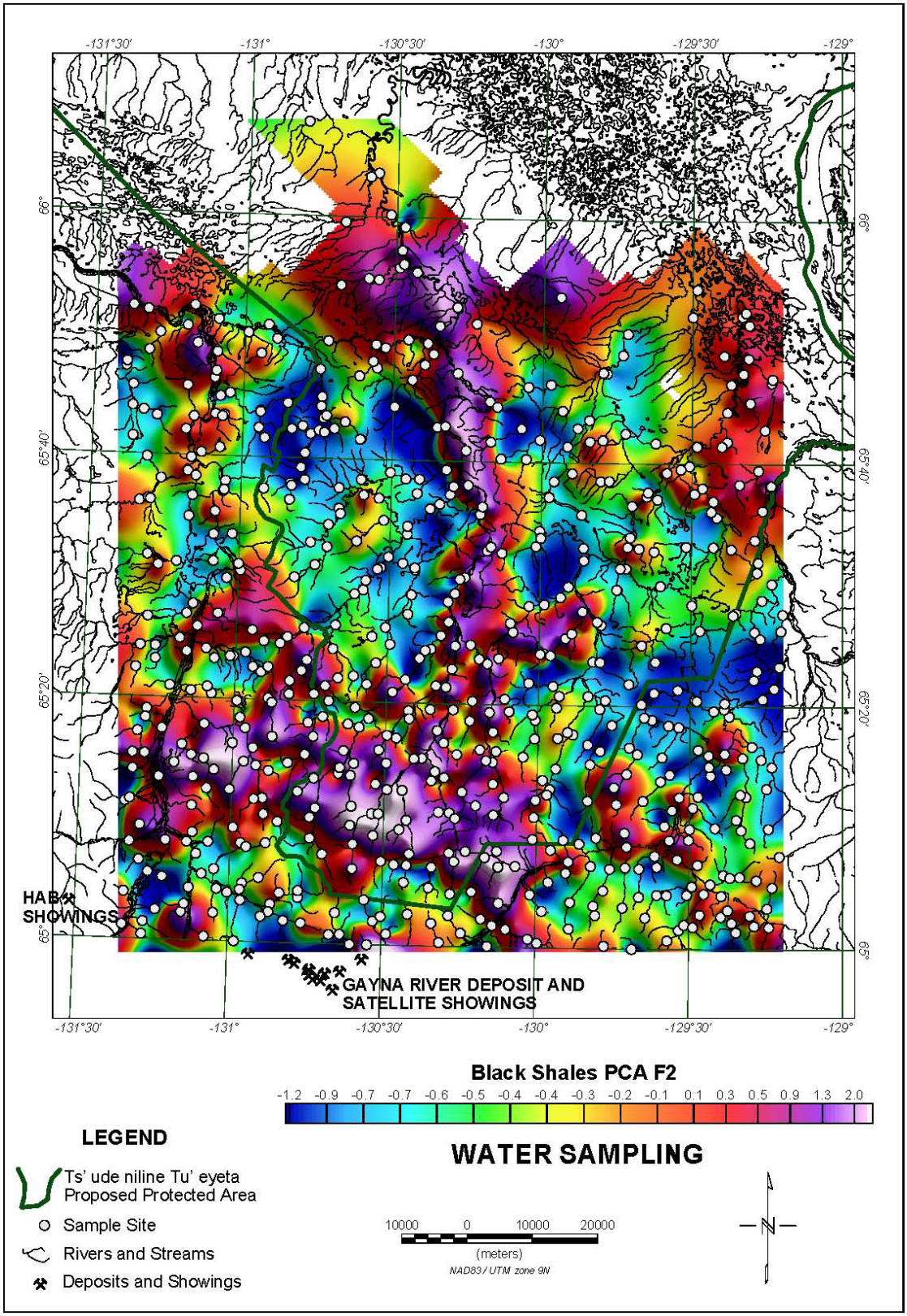


Figure 24 Gridded F2 factor values from the Principal Component Analysis for the Black Shale mineral assemblage model. It shows a predominant contribution from Mn (41%). Ni and Mn are both elevated in this factor and may be mapping the redox state of the water.

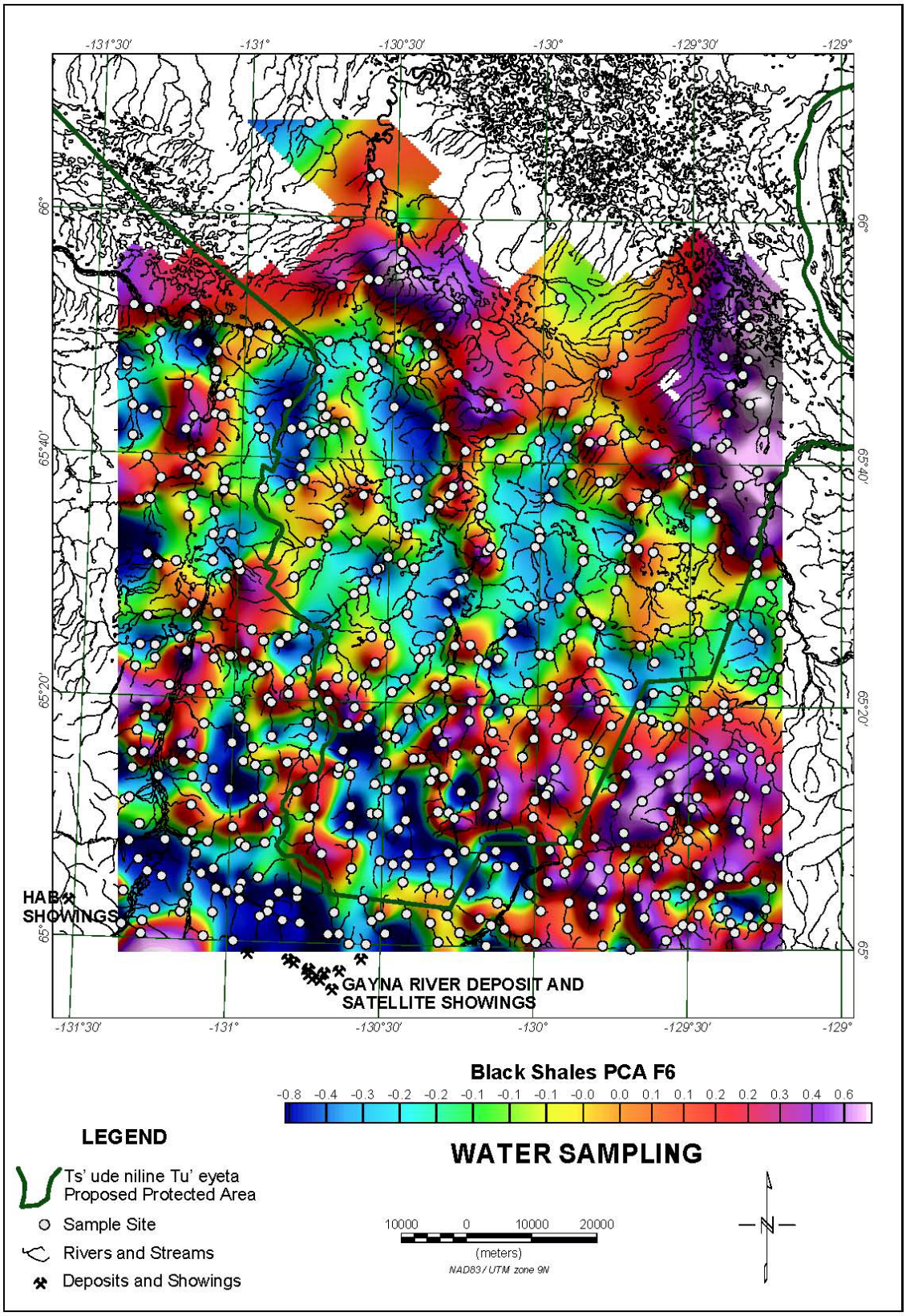


Figure 25 Gridded F6 factor values from the Principal Component Analysis for the Black Shale mineral assemblage model. It shows elevated concentrations of Fe, Cu and Ni and may map organic-rich shale units.

12 Conclusion

The Northwest Territories Geoscience Office conducted a stream sediment sampling program across portions of NTS mapsheets 106G, 106H, 106I and 106J during the summers of 2007 and 2008. This survey was completed to help assess the potential for the presence of economic mineral deposits in the Ts' ude niline Tu' eyeta Candidate Protected Area in west central Northwest Territories.

Analysis of the sampling data suggests the potential exists for several deposits of several different mineralisation types. The most obvious deposits to be expected in the southern, mountainous portion of the study area are limestone hosted, lead-zinc deposits similar to the Gayna River deposit and satellite showings just south of the survey area. The sample data show several locales with anomalous zinc and lead values in this area. There is also strong potential for the discovery of other base and precious metal deposits in the region. There are several locations which returned anomalous results for copper, silver, gold and nickel, often with several elements elevated in the same sample.

Wallace (2009) discovered an apparent correlation between copper, gallium and zinc in the ore mineralisation in the Gayna River deposits. This association has not been documented elsewhere in the cordillera. This is important because an analysis of the associations in the silt sampling univariate statistics also shows this correlation, indicating that there is a potential to discover Gayna River type mineralisation in the study area.

Further mapping and exploration work will no doubt result in the discovery of several showings and deposits in the cordillera region of the candidate protected area.

References

Aitken, J.D., 1981. Stratigraphy and Sedimentology of the upper Proterozoic Little Dal Group, Mackenzie Mountains, Northwest Territories; *in* Proterozoic Basins of Canada, edited by F.H.A. Campbell; Geological Survey of Canada, Paper 81-10, p. 47-72.

Aitken, J.D., 1993. Proterozoic sedimentary rocks; Subchapter 4A; *in* Sedimentary Cover of the Craton in Canada, edited by D.F. Stott and J.D. Aitken; Geological Survey of Canada, Geology of Canada, no.5, p.81-95.

Aitken, J.D., Ayling, M.E., Balkwill, H.R., Cook, D.G., Mackenzie, W.S., and Yorath, C.J., 1969. Fort Good Hope, District of Mackenzie; Geological Survey of Canada, Preliminary Map 4-1969.

Aitken, J.D. and Cook, D.G., 1974. Carcajou Canyon map-area, District of Mackenzie; Geological Survey of Canada, Paper 74-13.

Aitken, J.D., Cook, D.G., and Yorath, C.J., 1982. Upper Ramparts River (106G) and Sans Sault Rapids (106H) Map Areas, District of Mackenzie; Geological Survey of Canada Memoir 388.

Cook, D.G. and Aitken, J.D., 1975. Ontaratue River (106-J), Travaillant Lake (106-O), and Canot Lake (106-P) map-areas, District of Mackenzie, Northwest Territories; Geological Survey of Canada, Paper 74-17.

Cook, D.G., and B.C. MacLean 1995 The intracratonic Paleoproterozoic Forward Orogeny, and implication for regional correlation, Northwest Territories, Canada, Canadian Journal of Earth Sciences Vol.32, p.1991-2008.

Day S.J.A., Lariviere J.M., McNeil R.J., Friske P.W.B., Cairns S.R., McCurdy M.W., Wilson, R.S. 2007. Regional Stream Sediment and Water Geochemical Data, Horn Plateau area, Northwest Territories (Parts of NTS 85E, 85F, 85K, 85L, 95H, 95I and 95J) Including Analytical, Mineralogical and Kimberlite Indicator Mineral Data. Geological Survey of Canada, Open File 5478 / NWT Geoscience Office Contribution 0027 1 CD-ROM.

Dixon, J., 1999. Mesozoic–Cenozoic stratigraphy of the northern Interior Plains and Plateau, Northwest Territories; Geological Survey of Canada, Bulletin 536.

Duk-Rodkin, A. and Hughes, O.L., 1992a. Surficial Geology, Fort Good Hope, District of Mackenzie, Northwest Territories; Geological Survey of Canada, Map 1741A.

Duk-Rodkin, A. and Hughes, O.L., 1992b. Surficial Geology, Ontaratue River, District of Mackenzie, Northwest Territories; Geological Survey of Canada, Map 1742A.

Duk-Rodkin, A. and Hughes, O.L., 1993a. Surficial Geology, Sans Sault Rapids, District of Mackenzie, Northwest Territories; Geological Survey of Canada, Map 1784A.

Duk-Rodkin, A. and Hughes, O.L., 1993b. Surficial Geology, Upper Ramparts River, District of Mackenzie, Northwest Territories; Geological Survey of Canada, Map 1783A.

Dumont, R., Coyle, M., Oneschuck, D., and Potvin, J., 2000. Aeromagnetic total field map, Northwest Territories, NTS 106G/NW-NE; Geological Survey of Canada, Open File 3980.

Dumont, R., 2000a. Aeromagnetic total field map, Northwest Territories, NTS 106H/NW; Geological Survey of Canada, Open File 3759a.

Dumont, R., 2000b. Aeromagnetic total field map, Northwest Territories, NTS 106H/NE; Geological Survey of Canada, Open File 3759b.

Dumont, R., 2000c. Aeromagnetic total field map, Northwest Territories, NTS 106H/SW; Geological Survey of Canada, Open File 3759e.

Dumont, R., 2000d. Aeromagnetic total field map, Northwest Territories, NTS 106H/SE; Geological Survey of Canada, Open File 3759f.

Dumont, R., Coyle, M., Oneschuck, D., and Potvin, J., 2000. Aeromagnetic total field map, Northwest Territories, NTS 106G/NW-NE; Geological Survey of Canada, Open File 3980.

Dumont, R., Coyle, M., Oneschuck, D., and Potvin, J., 2001a. Aeromagnetic total field map, Northwest Territories, NTS 106I/SW-SE; Geological Survey of Canada, Open File 3981.

Dumont, R., Coyle, M., Oneschuck, D., and Potvin, J., 2001b. Aeromagnetic total field map, Northwest Territories, NTS 106I/NW-NE; Geological Survey of Canada, Open File 3982.

Dumont, R., Coyle, M., Oneschuck, D., and Potvin, J., 2001c. Aeromagnetic total field map, Northwest Territories, NTS 106J/SW-SE; Geological Survey of Canada, Open File 3983.

Dumont, R., Coyle, M., Oneschuck, D., and Potvin, J., 2001d. Aeromagnetic total field map, Northwest Territories, NTS 106J/NW-NE; Geological Survey of Canada, Open File 3984.

Eckstrand, O.R. and Barrie, C.T., 1996. Magmatic nickel-copper-platinum group elements; *in* Geology of Canadian Mineral Deposit Types, edited by O.R. Eckstrand, W.D. Sinclair, and R.I. Thorpe; Geological Survey of Canada, Geology of Canada, no.

8, p. 583-614 (also Geological Society of America, The Geology of North America, v. P-1).

Environment Canada, 2005. State of the Environment Infobase, Ecozones of Canada; website: http://www.ec.gc.ca/soer-ree/English/vignettes/default.cfm.

Gal, L.P., 2007. Ts' ude niline Tu' eyeta (Ramparts River and Wetlands) Candidate Protected Area Phase I Non-renewable Resource Assessment – Petroleum, Northwest Territories, Canada, NTS 106G, H, I, J; Northwest Territories Geoscience Office, NWT Open File 2007-01, 115 p.

Grunsky, E.C. (2007). The interpretation of regional geochemical survey data. In: Proceedings of Exploration '07: Fifth Decennial International Conference on Mineral Exploration. p139-182.

Hanley, P.T., Hodgson, D.A., Hughes, O.L., Kurfurst, P.K., Lawrence, D.E., Zoltai, S.C., Pettapiece, W.W., and Pilon, J., 1973. Four surficial geology and geomorphology maps of Fort Norman, Carcajou Canyon, Norman Wells and Sans Sault Rapids map areas, Mackenzie Valley; Geological Survey of Canada, Open File 155.

Harlan, S.S., Heaman, L., LeCheminant, A.N., and Premo, W.R., 2003. Gunbarrel mafic magmatic event: a key 780 Ma time marker for Rodinia plate reconstructions; Geology, v. 31, p. 1053-1056.

Hewton, R.S., 1976. Gayna River Project: Geology, Geochemistry and Diamond Drilling 1976, RT claims; Indian and Northern Affairs Canada, Northwest Territories Assessment Report 080567.

Hewton, R.S., 1982. Gayna River: a Proterozoic Mississippi Valley-Type Zinc-Lead deposit, Precambrian Sulphide Deposits, *in* H.S. Robinson Memorial Volume, edited by R.W. Hutchinson, C.D. Spence, and J.M. Franklin; Geological Association of Canada, Special Paper 25, p. 667-700.

Hughes, O.L., 1970. Five surficial geology maps of Mackenzie District, N.W.T.; Geological Survey of Canada, Open File 26.

Hunter, B., Geirholm, S., Krokosh, S., and McNeely, L., 2002. Protected Area Initiative: Ramparts River and Wetlands (Tsodehniline and Tuyat'ah) in the Sahtu Region of the Northwest Territories; unpublished report for Ducks Unlimited Canada.

Journeay, J.M. and Williams, S.P., 1995. GIS Map Library: a window on Cordilleran geology (version 1.0); Geological Survey of Canada, Open File 2948.

MacLean, B.C., 1999. Sub-Cambrian unconformity subcrop and seismic time structure map, Western Plains, Northwest Territories, Canada; Geological Survey of Canada, Open File D2998.

MacLean, B.C. and Cook, D.G., 2000. Salt tectonism in the Fort Norman area, Northwest Territories, Canada; Geological Survey of Canada, Open File 3857.

Mills, A.J., 2008. Ts' ude niline Tu' eyeta (Ramparts River and Wetlands) Candidate Protected Area Phase 1 Non-renewable Resource Assessment – Minerals; Northwest Territories Geoscience Office, NWT Open File 2008-01, 33 p.

Monroe, R.L., 1973. Three terrain classification and sensitivity maps of Upper Ramparts river, Sans Sault rapids, Carcajou canyon map-areas, District of Mackenzie; Geological Survey of Canada, Open File 132.

Morrell, G.R. (editor), 1995. Petroleum Exploration in Northern Canada: A Guide to Oil and Gas Exploration and Potential; Northern Oil and Gas Directorate, Indian and Northern Affairs Canada, 110 p.

Poulton, T.P., Braun, W.K., Brooke, M.M., and Davies, E.H., 1993. Jurassic; Subchapter 4H; *in* Sedimentary Cover of the Craton in Canada, edited by D.F. Stott and J.D. Aitken; Geological Survey of Canada, Geology of Canada, no.5, p. 321-357.

Pyle, L.P., Jones, A.J., and Gal, L.P., 2006. Geoscience knowledge synthesis: Peel Plateau and Plain, a prospective hydrocarbon province in the northern Mackenzie Corridor; Geological Survey of Canada, Open File 5234, NWT Open File 2005-01, 85 p.

Rainbird, R.H., Villeneuve, M.E., Cook, D.G., and MacLean, B.C., 1996. Detrital zircon ages from two wells in the Northwest Territories: implications for the correlation and provenance of Proterozoic subsurface strata; Geological Survey of Canada, Current Research, Paper 96-1B, p. 29-38.

Rampton, V. and Fulton, R.J., 1970. Surficial geology maps, Arctic coast, District of Mackenzie; Geological Survey of Canada, Open File 21.

Rogers, M.C., Thurston, P.C., Fyon, J.A., Kelly, R.I., and Breaks, F.W., 1995. Descriptive Mineral Deposit Models of Metallic and Industrial Deposits Types and Related Mineral Potential Assessment Criteria; Ontario Geological Survey, Open File Report 5916, 241 p.

Sangster, D.F., 1983. The Canadian experience in mineral resource assessment, Geoscience Canada, v. 10, no. 2, p. 70-76.

Seemann, D.A., Sweeney, J.F., Hearty, D.B., 1988. Gravity Anomaly Field, Northern Yukon, Northern District of Mackenzie and Beaufort Sea; Geological Survey of Canada, Open File 1832.

Stott, D.F., Caldwell, W.G.E. Cant, D.J. Christopher, J.E., Dixon, J., Koster, E.H., McNeil, D.H., and Simpson, F., 1993. Cretaceous, Subchapter 4I, *in* Sedimentary Cover of the Craton in Canada; edited by D.F. Stott and J.D. Aitken; Geological Survey of Canada, Geology of Canada no. 5, p. 358-438.

Thorkelson, Derek J., J. Grant Abbot, James K. Mortensen, Robert A. Creaser, Micheal E. Villeneuve, Vicki J. McNicoll, and Paul W. Layer 2005 Early and Middle Proterozoic evolution of Yukon Canada Canadian Journal of Earth Sciences Vol. 42, p. 1045-1071

Thorkelson, D.J., J.K. Mortensen, R.A. Creaser, G.J. Davidson, and J.G. Abbot 2001 Early Proterozoic Magmatism in Yukon, Canada: constraints on the evolution of northwestern Laurentia Canadian Journal of Earth Sciences, Vol. 38, p.1479-1494

Wheeler, J.O., Hoffman, P.F., Card, K.D., Davidson, A., Sanford, B.V., Okulitch, A.V., and Roest, W.R., 1996. Geological map of Canada; Geological Survey of Canada, "A" Series Map, 1860A.

Yorath, C.J. and Cook, D.G., 1981. Cretaceous and Tertiary stratigraphy and paleogeography, northern Interior Plains, District of Mackenzie; Geological Survey of Canada, Memoir 398.

Wallace, S.R.B., 2009. The Genesis of the Gayna River Carbonate-Hosted Zn-Pb Deposit. Unpublished M. Sc. Thesis, University of Alberta., 117 pages.

Welsch, E.P. and Chao, T.T. 1976. Determination of trace amounts of tin in geological materials by atomic absorption spectrometry; Anal. Chim Acta., Vol. 82, pp. 337-342.

APPENDIX 1

RAW DATA

LOG-TRANSFORMED DATA

BOX PLOT

Q-Q PLOT

HISTOGRAM PLOT

CUMULATIVE HISTOGRAM PLOT

HISTOGRAM PLOT

CUMULATIVE HISTOGRAM PLOT

Ag

Al

As

Au

B

Ba

Bi

Br

Ca

Cd

Ce

Co

Co

Cs

Cu

Eu

F_Fusion

Fe

Ga

Hf

Hg

La

Lu

Mg

RAW DATA

LOG-TRANSFORMED DATA

BOX PLOT

Q-Q PLOT

HISTOGRAM PLOT

CUMULATIVE HISTOGRAM PLOT

HISTOGRAM PLOT

CUMULATIVE HISTOGRAM PLOT

Mn

Mo

Na

Ni

P

Pb

Rb

S

Sb

Sc

Se

Sm

Sn

Sr

Ta

Tb

Te

Th

Ti

Tl

U

V

W

Yb

Zn

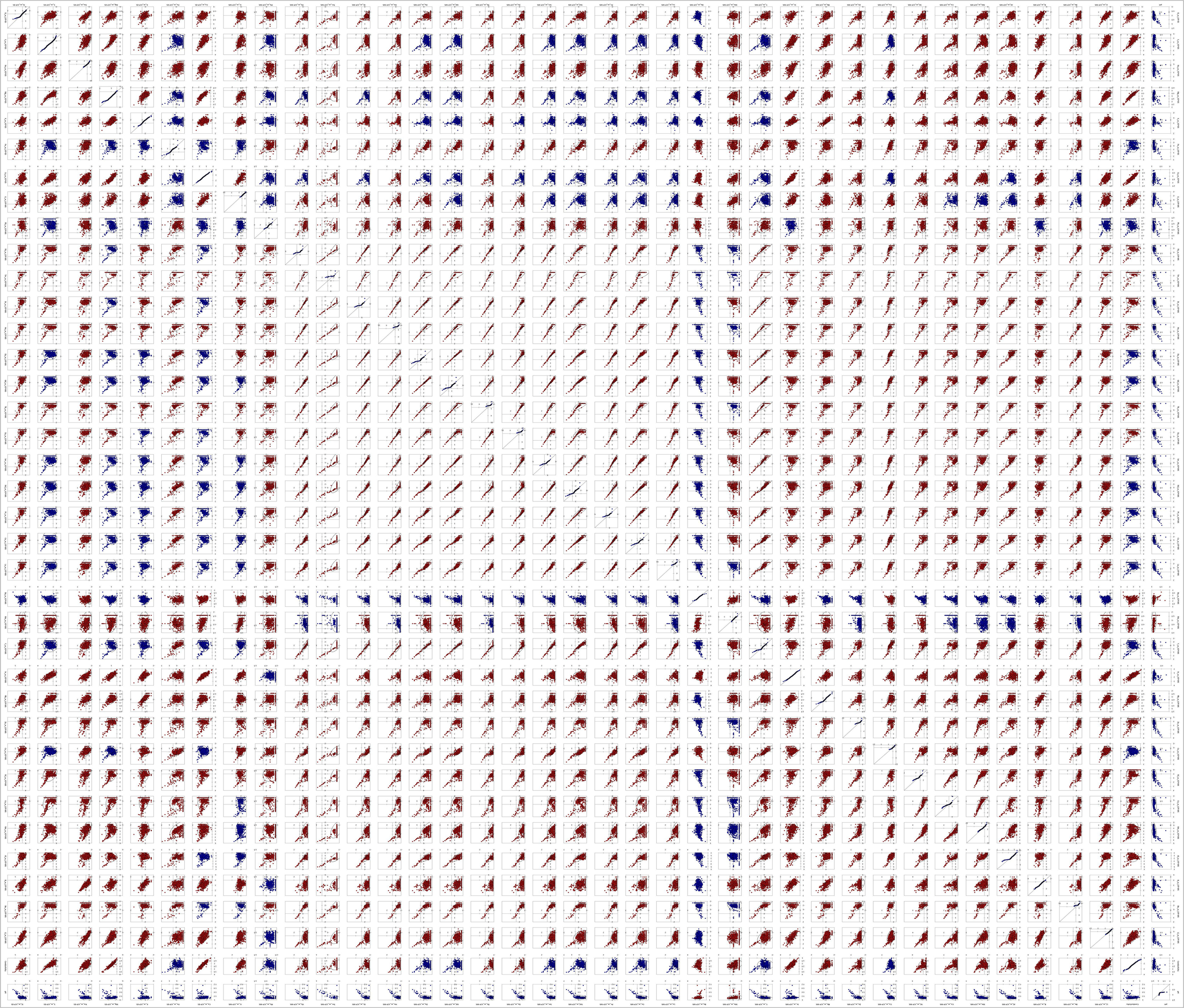
APPENDIX 2

APPENDIX 3

WATER GEOCHEMICAL DATA
UNIVARIATE STATISTICAL ANALYSIS
LOG-TRANSFORMED DATA

BOX PLOT | Q-Q PLOT | HISTOGRAM PLOT | CUMULATIVE HISTOGRAM PLOT

APPENDIX 4



APPENDIX B

Interpretation of Kimberlite Indicator Minerals (KIMs)
in stream sediments of the
Ts'ude niline Tu'eyeta Candidate Protected Area
Ramparts River Area,
Northwest Territories

INTERPRETATION OF KIMBERLITE INDICATOR MINERALS IN STREAM SEDIMENTS (MAP AREAS 106G & 106H)

for Stephen Day, GSC
by Ingrid Kjarsgaard, Consulting Mineralogist, Ottawa
December 6, 2008

Indicator Mineral Counts and Distribution

Only 394 indicator mineral grains were recovered from 94 samples in this area. They consist of 234 chromian spinels, 57 (Cr-)diopside , 22 Mg-ilmenite, 20 Cr-pyrope, 11 olivine and 50 other non-indicator minerals (see Table 1A, Appendix E). Most of the analyzed grains occur in the smallest size fraction (0.25 to 0.5 mm) but a few of the chromite, Mg-ilmenite and pyrope grains had larger sizes (0.5 to 1.0 mm).

Chromite grains occur in 57 of the 94 samples, but more than half of the grains are concentrated (with up to 37 grains per samples) in only five samples (106G-2007-2154, -2156, -2162, -2165, -2188). One of them also contains 9 of the 11 olivine grains. None of the chromite rich samples contains Cr-pyrope or Mg-ilmenite. The remainder of the chromite grains are dispersed over many samples with no more than 6 grains per sample. (Cr-) diopside occurs in 33 samples with up to 6 grains per sample (see Table 1A, Appendix E). Cr-pyrope occurs with one grain per sample in 17 out of the 94 samples and one sample (106G-2007-3004) contained three pyrope grains. Mg-ilmenite occurs with one to three grains per samples in 14 different samples.

Indicator Mineral Composition

Twenty-two of the 43 ilmenite grains are characterized by high MgO ranging from 7 to 15 wt.% (Fig. 1) and Cr_2O_3 ranging from 0.3 to 6.7 wt.% and fall well within the compositional range of kimberlitic megacryst ilmenite (Fig.2). The remainder of the ilmenites have low MgO ($\leq$ 1.15 wt.%) and are from crustal rocks (Fig. 2).

The 234 chromite grains show compositions similar to those in map areas 106B, which range from ca. 25 wt.% to 56 wt.% Cr_2O_3 and from 8 to 17 wt.% MgO, with a few grains scattering towards higher Cr_2O_3 and lower MgO (Fig. 3).

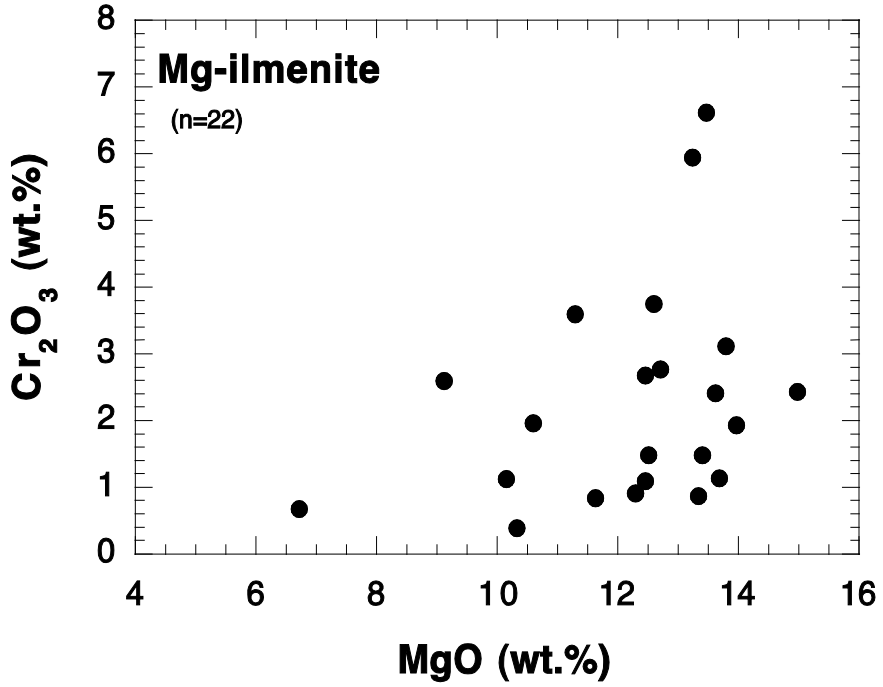


Figure 1: MgO vs. Cr_2O_3 for the 22 Mg-ilmenite grains showing the wide range of Cr_2O_3 and MgO content.

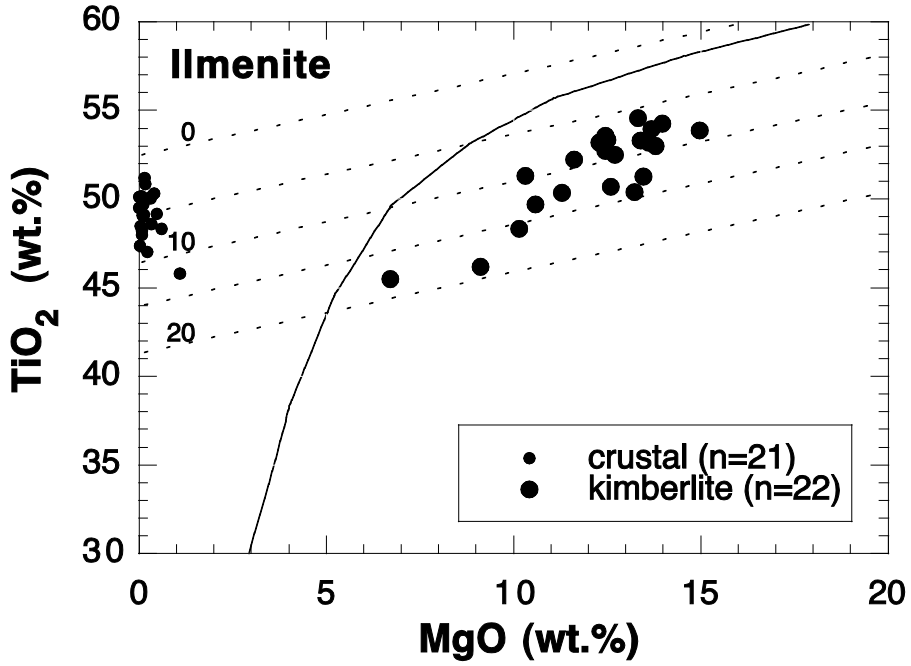


Figure 2: MgO vs. TiO_2 for ilmenites. The curve separates low MgO crustal ilmenites from high MgO kimberlitic megacryst ilmenite. The stippled lines are lines of equal hematite content - an indication of oxidation (curve and lines after Wyatt et al., 2004).

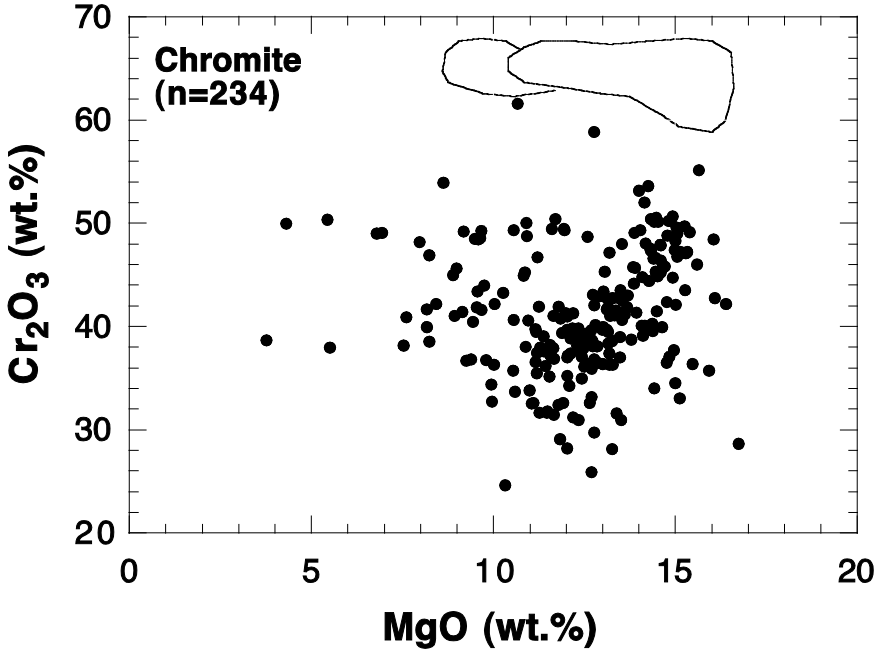


Figure 3: Chromite compositions shown in a Cr_2O_3 vs. MgO diagram. The fields outlined are for chromite compositions from diamond inclusions and intergrowth (after Fipke et al., 1995).

The bulk of the chromite grains has a fairly high amount of spinel component ($MgAl_2O_4$), which is higher than in chromites from garnet-peridotite typically found in diamondiferous kimberlites. Only a few chromite grains, which plot immediately below the diamond inclusion and intergrowth fields shown in Fig. 3 are likely from garnet-peridotite xenoliths.

The twenty garnets picked from the stream sediments are Cr-pyrope and plot above the 85% line of Gurney (1984) which is acts as a separation line between lherzolitic garnets which plot above and harzburgitic (subcalcic) garnets, which plot below the line (Fig. 4). This indicates that all of the garnets here came from garnet-lherzolite with the exception of one grain that is high in CaO and probably came from a wehrlite (olivine-clinopyroxenite). Garnet-lherzolite and wehrlite xenoliths are typically found in kimberlites, but are not indicative of high diamond potential.

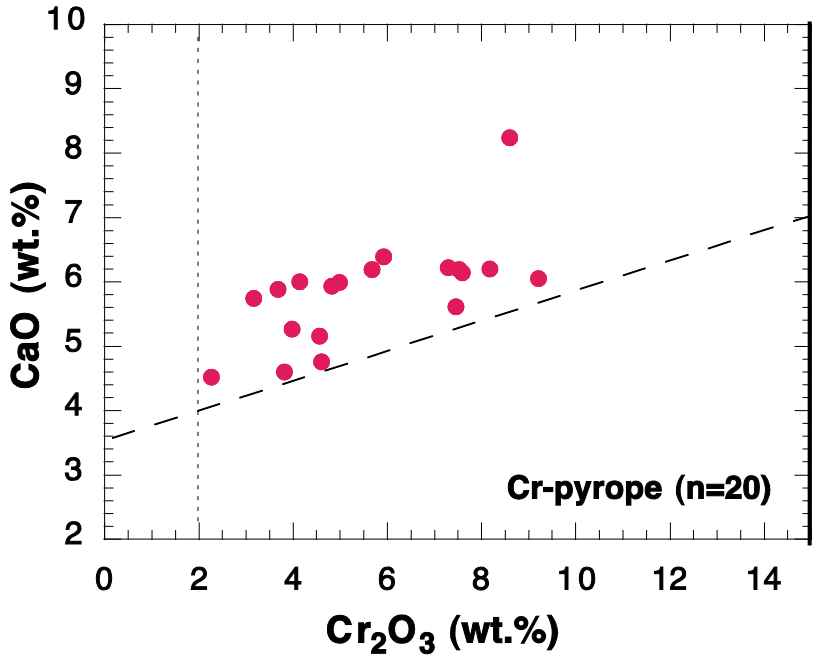


Figure 4: CaO vs. Cr_2O_3 for garnets. The diagonal stippled line is the 85% line from Gurney (1984) that separates lherzolitic (G9) garnets from subcalcic harzburgitic garnets (G10). The vertical stippled line separates peridotitic Cr-pyrope from Cr-poor megacrystic, eclogitic or pyroxenitic garnet.

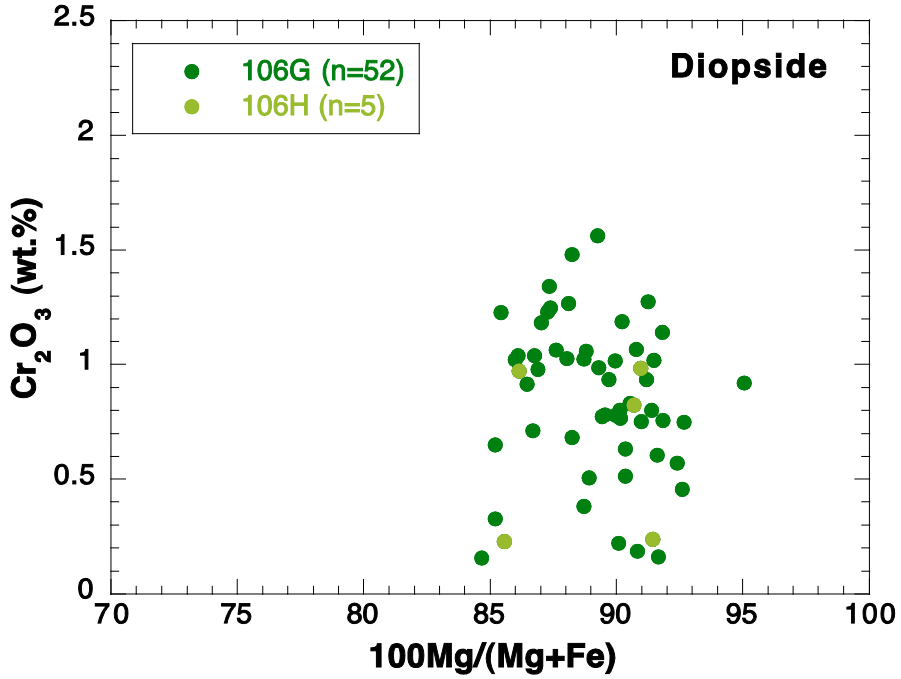


Figure 5: Cr_2O_3 vs. mg-# for diopsides.

The 57 diopsides picked from this map area consist of eight diopsides and 49 Cr-diopsides with mg-#s from 84 to 96 and Cr_2O_3 values from 0.25 to 1.6 wt.% (Fig. 5). Although many of the Cr-diopsides show similar compositions to Cr-diopsides from garnet-lherzolite (which typically have mg-# of > 90) it is suspected that they are from crustal ultramafic rocks rather than mantle xenoliths since not enough pyrope garnet and mantle olivine was recovered from the stream sediments to indicate abundant peridotite material. The most Mg-rich Cr-diopside(s), however, are likely to have come from mantle lherzolite.

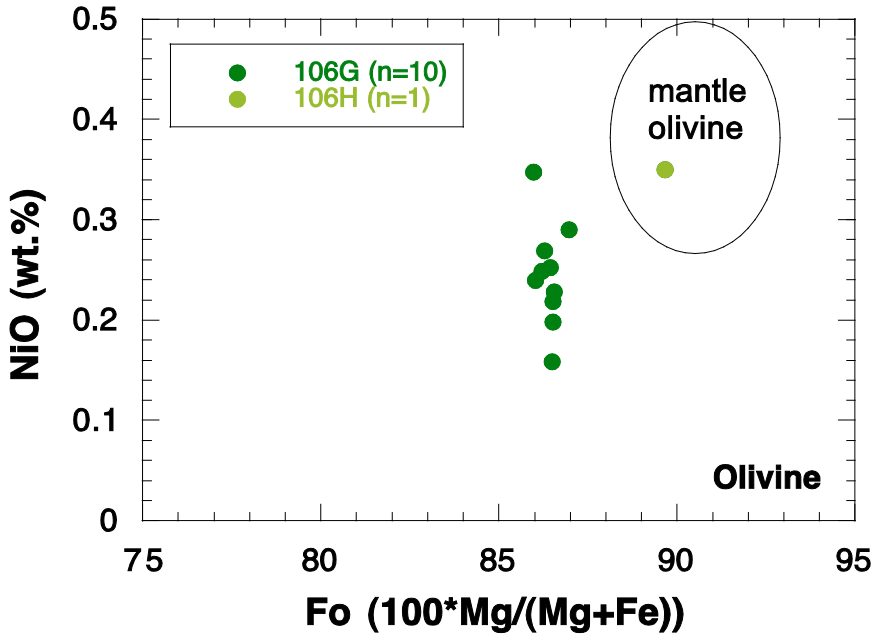


Figure 6: NiO vs. Fo content for olivine grains. The oval shows the compositional range of olivine from mantle peridotite and kimberlite megacrysts.

Nine of the eleven olivine grains found in this map area occur in sample 106G-2007-2154 and show compositions identical to those found in map area 106B, i.e. Fo content of 86-87 and variable NiO content from 0.15 to 0.46 wt.%. Only one olivine (from sample 106H-2007-1002) plots in the compositional field of kimberlitic megacryst olivine or mantle peridotite.

Summary and Discussion

Bona fide kimberlite indicator minerals in this map area are the 22 Mg-ilmenite, 20 Cr-pyrope grains, one olivine with Fo 92, one Cr-diopside with mg-# > 95 and a few Cr-rich chromite grains. The majority of the chromite and olivine grains and probably also the majority of the Cr-diopside grains are probably from regional ultramafic bedrock, most likely the same source as for indicator minerals in map area 106B. The presence of Mg-ilmenite in the stream sediments indicates that there is a kimberlitic source in the area and the composition of the Cr-pyrope grains indicates that it contained lherzolitic and wehrlitic mantle xenoliths. The abundance of both minerals, however, is low, indicating that the source kimberlite is either distal or poor in indicator minerals and xenoliths (aphanitic). Plotting the occurrences of Mg-ilmenite and Cr-pyrope grains on a sample map might help narrow down the kimberlite source area.

References

Fipke, C.E., Gurney, J.J. and Moore, R.O. (1995) Diamond exploration techniques emphasizing indicator mineral geochemistry and Canadian examples; Geological Survey of Canada, Bulletin 423, 86 p.

Gurney, J.J. (1984) A correlation between garnets and diamonds in kimberlites; in Kimberlite occurrence and origin: a basis for conceptual models in exploration; Geology Department and University Extension, University of Western Australia, Publication No. 8, p. 143-166.

Nimis, P. (1998) Evaluation of diamond potential from the composition of peridotitic chromian diopside. European Journal of Mineralogy 10, p. 505-519.

Wyatt, B.A., Baumgartner, M., Anckar, E. and Grütter, H. (2004) Compositional classification of "kimberlitic" and "non-kimberlitic" ilmenite; Lithos 77, p. 819-840.

Kimberlite Indicator Mineral distribution in map sheet 106G and 106H of the Ramparts area, Northwest Territories

KIMBERLITE INDICATOR MINERAL DISTRIBUTION IN MAP SHEET 106G AND 106H OF THE RAMPARTS AREA, NWT

for Stephen Day, GSC Canada and Carl Ozyer, NWT Geoscience Office
by Ingrid Kjarsgaard, Consulting Mineralogist, Ottawa
September 2010

Introduction

163 potential kimberlite indicator mineral grains were recovered from 42 stream sediment samples collected within the map sheets 106G (2 samples) and 106H (40 samples) in the lowlands bordering the Canyon Ranges in the Mackenzie Mountains, NWT, Canada. The grain distribution in each sample is listed in Table 1B, Appendix E. The grains were analyzed by microprobe at the GSC in Ottawa and the data labeled and sorted by mineral and listed in Appendix E.

1. Garnet

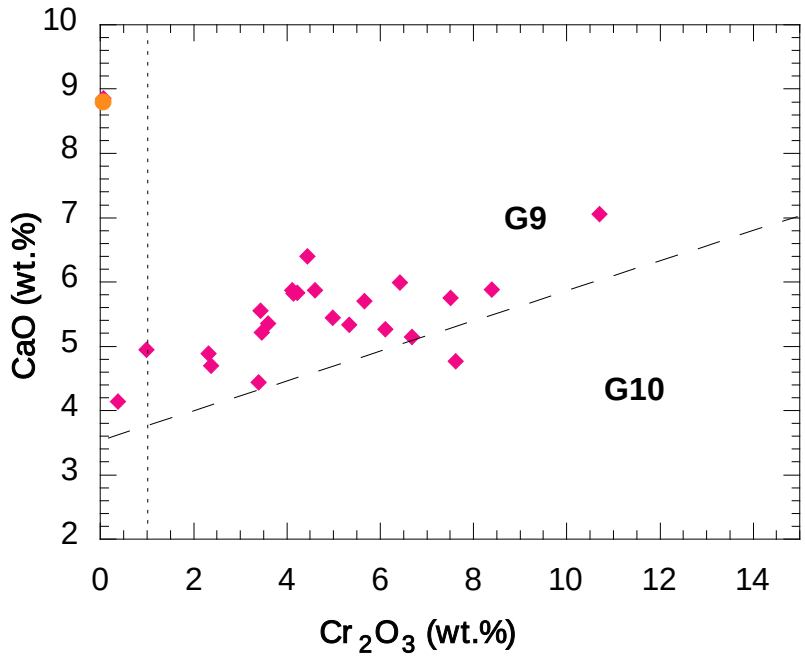


Figure 1: CaO vs. Cr_2O_3 showing the compositional variation in red and orange garnet. The vertical dashed line separates peridotitic Cr-pyrope (at right) from Cr-poor mega-crystic and eclogitic garnet (at left). A potentially eclogitic garnet is shown in orange. The diagonal dashed line is the 85% line of Gurney (1984) that is used to divide ca-rich lherzolitic (G9) from Ca-depleted harzburgitic (G10) garnets.

A total of 22 (Cr-)pyrope grains were recovered from samples in the 106H map sheet and one from a sample (106G-2008-3002) in the adjacent sheet 106G, very close to the boundary with 106H. One e-type orange garnet was also found in sample (106H-2008-3011) from 106H.

These garnet grains occur mostly in samples along the Hume and Mountain Rivers in the lowlands adjacent to the Canyon Ranges. Samples with more than one garnet are 106H-2008-1056 (3), -1085 (2), -2040 (2), -2050 (2), which were collected at approximately similar latitudes adjacent to the Hume and Mountain River. Two pyrope garnets have low Cr_2O_3 (< 1 wt.%) and elevated TiO_2 (> 0.5 wt.%) and are titanian pyrope characteristic of kimberlitic megacryst garnet (G1). The composition of the other pyrope grains is more chromian and their CaO levels suggest that they are G9 garnets from lherzolite xenoliths with the exception of one grain that falls below the 85% line and may be from fertile harzburgite (Fig. 1). Another grain picked as orange garnet (GO) in sample 106H-2008-3016 turned out to be a crustal almandine with > 27 wt.% FeO.

2. Mg-Ilmenite

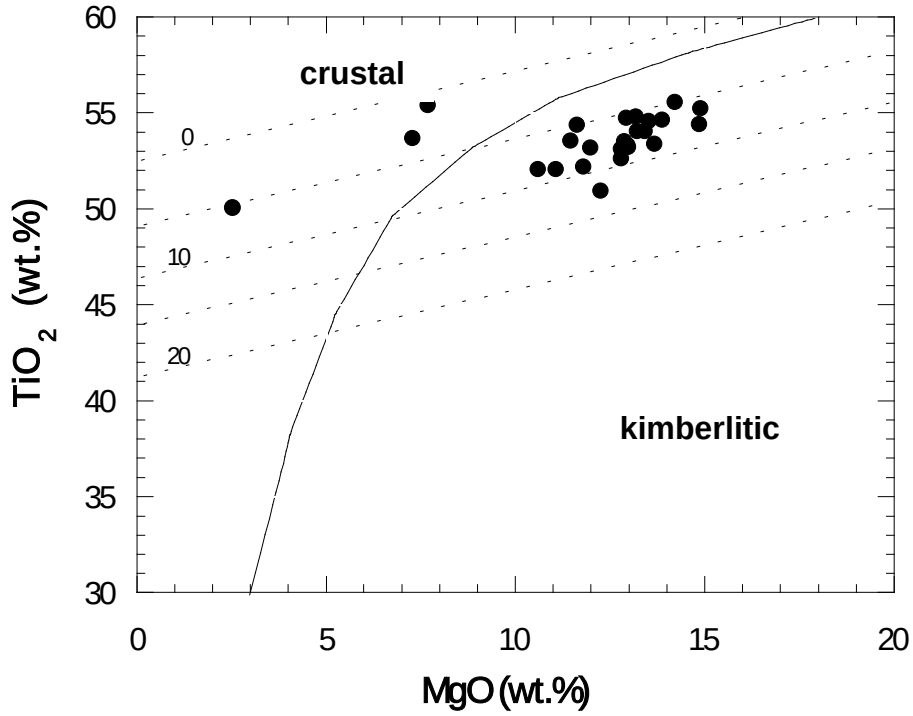


Figure 2: TiO_2 vs. MgO in 25 ilmenite grains with separation line between Mg-ilmenite megacryst from kimberlite and crustal ilmenite after Wyatt et al. (2004).

Twenty-five ilmenite grains were recovered and analyzed. Twenty-four of them were magnesian with MgO varying between 7.3 and 14.9 wt.%, one had only 0.4 wt.% MgO and is of crustal origin. However, two of the Mg-ilmenite grains, which have 7. 3 and 7. 7 wt.% MgO respectively, also plot outside the dividing line between kimberlitic megacryst

ilmenite and crustal ilmenite according to Wyatt et al. (2004). They also have lower Cr_2O_3 than the other Mg-ilmenite grains (Fig. 3). These fairly MgO-rich ilmenite grains could only be derived from crustal ultramafic rocks such as those found in ultramafic layered intrusions (e.g. dunite, peridotite, pyroxenite). The other Mg-ilmenites (MgO from 10.6 to 14.9 wt.% and Cr_2O_3 from 0.73 to 4.43 wt.%) are most likely kimberlitic megacrysts ilmenite. The grains have approximately the same distribution as the pyrope garnet grains in the lowlands N of the Canyon Ranges. Half of them (n=10) were found in one sample (106H-2008-3013BS), possibly fragments of a larger grain that broke apart (megacrysts can be several cm in diameter) or simply a pocket of heavy mineral accumulation.

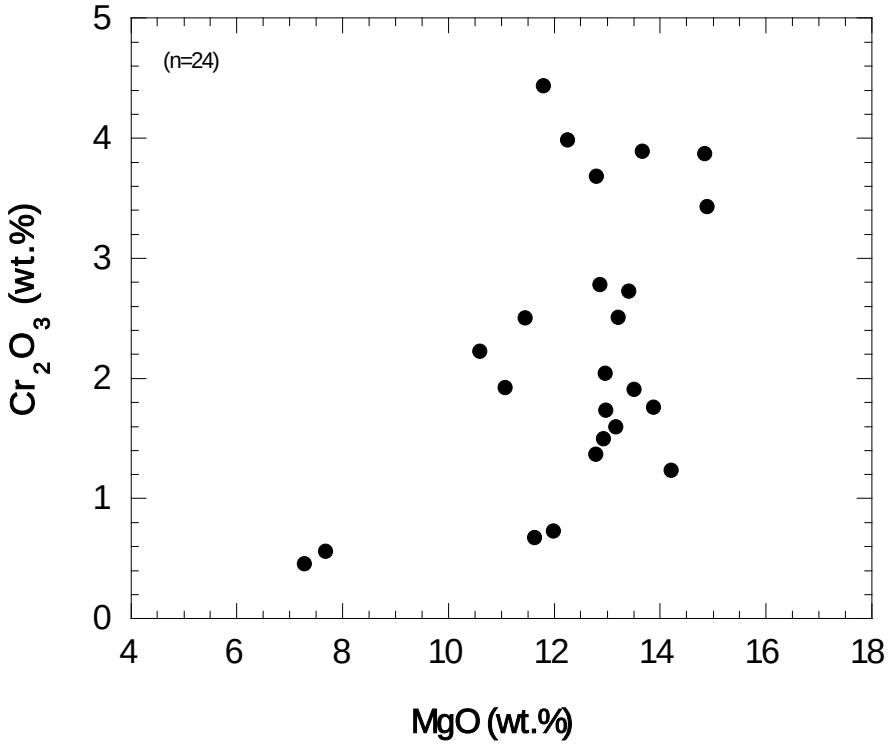


Figure 3: Cr_2O_3 vs. MgO in Mg-ilmenite.

3. Olivine

Only one olivine grain was found in this sample set (in sample 106H-2008-3009BS). It has a Fo value (100Mg/(Mg+Fe)) of 81 and NiO of 0.17 wt.%, which is too low to be from mantle peridotite, which typically has between Fo88 and 93 and NiO > 0.25 wt.% (Deer et al., 1997) Fig. 4) and more likely to be from a crustal ultramafic rock (peridotite, olivine pyroxenite, or olivine-gabbro from ultramafic layered intrusions, komatiite). However, it could also be a kimberlitic phenocryst olivine.

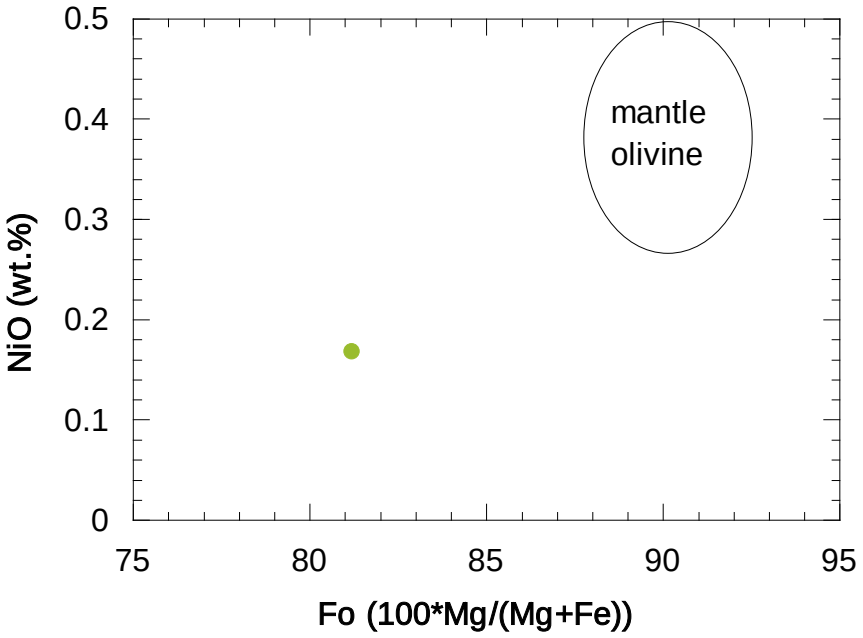


Figure 4: Fo vs. NiO in olivine with the compositional range of mantle olivine.

4. Chromite

Chromite is with 54 grains the second most numerous mineral in these samples. Sample locations are confined to the lowlands N of the mountains and overlap with those of pyrope and Mg-ilmenite. The highest number of chromite grains (n=15) was found in sample 106H-2008-3013BS, the same sample that also contained 10 Mg-ilmenite grains, which suggests a strong accumulation of heavy minerals in that area. The chromite grains are compositionally quite variable with 25.9 to 62 wt.% Cr_2O_3 and from 5.4 to 38.4 wt.% Al_2O_3, MgO from 2.5 to 17.6 wt.% MgO and 0.06 to 5.58 wt.% TiO_2. The most Cr-rich grain falls in the compositional field of chromites intergrown with diamond (see Fig. 5), but all others have below 53.5 wt.% Cr_2O_3. Several grains are Fe-rich and Al- and Mg-poor ferrochromites, characteristic of metamorphosed chromite from ultramafic layered intrusions. Cr-poor and Al- and MgO-rich chromian spinels are also present. Overall many of these chromites could come from mantle peridotite, with the possible exception of the most MgO-poor ferro-chromites, but many of the could also come from crustal ultramafic crustal rocks, which overlap compositionally. The high number of chromite grains compared to those of e.g. pyrope suggest that they may not entirely be mantle xenolith derived but come to some extent from crustal ultramafic rocks.

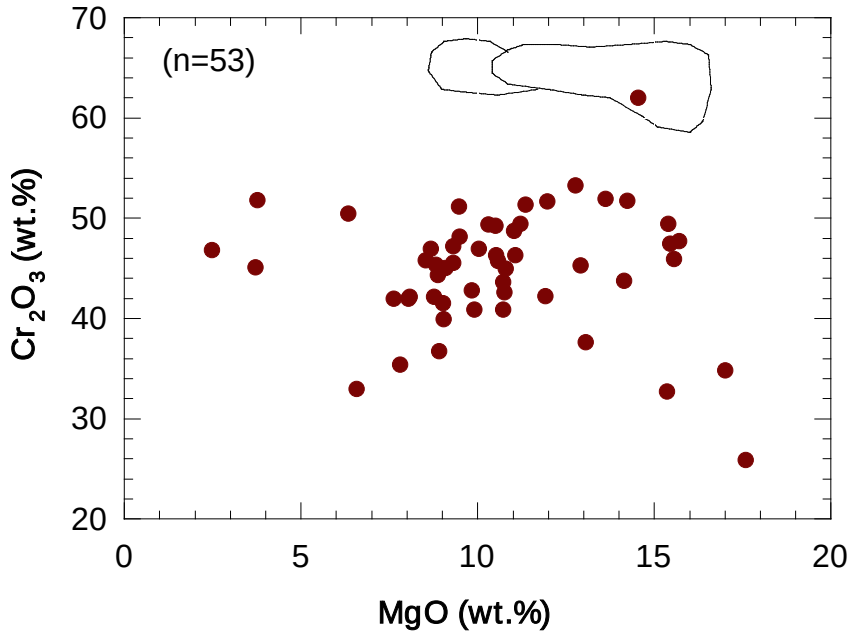


Figure 5: Cr_2O_3 vs. MgO for chromite and Cr-spinel. The black outlined fields are the compo-sitional ranges of chromite inclusions in diamond (right) and of chromite intergrown with diamond (left) after Fipke et al. (1995).

5. Diopside

Diopside is with 57 grains the most abundant kimberlite indicator mineral in this sample set. It is also the most widespread mineral and fairly evenly distributed over the 42 samples, with the highest concentration (n=6) occurring in sample 106H-2008-1056BS, which also contained three pyrope, three chromite and two Mg-ilmenite grains. Compositions vary from mg-# 76 to 95 and Cr_2O_3 from 0.20 to 1.47 wt.% (Fig. 6). Al_2O_3 ranges from 0.56 to 6.60 wt.% and a few grains are enriched in Na_2O (1.2 to 2.5 wt.%) while most contained below 0.5 wt.% Na_2O. The two most Al-rich grains fall into the compositional field for diopside derived from spinel peridotites (Nimis, 1998; Fig. 7), and the most Cr-poor cpx may represent megacryst or eclogitic cpx, but they could also come from crustal ultramafic rocks such as peridotite, komatiite, gabbro or pyroxenite from mafic layered intrusions (Deer et al, 1978). The three most Cr-rich diopsides are most likely to come from mantle peridotitic xenoliths since Cr-levels that high are rarely found in diopside from crustal rocks. Although most Cr-diopsides with $Cr_2O_3 > 0.5$ wt.% fall into the garnet-peridotite field (GP in Fig. 7) of Nimis & Taylor (1998), it needs to be mentioned that diopside from ultramafic crustal rocks have similar compositions with Cr_2O_3 up to 1.4 wt.% and mg-#s into the mid to high 80s.

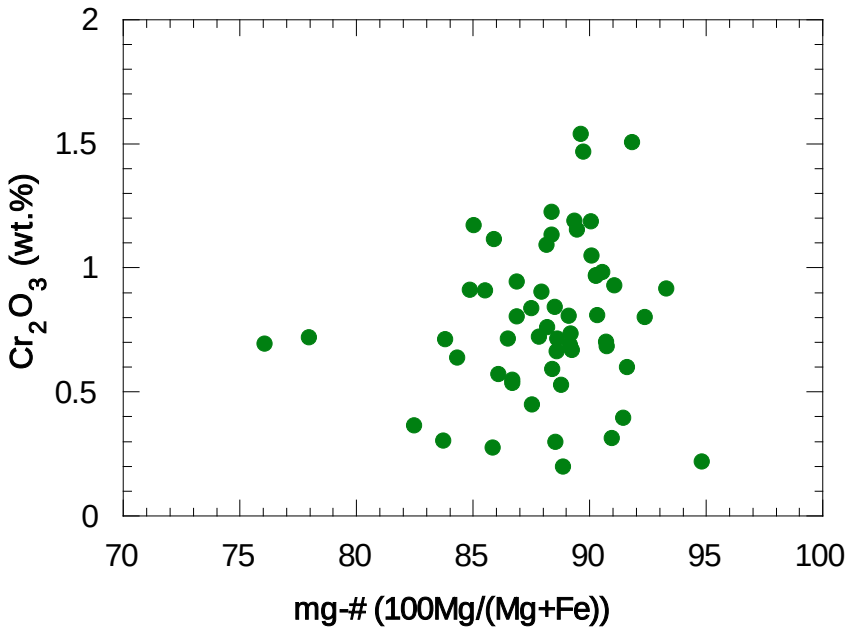


Figure 6: Cr_2O_3 vs. mg-# in diopside.

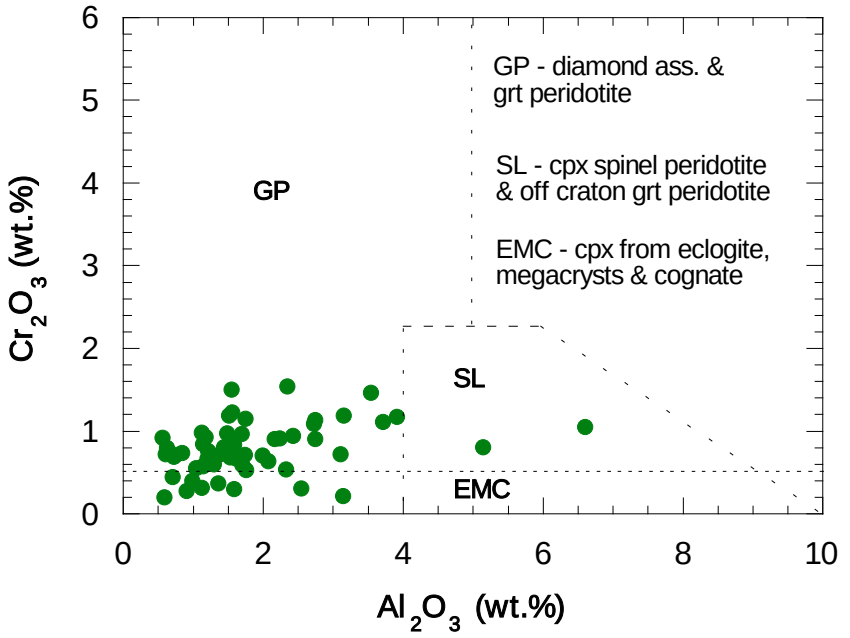


Figure 7: Cr_2O_3 vs. Al_2O_3 in diopside with field boundaries for kimberlite derived diopside according to Nimis (1998).

6. Summary

Cr-pyrope only occurs in garnet-peridotitic mantle xenoliths transported to the surface by kimberlite and is not found in crustal rocks. Mg-rich ilmenite is also unique to kimberlite, in which it occurs as megacrysts up to several centimeters in size. Olivine, chromite and Cr-diopside, however, although used as kimberlite indicator minerals, are not unique to kimberlite (or the mantle xenoliths it carries) but also occur in mafic to ultramafic crustal rocks and show compositional overlap with those derived from mantle peridotite.
The presence of moderate amounts of garnet peridotitic Cr-pyrope and megacrystic garnet and Mg-ilmenite and one eclogitic garnet strongly suggests the presence of kimberlitic material in the area drained by the streams sampled in this study. Whether or not this material is an actual kimberlite pipe (i.e. part of the bedrock geology) or just kimberlite debris carried into the area by glaciers from other sources cannot be determined. The relatively low abundance and wide distribution of the grains suggests the latter.

Chromite and (Cr)-diopside by far outnumber pyrope and Mg-ilmenite in this study suggesting that they have other source(s) than peridotitic mantle xenoliths (in which Cr-diopside typically has low modal abundances and chromite is a minor to trace mineral). The large compositional variation in these two minerals also suggests multiple sources involving garnet- and spinel-peridotite xenoliths and crustal mafic to ultramafic rocks. One olivine grain found in this study has a composition that also indicates derivation from crustal (ultra-)mafic rocks rather than mantle peridotite. Since the sample locations for pyrope, Mg-ilmenite, olivine and chromite widely overlap it is hard to determine the relative proportion of the different source rocks or narrow down the source region. The crustally derived material, however, seems to have higher concentrations in the N of the map sheet 106H (in samples 106H-2008-3009, -3010, -3011, and -3013). Kimberlitic material seems to be particularly prevalent in samples 106H-2008-1056, -1085, -3010 and -3013 but the grain counts are low overall and do not indicate a point source in the vicinity of the sample locations.

REFERENCES

Deer, W.A., Howie, R.A. & Zussman, J. (1978) Rock-Forming Minerals, Volume 2A Single-Chain Silicates, 2nd edition. Longman Group Ltd., London. 668 p.

Deer, W.A., Howie, R.A. & Zussman, J. (1997) Rock-Forming Minerals, Volume 1A Ortho-Silicates, 2nd edition. The Geological Society, London. 919 p.

Fipke, C.E., Gurney, J.J. and Moore, R.O. (1995) Diamond exploration techniques emphasizing indicator mineral geochemistry and Canadian examples; Geological Survey of Canada, Bulletin 423, 86 p.

Gurney, J.J. (1984) A correlation between garnets and diamonds in kimberlites; in Kimberlite occurrence and origin a basis for conceptual models in exploration;

Geology Department and University Extension, University of Western Australia, Publication No. 8, p. 143-166.

Nimis, P. (1998) Evaluation of diamond potential from the composition of peridotitic chromian diopside. *European Journal of Mineralogy* 10, p. 505-519.

Wyatt, B.A., Baumgartner, M., Anckar, E. and Grütter, H. (2004) Compositional classification of "kimberlitic" and "non-kimberlitic" ilmenite; *Lithos* 77, p. 819-840.

Kimberlite Indicator Mineral distribution in till samples from map sheets 106G, 106H, 106I and 106J of the Ramparts area, Northwest Territories

KIMBERLITE INDICATOR MINERAL DISTRIBUTION IN TILL SAMPLES FROM MAP SHEETS 106G, 106H, 106I AND 106J OF THE RAMPARTS AREA, NWT

for Carl Ozyer, NWT Geoscience Office
by Ingrid Kjarsgaard, Consulting Mineralogist, Ottawa
November 2010

Introduction

157 potential kimberlite indicator mineral grains were recovered from 60 till samples collected within the map sheets 106H, 106I and 106J west of Fort of Good Hope in the lowlands bordering the Canyon Ranges in the Mackenzie Mountains, NWT, Canada. The majority of the grains were Cr-diopside (n=60) and chromite (n=56), with considerably lower amounts of Mg-ilmenite (n=22) and pyrope garnet (n=17), as well as one epidote. The distribution of these minerals in each sample is given in Table 1C, Appendix E. The grains were analyzed by EMP at the GSC in Ottawa and the data labeled and sorted by mineral and listed in Appendix E. The critical compositional characteristics of each mineral are discussed below.

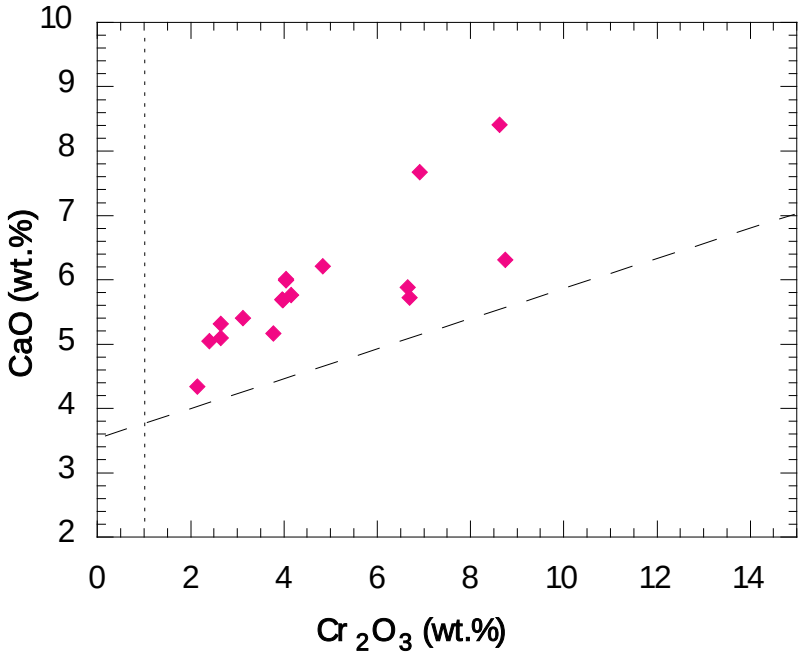


Figure 1: CaO vs. Cr_2O_3 in pyrope garnets. The vertical dashed line separates peridotitic Cr-pyrope (at right) from Cr-poor megacrystic and eclogitic garnet (at left). The diagonal dashed line is the 85% line of Gurney (1984) that is used to divide Ca-rich lherzolitic (G9, above) from Ca-depleted harzburgitic garnets (G10, below).

1. Pyrope Garnet

A total of 17 Cr-pyrope grains were recovered from 14 of the 60 samples in this study. These garnet grains occur mostly in samples from the northern periphery of the sampling area in map sheets 106J and 106I. Samples with more than one garnet are RA-26 (n=3) in the west of map sheet 106J, and RA-61 (n=2) at the border of map sheets 106J and I. Two pyrope garnets with elevated TiO_2 (> 0.5 wt.%) and comparatively low Cr_2O_3 (< 3 wt.%) are titanian pyrope characteristic of kimberlitic megacryst garnet (G1). The composition of the other pyrope grains is more chromian and their CaO levels suggest that they are G9 garnets derived from lherzolite xenoliths (Fig. 1) typically found in kimberlites.

2. Mg-Ilmenite

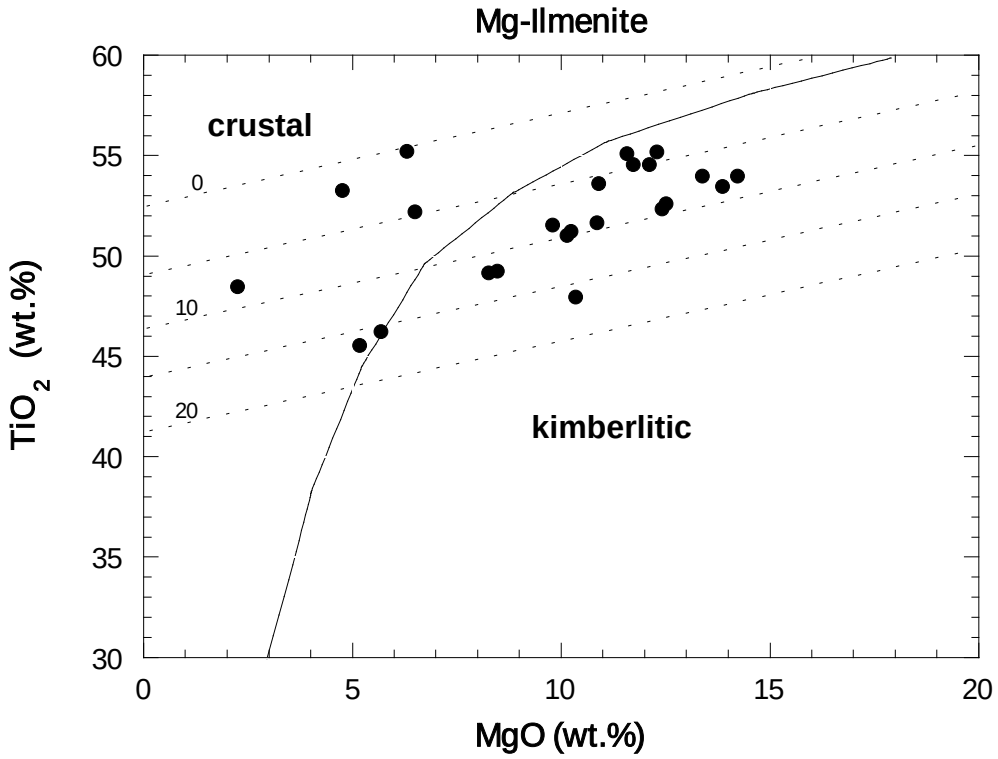


Figure 2: TiO_2 vs. MgO for 23 ilmenite grains recovered in this study. Six grains plot to the left of the separation line between Mg-poor crustal ilmenite and Mg-rich kimberlitic megacryst ilmenite (after Wyatt et al., 2004).

Twenty-two Mg-ilmenite grains and one Mg-poor ilmenite were recovered from 15 of the 60 samples in this study. These grains also occur mostly in samples from the northern periphery of the sampling area in map sheets 106J and 106I, none in map sheet 106H. Five of the Mg-ilmenite bearing samples also contained Cr-pyrope. Samples RA-57 and RA-88 (n=3), and RA-65 (n=2) collected east of the Mackenzie River in map sheet 106I contain more than one Mg-ilmenite each, whereas samples further west contained only 0 to 2 ilmenite grains each.

The MgO content in the ilmenite grain ranges from 2.25 to 14.22 wt.% (Fig. 2). Six ilmenite grains with less than 6.5 wt.% MgO plot left of the dividing line between crustal ilmenite and kimberlitic megacryst ilmenite according to Wyatt et al. (2004)(Fig. 2). They contain between 0.53 and 1.04 wt.% Cr_2O_3 (Fig. 3). These - for crustal ilmenite - unusual-ly Mg- and Cr-rich ilmenite grains are probably derived from ultramafic rocks such as those found in ultramafic layered intrusions (e.g. dunite, peridotite, pyroxenite). They occur in four samples (RA-16, R68, RA-70, RA-62, that lie in map sheet 106J just west of the boundary to 106I. The other Mg-ilmenite grains have MgO from 8.27 to 14.22 wt.% and Cr_2O_3 from 0.19 to 5.59 wt.%, compositions characteristic of (and unique to) kimberlitic megacryst ilmenite. The grains have similar geographic distributions as the pyrope garnet grains.

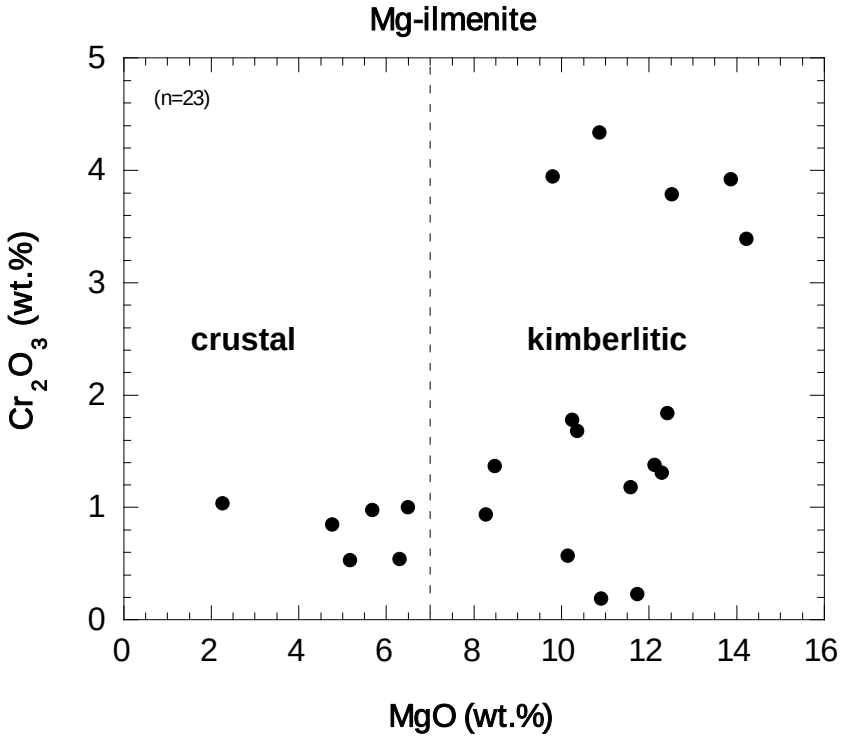


Figure 3: Cr_2O_3 vs. MgO ilmenite grains recovered in this study. Six grains plot to the left of the separation line between Mg-poor crustal ilmenite and Mg-rich kimberlitic megacryst ilmenite (after Wyatt et al., 2004).

3. Chromite

Chromite is the second most abundant kimberlite indicator mineral in this study after Cr-diopside. It occurs in abundances of 1 to 5 grains in about half of the sixty till samples from this study, particularly in samples just west of the Mackenzie River in map sheet 106I and from there diagonally across map sheet 106J (from ENE to SW), overlapping with samples that also contain pyrope and ilmenite.

The composition of these chromite grains is shown in Fig.4. Most chromite grains are only moderately chromian with 30 to 48.7 wt.% Cr_2O_3, only six grains have more than 50 wt.% Cr_2O_3 but none more than 58 wt.%. Chromite from mantle xenoliths found in kimberlites typically cluster between 45 to > 60 wt.% Cr_2O_3 suggesting that the chromites in this study are probably also largely crustal and from the same source as the less magnesian ilmenites, i.e. crustal ultramafic igneous rocks.

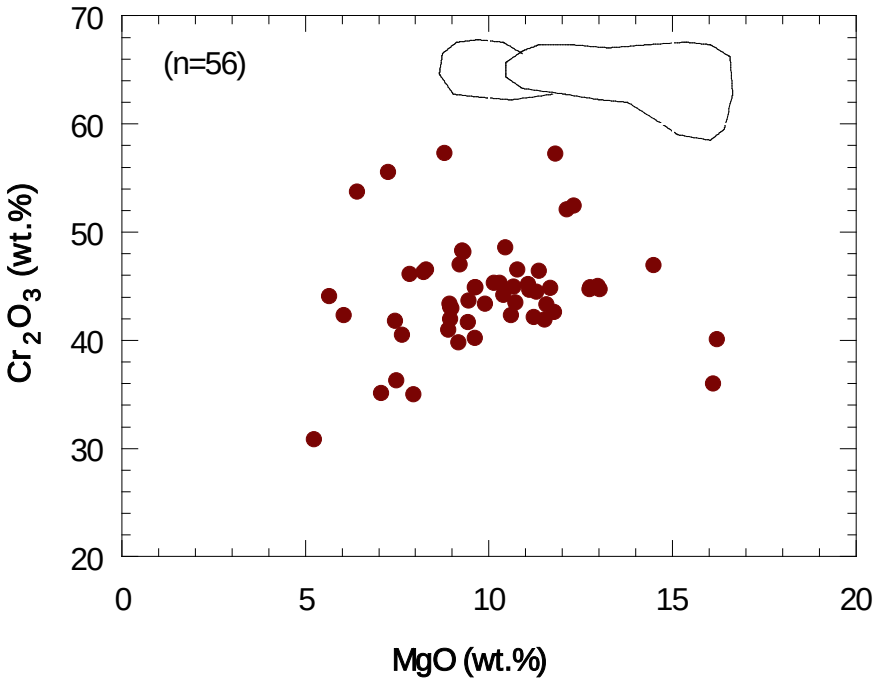


Figure 4: Cr_2O_3 vs. MgO for chromite and Cr-spinel. The black outlined fields are the compositional ranges of chromite inclusions in diamond (right) and of chromite intergrown with diamond (left) after Fipke et al. (1995).

4. Cr-diopside

Cr-diopside is with 60 grains the most abundant mineral in the till samples from this study. It occurs with 1 to 6 grains in about thirty till samples. Only 10 of these samples also contain chromite. The sample with the most Cr-diopside grains (n=6) is R-65 (which also contained 4 chromites, 1 pyrope and 2 ilmenite), followed by R-20 and R-88 (n-4 each). All other samples had between 0 and 3 diopside grains.

The composition of the diopside grains is predominantly chromian with only four grains < 0.5 wt.% and Cr_2O_3 values up to 1.6 wt.% (Fig. 5). Mg-#s vary from 80.5 to 90.5 (Fig.5), i.e. they are mostly derived from mafic to ultramafic host rocks (Deer et al. 1978). Figure 6 (after Nimis, 1998) classifies kimberlitic cpx by their composition into grt-peridotitic, spinel-peridotitic and other sources, however, the diagram does not discriminate between mantle and crustal sources. In Figure 6 most Cr-diopside grains form a cluster in the field of garnet-peridotitic compositions (GP), three grains are clearly more aluminous and plot in the spinel-peridotite field (SL) although all of them including

those with < 0.5 wt.% Cr_2O_3 could also be from crustal ultramafic rocks such as layered intrusions or komatiitic rocks.

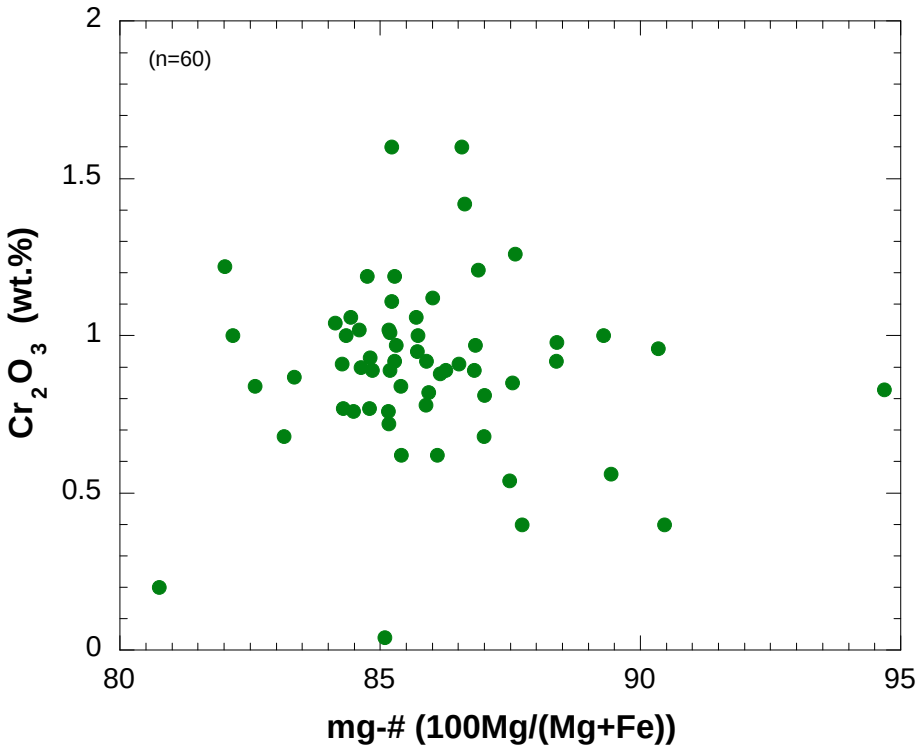


Figure 5: Cr_2O_3 vs. mg-# in Cr-diopside grains.

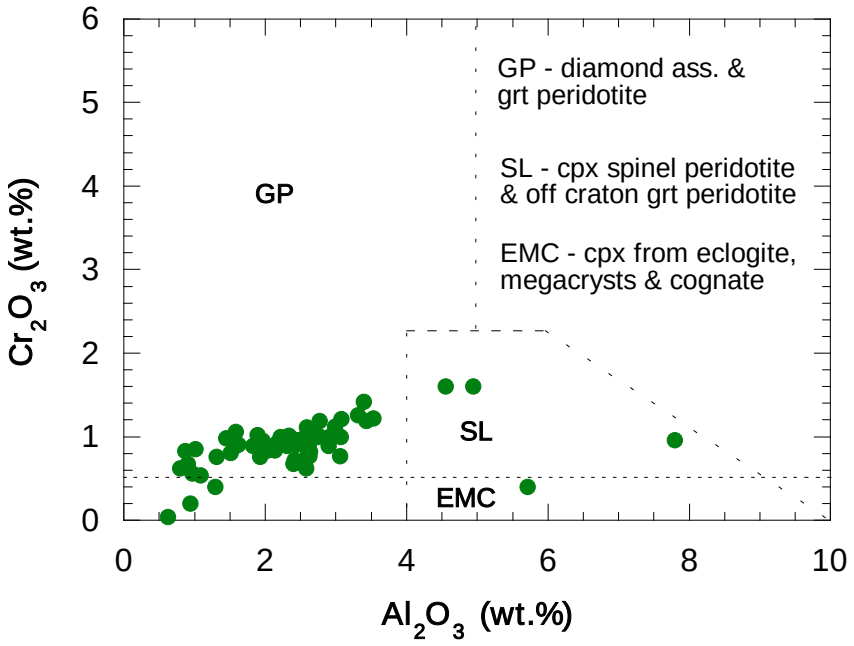


Figure 6: Cr_2O_3 vs. Al_2O_3 in Cr-diopside grains with discrimination fields according to Nimis (1998). Note that these fields were developed for kimberlite derived diopside and do not discriminate between those and diopside from regional crustal sources.

Summary and Discussion of Provenance

Over 150 grains of four different kimberlite indicator minerals (chromite, Cr-diopside, Mg-ilmenite and pyrope) were picked from ca. 60 till samples in map sheets 106,I, 106, J, 106G, and 106H in the Mackenzie river low lands (Ramparts area), NWT. Cr-diopside and chromite are with 60 and 56 grains, respectively, the most abundant kimberlite indicator minerals in these samples, but also the most ambiguous, since they could also be derived from crustal mafic to ultramafic rocks. Mg-ilmenite and pyrope are less abundant (22 and 17 grains, respectively) but more likely to be derived from kimberlite or its xenoliths. More specifically 17 of the 22 Mg-ilmenite grains could be positively identified as kimberlitic megacryst-ilmenite and 15 of the Cr-pyrope grains are derived from mantle lherzolite (xenoliths transported to the surface by kimberlite) whereas two more titanian Cr-pyrope grains are kimberlitic megacryst garnet.

Thus, the presence of Mg-rich ilmenite, Cr-pyrope and megacryst garnet strongly indicate a kimberlitic source up-ice from the sample area. However, the low grain count per sample and the wide distribution of the grains suggests that the source is distal and the material was widely distributed before deposition. The most indicator rich samples (in absolute numbers, without normalization to sample weight) are generally in the North of the sample area close to the Mackenzie river in map sheet 106I (RA-065, RA-061 and RA-088) and in the west of map sheet 106J around sample RA-026. The samples closer

to the foothills (i.e. South) are comparatively indicator mineral poor, containing only occasional Cr-diopside. This suggests that the indicator mineral sources are up-ice (i.e. E) of the sample area (Fig.7).

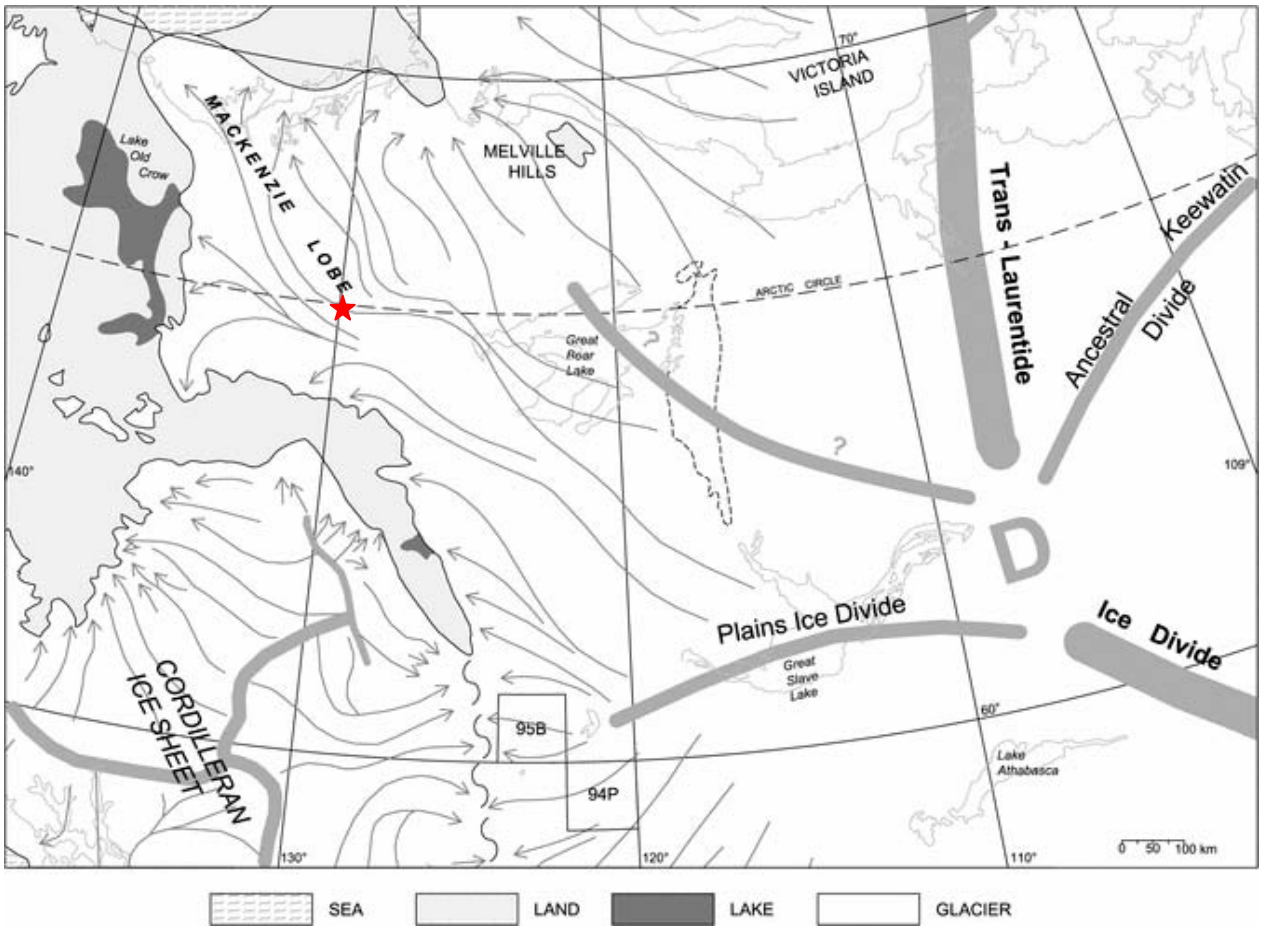


Figure 7: Ice flow direction of the Laurentide and Cordilleran ice sheets about 18 ka BP in the NWT. Red star indicates location of study area. *(from Bednarski, 2008; after Dyke and Prest, 1987; Dyke et al. 2003).*

Since chromite and Cr-diopside are typically minor minerals in mantle lherzolite, the high abundance of chromite and Cr-diopside versus pyrope suggests that not all grains of the two former minerals are derived from the same lithologies as Cr-pyrope, i.e. only a small percentage of the chromite and Cr-diopside are likely from garnet-lherzolite. A few Al-rich Cr-diopside grains suggest the presence of spinel-lherzolitic material (which does not contain garnet). This is consistent with the generally more Al-rich and less- Cr-rich compositions of the chromite/Cr-spinel grains (chromite is more Cr-rich in garnet-peridotite than in spinel lherzolite and crustal ultramafic rocks). Another explanation is that many of the Cr-diopside and chromite grains, as well as the Mg-ilmenites with < 7 wt.% MgO are derived from crustal mafic to ultramafic sources such as those found in layered intrusions. This is supported by the fact that many of the chromite and Cr-diopside grains occur in samples that do not contain pyrope or Mg-ilmenite and are far removed from those which do.

REFERENCES

Bednarski, J.M., 2008. Landform assemblages produced by the Laurentide Ice Sheet in northeastern British Columbia and adjacent Northwest Territories — constraints on glacial lakes and patterns of ice retreat, Canadian Journal of Earth Sciences, 45, p. 593-610.

Deer, W.A., Howie, R.A. & Zussman, J. (1978) Rock-Forming Minerals, Volume 2A Single-Chain Silicates, 2nd edition. Longman Group Ltd., London. 668 p.

Dyke, A.S., and Prest, V.K., 1987. Paleogeography of northern North America, 18,000 – 5,000 years ago, Geological Survey of Canada, Map 1703A, scale 1:12 500 000.

Dyke, A.S., Moore, A., and Robertson, L., 2003. Deglaciation of North America, Geological Survey of Canada, Open File 1574.

Fipke, C.E., Gurney, J.J. and Moore, R.O. (1995) Diamond exploration techniques emphasizing indicator mineral geochemistry and Canadian examples; Geological Survey of Canada, Bulletin 423, 86 p.

Gurney, J.J. (1984) A correlation between garnets and diamonds in kimberlites; in Kimberlite occurrence and origin a basis for conceptual models in exploration; Geology Department and University Extension, University of Western Australia, Publication No. 8, p. 143-166.

Nimis, P. (1998) Evaluation of diamond potential from the composition of peridotitic chromian diopside. *European Journal of Mineralogy* 10, p. 505-519.

Wyatt, B.A., Baumgartner, M., Anckar, E. and Grütter, H. (2004) Compositional classification of "kimberlitic" and "non-kimberlitic" ilmenite; *Lithos* 77, p. 819-840.

APPENDIX C

Sample field card data for Silt Water Geochemistry
from 2007-2008 field surveys of the
Ts'ude niline Tu'eyeta Candidate Protected Area
Ramparts River Area,
Northwest Territories

Note: This appendix contains 1 Microsoft Excel® Spreadsheet available on the CD that accompanies this report. These files can also be downloaded from www.nwtgeoscience.ca .

APPENDIX D

Data Transmittal Reports
from 2007–2008 field surveys of the
Ts'ude niline Tu'eyeta Candidate Protected Area
Ramparts River Area,
Northwest Territories
prepared by Overburden Drilling Management Ltd.

Note: This appendix contains 3 Microsoft Excel® Spreadsheets available on the CD that accompanies this report. These files can also be downloaded from www.nwtgeoscience.ca .

APPENDIX E

HMC and Till Microprobe data
from 2007-2008 field surveys of the
Ts'ude niline Tu'eyeta Candidate Protected Area
Ramparts River Area,
Northwest Territories

Note: This appendix contains 3 Microsoft Excel® Spreadsheets available on the CD that accompanies this report. These files can also be downloaded from www.nwtgeoscience.ca .